Telomeric silencing, Nucleotide Excision Repair and chromatin organisation in *Saccharomyces cerevisiae*

Agurtzane Irizar Oña

Doctor of Philosophy

Department of Pathology
Cardiff University
Ph.D. 2009

ProQuest LLC
789 East Eisenhower Parkway
P.O. Box 1346
Ann Arbor, MI 48106-1346

Declaration

This work has not previously been accepted in substance for any degree and is not concurrently submitted in candidature for any degree.

Signed ..... (candidate) Date 16/11/'09

STATEMENT 1

This thesis is being submitted in partial fulfillment of the requirements for the degree of PhD.

Signed ..... (candidate) Date 16/11/'09

STATEMENT 2

This thesis is the result of my own independent work/investigation, except where otherwise stated. Other sources are acknowledged by explicit references.

Signed ..... (candidate) Date 16/11/09

STATEMENT 3

I hereby give consent for my thesis, if accepted, to be available for photocopying and for inter-library loan, and for the title and summary to be made available to outside organisations.

Signed ..... (candidate) Date 16/11/09

STATEMENT 4: PREVIOUSLY APPROVED BAR ON ACCESS

I hereby give consent for my thesis, if accepted, to be available for photocopying and for inter-library loans **after expiry of a bar on access previously approved by the Graduate Development Committee.**

Signed ..... (candidate) Date .....

Acknowledgments

Firstly and foremost I would like to thank my supervisor Professor Raymond Waters for giving me the opportunity to do a PhD in his group. I would also like to thank him for his continuous support, encouragement and his constructive advice throughout my PhD studies.

Many people in Ray Waters and Simon Reed groups (Yuming Teng, Shirong Yu, Huayun Jackson, Yachuan Yu, Julia Smirnova....) have provided me with technical advises and support, helping me not to get lost in the lab.

I would like to give special thanks to those friends who read versions of my thesis: Aaron Mendez Bermudez, Virginie Reuter, Neil Humphreys and Emeline Furon. I would also like to thank Oscar Silvestre for the enjoyable chats walking home and coffee breaks that we used to have at unusual hours in the Tenovus building. A general thanks to all the nice people I met in Cardiff: Rhiannon Jones, Nicole Heppel, Marcela Rosas, Jean Paul, Emeline furon, my housemates at 49, Lisvane Street; Deborah Bacciu, Virginie Reuter, Ehab Almoubarak, and Paola Murciani. I would also like to express my gratitude to my friends back at home. Thanks for their support in this three years and mostly when I was writing this thesis; Amagoia Aguado, Edurne de Albiz, Irene Lopez and Maider Solana.

Special thanks to my boyfriend Aaron Mendez Bermudez for being so comprehensive, patient and supportive.

I would like to thank the MRC for financial support, without their support this research will not have being possible.

Last, but not least, I acknowledge my parents, Inaki Irizar Aurtenetxe, Argine Ona Ona and my Sister Alaitz Irizar Ona, who supported and encouraged me to continue with my studies.

Summary

In this thesis, the influence of subtelomeric silencing on chromatin structure and Nucleotide excision repair (NER) efficiency in *Saccharomyces cerevisiae* is addressed.

To assess the chromatin organisation, NER efficiency and acetylation levels; yeast strains containing the *URA3* marker gene at two subtelomeres with distinct levels of silencing were used. All the analyses were undertaken at the coding region of the *URA3* sequence.

Overall, the results presented in this thesis showed that at subtelomeres with high levels of silencing, the DNA is less accessible to the NER machinery; therefore, the repair is slower. This is probably due to the variations in chromatin organisation since the chromatin structure is more compact at highly silenced subtelomeres. When telomeric silencing is abrogated by the deletion of the *SIR2* gene, the NER efficiency and the chromatin organisation became similar at both subtelomeres, enforcing the idea that the differences in NER and chromatin organisation are due to variations in silencing levels. Furthermore, there was a considerable difference at the highly silenced subtelomere between the $SIR2^{+}$ and *sir2Δ* strains. However, the differences at the non-highly silenced telomeres between $SIR2^{+}$ and *sir2Δ* were not so dramatic.

This work also concentrated on the inhibitory role of Sir2p on the acetylation response after UV irradiation. The results showed an incremental increase in acetylation levels after UV treatment when the *SIR2* gene was deleted at the highly repressive end. However, the acetylation levels remained the same after and before the UV treatment when *SIR2* was not deleted. In contrast, there were not significant differences in acetylation levels between the $SIR2^{+}$ and the *sir2Δ* strains after UV irradiation at the non-repressive end. These findings imply that silencing influence NER efficiency and DNA accessibility. Furthermore, *SIR2* suppresses any UV induced response in acetylation at highly silenced subtelomeres.

Abbreviations

AADPR	0-acetyl ADP ribose
AP	Apurinic / Apyrimidinic
ARR	Access repair restore
BER	Base excision repair
BSA	Bovine serum albumin
CAF-1	Chromatin assembly factor-1
ChIP	Chromatin immunoprecipitation
CPD	Cyclobutane pyrimidine dimer
CR	Caloric Restriction
COFS	Craneo-oculofacial-skeletal syndrome
CS	Cockayne Syndrome
DDB	Damaged DNA-binding (protein)
DDT	DNA damage tolerance
DHO	Dihydroorotic acid
DNA	Deoxyribonucleic Acid
dsDNA	Double-stranded DNA
DSB	Double-strand breaks
DTT	Dithiothreitol
EDTA	Ethylenediaminetetraacetic acid
Endo III (IV)	Endonuclease III (IV)
ERCC	Excision repair cross complementing
FAD	Flavin adenine dinucleotide
5-FOA	5-fluoroorotic acid
GG-NER	Global genomic-nucleotide excision repair
GNAT	Gcn5p-related *N*-acetyltransferases
HAT	Histone acetyltransferases
HAST	Hda1-Affected SubTelomeric
HDAC	Histone deacetylase
HR	Homologous recombination
HST	Homologues of Sir Two
IP	Imunoprecipitation
IR	Ionizing radiation
LB	Lysogeny broth
ML endo	*Micrococcus luteus* CPD endonuclease
MMR	Mismatch repair
MMS	Methyl methane sulphonate
MPC	Magnetic particle concentrator
MTHF	5, 10 methenyltetrahydrofolate
NAM	Nicotinamide
NER	Nucleotide excision repair
NHEJ	Non-homologous end joining
NRE	Non-repressive end
NTS	Non-transcribed strand
OA	Orotic acid
OGG1	Oxoguanine glycosylase
ORC	Origin recognition complex
ORF	Open reading frame
PBS	Phosphate buffered saline
PCNA	Proliferating nuclear antigen
PCR	Polymerase chain reaction
PD	Pyrimidine dimers

PEV	Position effect variegation
PIC	Pre-initiation complex
PNKP	Polynucleotide kinase/phosphate
Pol I (II)	Polymerase I (II)
Pd(A)	Polydeoxyadenosine
Pd(C)	Polydeoxycytidine
Pd(G)	Polydeoxyguanosine
Pd(T)	Polydeoxythymine
(6-4) PPs	Pyrimidine-pyrimidone (6-4) photoproducts
PR	Photoreactivation
RE	Repressive end
PSI	Pounds per square inch
RNA	Ribonucleic acid
ROS	Reactive oxygen species
RPA	Replication protein A
RPM	Revolution per minute
r.t.	Room temperature
RT-PCR	Reverse-Transcription PCR
ssDNA	Single-stranded DNA
SDS	Sodium dodecyl sulfate
STR	Subtelomeric repeats
SSC	Standard saline citrate
T	Timine
TAE	Tris-acetate-EDTA
TBE	Tris-borate- EDTA
TC-NER	Transcription coupled-nucleotide excision repair
TE	Tris-EDTA
TEMED	Tetramethylethylenediamine
TFIIH	Transcription factor II H
TPE	Telomere position effect
TS	Transcribed strand
TTD	Trichothiodystrophy
UAS	Upstream activation sequence
YC	Yeast complete media
UV	Ultraviolet light
WCE	Whole cell extract
YNBD	Yeast nitrogen base difco
XP	Xeroderma pigmentosum
YPD	Yeast peptone dextrose
XCR	X-combinatorial repeats
XRCC	X-ray cross-complementing

Contents

Chapter I

GENERAL INTRODUCTION

1.1 DNA Damage

There are two classes of mutagen sources that can modulate the genome; endogenous sources (e.g. oxygen free radicals, methylating agents, loss of glycosylic bond by hydrolysis of purine residues or transformation of cytosine to uracil by deamination, replication errors) and exogenous sources (e.g. ultraviolet radiation (UV), ionizing radiation (IR) from radioactive materials, some chemicals).

The DNA damage produced by these sources can generate genome instability, altering cellular functions and causing diseases such as cancer. However, plasticity of the DNA allows organisms to survive, acclimatise to the environment and to changes within the environment.

This thesis focuses primarily on the nucleotide excision repair of DNA damage produced by UV light.

1.1.1 DNA damage induced by UV light

UV light can be divided into three categories depending on the wavelength: (i) UV-A, where the wavelength ranges between 320 nm and 400 nm; (ii) UV-B from 295 nm to 320 nm and (iii) UV-C from 100 nm to 295 nm. Mainly UV-C and to some extent UV-B can be absorbed by the DNA and this produces DNA damage. However, it has been recently reported that UV-A can also produce DNA damage (Runger and Kappes, 2008).

The DNA damages by UV-C and UV-B are named photoproducts. The most abundant of these produced in the genome are cyclobutane pyrimidine dimers (CPDs) which constitute around 70% of the lesions at 260 nm of UV and pyrimidine pyrimidone (6-4) photoproducts [(6-4)PPs], which are helix distorting lesions (Friedberg et al., 2005) and which constitute around 25% of the lesions induced.

UV induced CPDs are pre-mutagenic lesions and the chemical nature of the dimer can influence the type of the resulting mutation, the most common lesions are transition mutations from C to T (Friedberg et al., 2005; Mitchell, 2000; Runger and Kappes, 2008; You et al., 2001).

The formation of CPDs is heterogeneous throughout the genome and it can be influenced by various factors:

DNA sequence

Studies had showed that dimer formation depends on the DNA sequence, these being in the ratio of T^T: C^T: T^C: C^C; 68: 13: 16: 3 in irradiated plasmid DNA. Moreover, the induction of CPDs is correlated with the maximum absorbance of pyrimidines. Actually, when cells are irradiated with UV-C, the yield of CPDs in polyd(A): polyd(T) is much higher than in polyd(C): polyd(T) and in polyd(m^5C): polyd(G). Furthermore, polyd(A): polyd(T) tracts have been shown to create hot spots for PD formation since they adopt a characteristic chromatin structure affecting the nucleosome formation rendering the DNA more accessible to transcription factors and the T homodimer is the predominant photoproduct induced by UV-C radiation (Schieferstein and Thoma, 1996; Shimizu et al., 2000; Tijsterman et al., 1999).

However, when cells are irradiated with UV-B there is an increment of CPD formation in polyd(m^5C): polyd(G) in comparison to polyd(C): polyd(G) and polyd(A): polyd(T) (Mitchell, 2000).

The yield of CPDs also depends on the nature of the nucleotides flanking potential dimer sites. For instance, dimerisation is more efficient when the sequence is 5'-ATTA-3' than when it is 5'-ATTG-3' (Gordon and Haseltine, 1982).

Protein-DNA binding

Another factor influencing CPD distribution is the binding of proteins to the DNA. In the genomic nucleosome core DNA, CPDs are originated with a 10.3 bp periodicity, generally situated in the minor groove of the DNA facing away from the histone surface (Ataian and Krebs, 2006). However, (6-4) PPs are preferentially found in the linker region. Overall, protein-DNA interaction can create a distortion in the DNA helix, facilitating the formation of pyrimidine dimers after UV. For instance, nucleosomes can influence the damage formation, since the flexibility and mobility of the DNA around the nucleosome create structural changes that alter the damage formation (Thoma, 1999).

The removal of the damage is also influenced by positioned nucleosomes. Indeed, the CPDs found within the internal protected region of the nucleosomes are repaired slower than CPDs in the linker region. This difference in repair rate between

the linker region and the internal protected region has been reported by several groups (Ferreiro et al., 2004; Powell et al., 2003; Teng et al., 2002; Wellinger and Thoma, 1997); however, these differences are relatively small.

Transcription factors are another example of a DNA-protein interaction that can influence the CPD formation throughout the genome. Transcription factors, apart from forming hyper-reactive regions for CPD formation, can also form hypo-reactive regions frequently found near the hyper-reactive site (Becker and Wang, 1984; Pfeifer et al., 1992; Selleck and Majors, 1987; Tornaletti and Pfeifer, 1995). Therefore, UV light can be used to investigate the binding of transcription factors to DNA and the distribution of the nucleosomes due to heterogeneity in the CPD formation and NER (Axelrod et al., 1993).

CPDs formation is also influenced by single-stranded DNA and double-stranded DNA, and they are more easily formed in single-stranded DNA. CPDs and (6-4) PPs are described below in more detail.

1.1.1.1 Cyclobutane pyrimidine dimers (CPDs)

CPDs are the most studied lesion due to their abundance, their highly mutagenic properties and the ability to detect them relative easily in DNA from UV irradiated cells or tissues.

These bulky lesions in the DNA are created by two covalent bonds between adjacent pyrimidines, forming four members ring structure due to saturation of pyrimidine 5, 6 double bonds (figure 1.1). The most predominant conformation is the Cis-syn form (figure 1.2); other forms such as trans-syn (figure 1.2) can be detected in single-stranded and in duplex DNA with special conformations, for example B-DNA and Z-DNA. CPDs in DNA are also stable at extreme pH and temperature (Friedberg et al., 2005).

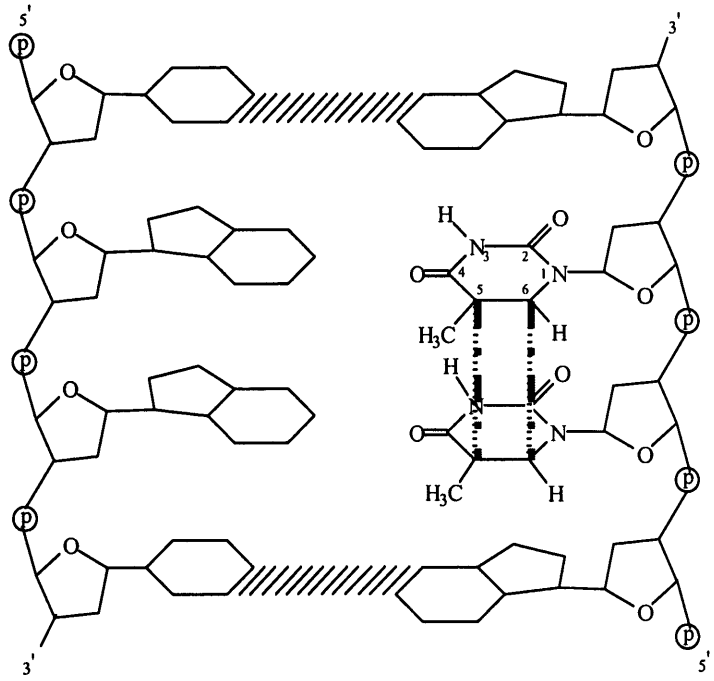

Figure 1.1 *Structure of CPD in a dsDNA.* Covalent interaction of two adjacent pyrimidines in the same polynucleotide chain forms a four-membered cyclobutyl ring linking the two pyrimidines. The formation of two new bonds (C^5-C^5, C^6-C^6) results from the saturation of the two C^5=C^6 double bonds in two pyrimidines (adapted from Friedberg et al., 2005).

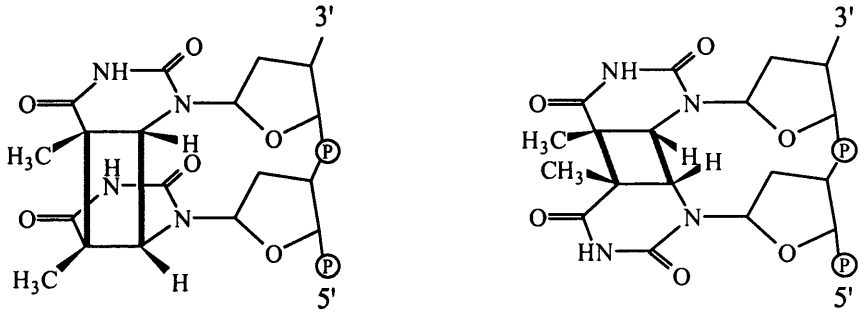

Cys-syn (T-T) *Trans-syn* (T-T)

Figure 1.2 *Structures of cys-syn and trans-syn CPD* (adapted from Friedberg et al., 2005).

1.1.1.2 Pyrimidine-Pyrimidone (6-4) photoproducts, [(6-4) PPs]

(6-4) PPs are created by the linkage of the 5'pyrimidine C_6 position with the 3'pyrimidine C_4 position with a single covalent bond (figure 1.3). These lesions are less frequent than CPDs and are repaired faster than CPDs in the non-transcribed strand (NTS) (Tijsterman et al., 1999), probably because NER proteins bind with more affinity to (6-4) PPs lesions and they can excise these more efficiently than CPDs (Kusumoto et al., 2001).

The faster repair may also be linked to the fact that they generate major distortions in the DNA helix, producing a 44° bend and do not retain the hydrogen bonds at the 3' side of the photolesion (Friedberg et al., 2005). It is likely that the generation of a major distortion in the DNA helix and the fact that they are located in the linker region may facilitate better/easier recognition by repair proteins so these lesions are repaired more efficiently than CPDs.

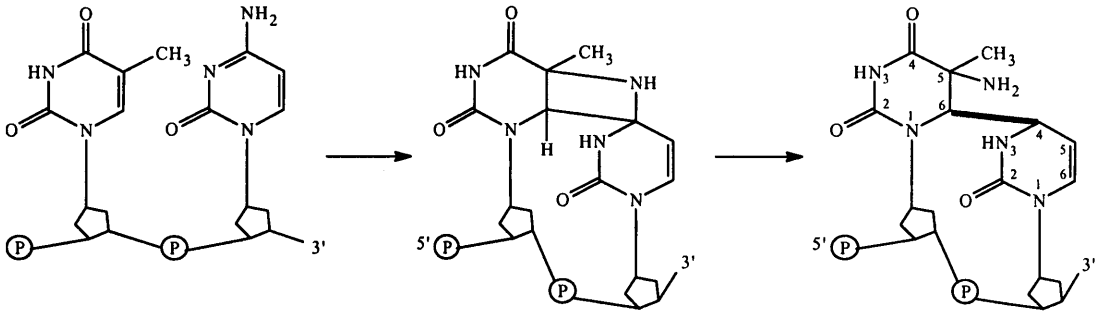

Figure 1.3 *Formation of UV induced T-C (6-4) PPs.* The covalent linkage between the C^6 position of one thymine and the C^4 position of the 3' adjacent cytosine formed due to UV radiation. The plane of the 3' base moiety is shifted 90° relative to that of the 5' thymine. The 3' pyrimidine in the (6-4) PP is typically cytosine rather than thymine (adapted from Friedberg et al., 2005).

1.1.1.3 Other DNA photoproducts

These are other UV-induced photoproducts found in a lower proportion. For example, spore photoproducts also called 5'-thyminyl-5, 6-dihydrothymine, are major photoproducts found in the spores of *Bacilus subtilis* (Slieman et al., 2000; Varghese, 1970) and in the dehydrated A-DNA form.

Pyrimidine hydrates are formed by the addition of a water molecule to form a 5, 6, double bond resulting in a 5, 6-dihydro-6-hydroxy derivative named cytosine hydrate. Hydrates of cytosine or deoxycytosine are highly unstable; they can rehydrate and revert to the parent form. Cytosine hydrates can also undergo dehydration to yield uracil (Boorstein et al., 1990). The photoproduct formed from methyl cytosine, 5' methylcytosine hydrate, may undergo deamination to yield 5'-thymine hydrate which can convert to thymine upon dehydration.

Thymine glycols result from the saturation of the 5, 6 double bond in the pyrimidines forming 5, 6-dihydroxy dihydrothymine. These DNA lesions are formed by IR or UV (Demple and Linn, 1982).

1.1.2 Oxidative DNA damage

Reactive oxygen species (ROS) are created by products of cellular metabolism but can also be generated by exogenous IR, ultraviolet light (UV-B and UV-C), and exposure to chemical oxidants and transition metals. ROS are molecules that contain one or more unpaired electrons. Therefore, they are more reactive than non-radical molecules since they have the ability to act as oxidizing agents. Indeed, these molecules can interact and modify biomolecules (lipids, proteins, nucleic acids) producing alterations to the cell. In nucleic acids, the oxidative lesions are base modifications, such as the formation of abasic sites and deoxyribose damages. These damages are repaired by the base excision repair (BER) mechanisms and in some instances by the nucleotide excision repair mechanisms (Herrero et al., 2008; Scott et al., 1999).

Due to its low redox potential, guanine is the most vulnerable base to oxidisation creating the most common lesion; 7, 8 dihydro-8-oxoguanine (8-oxoG). 8-oxoG can base pair with adenine and cytosine 2-hydroxyadenine. Therefore, if the lesion is not removed during replication, a transversion mutation from G to T can be generated. There are many glycosylases in the BER mechanism that specifically recognize abnormal DNA bases and, when the modified base is removed, other enzymes repair the damage (the BER mechanism is described in section 1.3.2.2). An example of a glycosylase is the product of the gene OGG1 in humans. This gene encodes a mithochondrial glycosylase/lyase enzyme that specifically excises 7,8 dihydro 8 oxoguanine residues located opposite cytosine or thymine residues in the DNA (Cooke et al., 2003; David et al., 2007; Maynard et al., 2009; Tsuzuki et al., 2007).

1.2 Cellular responses to DNA damage

DNA damage checkpoints are required for the maintenance of genome integrity. Throughout the cell cycle, there are four main damage checkpoints, G_1, G_2/M and two in S-phase. During these checkpoints, the DNA damage or failures in DNA replication are detected so facilitating a hiatus in the cell cycle to enable DNA repair. Indeed, in response to DNA damage, eukaryotic cells generate post-translational modifications in the genome, regulating the expression of some genes. Thus, there is a transcriptional response to DNA damage and many of the genes that are transcriptionally activated are involved in the repair of DNA.

In addition to repair pathways, cells have developed DNA damage tolerance (DDT) mechanisms to allow DNA replication when replication forks collapse due to DNA damage. The DDT consists of pathways that allow replication without repairing the damage.

One pathway is called translesion synthesis, where several lower fidelity DNA polymerases can replicate a damaged template producing some errors during replication. The family of polymerases involved in this pathway is termed Y-polymerases (reviewed by Plosky and Woodgate, 2004). These Y-polymerases have a low fidelity activity and can replicate damaged DNA. One of the Y-polymerases is the Pol η which can replicate the damaged DNA produced by UV exposure. The extent of fidelity varies with the polymerases in question and surprisingly some can replicate damaged templates with considerable accuracy.

The other pathway implicated in DDT is error free. This pathway bypasses the damage without creating any mutation in the DNA since the sister chromatid is used to restore the sequence opposite to the lesion (Ulrich, 2007).

Finally, when the damage cannot be tolerated or repaired due to a huge amount of DNA lesions, the cells in metazoans initiate programmed cell death or apoptosis (Friedberg, 2003; Hoeijmakers, 2001). In the unicellular organisms such as *Schizosaccharomyces pombe* and *S. cerevisiae* DNA damage can induce cell death (Madeo et al., 2009). Figure 1.4 shows the possible external and internal DNA damage sources and cellular response to these attacks.

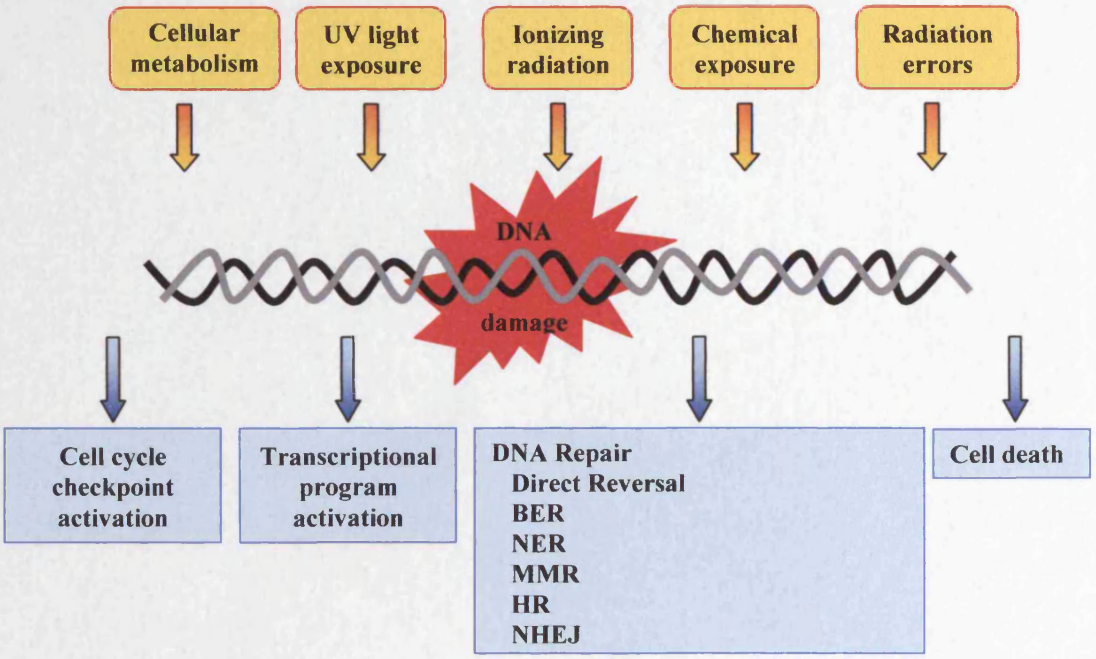

Figure 1.4 *Summary of the cellular response and mechanism to process DNA damage.*

1.3 DNA repair pathways

The multiple repair mechanisms that cells can use are divided into two main groups based on the molecular procedure to repair the damage; excision repair pathways and double-strand break (DSB) repair.

In the DSB repair group there are two main pathways, non-homologous end joining (NHEJ) and homologous recombination (HR). DSBs are caused by ionizing radiation or chemical exposure, but they can occur after UV (for example when a replication fork encounters an incised CPD). In the HR repair mechanism the information of the homologous sequence of the damaged DNA is used as a template for DNA repair (San Filippo et al., 2008). When the homologous template is not present, the NHEJ mechanism repairs the DNA lesion. In this pathway the ligation of two broken DNA ends can occur with no or minimal homology (Ataian and Krebs, 2006; Friedberg, 2003).

In the excision repair group there are three main pathways; nucleotide excision repair (NER), base excision repair (BER) and mismatch repair (MMR). The general repair mechanism for excision repair consists of the recognition of the damage, incision of the DNA phosphodiester backbone in the damaged strand, excision of the lesion and gap filling by DNA polymerase (Ataian and Krebs, 2006) with the final ligation. NER repairs helix distorting DNA damage. BER repairs DNA lesions

formed by endogenous and exogenous sources such as oxidative lesions or base alkylations. MMR repairs DNA damage produced by minor deletions, insertions and incorrect base incorporation during replication (Friedberg, 2003). Figure 1.5 shows a summary of the specific DNA lesions that are repaired by each DNA repair pathway followed by the main enzymes involved in each pathway in humans.

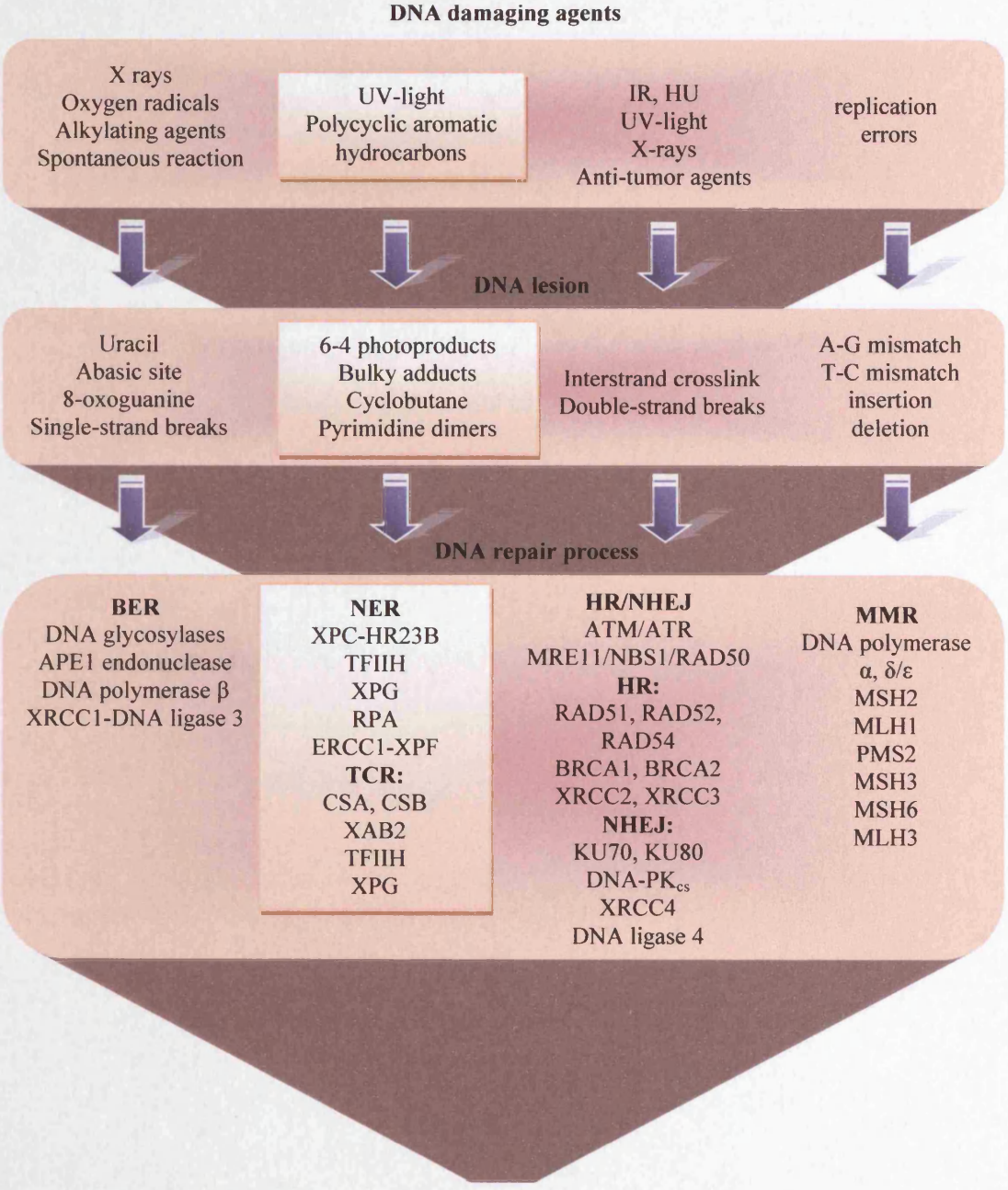

Figure 1.5 *Summary of the DNA repair pathways*. At the top, the main damaging agents are shown. In the middle, the possible DNA damage produced by these damaging agents is described. At the bottom, the precise DNA repair pathway for a specific damage is described together with the main genes and enzymes involved in each DNA repair pathway in humans (adapted from Allinen, 2002; Hoeijmakers, 2001).

1.3.1 Double-strand break repair (DSBR)

1.3.1.1 Homologous recombination mechanism (HR)

HR is a mechanism to repair DSBs that uses homologous sequences as a template to re-synthesise damage of missing information at the break site. However, if HR is not properly regulated or there is a deficiency in the mechanism, the HR products can lead to genomic instability. The process of strand invasion in search for homologous sequences and the formation of heteroduplex DNA displace one strand of the template. Once the damaged strand is paired with a homologous sequence, DNA synthesis takes place. In most of the cases the template strand is the sister chromatid and the repair process is mediated by a gene conversion event (Aylon and Kupiec, 2004; Richardson et al., 1998). After DNA synthesis the remaining gaps are filled by polymerases and ligated by DNA ligase I (Bugreev et al., 2006; Constantinou et al., 2000). In this model, only one end of the DSB invades the template strand and it is called synthesis-dependent strand annealing (SDSA). Alternatively, a model where both ends of a DSB invade the template strand has been proposed and it is known as double holiday junction model (DSBR) (Holliday, 1964).

1.3.1.2 Non-homologous end joining (NHEJ)

The NHEJ pathway directly rejoins two damaged DNA strands independently of their sequences. Therefore, if the ends are not compatible, the repair of DSBs can lead to loss of DNA material at the breakpoint. However, a very short stretch of DNA homology near the end of the DNA (1 – 6 bp) facilitates the rejoining and the accuracy of DSB repair. It is not clear how a cell decides between the use HR or NHEJ after a double-strand break. However, these two repair pathways are cell cycle-dependent, thus the choice of either pathway may depend on the cell cycle stage at which the DSB is originated. HR plays a major role during the S/G2 phases when sister chromatids are paired whereas NHEJ is mainly active in G1/early S phase (Aylon and Kupiec, 2004; Hefferin and Tomkinson, 2005; Hendrickson, 1997).

1.3.2 Excision repair pathways

In all the excision repair pathways the DNA fragment containing the damage is excised, new DNA is synthesized and ligated to fill the post-excision gap. Figure 1.6 shows an outline of the excision mechanisms that operate.

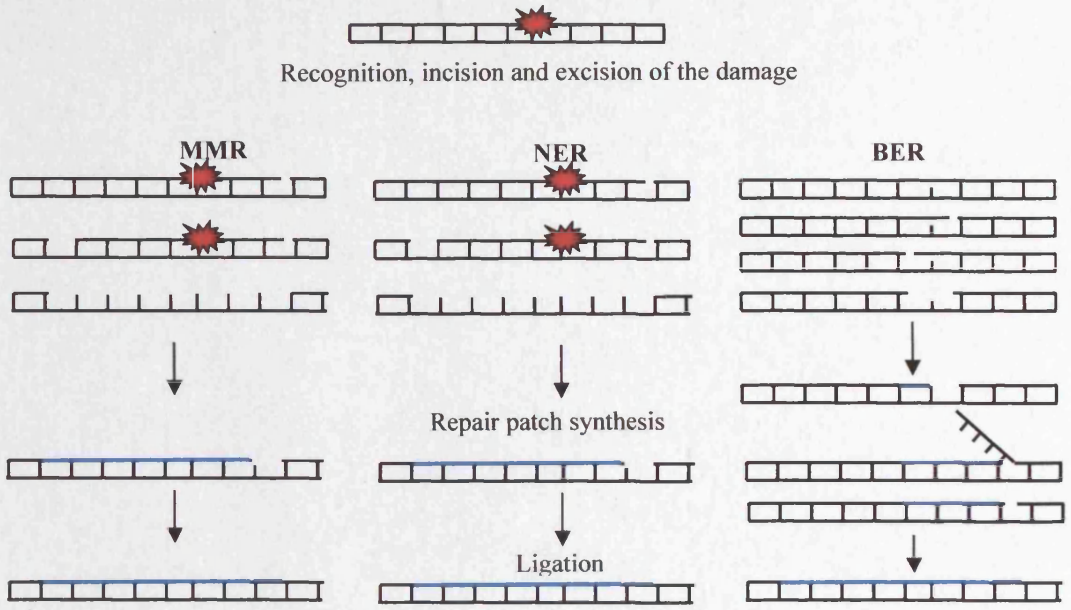

Figure 1.6 *General mechanisms of the excision repair pathways.* All three pathways share the same steps: excision of the damage, re-synthesis of DNA and the ligation of the remaining gap. Adapted from (Cline and Hanawalt, 2003).

1.3.2.1 Mismatch repair (MMR)

Errors generated during the replication process such as mis-incorporation of nucleotides or DNA-loops can be repaired by MMR. Furthermore, MMR is involved in the inhibition of recombination between non-identical sequences (homeologous recombination) and in promoting recombination events during meiosis (Kunkel and Erie, 2005).

The molecular mechanism of MMR consists of several steps: (i) the recognition of the mismatch by MutSα (a complex formed by Msh2p and Msh6p) or MutSβ (a complex formed by Msh2p and Msh3p). It has been reported that the proliferating nuclear antigen (PCNA) interacts with Msh2p in yeast and humans, thus, it may transfer or facilitate the binding of MutSαp or MutSβp to the mismatch (Lee and Alani, 2006); (ii) in the excision step, the exonuclease ExoI is involved in the excision of the strand containing the mismatch (Dzantiev et al., 2004); (iii) in the next step the gap is filled. Replication Protein A (RPA) protein binds to the nicked heteroduplex DNA at an earlier stage than PCNA or MutS proteins and it remains bound to the DNA during most of the repair process. Unphosphorylated RPA binds to DNA initially; however after extensive excision of the damage this protein gets phosphorylated. The phosphorylation of RPA reduces its affinity to bind to DNA, making the DNA template accessible to polymerase that re-synthesises the gap

created by the ExoI enzyme. Finally, the repair is completed by DNA ligase that seals the remaining nick.

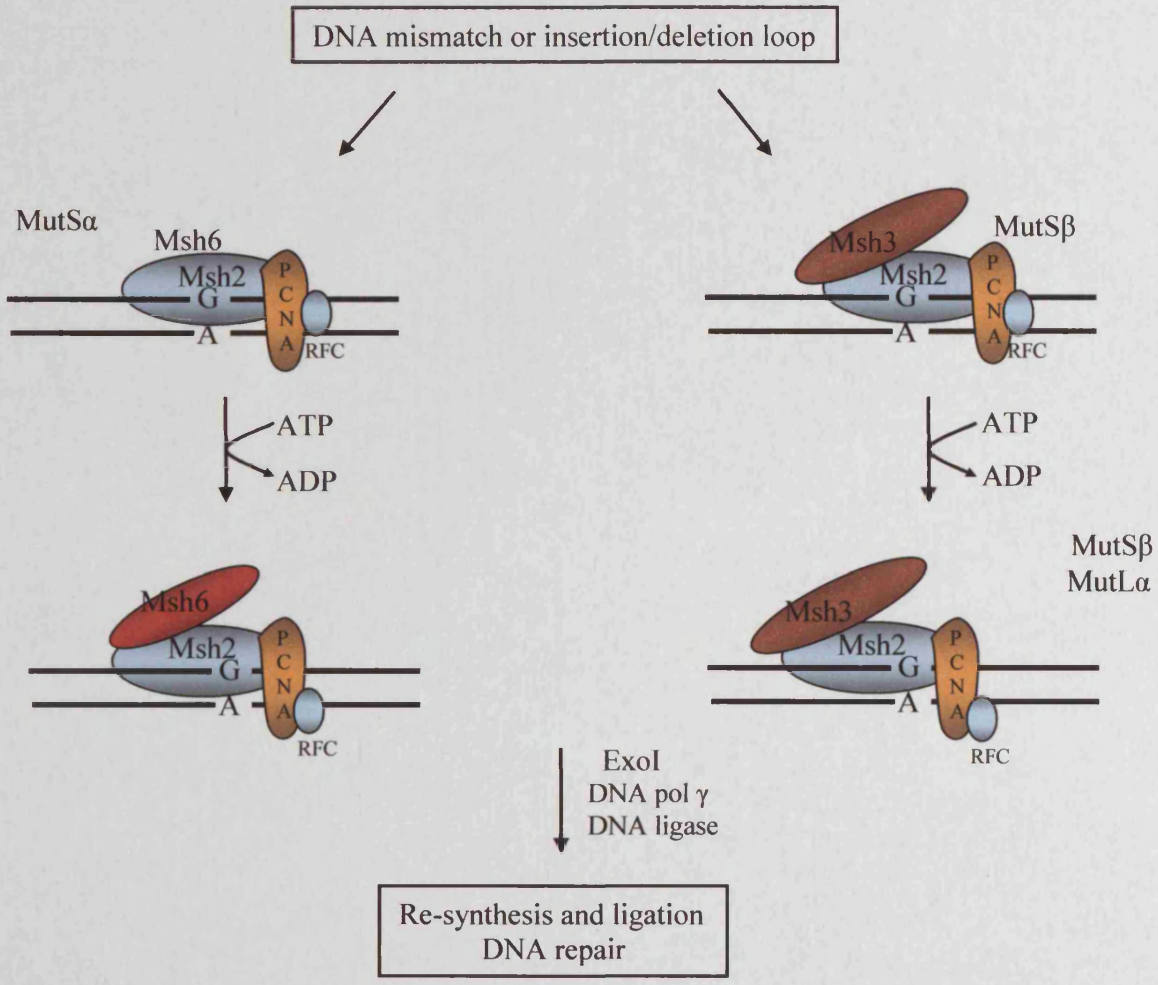

Figure 1.7 *Mismatch repair pathway*. MutSα and MutSβ bind to base mispairs and extrahelical loops. PCNA protein may be involved in the mismatch recognition and in the stabilisation of the MMR complex. Once MutS is bound, hMutLα binds the complex in an ATP dependent way. ExoI removes the mismatch segment while DNA polymerase δ re-synthesise the new DNA fragment.

1.3.2.2 Base excision repair (BER)

BER corrects the most common lesions that occur in DNA. The mechanism can be divided into five steps: (i) recognition and excision of the base that carried the damage by specific DNA glycosylases. These enzymes hydrolyses the N-glycosilic bond, generating an abasic site with a phosphodiester backbone (Wilson and Barsky, 2001); (ii) the next step is the incision of the abasic site. AP-Endonucleases are enzymes that remove the abasic site from the DNA. For example, in mammalian cells, APE1 endonuclease removes the abasic sites from the DNA by making an incision in

the first 5'phosphate to the AP site. Furthermore, it has been shown that the suppression of APE1 increases the levels of abasic sites in the DNA which can lead to apoptosis. However, experiments in budding yeast have shown that cells can use alternative pathways to remove the abasic sites when the yeast endonuclease Apn1 is deleted (Demple and Sung, 2005; Wilson and Barsky, 2001); (iii) afterwards, the excised nucleotide is replaced. The polynucleotide kinase/phosphate (PNKP) or AP lyase is responsible for excision at 3' termini (Rasouli-Nia et al., 2004; Wiederhold et al., 2004); (iv) The gap is filled by DNA polymerase. In humans, Pol β is implicated in the DNA synthesis an has also been shown to participate in the excision of the damage by removing the 5' terminal abasic fragment (Bennett et al., 1997; Wilson, 1998); (v) finally, the nick is sealed. Either a complex of X-ray cross-complementing 1 (XRCC1) protein and DNA ligase III or DNA ligase I (LIG1) seal the nick in the last step (Wilson and Bohr, 2007). In *S. cerevisiae* Cdc9p is involve is involved in the ligation.

DNA glycosylases

These enzymes have a great diversity of substrate specificities. DNA glycosyases flip the damaged nucleotides 180° out of the base stack into damage specific pockets within the enzyme. In the chromatin they bind to the minor groove, bend the DNA at the site of the damage and flip out the damaged base to the DNA major groove. There are two types of DNA glycosylases. The monofunctional glycosylases remove the damaged base by hydrolysing the N- glycosidic bond so generating apurinic sites and then they protect the abasic site until the involvement of AP endonuclease. In contrast, the bifunctional glycosylases have also AP lyase activity, hydrolyzing the 3' phosphodiester bond of the AP site. These enzymes require lysine side chain or N-terminal praline to be functional. All glycosylases that operate in BER act co-ordinately with the repair machinery (Dizdaroglu, 2005).

In some organisms there are glycosylases that specifically act on DNA lesions produced by UV irradiation. Nowadays, these enzymes are used for research purposes to analysed the incidence and location of UV lesions in DNA, both *in vitro* and *in vivo*. For example, in this thesis the *Micrococcus luteus* UV endonuclease enzyme has been used for the examination of the NER efficiency. These UV damage-specific glycosylases are briefly described below.

Pyrimidine dimer DNA glycosylases

a. T4 endonuclease V

T4 endonuclease V (T4 endo V) is derived from the bacteriophage T4 and is encoded by the *DENV* gene. It recognizes CPDs formed in DNA due to UV exposure and hydrolyzes the C-N glycosylic bond of the 5'CPD base. The AP site is cleaved by its AP lyase activity at the 3' side, resulting in a nick at the 5' side of the CPD. These enzymes are small proteins of 137 amino acids. The T4 endo V does not require divalent cations or other cofactors for its activity. T4 endo V can also target CPDs located in single-stranded DNA (Friedberg et al., 2005; Krokan et al., 1997).

b. *M. luteus* UV endonuclease

This UV endonuclease is encoded in the *M. luteus* genome and it is also a CPD-DNA glycosylase/AP lyase enzyme with a molecular mass of 31-32 kDa. Just as for T4 endo V, the *M. luteus* enzyme does not require ATP or divalent cations. The *M. luteus* UV endonuclease cleaves the CPD 5'- glycosylic bond. However, it only cleaves the *cis-syn* thymine dimer and not the *trans-syn* (6-4) or Dewar photoproducts (Krokan et al., 1997). Following the glycosylase activity, the AP lyase activity of the *M. luteus* endonuclease cleaves the phosphodiester backbone between the pyrimidines of the CPDs. This UV endonuclease has a preference for duplex rather than single-strand DNA. Although, only 27% amino acid residues are identical between both enzymes, the T4 endo V and *M. luteus* UV endonuclease functional catalytic residues are conserved (Friedberg et al., 2005; Krokan et al., 1997). The incision of DNA at CPDs by the N-glycosylase/AP lyase activity of T4 endo V and the *M. luteus* enzyme is shown in figure.1.7.

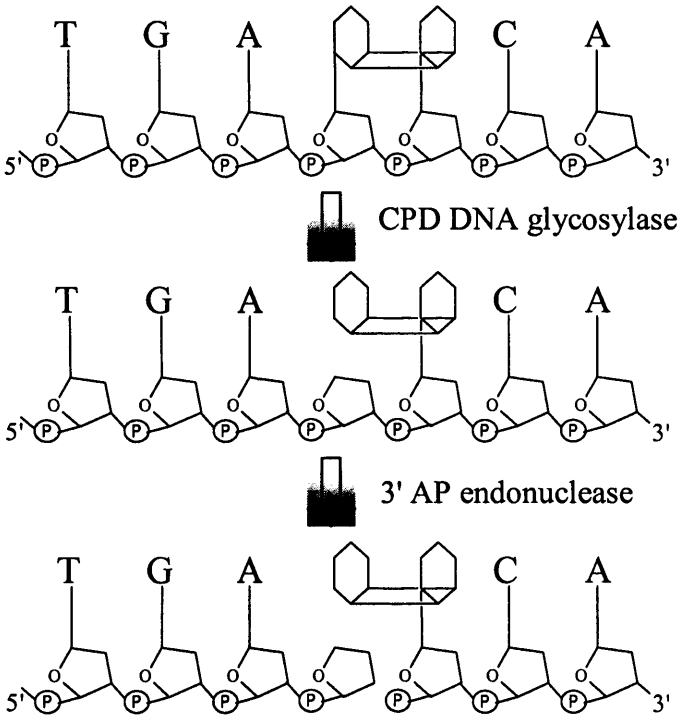

Figure 1.7 *Incision of DNA by CPD specific enzymes.* N-glycosylase specifically recognizes a CPD in DNA and cuts the 5' glycosyl bond of the dimer generating an AP site. AP lyase cleaves the phosphodiester bond 3' to the AP site.

1.3.2.3 Nucleotide excision repair (NER)

NER is a repair mechanism which removes helix distorting bulky DNA adducts produced by exposure to UV light, radiation or chemicals. This mechanism has been found in all cellular organisms and it repairs a wide range of DNA lesions.

The basic components of NER are conserved in prokaryotes and eukaryotes. In eukaryotes there are numerous differences from prokaryotic NER and many of these are related to the more complex structure of the eukaryotic genome. In prokaryotes the incision stage of NER is carried out by three specific proteins, UvrAp, UvrBp and UvrCp, whereas in eukaryotes around 20-30 proteins are involved in this mechanism and some of these proteins are also implicated in transcription (for example, TFIIH), replication (for example, RPA) and recombination (for example, XPF, ERCC1).

In both prokaryotes and eukaryotes, the DNA that is transcriptionally active is repaired faster than the non-transcribed DNA (Petit and Sancar, 1999; Sancar et al., 2004). Additionally, the chromatin structure can also affect NER. Consequently, eukaryotic cells contain chromatin remodelling factors, histone modifiers and histones

variants that can facilitate the accessibility of the repair proteins to the DNA (Cairns, 2005; Lee et al., 2004; Reed, 2005; Waters et al., 2009; Yu et al., 2005).

In humans, defective NER can have severe consequences, causing several diseases with increased UV sensitivity. These autosomal recessive inherited diseases are Xeroderma Pigmentosum (XP), the photosensitive form of Cockayne Syndrome (CS), combined XP/CS, Craneo-Oculofacial-Skeletal Syndrome (COFS) and Trichothiodystrophy (TTD) (Friedberg et al., 2005).

CS is due to a defect in the transcription-coupled nucleotide excision repair (TCNER) subpathway by mutations in *CSA* or *CSB* genes. This subpathway acts on the TS of transcriptionally active regions in the genome (Friedberg et al., 2005).

TTD patients are more complex and most of them show mutations on both alleles of the *XPD* gene. In others, *XPB* and *XPD* containing helicase activities are found to be damage. Hence, the phenotype presented can vary depending on the nature and location of the mutations (Friedberg et al., 2005).

Patients with XP show at least 7 different gene abnormalities (*XPA* to *XPG*) resulting in varying the diseases severity together with a defect in the global genomic nucleotide excision repair (GGNER) subpathway. The DNA damage from UV light remains unrepaired leading to cancerous cells or cell death (Friedberg et al., 2005).

There are cases where the combined XP/CS is present; this abnormality is produced by mutation in XPB helicase subunit. In addition, mutation in both helicases can lead to TTD or combined form of XP/TTD (de Boer and Hoeijmakers, 2000; Hoeijmakers, 2001; Leibeling et al., 2006).

1.3.2.3.1 The molecular mechanism of NER in *S. cerevisiae*

As mentioned before, the molecular mechanism of NER is based on five steps: a. damage recognition, where the lesion is recognized by the repair proteins; b. dual incisions are introduced at the flanking region of the damage; c. excision of the fragment containing the damagedDNA by excision nucleases; d. filling the gap using the complementary DNA strand as a template, e. ligation of the newly synthesized DNA. Figure 1.8 illustrates the general molecular mechanism of NER in *S. cerevisiae*.

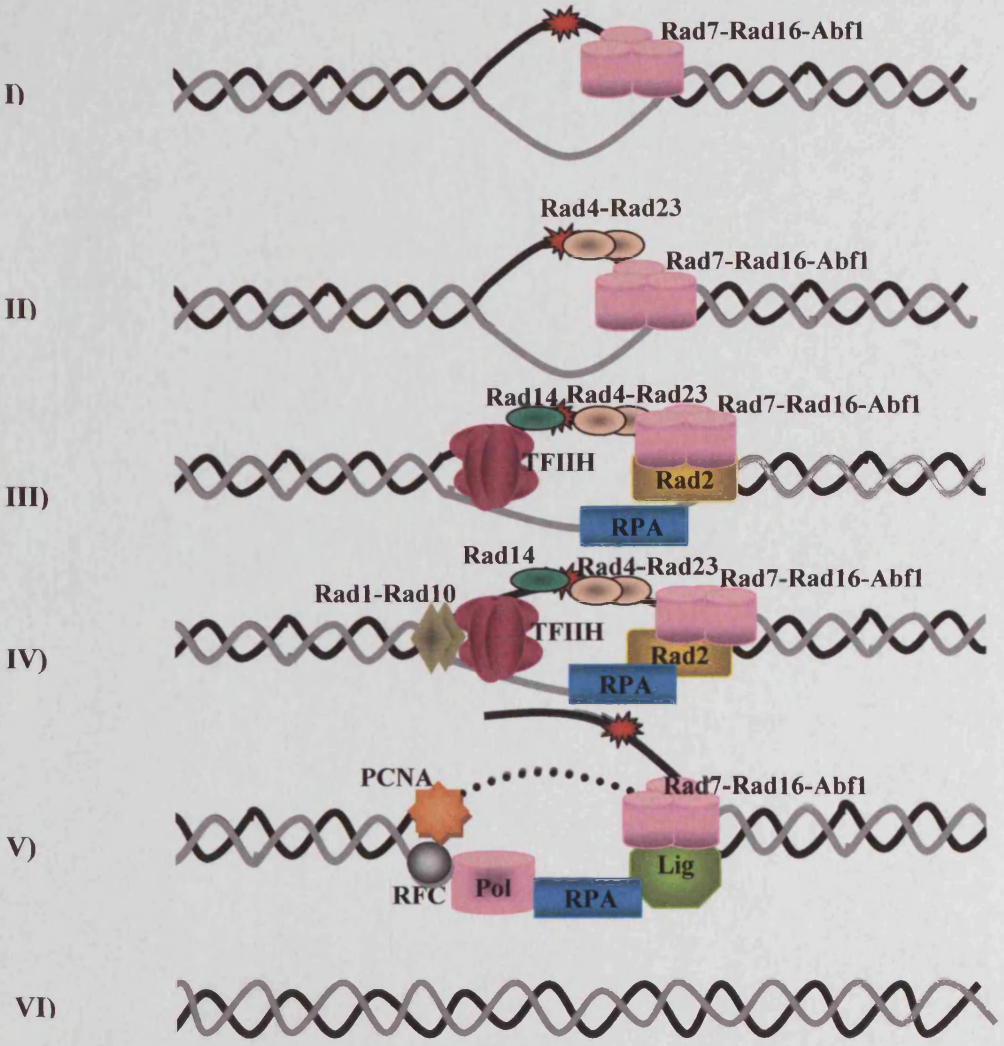

Figure 1.8 NER in S. cerevisiae with the GGNER recognition step. **(I)** Helix distorting damage is induced by UV irradiation; **(II)** after the early stages of recognition the damage is recognized by the Rad23p-Rad4p complex; **(III)** Rad14p, RPA and TFIIH bind to the DNA damage. The TFIIH contains Rad25p and Rad3p subunits with helicase activities that unwind the DNA forming a 'bubble'. Rad2p endonuclease is also recruited to the DNA damage; **(IV)** Rad1p-Rad10p endonuclease complex is recruited to the DNA damage site; **(V)** dual incision at both sites of the damage is generated by the endonucleases and the fragment containing the damage is excised with the help of Rad7p-Rad16p-Abf1p; finally **(VI)** the gap is filled by DNA polymerase and the remaining gap is sealed by DNA ligase.

a. Damage recognition

The repair rate is heterogeneous throughout the genome, being faster in the TS of RNA polymerase II transcriptionally active regions. However, repair is slower in the NTS of the transcriptionally active and inactive regions together with the TS of the transcriptionally inactive regions. Consequently, as mentioned before, NER has

been divided in two subpathways, TC-NER and GG-NER. TC-NER repairs DNA lesions found in the TS of transcriptionally active genes whereas GG-NER repairs the DNA damage in the NTS and also in the TS of transcriptionally inactive genes and in upstream regulatory sequences which are not transcribed. The difference between these subpathways is based on the recognition step which is an ATP-dependent multi-step process. Figure 1.9 shows the differences in the recognition step between TC-NER and GG-NER at the budding yeast. The differences between GG-NER and TC-NER in the DNA damage recognition step are also described below.

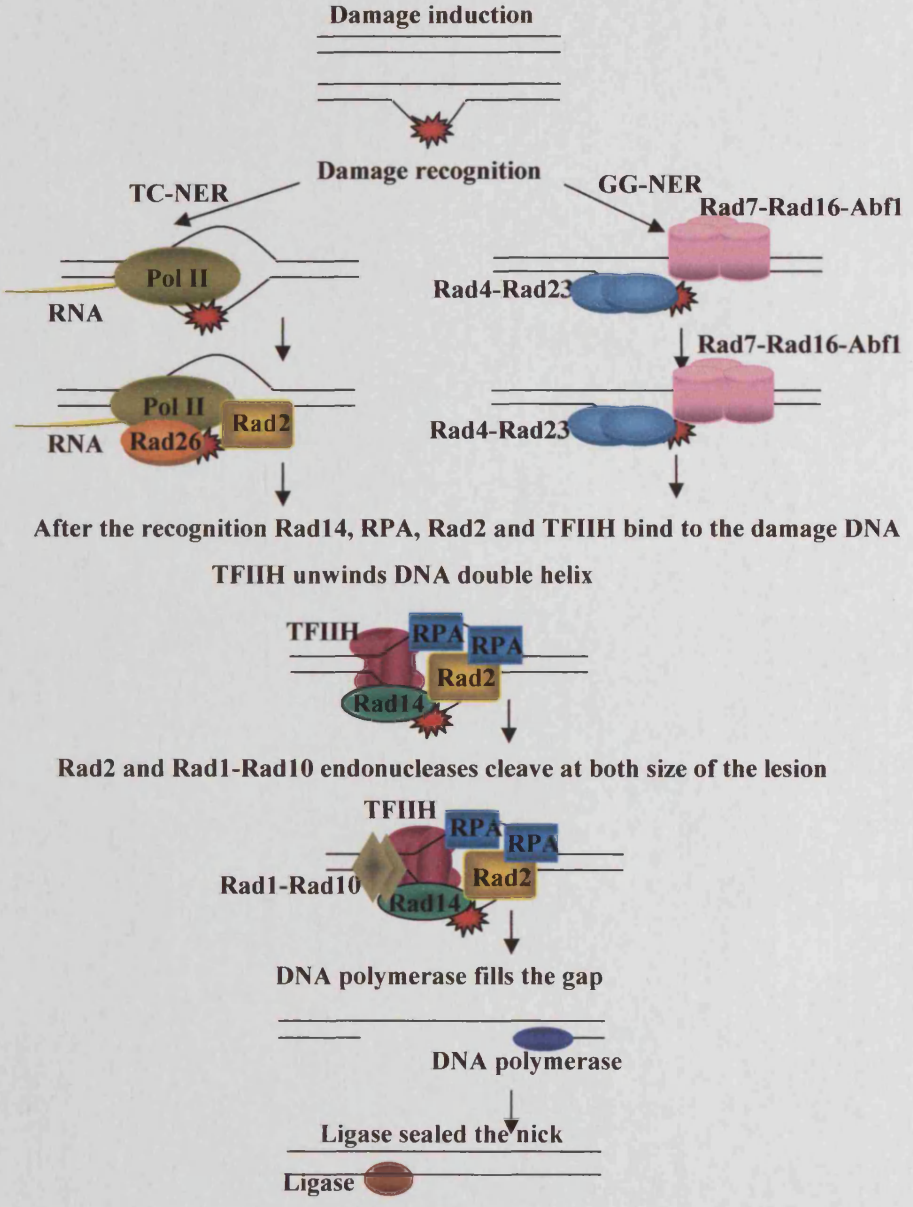

Figure 1.9 NER in S. cerevisiae. The GG-NER and TC-NER pathways differ in the recognition step. In TC-NER, the recognition of the damage begins with RNA pol II, which recruits Rad26p and Rad2p. In the GG-NER the recognition requires Rad4p-Rad23p and Rad7p-Rad16p.

Damage recognition in GG-NER

Rad14p (XPA in humans), Rad4p-Rad23p (XPC-HhR23b in humans) are involved in the pre-incision recognition step (Prakash and Prakash, 2000) and they have higher affinity for damaged than undamaged DNA. This recognition step is ATP-dependent since it has been shown that there is an increment of an interaction between Rad4p-Rad23p heterodimer and SWI/SNF ATP-dependent chromatin remodellers in the present of UV damage (Gong et al., 2006). Moreover, it is believed that the SWI/SNF recruitment to the damage site is to facilitate NER (Gong et al., 2006). In the absence of UV damage this interaction can also be observed, however, it increases when the DNA is damaged by UV irradiation. Rad7p (not known in humans), Rad16p (not known in humans) and Rad23p (HhR23bp) are also indispensable for transcription-independent NER and are physically associated with Rad4p. Hence, Rad4p is associated with Rad23p and in another complex with Rad7p and Rad16p (Wang et al., 1997). These proteins, Rad7p and Rad16p, are only involved in GG-NER (Verhage et al., 1994), and in the post-incision step they are complexed with Abf1p (Yu et al., 2004). However, in the upstream promoter region of *MFA2* Rad16p is not totally needed for the repair of UV lesions but in the NTS and downstream Rad16p is indispensable (Constantinou et al., 2000). Recent evidence has suggested that Rad16p is required for chromatin remodelling after cells are exposed to UV due to the involvement of the Rad16p in the acetylation of histone H3. Thus, knowing that Rad16p has an ATPase domain, it is suggested that Rad16p can generate a superhelical torsion resulting in changes in chromatin structure which can cause further changes such as acetylation in the histone H3 (Teng et al., 2008). In addition, Rad7p and Rad16p are also required for efficient NER at nucleosome free regions (Lettieri et al., 2008). The roles of Rad7p and Abf1p are discussed below.

Overall, The recognition complex is ATP-dependent with high affinity to damage DNA and it is formed by RPA, Rd14p (XPA), Rad4p (XPC), Rad23p (HhR23b) and TFIIH (Petit and Sancar, 1999).

Damage recognition in TC-NER

The damage is recognized by RNA polymerase II and Rad26p (CSB in humans) is required for the efficient repair in the TS of transcriptionally active genes (van Gool et al., 1994). For example, in the *MFA2* gene of *rad26* mutants, slower repair was observed in the TATA box and in the coding region where TC-NER operates. On the

contrary, where the transcription terminates, the NER rate in the *RAD26* mutant was not affected (Teng and Waters, 2000).

The precise role of Rad26p is not known; however, it is known that Rad26p has ATPase activity, suggesting its involvement in the removal of RNA polymerase II after the recognition of the damage for the recruitment of TFIIH.

Another study in *S. cerevisiae* had shown that in *rad26* mutants the TC-NER efficiency in the *MFA2* gene sequence decreases at the level of the NTS repair rate, suggesting that Rad26p is required for the TCNER pathway and when the TCNER is dysfunctional, GG-NER subpathway is involved in the TS of transcriptionally active genes (Constantinou et al., 2000).

However, it has been recently suggested that TC-NER might be divided into two pathways, Rad26p-mediated TC-NER and RNA binding protein 9 (Rpb9p)-mediated TC-NER (Ataian and Krebs, 2006). The Rpb9p-mediated TC-NER pathway operates more efficiently in the coding region than in the region upstream of the transcription start site. In contrast, Rad26p-mediated TC-NER has the same efficiency in both regions. The UAS and TATA regions are needed for the TC-NER mediated by Rad26p in the TS of transcriptionally active genes. Moreover, the Rad26p-mediated repair can be affected by the presence of mutations in TATA or UAS regions but not the Rpb9p-mediated repair. The Rpb9p-mediated TC-NER always acts on the TS and its efficiency is influenced by UAS, TATA, but the UAS and TATA box are not absolutely required for this repair pathway (Ataian and Krebs, 2006).

b. Dual incision

After the recognition of the damage, the molecular mechanism at the TC-NER and GG-NER are identical.

Rad2p endonuclease (XPG in humans) binds to increase the stability of the DNA-protein complex. Rad2p has 3' nuclease function and one of its roles in the repair mechanism is the recruitment of Rad1p-Rad10p heterodimer (XPF-ERCC1 in humans) which is less stable in the complex and has 5' endonuclease function.

Another protein complex involved in NER in *S. cerevisiae* is TFIIH. This transcription factor can adopt two molecular conformations. The form involved in NER is named Ssl2-core TFIIH and it is composed of 5 tightly associated subunits (Rad3p, Tfb1p, Tfb2p, Ssl1p, and Tfb4p) and the loosely associated Ssl2p (also called Rad25p). The transcriptional form of TFIIH is named holo-TFIIH an it is formed by

the Ssl2p-core TFIIH and TFIIK (Kin28p, Ccl1p and Tfb3p) which has a kinase activity and it is involved in the phosphorylation of the C-terminal RNA polymerase II largest subunit. Ssl2p (Rad25p) and Rad3p in yeast are DNA-dependent ATPase/helicases (Wang et al., 1995). Thus, following the recognition of the damage by the NER mechanism, Rad3p helicase (XPD in humans) which works from 5' to 3' and Ssl2p (Rad25p) (XPB in humans) which contain 3' to 5' helicase activity, unwind the DNA generating a "bubble" at the damaged region of the DNA.

Following the generation of the 25-30 nucleotide "bubble" containing the damaged DNA by Rad3p and Rad25p helicases, the Rad1p-Rad10p endonuclease heterodimer makes and incision at 5' end of the bubble (ERCC1-XPF in humans) and the Rad2p endonuclease (XPG in humans) cleaves the 3' end of the bubble, generating a fragment of 24-32 nucleotide long which contain the damaged DNA. The Rad1p-Rad10p nuclease complex has no affinity for the damaged DNA but it is recruited by Rad2p. The Rad1p-Rad10p complex is associated with Rad14p which has affinity for the damaged DNA. After, Rad1p-Rad10p endonuclease can effectively generate an incision at the 5' side of the DNA damage (Guzder et al., 2006).

The incision is generated at the 3' side of the lesion, precisely 2 to 8 nucleotide from the DNA damage, whereas, the incision at the 5' is at 15 to 24 nucleotide from the UV lesion. However, the exact cutting is determine by the nature of the lesion and the sequence of the DNA at that location. This dual incision is also asynchronous since the 3' incision occur a fraction of a second earlier than the 5' incision. The activity of these endonucleases is enhanced by RPA protein which bind to the single-stranded DNA to protect it (Petit and Sancar, 1999).

c. Excision of the fragment containing the damage

It has been recently shown that Rad7p/Rad16p/Abf1p protein complex is likely to be required for the excision of the oligonucleotide containing the damage. This protein complex could generate the super helical torsion essential for the excision of the damaged oligonucleotide. The generation of superhelical torsion is ATP-dependent and it is most likely to be introduced by Rad16p, which has ATPase domain (Lee et al., 2004).

Recently, it has been observed that the binding of the Abf1p to its DNA binding site is required for the efficient GG-NER since Abf1p recruits Rad16p and Rad7p to the damage site (Yu et al., 2009). Furthermore, the mutation of Abf1p binding site at

HMLα locus affects the recruitment of Rad7p and Rad16p to the damage DNA as well as Abf1p (Yu et al., 2009). It has been also observed that in the absence of Rad16p, Rad7p interacts physically with Rad4p/Rad23p complex and binds to DNA, however, does not have specificity to damaged DNA (Guzder et al., 1999).

d. Gap filling

The single-strand DNA is protected from degradation by some repair proteins such as RPA. The formed gap is filled by DNA polymerase ε/δ For this reaction, PCNA and RFC allow detection of primer terminus and it is required for the synthesis of DNA in the present of RPA. In contrast, in the absence of RPA, repair synthesis is independent of PCNA (Petit and Sancar, 1999).

e. Ligation

The phosphodiester backbone of the repaired DNA is completed by DNA ligase I (in humans) or Cdc9p (in budding yeast).

Table 1.1 shows a summary of proteins involved in NER in budding yeast and their human counterparts.

There are other proteins such as Mms19p and Tfb5p, termed NER accessory proteins. The absence of these proteins leads to a moderate rather than severe cellular UV sensitivity. For example, it has been recently reported that Mms19p is required to control the concentration of Rad3p in the cell (Kou et al., 2008).

Table 1.1 *Genes involved in NER in S. cerevisiae and their human homologues.* The biochemical activity is described for each gene if it is known.

S. cerevisiae	Human gene	Biochemical activities
RAD7	Not known	Rad7p-Rad16p complex
RAD16*	Not known	ATPase, translocase
RAD14	*XPA*	Damage binding protein
RAD4	*XPC*	Rad4-Rad23 complex binds UV damaged DNA
RAD23	*HR23B* *HhR23A*	Rad4-Rad23 complex binds UV damaged DNA
ABF1	Not known	DNA binding protein. Rad7p-Rad16-Abf1p complex
RAD3	*XPD*	5'→3' DNA helicase
RAD25 (SSL2)	*XPB*	3'→5' DNA helicase
RAD1	*XPF*	5'incision subunit
RAD10	*ERCC1*	5' incision subunit
RAD2	*XPG*	Rad2 endonuclease, 3'incision
RAD26	*CSB*	DNA dependent ATPase
CDC9	*LIG1*	Ligase
RFA1	*RPA1*	Subunit of RPA which binds to ssDNA
RFA2	*RPA2*	Subunit of RPA which binds to ssDNA
RFA3	*RPA3*	Subunit of RPA which binds to ssDNA
MMS19	*MMS19L*	Sustain an adequate concentration of the Rad3p
TFIIH subunits:		
TFB1	*GTF2H1*	?
TFB2	*GTF2H4*	?
SSL1	*GTF2H2*	Zn finger, DNA binding?
TFB4	*GTF2H3*	Ring finger, DNA binding?
TFB5	*GTF2H5, TTD-A*	Stabilisation of TFIIH
TFB3	*MAT1*	CDK assembly factor
KIN28	*CDK7*	CDK, C terminal domain kinase, CAK
CCL1	*CCNH*	Cyclin

* The functional human homologue of *RAD16* could be *DDB2*.

1.3.2.4 Photoreactivation (PR)

PR is a reversal mechanism involved in the repair of CPDs and (6-4) PPs using blue light photons as source of energy. It is evolutionary conserved as far as marsupials but is absent in mammals (Sancar, 2000; Tuteja et al., 2009). The mechanism is simple and contains a unique monomeric enzyme called photolyase (Phr1) which has a molecular mass of 55-65 kDa. Moreover, there are two different photolyases that specifically repair CPDs or (6-4) PPs (Sancar, 1994; Todo et al., 1993). This enzyme uses the blue light as a source of energy to carry out the photoreactivation. Figure 1.10 describes this repair mechanism. Firstly, in the absence of blue light photolyase bind to CPDs. Afterwards, in the presence of blue light the photo-antenna (folate) located at the surface of the photolyase absorbs a violet/blue-light photon (350-450 nm) and the chromophore MTHF is stimulated to the excited singlet state. Afterwards, it transfers the energy to the chromophore cofactor of

reduced form of flavin adenine dinucleotide ($FADH^-$) to generate the excited state of $FADH^-$. Subsequently, $FADH^-$ donates an electron to the CPD, producing an unstable anion which gives rise to two pyrimidines (Carell et al., 2001; Sancar, 1994; Sancar, 1990, 2000; Tuteja et al., 2009). $FADH^-$ can re-acquire its catalytic function since an electron returns to its chromophore (Baer and Sancar, 1989). Photolyase enzyme preferentially reverse CPDs originated in the NTS of certain active genes (Aboussekhra and Thoma, 1998; Livingstone-Zatchej et al., 1997) and it can also assist NER mechanism if there are no suitable conditions for PR to happen (Baer and Sancar, 1989). CPD photolyase is more widespread than (6-4) photolyase and it has been found in many organism including bacteria, fungi and plants whilst (6-4) photolyase has only been found in some higher eukaryotes, e.g. *Drosophila melanogaster* (Todo et al., 1996; Todo et al., 1993) and *Xenopus laevis* (Hitomi et al., 1997). Both enzymes follow a similar mechanism to bind and repair their targets (Hitomi et al., 1997; Tuteja et al., 2009; Zhao et al., 1997).

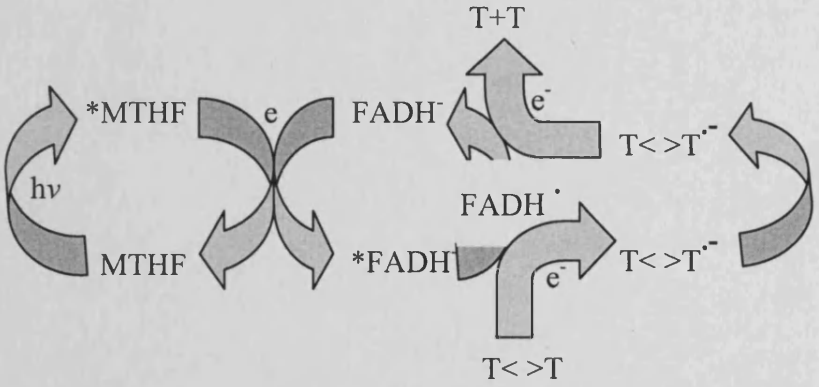

Figure 1.10 *Transference of energy in S. cerevisiae photoreactivation.* Both chromophores from the photolyase enzyme, $FADH^-$ and 5, 10-methenyl tetrahydrofolate (MTHF) absorb light and transfer it to dimers for their splitting. MTHF absorbs blue-light and transfers the energy to $FADH^-$. $FADH^-$ gives an electron to a CPD bound to the photolyase and generates unstable CPD radical anions that enhance the splitting into two pyrimidines. An electron is also transferred back to $FADH^-$ to generate the original $FADH^-$.

1.4 Chromatin structure

Chromatin can influence the rate of metabolic processes such as transcription and repair. Furthermore, it is known that chromatin structure differs between transcriptionally active and inactive regions (Biddick and Young, 2009). The influence of chromatin structure over NER has been reported by several groups and is further described below (Morrison and Shen, 2005).

1.4.1 Chromatin composition and organisation

The nucleosome is the basic unit of chromatin and is formed by a histone octamere composed of H2A, H2B, H3 and H4 histones. Histones H3 and H4 are highly conserved having similar function in all eukaryotes. However, H2A and H2B are less conserved than H3 and H4 since they show a degree of speciation. Each nucleosome contains approximately 147 bp of DNA wrapped around the outside of the histone octamer. Nucleosomes are repeated and connected by linker DNA forming the structure called "beads on a string". This structure is compacted into higher order chromatin structure by folding and coiling. Nucleosomes can form two types of chromatin; an open and relaxed form named euchromatin that is associated with active genes and a highly condensed chromatin named heterochromatin that is associated with repressed transcription sites. In *S. cerevisiae*, the repressive chromatin form is called silenced chromatin. The structure is very similar to heterochromatin and is mainly located at the mating type loci (cryptic mating type *HML* and *HMR*), telomeres and rDNA (Kornberg, 1977; Luger, 2006). The highest compacted chromatin structure found in mammal cells is the metaphase chromosome that is visible under a light microscope. Figure 1.11 shows the different levels of chromatin condensation in a chromosome.

The linker histone protein (H1), which is located outside the core nucleosome, plays important roles in the chromatin structure of many eukaryotes including humans. The precise function of histone H1 is not known, but it has been proposed that it may have a structural function to help secure DNA to the core histone octamer (Georgel and Hansen, 2001) and it may also be involved in chromatin modification (Veron et al., 2006). The budding yeast homologue of histone H1 is encoded by the *HHO1* (Histone H One) gene (Veron et al., 2006). The role of the yeast H1 homologue is unclear but it may be involved in recombination and transcriptional silencing inhibition rather than chromatin structure since it is not found in the linker region of the chromatin (Downs et al., 2003; Veron et al., 2006).

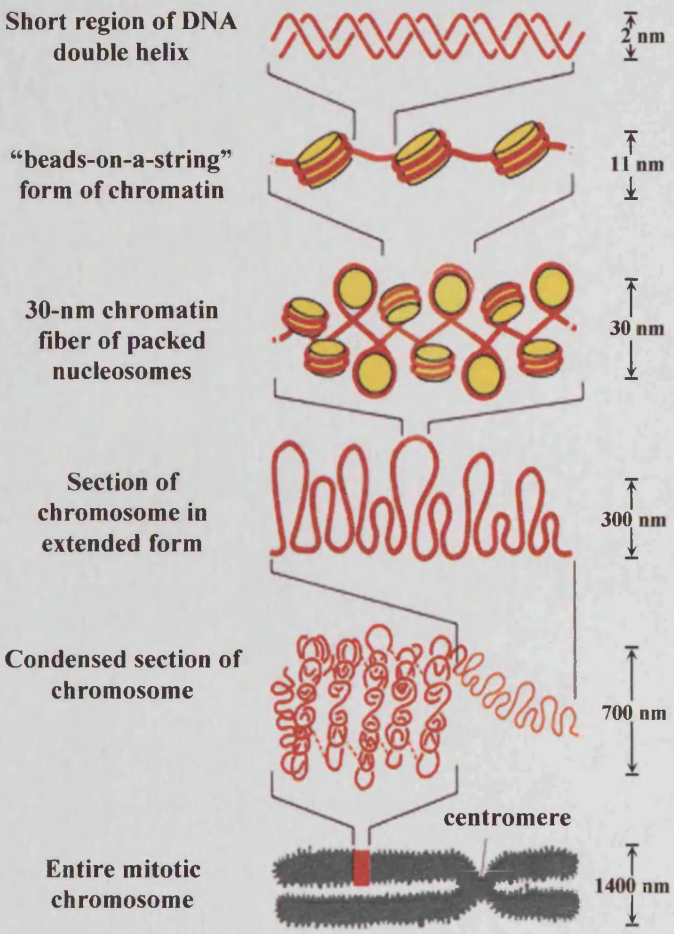

Figure 1.11 *Chromatin and DNA organisation.* The DNA is associated with histone octamers forming a 'beads on a string" conformation. This structure is further packaged by folding and coiling forming a condensed chromosome structure.

1.4.2 Implications of chromatin structure

Chromatin structure and nucleosome positioning influence the formation of CPDs and (6-4) PPs. Furthermore, the NER mechanism can also be affected by chromatin structure so the chromatin needs to be remodelled for NER to take place.

1.4.2.1 NER in a chromatin environment

The link between chromatin remodelling and NER was initially proposed 25 years ago (Smerdon and Lieberman, 1978, 1980). It was (showed by Wang et al., 1991) that the repair of UV damage is affected in nucleosomal DNA compared to naked DNA. However, many aspects of chromatin modulation during NER remain unresolved.

It has been shown that the damage recognition affinity and the damage excision by the NER machinery are less efficient in the nucleosomal DNA than in the

naked DNA (Constantinou et al., 2000). In addition, in the nucleosomal DNA, chromatin assembly and remodelling factors are implicated in the movement of the nucleosomes to permit repair by NER (Ataian and Krebs, 2006). After the DNA is repaired, chromatin assembly factor 1 (CAF1) is reloaded and the chromatin is reassembled to adopt its original structure (Gong et al., 2005). Hence, highly compacted chromatin needs to be remodelled for the detection and repair of DNA lesions. After the damage is repaired, the nucleosomes are reassembled and the highly compacted chromatin is restored.

This process is explained by a model called access repair restore (ARR) consisting of the unfolding and refolding of chromatin during NER (Gong et al., 2005; Green and Almouzni, 2002; Moggs and Almouzni, 1999; Smerdon and Conconi, 1999; Thoma, 1999). This model is discussed and explained further in Chapter V (page 110).

The rate of repair by NER is heterogeneous in transcriptionally inactive regions and in the NTS of transcriptionally active genes. This is in part due to faster repair in the linker DNA region compared to the core nucleosomal DNA. In addition, the repair rate is slightly faster towards the 5' end of the nucleosome region. This pattern of repair has been observed at various genes in budding yeast such as *MET16, URA3, MET17* and *GAL1-10* (Allinen, 2002; Ferreiro et al., 2004; Powell et al., 2003; Tijsterman et al., 1999; Wellinger and Thoma, 1997). However, the differences in repair efficiency between the linker and the protected regions are weak. Moreover, this pattern have not been observed in human chromatin (Jensen and Smerdon, 1990).

The chromatin structure at the TS of transcriptionally active region is more relaxed since chromatin remodelling has already occurred during transcription. Therefore, the NER efficiency appears to be homogeneous throughout this region.

1.4.2.2 Chromatin remodelling and DNA-mediated processes

Chromatin structure acts as a barrier to metabolic processes such as transcription, replication and repair (Widom, 1998; Workman and Kingston, 1998). Highly compacted DNA can inhibit the access of proteins that participate in such processes (Luger et al., 1997; Moggs and Almouzni, 1999). On the contrary, euchromatin adopts a more relaxed form and the DNA is more accessible to proteins and enzymes.

Cells have evolved mechanisms to remodel the chromatin. Chromatin is a flexible and dynamic structure that can be modified and this can also influence the position of the nucleosomes facilitating DNA metabolism. The dynamics of the chromatin are modulated by several mechanisms. One of them is addition of post-translational modifications such as acetylation, phosphorylation, deacetylation and methylation of the histone tails. The other one is the ATP-dependent chromatin remodelling (Kimura et al., 2002; Saha et al., 2006). Most of the time, post-translational modifications of the histone tails are recognised by ATP-dependent chromatin remodellers that change the conformation of the chromatin. Chromatin modifications can be local, affecting a specific locus or can be global, affecting the overall chromatin structure (Becker and Horz, 2002; Kunkel and Erie, 2005; Peterson and Cote, 2004).

Post-translational modifications of histone tails can change the charges of them, affecting the interaction between histones, with other proteins and with the DNA (Karow et al., 2000). The best characterised modification is the acetylation and the deacetylation of histone tails (Kouzarides, 2007). It has been shown that acetylation and deacetylation regulate some metabolic functions such as replication, transcription and DNA repair (Altaf et al., 2007; Verger and Crossley, 2004). For example, the acetylation state of histone tails is associated with transcriptionally active regions and the deacetylation state with repressive or silenced regions (Fukuda et al., 2006)

1.4.3 Histone acetylation and deacetylation

Histones are acetylated by histone modifiers enzymes called histone acetyltransferases (HATs) and deacetylated by histone modifiers enzymes called histone deacetyltransferases (HDACs). HDACs can remove the acetyl group from lysine residues. Figure 1.12 shows the acetylation and the deacetylation reaction of the histone octamer.

The acetylation reaction is reversible and consisted in the transfer of acetyl groups from acetyl-CoA to the ε-amino group of specific lysine residues at the histone tails. However, it has been recently shown that covalent modifications also occurred at specific amino acids of the histone globular domain and these modifications are involved in chromatin remodelling and in regulation of biological processes such as the DNA damage response and transcriptional silencing (Cairns, 2005; Haldar and Kamakaka, 2008; Masumoto et al., 2005; Xu et al., 2007).

The addition of acetyl groups to histone tails can affect chromatin structure at two levels. Firstly, histone charges are neutralised, thus inter- and intranucleosomal interactions become weaker facilitating the accessibility to the nucleosomal DNA (Annunziato and Hansen, 2000; Kouzarides, 2000). Secondly, acetylation can be recognized by transcription regulators or ATP-dependent remodellers.

Acetylation and deacetylation are more frequent on histone H3 and H4. Furthermore, each core histone has specific acetylation sites. For example, in the case of histone H3 the acetylation sites are located at lysines 9, 14, 18 and 23 whilst histone H4 has acetylation sites at lysines 5, 8, 12 and 16 (Roth et al., 2001).

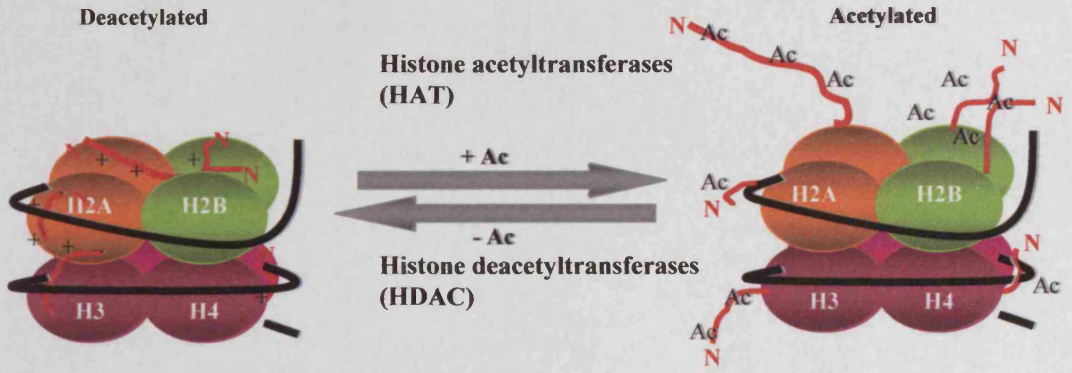

Figure 1.12 *Acetylation and deacetylation at histone terminal tails.* Histone acetylation by HATs required the addition of acetyl groups to N-terminal tails of core histones. The acetylation neutralise the positive charge at specific amino acids in the histone, thus the interaction of histones with the DNA and with other proteins is altered and the DNA is rendered more accessible to transcription and repair proteins. HDACs can remove the acetyl groups at specific amino acids and with positive charges the chromatin becomes repressed.

1.4.3.1 Histone acetylation and deacetylation in transcription regulation

Histone acetylation has been linked with the accessibility of DNA to transcription factors (Lee et al., 1993; Vettese-Dadey et al., 1996), whereas increase in deacetylation is correlated with the inhibition of transcription (Karow et al., 2000). Nevertheless, there are some examples where histone acetylation is related to silencing in *S. cerevisiae* (Braunstein et al., 1996; Kelly et al., 2000) and deacetylation with transcription (Nusinzon and Horvath, 2005, 2006; Wang et al., 2002).

Chromatin structure can influence the transcriptional level of a particular region; and acetylation/deacetylation contributes to the formation of chromatin structures. Sometimes, a particular HAT and HDAC form functional complexes helping to maintain appropriate equilibrium between acetylation and hypoacetylation

(Wade, 2001). For example, the Sir2p HDAC is implicated in the deacetylation of histone H3 and H4 at telomeres (primarily at H4K16) increasing the spreading of silencing by its activity. The Sir2p counterpart Sas2p HAT counteracts the deacetylation function of Sir2p, blocking the spread of silencing and establishing a gradient of acetylation along the chromosome. The balance between Sir2p and Sas2p can also regulate the deposition of histone variants and the acetylation stage at a particular position (Kimura et al., 2002; Shia et al., 2006; Suka et al., 2002).

Apart from regulating chromatin structure, histone acetylation and deacetylation are also implicated in cell cycle progression, DNA recombination, repair, and, in higher eukaryotes, in apoptosis and cancer (Roth et al., 2001).

1.4.4 Histone acetyltransferases (HATs)

Gcn5p was the first HAT identified (Brownell and Allis, 1996; Kuo et al., 1998). Since then, many more have been identified and they have been classified into families (Roth et al., 2001):

1) The GNAT (Gcn5p-related *N*-acetyltransferases) superfamily. These HATs contain highly conserved acetylation motifs and they are mainly involved in transcriptional initiation (Gcn5p, PCAF), elongation (Elp3p), histone deposition, telomeric silencing (Hat1p), and repair DNA lesions (Rtt109p) (Fillingham et al., 2008; Vetting et al., 2005).

2) The p300/CBP or PCAT family. These acetylate histones and other transcription factors, such as those acting as coactivators (Yuan and Giordano, 2002).

3) The MYST family. In this family MOZ-YBF2/SAS3-SAS2-TIP60 and ESA1 HATs are included. These enzymes contain a MYST domain which is the most conserved region and comprises an acetyl-CoA binding motif and a zinc finger domain (Avvakumov and Cote, 2007). Sas2p is involved in silencing at telomere in budding yeast. Both, Sir2p and Sas2p maintain the boundaries between silenced chromatin and euchromatin (Lafon et al., 2007; Suka et al., 2002). This is further explained below.

4) Basal transcription factor HATs. This group includes TAFII250 (a component of TFIID) and nuclear receptor cofactors such as ACTR and SRC1 (Grant and Berger, 1999; Roth et al., 2001).

HATs have been shown to recruit chromatin remodelling complexes or cause structural changes in gene activation and repair. For example, the modification of the

histone H4 terminal tail is important for nucleosome assembly (Berger, 2007; Downs et al., 2007; Lydall and Whitehall, 2005; Mitra et al., 2006).

HDACs are also involved in the recruitment of chromatin remodelling complexes and in changing the chromatin structure (Tong et al., 1998; Witt et al., 2009). Furthermore, it has been reported that HDACs inhibit the recruitment of the repair machinery and reconstitute the positive charges of histones (Deckert and Struhl, 2002). The different classes of HDACs are described below.

1.4.5 Histone deacetylases (HDACs)

All HDACs are classified based on the similarities with *S. cereviciae* HDACs (Witt et al., 2009) and they can be divided into three classes:

Class I HDACs are homologs of Rpd3p HDACs and they can associate with Sin3p or N-CoR, which are necessary for targeting the chromatin and for enhancing their enzymatic activity.

Class II HDACs are similar to Hda1p HDAC and to Class I enzymes. Class I and Class II HDACs need zinc for the hydrolysis of acetyl groups which are released in the form of acetate groups.

Class III HDACs are named sirtuins and are similar to yeast silent information regulator 2 (Sir2p) HDACs family members. Human sirtuins are included in Class III and they require NAD^+ as a cofactor to carry out the deacetylation of the lysine residue. Sir2p, not only has deacetylase activity, but also ADP ribosiltransferase activity (Gregoire and Yang, 2005; Imai et al., 2000; Landry et al., 2000; Tanny and Moazed, 2001).

1.4.5.1 Sir2p histone deacetylase

Sir2p is a Class III Histone deacetyltransferase which deacetylates mainly lysine residues at H4K16 and H3K (9, 14). Sir2p is involved in several processes:

(1) The formation of the compact chromatin structure such as silenced chromatin at telomeres, mating type loci and ribosomal DNA (Bryk et al., 1997; Gottschling et al., 1990; Moazed et al., 2004; Rine and Herskowitz, 1987).

(2) Caloric Restriction (CR) and aging: Sir2p extends the cell lifespan the number of divisions a cell can undergo prior to death suppressing DNA instability. In *S. cerevisiae*, the Sir2p is activated by CR since there is an increase of NAD^+ in the cell (Borra et al., 2004; Cairns, 2005; Sandmeier et al., 2002; Sauve et al., 2001). Thus,

overall, the activity of Sir2p is regulated by the metabolism due to the requeriment of NAD^+ cofactor (Kaeberlein and Powers, 2007; Sandmeier et al., 2002).

Sir2p HDAC is part of two protein complexes in the cell. One complex is formed by Sir2p and Sir4p and the function is NAD^+-dependent (discussed in more detail in 1.5.3 section). In the second complex, the requirement for NAD^+ cofactor is weak and Sir2p is associated with Net1p (discussed further in section 1.5.1). Both complexes bind to nucleosomal DNA (Ghidelli et al., 2001).

Several homologs to budding yeast Sir2p have been identified. The closest is *S. pombe* Sir2p (spSir2p) which is capable of deacetylating H4K16 and H3K9 in an NAD^+-dependent fashion. The enzyme spSir2p is involved in silencing at telomeres, mating type and the inner centromeric repeats, whereas little effect has been observed in the outer centromeric repeats and ribosomal DNA (Freeman-Cook et al., 2005; Shankaranarayana et al., 2003).

The enzyme CobB from *Salmonella enterica* is also a Sir2p homologue and deacetylates the acetyl-Coa synthetase enzyme in an NAD^+-dependent manner to activate this enzyme which it is required for the acetate and propionate activation (Starai et al., 2002).

The ssSir2p is the Sir2p homologue of *Sulfolobus solfataricus* and like Sir2p, it has a NAD^+-dependent deacetylase and mono-ADP-ribosyltransferase activity. The ssSir2p enzyme deacetylates Alba protein, which is the major archaeal chromatin protein, and represses transcription (Bell et al., 2002).

There are five proteins belonging to the Sir2p family in *Drosophila*. The closest homologue to Sir2p is dSir2p which is an NAD^+ -dependent histone deacetylase and is required for the formation of heterochromatin and silencing. This enzyme is located in heterochromatic regions (Newman et al., 2002; Rosenberg and Parkhurst, 2002); however, it is not required for position effect variegation (PEV) at telomeres (Rosenberg and Parkhurst, 2002). The expression of dSir2p is regulated during development (Newman et al., 2002).

There are seven genes in the mammalian Sir2p gene family. The best characterised is the human orthologous Sirt1p which is an NAD^+-dependent histone deacetyltransferase and it is located in the nucleus. One of the roles of Sirt1p is to inactivate p53 by hypoacetylation, preventing it activating genes involve in cell cycle arrest, apoptosis and senescence (Sandmeier et al., 2002). The other proteins are Sirt2p which deacetylate α-tubulin, Sirt3p histone deacetylase which it is located in

the mitochondria, Sirt4p, Sirt5p, Sirt6p and finally Sirt7p (Blander and Guarente, 2004; Vaquero, 2009).

In *S. cerevisiae*, four homologues to Sir2p have been identified. These are the Homologues of Sir Two (HST), (Hst1p-4p). It has been shown that Hst1p is involved in transcriptional silencing at HMR. Whereas, Hst3p and Hst4p are involved in telomeric silencing (Brachmann et al., 1995) and Hst2p in enhancing silencing at rDNA, however, Hst2p disrupt the Telomere Position effect (TPE) (Perrod et al., 2001).

Overall, the NAD^+ dependent histone deacetylase activity of Sir2p homologues enzymes is evolutionary conserved in eubacteria, archaea and humans. Furthermore, all eukaryotes studied so far have multiple homologues of Sir2p (Mitchell, 2000).

The mechanism of NAD^+ dependent deacetylation reaction

As mentioned before, Sir2p is a Class III histone deacetyltransferase with two main functions, deacetylation and ADP ribosylation (Landry et al., 2000). The deacetylation reaction by Sir2p is believed to be the principal mechanism to convert active chromatin to silent chromatin (Braunstein et al., 1993; Imai et al., 2000; Parsons et al., 2003).

The reaction is stoichiometric (it requires one NAD^+ molecule for each acetyl lysine) and consists of three steps, two reversible and one irreversible (Landry et al., 2000). The products obtained from Sir2p-mediated deacetylation are deacetylated peptide, 0-acetyl ADP ribose (AADPR) and nicotinamide (NAM) (figure 1.13). Sir2p has also ADP-ribosyltransferase activity and it is coupled with deacetylation, acting on the deacetylated peptide. Thus, ADP-ribosyltransferase, transfers the acetyl group to the NAD^+ breakdown product during deacetylation reaction forming 0-acetyl-ADP-ribose (Sauve et al., 2001; Tanny and Moazed, 2001). In the reaction, nicotinamide is cleaved first and after that, the acetyl group is transferred from acetylated peptide to the ADP-ribose (Borra et al., 2004). NAM is a product of the deacetylation and is involved in the inhibition of the Sir2p activity. So, NAM regulates Sir2p activity by switching from deacetylation to base exchange (Sauve et al., 2001).

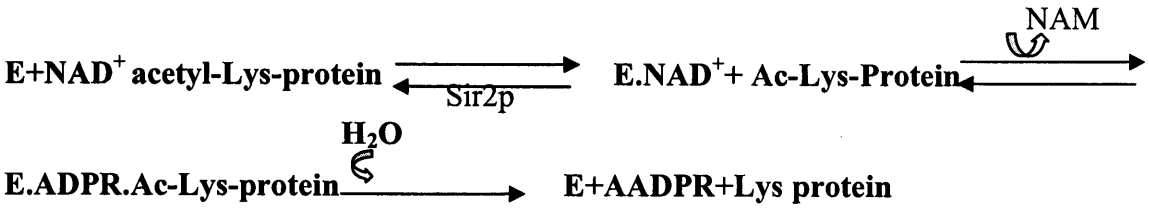

Figure 1.13 *Sir2p catalytic reaction in S. cerevisiae.* In the first reaction, the enzyme (E) binds to NAD^+, then, in the presence of acetylated protein, NAD^+ is processed forming nicotinamide (NAM) which is release together with ADP-ribose. In the last reaction the enzyme transfers the acetyl group from the acetylated substrate to ADP-ribose, forming O-acetyl-ADP ribose and deacetylated substrate.

1.5 Heterochromatin in the chromosome

Heterochromatin is highly condensed chromatin and is associated with a transcriptionally repressed state. In budding yeast, heterochromatin akin to that in mammalian cells is not found, however, the repressive chromatin is called silenced chromatin and the structure is similar to heterochromatin. There are two types of heterochromatin:

Facultative heterochromatin; generated by the repression of sequences rich in genes. The facultative heterochromatin can be remodelled to confer an open chromatin structure.

Constitutive heterochromatin is condensed in all somatic cells and is formed in regions of DNA poor in genes and repetitive sequences. The genes which are positioned nearby can be repressed epigenetically and can lead to transcriptional silencing indirectly. This silencing phenomenon is known as PEV. In *S. cerevisiae*, constitutive heterochromatin is mainly located at the mating type loci (*HML* and *HMR*), telomeres and rDNA (Moazed et al., 2004).

1.5.1 The structure of ribosomal chromatin

In budding yeast, ribosomal genes are located on chromosome XII, organised in clusters of 100-200 tandem repeats and separated by 5S genes and origins of replication (Nomura, 2001; Planta and Raue, 1988; Warner, 1989). In each cell, there are two types of rDNA at the nucleolus. One type is transcriptionally active and the other type is transcriptionally inactive or silenced (Grummt and Pikaard, 2003). The active ribosomal genes are transcribed at high levels having the maximal density of RNA polymerase I (Pol I) since each cell has to produce millions of new ribosomes for each generation (Moss, 2004). The transcription of ribosomal DNA generates 35S rRNA precursors which it is processed into 28S, 18S and 5.8S ribosomal RNA.

Afterwards, the ribosomal RNA is packaged with proteins forming the large subunit of the ribosomes (Planta and Raue, 1988).

In contrast to higher eukaryotes, in *S. cerevisiae* all rRNA genes have the same probability of being silenced. Furthermore, the silenced and active copies are randomly distributed and the number of active genes can be regulated by the cellular growth rate (Santoro, 2005). The mitotic silencing of the transcriptionally inactive copies occurs from prophase to metaphase. As in the telomeres and mating type loci, the silencing requires Sir2p, however, no other Sir proteins are involved (Yang and Seto, 2003).

In the rDNA, Sir2p binds to Net1p and not to Rap1p as at telomeres. Net1p associates with rDNA and recruits Sir2p to the nucleolus. However, Sir2p-dependent silencing is only carried out in the non transcribed spacer and in the 18S RNA coding region (Fritze et al., 1997). Therefore, there is another type of silencing at the rDNA that does not require Sir2p. Thus, there are two types of silencing when the transcription is mediated by RNA polymerase I (Sandmeier et al., 2002).

There are several lines of evidence suggesting that chromatin structure influences the expression of the rDNA regulating silencing and gene expression since the rDNA the chromatin can adopt two main conformations. The inactive chromatin structure is formed with arrays of nucleosomes and the active chromatin has an open conformation with no nucleosomes. In addition, it has been shown that *S. cerevisiae* cells can modify their chromatin structure rapidly when the rDNA is transcriptionally switched from on to off or inversely (Dammann et al., 1993). Recently, it has been reported that non-nucleosomal DNA is repaired faster than the nucleosomal DNA due to the open chromatin structure (Tremblay et al., 2008).

1.5.2 Structure of the mating type loci chromatin

HMR and *HML* are located in the right and left ends of the chromosome III. They are trancriptionally silenced and responsible for the mating type switch (Haber, 1998). The HM loci are flanked by silencers named E and I. For *HMR*, there are *HMR*-E and *HMR*-I silencers. For the *HML* locus, there are *HML*-E and *HML*-I silencers. These silencers contain binding sites for Origin Recognition Complex (ORC), Rap1p, and Abf1p which are involved in the recruitment of the SIR complex (Sir1p, Sir2p, Sir3p and Sir4p) to the DNA (Loo et al., 1995; Lustig, 1998).

The consensus sequence of Abf1p, Rap1p or ORC differs between silencers; therefore, the proteins have distinct affinity at each binding site. For example, the effect of silencing is stronger at *HMR*-E than at *HML*-E which is stronger than *HML*-I (Boscheron et al., 1996; Buchman et al., 1988; Shei and Broach, 1995). Silencer I is also involved in insulating the silenced chromatin from the active chromatin (Bi et al., 1999) however, the HMR-I silencers only operate as assistant to silence HMR locus (Rivier et al., 1999). There are also protosilencers for any silencer protein which can enforce the silencing effect (Boscheron et al., 1996).

The chromatin structure is also different at both sides of the silencers, the nucleosomes are stably located near the Abf1p where the silencing is stronger but not at the ORC where the silencing effect is weaker (Bi et al., 1999; Shei and Broach, 1995; Veron et al., 2006). All the proteins implicated in silencing at the mating type loci can also modulate the chromatin structure. However, the Abf1p binding site mutation does not alter nucleosome organisation so does not alter the chromatin structure significantly (Yu et al., 2009).

The current model of mating type silencing is as follows; Rap1p recruit Sir3p and Sir4p to the chromatin, however, Sir4p can also be recruited by Sir1p which can bind to the DNA (Buck and Shore, 1995; Cockell et al., 1995; Moretti et al., 1994; Triolo and Sternglanz, 1996). Not all the Sir proteins have the same degree of silencing; for example, deletion of the *SIR2, SIR3*, or *SIR4* genes completely eliminates silencing. However, deletion of *SIR1* has a partial effect on silencing. Furthermore, the function of Sir1p can be complemented by the overexpression of Esc2p which can also recruit and stabilize Sir proteins (Dhillon and Kamakaka, 2000). Sir2p HDAC, interact with Sir4p and deacetylate H3 and H4 histone tails. Sir3p and Sir4p have more affinity for hypoacetylate H3 and H4 tails, therefore, they can be recruited and the silenced chromatin is spread (Braunstein et al., 1993; Hecht et al., 1995; Liou et al., 2005; Rusche et al., 2003; Yang et al., 2008). It is believed that Sir1p, Sir2p, Sir3p and Sir4p are also implicated in the maintenance of transcriptional silencing through the cell cycle (Gardner and Fox, 2001; Pillus and Rine, 1989).

There are other proteins such as Sum1p, Mga2p and Spt23p which are also involved in the silencing at the HM loci. For instance, Sum1p mediated silencing needs Hst1p, a protein homologue to Sir2p, which forms a complex with Sum1p (Xie et al., 1999). Mga2p and Spt23p are transcription factors which can also regulate chromatin structure and influence transcription (Rusche et al., 2003).

1.5.3 Telomeres

Telomeres are specialized structures located at the end of eukaryotic chromosomes. They protect the chromosomes from end to end fusions and rearrangements. Thus, telomeres are important for the maintenance of genome integrity.

1.5.3.1 Telomere structure

The telomere sequence and organisation is highly conserved. The G-rich DNA is orientated 5' → 3' towards the end of the chromosome forming a 3' overhang. In *S. cerevisiae* the telomere are composed of repeat arrays of $G_{2-3}(TG)_{1-6}$ with a length ranging from 200 to 300 bp (Shampay et al., 1984). In humans, telomeres are much longer in length (2 to 20 Kb) and are composed of 5'TTAGGG3' arrays.

1.5.3.2 DNA structure of the subtelomeric region

The *S. cerevisiae* subtelomeric region is one of the best characterised. They comprise ~25 kb and contain two elements: The Y' element and the conserved core X element.

The Y' elements are not found at all chromosome ends, however, up to four of them can be found in a single subtelomeric region. They are organised in tandem arrays and separated by short regions of telomeric repeats $G_{2-3}(TG)_{1-6}$.

The other major component of the subtelomeric region is the Core X element. This element is found at all chromosome ends. It is 473 bp in length and is found proximal to the Y' elements. The Core X element has binding sites for the yeast origin recognition complex (ORC) and the Abf1 transcription factor. Therefore, this element could have functional roles at telomeres, probably facilitating the silencing at chromosome ends (Pryde and Louis, 1999). Figure 1.14 illustrates the structure of yeast telomeric and subtelomeric regions.

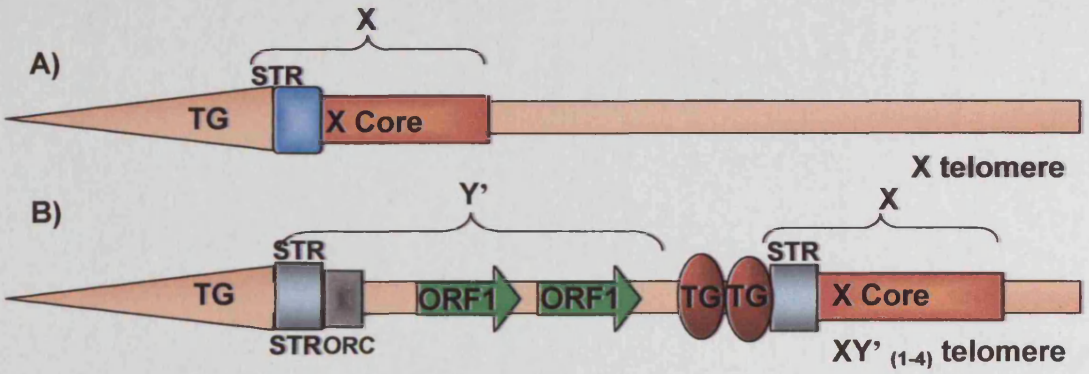

Figure 1.14 *Examples of some telomeric structures in S. cerevisiae*. In budding yeast, subtelomeres contained X (a) or X and Y' (b) elements. Protosilencers involved in the induction of the repression as well as anti-silencing regions are found in these elements. TG are the telomeric repeats $TG_{1\text{-}6}$.

1.5.3.3 Silencing at telomeres

Silenced chromatin at telomeres is formed when Rap1p, with the help of yku80p and yku70p, recruits the SIR complex. This protein complex consists of an enzymatic component (Sir2p) and a structural component (Sir3p and Sir4p). Sir3p and Sir4p are recruited by Rap1p to the telomeres. The interaction between Rap1p-Sir3p and Rap1p-Sir4p are independent of each other and the loss of these interactions can abolish transcriptional silencing. Telomere silencing can spread due to the binding affinity of Sir3p and Sir4p to the hypoacetylated form of H3 and H4 N-terminal tails at lysine residues, mainly at H4K16. This site is deacetylated by Sir2p creating high affinity binding sites for structural proteins Sir3p and Sir4p (Perrod and Gasser, 2003). Therefore, the activity of Sir2p is extremely important for the creation of silenced chromatin structure at telomeres (Chen and Widom, 2005).

Telomere silencing can be propagated from the end of the chromosome towards the centromere, a phenomenon called telomere position effect (TPE). The silencing or TPE at chromosome ends can be measured by the insertion of a reporter gene such as *URA3* at the subtelomeres (Sandell and Zakian, 1992). In the silenced chromatin structure close to the telomere, the presence of RNA polymerase II, TFIIE and TFIIB at the promoters is reduced (Chen and Widom, 2005).

In truncated ends, as the distance from telomeric TG repeats increases, the TPE decreases. However, at native ends there are protosilencers in the subtelomere where the repression is greater. For example, the silencing is maximal at X-ACS region which is located at the Core X element. However, immediately internal to the

telomeric sequence and in Y' elements there is no repression (Pryde and Louis, 1999). Furthermore, the protein binding sites at subtelomeric region (mainly ORC but also Abf1p and Rap1p) are involved in the recruitment of the silencing complex.

The binding sites for Rap1p are approximately every 35 bp in the whole telomere, however, if Rap1p is removed TPE is alleviated (de Bruin et al., 2000). Chromatin in telomeres is more compacted when is not replicated facilitating the silencing (Sandell et al., 1994). Another factor that can impinge on transcriptional silencing is the temperature, at high temperature transcriptional silencing is enhanced and it is weakened by low temperature (Aylon and Kupiec, 2004).

Proteins involved in the SIR complex are very important for the telomeric silencing. For instance, there is an increase in silencing in *SIR3* mutants when the *SIR4* gene dose is increased but there is loss of telomeric silencing when *SIR4* and *YKU80* genes are mutated (Benbow and Dubois, 2008). Mutations at natural telomeres in *SIR2* and *SIR4* genes eliminate the silencing completely. Another protein involved in telomeric silencing is Hdf1p, also called Yku70p. It has been reported that its deletion reduces the silencing at native telomeres (Pryde and Louis, 1999).Figure 1.15 illustrates some proteins involved in telomeric silencing

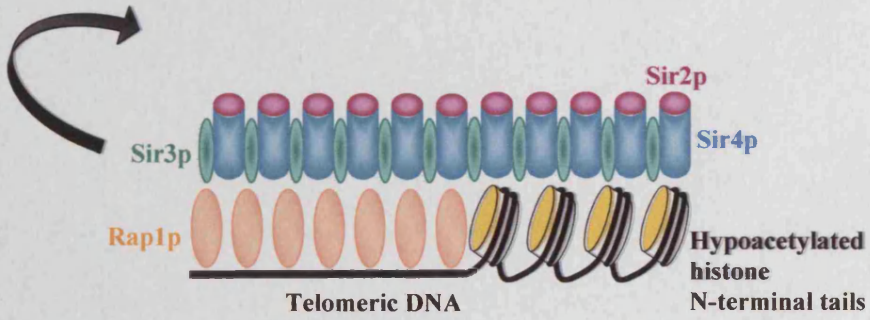

Figure 1.15 *Silencing at telomeres*. Rap1p binds to the telomere and recruits Sir3p and Sir4p which can interact with each other. The telomere folds back and silencing is propagated throughout the subtelomeric region towards the centromere.

1.7 Aims of the project

The aim of my project was to study how chromatin structure and silencing at chromosome ends can affect NER efficiency. To eliminate any variation due to DNA sequence, yeast strains where the *URA3* gene was moved to the subtelomeric region at different chromosome ends were employed. The *URA3* gene was inserted where the promoter is approximately 1.75 Kb centromere proximal to the $TG_{1\text{-}3}$ telomeric sequence and 1 Kb centromere proximal to the Core X-ACS. The *URA3* was inserted

at the subtelomere of the IIIR chromosome end and at the subtelomere of the XIL chromosomes end in a different strain.

In both strains *URA3* was inserted at the same position in the subtelomere. However, the difference between these two locations is the silencing level. When *URA3* is inserted at the XIL chromosome end, the silencing is higher than at the IIIR chromosome end (Pryde and Louis, 1999).

To investigate whether the disruption of silencing has a different effect in both strains, the *SIR2* gene was deleted and the chromatin structure together with NER efficiency were studied.

All the studies were carried out by examining events in the coding region of *URA3*. Figure 1.16 shows the different strains utilized in this thesis. The insertions of the *URA3* gene at the subtelomeres were performed previously (Pryde and Louis, 1999).

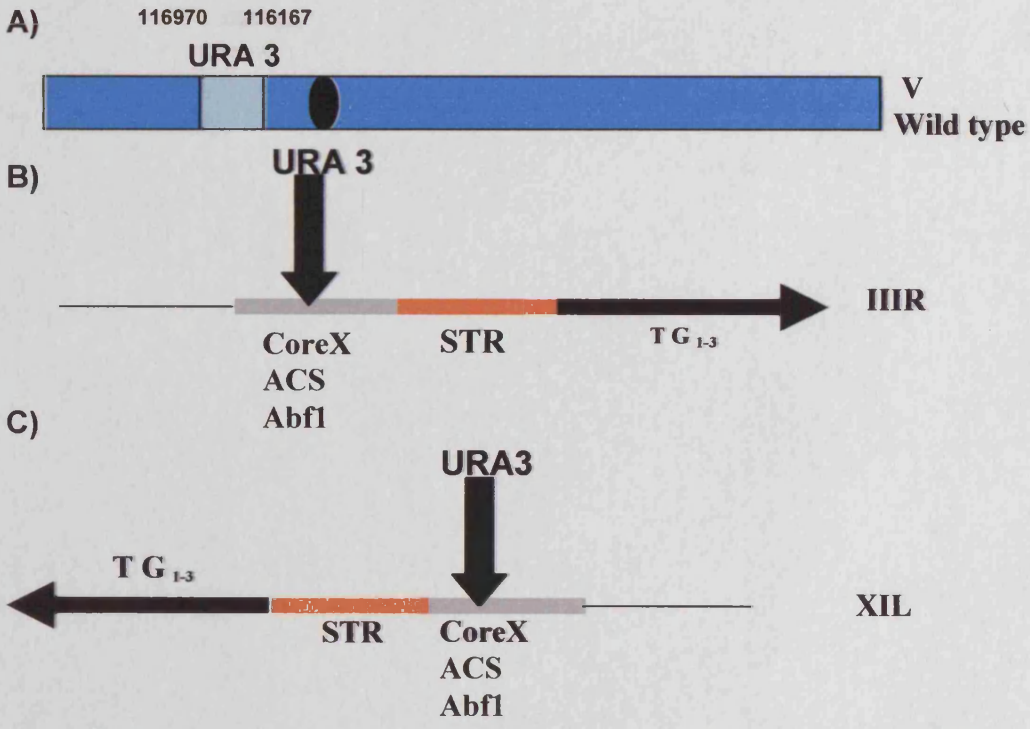

Figure 1.16 *Structure of the chromosome ends with URA3 insertion.* For this work three strains were employed. The wild type strain where *URA3* gene is located at its natural location (chromosome V), a strain where *URA3* is located at the IIIR chromosome end and a strain where *URA3* was inserted at the XIL chromosome end. STR = several subtelomeric repeats. In Chapter III (page 68) the strain where *URA3* is inserted in the IIIR was termend non-repressive end (NRE) and the strainwhere *URA3* is inserted in the XIL was termed the repressive end (RE).

Chapter II

MATERIALS AND METHODS

In this chapter, the general materials and methods used for this research are outlined. In each result chapter, the materials and methods for any specific study will be described.

All the solutions used are shown in Appendix I (page 138).

2.1 Yeast strains

The genotypes of the *S. cerevisiae* strains used in this study were as follows:

FEP 178 *ura3-52Δ* (MAT a, *ura3-52, can1-1, ade2Δ, leu2*Δ, *URA3 at CHRIII-R*)

FEP 100-10 *ura3-52Δ* (MAT a, *ura3-52, can1-1, ade2Δ, leu2*Δ, *URA3 at CHRXI-L*)

FEP 100-10 (MAT a, *ura3-52::KanMX can1-1, ade2Δ, leu2Δ, URA3 at CHRXI-L*)

FEP 178 (MAT a, *ura3-52::KanMX can1-1, ade2Δ, leu2Δ URA3 at CHRIII-R*)

FEP178*sir2** (same as FEP178, except *sir2::LEU2*)

FEP100-10*sir2** (same as FEP100-10, except *sir2::LEU2*)

The FEP178 and FEP100-10 strains were kindly provided by Professor Edward J. Louis (Institute of Genetics, The University of Nottingham, Queen's Medical Centre, Nottingham). In these strains, *URA3* was inserted into the subtelomeric region of chromosome end IIIR and chromosome end XIL. The promoter is found approximately 1.75 kb centromere-proximal to the consensus $TG_{1\text{-}3}$ telomere sequence and 1 kb centromere proximal to the Core X-ACS (Pryde and Louis, 1999). In the FEP178*ura3-52Δ* and FEP100-10*ura3-52Δ* strains, the genomic *ura3-52* was replaced by *KanMX* and in the FEP178sir2*and FEP100-10sir2* the *SIR2* gene was replaced by *LEU 2* (see Chapter III for details).

2.2 Storage and growth conditions

The strains were stored at -80°C in 1 ml of complete medium YC (1% yeast extract, 2% peptone, 2% glucose, 2% agar) containing 30% glycerol previously filtered once they reached exponential growth.

Before every experiment, a pre-culture was made from the stock by inoculating 25 ml of medium. Then, the culture was incubated at 28°C to stationary phase and subsequently stored at 4°C.

When the strains were grown in minimum media, the essential amino acids were added accordingly to the requirements of each strain. All the cultures were grown over night by shaking at 30°C. The amount of pre-culture used for inoculation was different for each strain due to different growth rates.

For the repair and mapping experiments large volumes of cultures were needed. Thus, an inoculate was taken from the pre-culture and grown in fresh media to a density of 2-4x10^7 cells/ml. All the repair and mapping experiment were in log phase and at a growth stage similar to that used to examine repair and nucleosome positions or modifications by our group (Ferreiro et al., 2004; Powell et al., 2003; Teng et al., 2002; Vetting et al., 2005).

2.3 Oligonucleotides

DNA oligonuleotides were synthesised by Eurofins MWG operon (Germany) and by Eurogentec (Belgium). The oligonucleotide sequences are shown in Appendix I **(page 143)**.

2.4 *URA3* expression and silencing measurement

The *URA3* gene product converts 5-fluoroorotic acid (5-FOA) into a toxic substance. Thus, cells that express *URA3* in the presence of 5-FOA cannot survive. Therefore, this chemical can be used as a negative selection of *URA3* expression.

Cells were grown in YPD overnight until stationary phase and then dilutions of these cultures with the same density were carried out. These dilutions were plated in minimum media lacking uracil and minimum media with uracil both containing 5-FOA. The experiment was repeated three times and at each time the same dilution was plated in triplicate. Petri dishes were incubated for 3-4 days at 30°C and then the colonies were counted. Steps for this technique are described more thoroughly below.

2.4.1 5-FOA plates

The plates for this analysis were prepared as follows:

1) 4% agar dissolved in 250 ml of water was autoclaved and kept at 65°C in a water bath (Bennett Scientific limited, UK).

2) A second solution was made with 0.1% 5-FOA, 0.7% YNB, 2% glucose, 0.37% CAA, adenine (0.4 mg/ml final concentration), 2 ml tryptophan and lysine (0.4 mg/ml final concentration). These components were mixed and dissolved in 250 ml of water. For the uracil plates, a final 0.2 mg/ml concentration of uracil was added. As a control, the same mixture was prepared, but without 5-FOA. This solution was filtered and kept in a water bath at 50°C.

3) The solution from step 2 was mixed with the 4% agar and Petri dishes were prepared with 10 ml of this mixture.

2.4.2 Growing conditions

The study of *URA3* expression was performed as follows:

1) The strains were grown over night in YPD to a density of $2x10^7$cells/ml.

2) Next morning, cells were diluted to 10^{-1}, 10^{-2}, 10^{-3}, 10^{-4} and 10^{-5}. For each dilution, 100 µl were plated on minimum media plates with uracil and minimum media without uracil in triplicates and in the presence of 5-FOA.

3) The cells were allowed to grow for 2-4 days at 30°C.

These experiments were carried out three times and each time the plates were grown in triplicate.

2.4.3 Analysis of the results

The expression of *URA3* was determined by measuring the fraction of cells that were able to grow on plates containing 5-Fluoroorotic acid (5-FOA) *versus* the colonies able to grow on plates without 5-FOA.

2.5 MNase accessibility at high resolution

In order to analyse the accessibility to the DNA in the chromatin, cells were grown to a density of $2x10^7$cells/ml. The chromatin and the DNA were extracted and treated with increasing concentrations of MNase (Roche Molecular Biochemicals) which preferentially cuts in the linker region (described below). The DNA was purified and digested with *Mse*I restriction endonuclease to select the fragment of interest. Afterwards, each strand was purified and labelled as described in the sections 2.8.3 and 2.8.4. The DNA fragments were resolved in a polyacrylamide gel as in 2.8.5 section. The procedure is illustrated in figure 2.1.

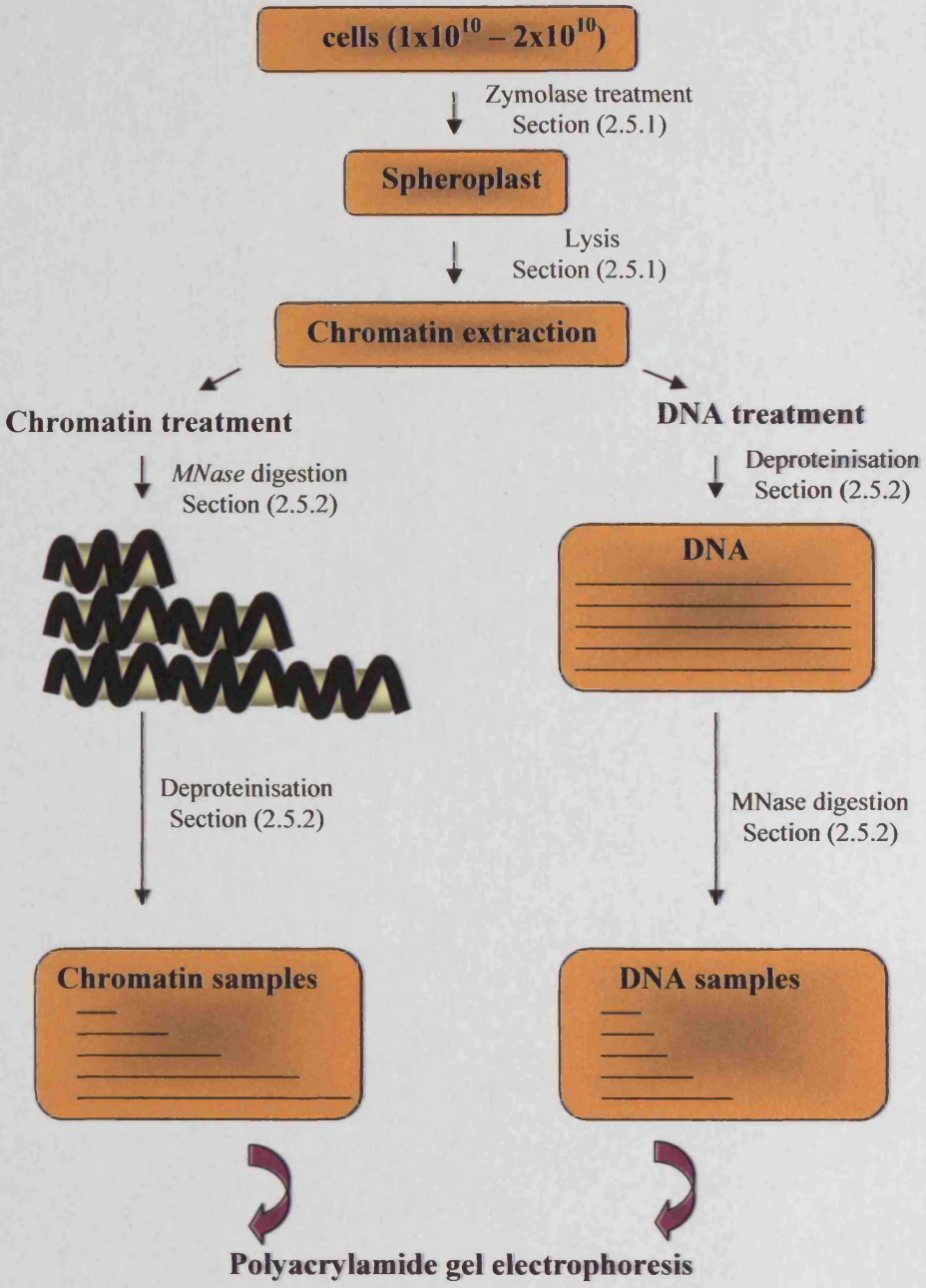

Figure 2.1 *Schematic representation of the mapping at high resolution.* The chromatin is extracted and treated with MNase and then is deproteinisation. To obtain the DNA samples, the chromatin is first deproteinizated and then treated with MNase.

2.5.1 Chromatin extraction

This was undertaken as follows:

1) Cells were grown to a density of $2x10^7$cells/ml over night, pelleted and washed with pre-chilled 1 M sorbitol. The pellets were dried and weighted.

2) The cells were digested with zymolase (section 2.7) and the spheroplast pellets obtained (section 2.7) were resuspended in 5 ml of lysis solution (1 M sorbitol, 5 mM

2-mercaptoethanol and 25 mg of zymolase per 1 g of cell pellet) and incubated at 30°C for 20 mins.

3) To extract nuclei, spheroplasts were collected by centrifugation at 3,000 rpm for 5 mins (Beckman Avanti J-25 centrifuge, JA-17), washed once with pre-chilled 1 M sorbitol and resuspended in 7 ml ficoll solution (18% w/v ficoll, 20 mM KH_2PO_4 pH 6.8, 1 mM $MgCl_2$, 0.25 mM EGTA and 0.25 mM EDTA) per 1 g of cell pellet until the cell clumps were dispersed. When the suspension was homogeneous, the spheroplasts were broken mechanically with a syringe.

4) The nuclei were separated from the rest of the cell organelles and debris by centrifugation at 17,000 rpm 4°C for 30 mins (Beckman Avanti J-25 centrifuge, JA-17). After centrifugation, the supernatant was discarded with a Pasteur pipette.

5) The nuclei were washed in digestion buffer (15 mM tris-HCl pH 7.4, 75 mM NaCl, 3 mM $MgCl_2$, and 1.5 mM $CaCl_2$ and 1 mM 2-mercaptoethanol) and step 4 was repeated.

2.5.2 Treatment with MNase and restriction enzyme

The chromatin extraction was followed by MNase digestion. This enzyme is an extracellular nuclease or S7 nuclease from *Staphylococcus aureus* and it is used to study chromatin structure because it cleavages in the inter-nucleosomal linker region.

1) The nuclear fraction was resuspended in 1.5 ml of digestion buffer and aliquoted (250 µl) into six 1.5 ml tubes. Four of then were treated with MNase (chromatin samples) and the other two were kept on ice for following deproteinisation and purification of naked DNA (DNA samples).

2) Each chromatin sample was digested with different amount of MNase (1 to 40 U/ml) and incubated at 37°C for 10 mins.

3) To avoid overdigestion of chromatin, immediately after the incubation period, the samples were kept on ice followed by the addition of 1% SDS, 5 mM EDTA and 3 mg of proteinase K. Subsequently, the samples were incubated for at least 2 hrs at 55°C in a water bath for deproteinisation to take place.

4) The deproteinized DNA was purified by adding 1 volume of phenol/chloroform/isoamyl alcohol (24:24:1). Aqueous and organic layers were mixed by vortexing and the mixture was centrifuged for 10 mins at 13,000 rpm (Eppendorf 5415D centrifuge, rotor F45-24-11). Afterwards, the aqueous layer was

transferred to a new tube and the step was repeated. Finally, chloroform/isoamyl alcohol (24:1) was used to remove any organic residues in the purified DNA.

5) For the precipitation of the DNA, 2.5 volume of pre-chilled ethanol was added to each tube and the samples were incubated at -20°C over night. Next morning, the DNA pellets were collected by centrifugation at 10,000 rpm for 20 mins (Eppendorf 5415D centrifuge, rotor F45-24-11) and resuspended in 360 µl 1xTE for the following re-precipitation with 40 µl of 3 M sodium acetate and 1 ml of cold ethanol.

6) Pellets were collected by centrifugation at 10,000 rpm for 10 mins and finally dissolved in 0.5 ml of 1xTE buffer.

7) To obtain naked DNA for treatment with MNase, the two samples from step 1 were deproteinized by adding 30 µl of 1xTE buffer, 3 mg of proteinase K and incubated at 55°C for 2 hrs in a water bath. Afterwards, the DNA was purified and precipitated as previously described above in this section.

8) Next, samples were resuspended in 250 µl digestion buffer and naked DNA was digested by the addition of MNase (1 to 40 U/ml). The digestion reaction was incubated at 37°C for 10 mins and the steps 4, 5, 6 were carried out again.

9) All the samples were digested with *Mse*I restriction endonuclease (section 2.8.1) to obtain the *URA3* fragment of interest.

10) Finally, the samples were resolved in a polyacrylamide gel as described in sections 2.8.3, 2.8.4 and 2.8.5.

2.5.3 Analysis of the gel

The sequencing gel was exposed overnight to a phosphorimage screen and then the screen was scanned using the phosphorimager (Typhoon, GE Healthcare life Science). In the resulting image, the bands at the top of the gel were considered as fragments not digested by MNase because the amount of MNase was not sufficient to digest all the fragments. Hypothetically, MNase cleaves only at the internucleosomal linker region of the chromatin.

2.6 UV irradiation and DNA repair analysis

The details are as follows:

1) Cells were grown over night to a density of 2-4x10^7cells/ml. These cells were collected by centrifugation (Beckman Avanti J-25 centrifuge, JA-10) at 5000 rpm for 5 mins.

2) Pellets were re-suspended and washed with pre-chilled PBS. If the cells clumped together, brief sonication was applied to disperse the cells and homogenise the sample. The concentration of cells was adjusted to 2x10^7cells/ml with chilled PBS in a final volume of 1200 ml.

3) Before the UV treatment, 200 ml were collected and kept on ice in the dark (untreated sample).

4) The cells were irradiated at a dose rate of 150 J/m^2 using VL-215G (Vilber Lourmat, France) UV lamp which was switched on 30 mins before used and calibrated with a UVX radiometer (UVP Inc., CA, USA).

5) Immediately after the cells were irradiated, 200 ml were taken (0 hrs repair time) and kept on ice in the dark.

6) The rest of the cells were centrifuged as above and re-suspended in pre-warmed YPD medium at 30°C. These cells were incubated at 30°C with agitation to enable DNA repair. Samples of 200 ml were taken for each repair point (1, 2, 3 and 4 hrs).

7) All samples were centrifuged after the repair times and re-suspended in a 20 ml final volume of 1xPBS containing 1% EDTA (Beckman Avanti J-25 centrifuge, JA-10).

2. 7 Extraction of yeast DNA

The details of the DNA extraction are as follows:

1) The cells in PBS and 1% EDTA were pelleted and resuspended in 5 ml of sorbitol-TE (Beckman Avanti J-25 centrifuge, JA-10).

2) To this cell suspension, a final concentration of 0.28 M 2-mercaptoethanol (Sigma-Aldrich Ltd, USA) and zymolase (1 mg/ml final concentration) (Immuno^{TM}, MP Biomedicals, U.S.A.) were added to each sample. Then, the samples were incubated in the dark at 4°C over night to allow digestion of the cell wall.

3) The spheroplasts generated were collected by centrifugation at 3,000 rpm for 5 mins (Beckman Avanti J-25 centrifuge, JA-17). Subsequently, the samples were washed with PBS and incubated with 5 ml of 1:1 (v/v) lysis buffer/1xPBS solution.

4) Proteinase K (Sigma-Aldrich Ltd, USA) was added to a final concentration of 0.5 mg/ml and the samples were incubated at 37°C for 1 h with a following incubation at 65°C for 1-2 hrs.

5) RNase was added to a final concentration of 0.4 mg/ml and incubated at 37°C for 1 h.

6) An equal volume of Phenol:Chloroform:isoamyl alcohol (Sigma-Aldrich Ltd, USA) at 24:24:1 in volume was added to each sample. The samples were mixed well and centrifuged for 10 mins at 10,000 rpm (Beckman Avanti J-25 centrifuge, JA-17).

7) This extraction was repeated and then a third extraction was carried out with Chloroform:isoamyl alcohol at 24:1 (Sigma-Aldrich Ltd, USA) to eliminate phenol residues.

8) The extracted DNA was precipitated with 2 volumes of 100% cold ethanol (stored at -20°C), mixing gently and the samples incubated over night at -20°C.

9) The samples were centrifuged for 20 mins at 10,000 rpm (centrifuge 5810R, rotor F-45-24-11). The pellets were allowed to air-dry and were resuspended in 0.5-1 ml of 1xTE.

10) Afterwards, a second precipitation was carried out by adding one volume of isopropanol stored at -20°C. The samples were incubated at room temperature for 20-30 mins and mixed occasionally by inverting the tubes. The pellets were air dried and were resuspended in 600-800 µl of TE buffer.

11) The quality of the DNA was analysed in a 1% non-denaturing agarose gel; good quality samples give a sharp bright band under the UV transilluminator.

12) The DNA samples were stored at -20°C or alternatively at 4°C if they were to be used immediately.

2. 8 CPD repair at the nucleotide level

The main steps of this procedure are illustrated below. Figure 2.2 described the treatment of the extracted DNA.

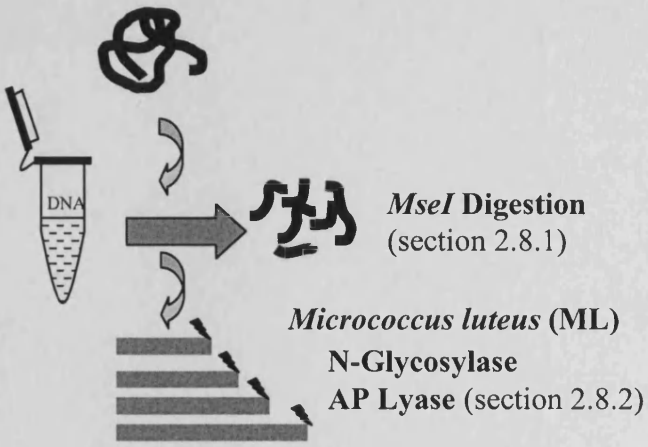

Figure 2.2 *DNA treatments.* The DNA was digested with *Mse*I restriction enzyme and then treated with crude extract of *M. luteus* (ML) (Teng et al., 1997) .

After the digestion with *M. luteus* (ML), purification of the non transcribed strand and transcribed strand where carried out as shown in figure 2.3. This step is explained in section 2.8.3.

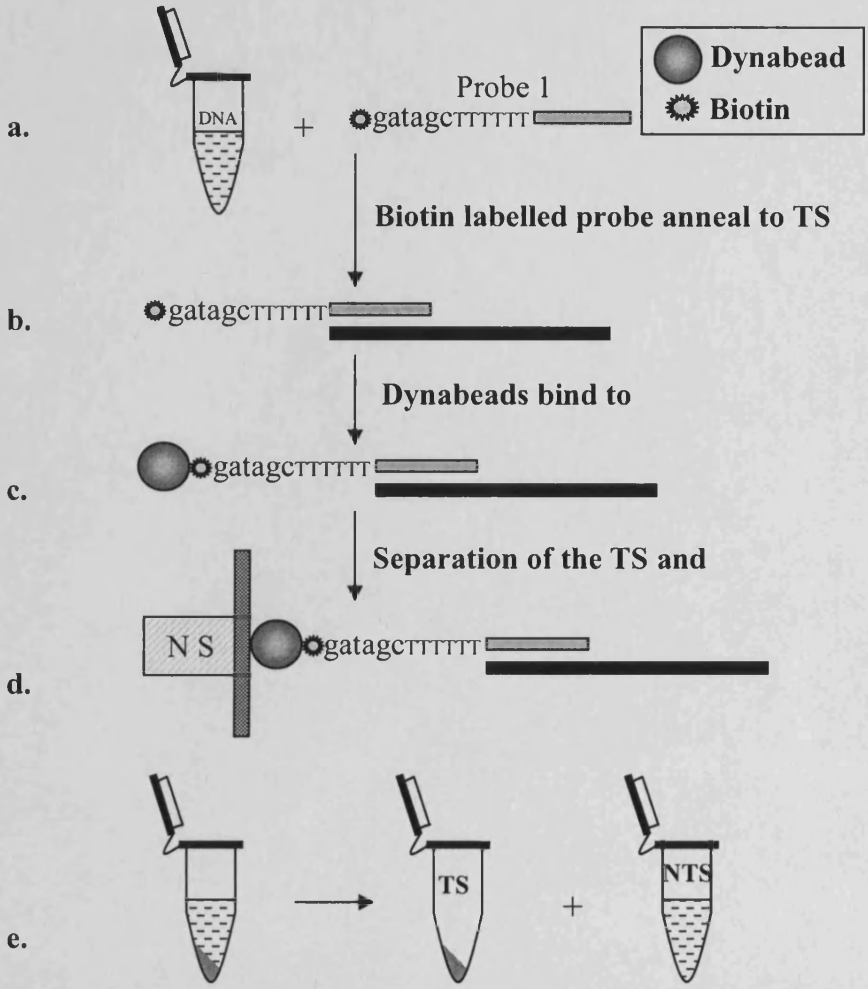

Figure 2.3 *Purifying the* URA3 *fragments.* **a.** Probe 1 is added to the restricted and ML treated DNA. **b.** Probes anneal to the complementary TS sequences. **c.** Dynabeads are added to bind the biotin at the 5' end of the probe. **d.** Dynabeads and the associated DNA fragments are immobilized on the tube wall. **e.** the supernatant is transferred to a fresh tube for NTS purification (Teng et al., 1997).

After purification of the two strand, end labelling was performed using sequenase enzyme and [α^{32}P]dATP as shown in figure 2.4 and described in section 2.8.4. Then, labelled fragments were loaded in a sequencing gel (section 2.8.5.).

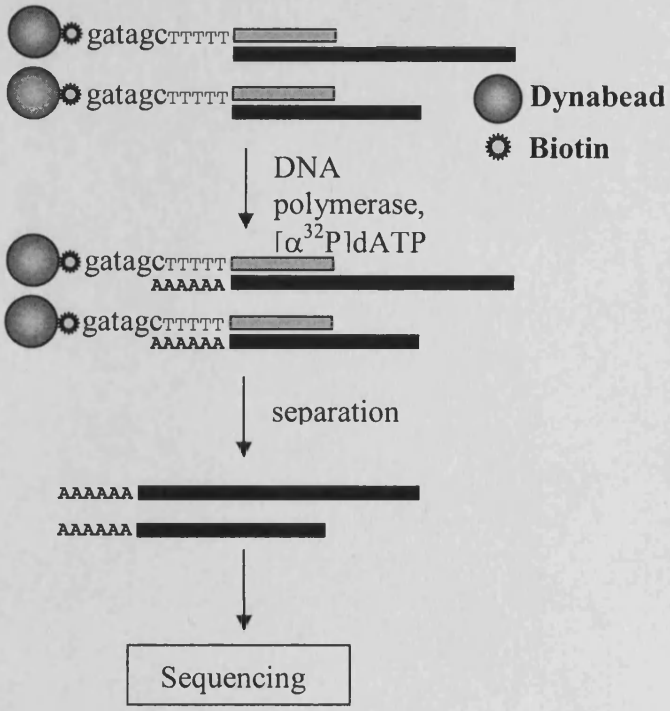

Figure 2.4 *End-labelling of URA3 fragments.* DNA polymerase adds 6 [α^{32}P]dAs at the 3' end of the purified *URA3* fragments, using the six dTs in the probe overhang as template. The labelled fragments are eluted from the probe with a formamide solution and separated from Dynabeads for sequencing gel electrophoresis using a magnetic particle collector (MPC) (Teng et al., 1997).

2.8.1 Digestion with *Mse*I restriction enzyme

In this thesis, the DNA repair at the *URA3* gene was examined. The genomic DNA was treated with *Mse*I restriction endonuclease which cuts at the position +221 bp and +861 bp of the *URA3* gene where +1 is the first base of the start codon; this generates a 640 bp fragment. The treatment of the genomic DNA with the restriction endonuclease was carried out as described at the manufacturer's guidelines (New England Biolabs, Inc). The procedure was as follows:

1) The following reagents (New England Biolabs, Inc) were mixed in a 1.5 ml tube in a final volume of 300 µl: 100 µl of genomic DNA (50-60 µg), 60 units of *Mse*I restriction endonuclease, buffer 4 (1x final concentration), BSA (1x final concentration)

2) The samples were incubated at 37°C for 3 hrs.

3) The digestion was resolved in 1% agarose gel at 80 V for 1 h (Bio-Rad, Wide Mini Sub Cell GT Cell with 7x10 cm tray). A good quality digestion result is seen as a smear under a trans-illuminator.

4) Phenol/chloroform extraction was used to remove the enzyme from the sample, followed by chloroform extraction (see section 2.5.2). Then, the aqueous layer which contains the DNA was transferred into another tube.

5) This DNA was precipitated with 1 volume of pre-chilled (-20°C) isopropanol and 1/10 volume of 3 M sodium acetate pH 5.3. The samples were mixed by inverting the tubes several times and kept at -20°C for at least 1 h.

6) The pellets were collected by centrifugation at 10,000 rpm for 20 mins (Eppendorf 5415D centrifuge, rotor F45-24-11) and the supernatant was removed by suction. The pellets were left to air dry and were re-suspended in 120 µl of 1xTE.

2.8.2 Incision of DNA at the sites of CPDs

Subsequently, the DNA from 2.8.1 was treated with a crude extract of *M. luteus* (ML) which contains a UV endonuclease that has cyclobutane pyrimidine dimer (CPyD)-DNA glycosylase and abasic lyase activity. Thus, it cuts where CPDs were generated. To each sample 10 µl of ML extract was added and these were incubated at 37°C for 1 h. After the ML treatment, phenol/chloroform extraction was used to eliminate ML and a final chloroform extraction was employed to remove phenol residues from the sample.

2.8.3 Purification of CPD-incised single stranded DNA fragments

1) A final concentration of 1 M NaCl was added to each 120 µl DNA sample since was the optimal concentration for the Dynabeads-biotin binding.

2) 2 µM biotinylated probe called AntoTSMseIb (1 µl) (appendix I) and complementary to the 3' end of the TS of the *URA3* fragment was added. The samples were incubated at 95°C for 5 mins to denature the DNA followed by 55°C for 15 mins. In this step, the probe anneals to the TS of the *URA3* fragment.

3) 10 µl of Dynabeads (Invitrogen) per sample were placed into a 0.2 ml tube. The Dynabeads were washed twice with 1×PBS 0.1% BSA, twice with 1×BW buffer and re-suspended in 1 volume of 1×BW buffer. After, 10 µl of dynabeads were added to each sample and those were incubated at room temperature for 15 mins with occasional mixing by pipetting.

4) The beads containing the TS strand were isolated with a MPC and the supernatant was transferred to a fresh tube for isolation of the NTS of the same *URA3* fragment.

5) 50 µl of 1×BW buffer was added to the beads and the samples were incubated for 5

mins at 55°C to remove non-specific binding. The supernatant was immediately removed and discarded.

6) The beads were washed twice with water and re-suspended in 6 µl of water.

7) For the *URA3* NTS isolation, steps 2-6 were repeated but using a probe called AntoNTSMselb (appendix I) complementary to the 3' end of the NTS.

2.8.4 End labelling the DNA fragments with α-[^{32}P] dATP

After strand purification, the pool of fragments from TS and NTS were labelled with α-[^{32}P] dATP followed by band identification. The procedure was as follows:

1) 1µl of Sequenase buffer, 0.7 µl of 0.1 M DDT, 1 µl (5 µCi) of α-[^{32}P] dATP (6000 Ci/mmol. GE healthcare) and 2 µl of Sequenase (diluted 1:30 in dilution buffer) were added to the beads (USB Corporation, USA).

2) The solution was incubated at room temperature for 10 mins to enable labeling, the beads were collected using the MPC and washed twice with TE buffer.

3) The labelled DNA fragments were eluted from the beads by adding 3 µl of formamide loading buffer (95% formamide, 20 mM EDTA, 0.05% Bromophenol blue) and incubating at room temperature for 5 min. The samples were loaded onto the gel and resolved by electrophoresis on a 6% denaturing polyacrylamide gel as described below.

2.8.5 Denaturing polyacrylamide gel electrophoresis

The single stranded DNA fragments were resolved in a 0.4 mm thick denaturing polyacrylamide gel. The steps were as follows:

1) The mould for the gel was constructed with two glass plates measuring 20 cm × 60 cm and 20 cm × 62 cm. The plates were washed thoroughly with detergent and water and then washed using absolute ethanol. Dimethyldichlorosilane solution (2% in 1, 1, 1-trichloroethane, BDH Chemicals) was applied to the inner surface of the shorter plate so the gel sticks only to one plate. The plates were separated at the edges with 0.4 mm spacers and sealed with vinyl insulation tape.

2) 80 ml of 6% acrylamide EASI gel (acrylamide: bis-acrylamide = 19:1, 7 M urea, 1×TBE, Scott-Lab) was mixed with 650 µl 10% ammonium persulfate (Sigma-Aldrich Ltd, USA) and 35 µl of TEMED.

3) An electrophoresis system (Gibco Model SA) and a power pack (Pharmacia EPS 3500) were used to run the sequencing gel. First, 3 µl of loading buffer was loaded in

each well and the gel was pre-run for 30 mins in 1xTE at an output of 70 W to achieve the optimum temperature of 50°C for gel electrophoresis.

4) 2.5 µl of loading buffer was added to the DNA samples and the samples were incubated for 5 mins at room temperature to enable the separation of the labeled strand from the dynabeads. After, they were loaded onto the gel; electrophoresis was carried out for 2.5 hrs at 70 W.

5) Next, the glass plates were separated and a piece of Whatman filter paper was placed on top of the gel. The gel was dried using a gel dryer (BioRad) for 2 hrs at 80°C under vacuum.

6) Once dried, the gel was exposed to a phosphorimager screen and left over night. The screen was then scanned with a phosphorimager scanner (Typhoon 9410, Molecular Dynamics, Inc.) to obtain the resulting image which was then analysed as below.

2.8.6 Quantification and repair analysis

The analysis of the results was undertaken using ImageQuant software version 5.0 (Molecular Dynamics, Inc.):

1) The DNA damage at a specific site was measured as the intensity of each band which reflects the frequency of collective pixel values. To eliminate loading errors, an adjustment was made and the total signal from individual lanes was multiplied by a factor to give equal values. Then, the signal of each band was accordingly multiplied.

2) The non-specific background was measured using the signal from non-irradiated DNA or the untreated sample. The damage remaining after particular repair times was presented as a percentage with respect to the initial damage (0 lane, 100% damage).

$$\% \text{ Damage} = \frac{[\text{Damage}]_t}{[\text{Damage}]_0} \times 100$$

(Where t = a given repair time, 0 = the time point immediately after UV)

3) Data points representing the percentage of damage at defined sites at each repair time were applied to an exponential curve.

4) Finally the time point where 50% of the damage is repaired ($T_{50\%}$ value) was selected to compare repair rates of individual CPDs.

2.9 Chromatin immunoprecipitation (ChIP)

Cell samples were grown and treated with formaldehyde to generate protein-protein and protein-DNA cross-links. The cross linked chromatin was sonicated to generate fragment sizes of ~ 400 bp. Afterwards, the chromatin was deproteinized, the DNA was purified and the sonicated DNA fragments were checked in a non-denaturing agarose gel electrophoresis. Subsequently, the DNA was immunoprecipitated with specific antibodies and then heated to allow a reversal of formaldehyde cross-link. This step allows the quantification of precipitated DNA by quantitative PCR.

2.9.1 Preparation of chromatin and cross-linking

1) The cells were grown to 2 x10^7cells/ml density over night and treated with UV as previously described in section 2.6. The repair points taken were U (untreated), 30 and 60 mins after UV treatment. For each repair point 50 ml of culture were taken. Then, 3 ml of formaldehyde at 37% were added to the 50 ml culture to allow protein-DNA and protein-protein cross link. The culture was incubated at room temperature for 20 mins by shaking slowly on a platform. Immediately after the incubation, 2.5 M glycine, which reacts with the formaldehyde, was added to stop the cross linking and the culture were further incubated with shaking for 5 mins at room temperature.

2) The cells were collected by centrifugation at 3,000 rpm for 5 mins (Beckman Avanti J-25 centrifuge, JA-10) and resuspended in pre-chilled 1xPBS. The cells in 1xPBS were centrifugated again at 3,000 rpm for 5 mins (Beckman Avanti J-25 centrifuge, JA-10) and the supernatant was discaterted. Afterwards, the pellets were resuspended in ice cold FA/SDS (+ PMSF) solution which contains 50 mM HEPES KOH pH7.5, 150 mM NaCl, 1 mM EDTA, triton X-100 and PMSF. Subsequently, the cells were transferred to a 2 ml tube and resuspended in 500 µl of cold FA/SDS (+ PMSF).

3) The cell wall was lysed mechanically by adding 0.5 ml glass bead (Sigma-Aldrich Ltd, USA) to each 2 ml tube and vortexing for 10 mins at 4°C (it is important not to use 1.5 ml microcentrifuge tubes with conical bottoms because they could restrict the beads movement resulting in an unequal breakage of the cells along the tube). Then, the chromatin was purified by puncturing a hole in the bottom of each tube and sitting them on the top of the 15 ml tube. The lysate was collected into the 15 ml tube by centrifugation at 2,000 rpm for 2 mins (Eppendorf centrifuge 5810R, rotor A-4-81).

The samples with the beads were washed once with 500 µl cold FA/SDS (+ PMSF) and similarly centrifuged to collect the rest of the lysate.

4) To remove soluble proteins which are not cross-linked to the DNA and to reduce background in the immunoprecipitation step, the lysate was transferred to 2 ml tubes and centrifuge at 13,000 rpm for 20 mins at 4°C (Beckman microfuge 22R, rotor F241.5P). After centrifugation, the supernatant was removed by aspiration and the pellets were resuspended carefully in 950 µl FA/SDS (+ PMSF) to avoid the formation of bubbles in the solution which could affect the outcome of sonication.

5) In the sonication step, the DNA is sheared to an optimal size (400 bp approximately). The biorupter used for this step was switched on 30 mins before the experiment or until the temperature reached 4°C. The cells were transferred into 15 ml tubes (Becton Dickinson Labware, USA) and the biorupter was set up appropriately (20 secs on and 40 secs off at 4°C for 5 cycles at high power). This settings result in chromatin fragments of a 400 bp. After sonication, samples were centrifuged at 4,000 rpm for 5 mins (Eppendorf centrifuge 5810R, rotor A-4-81) and the supernatants were removed to 1.5 ml tubes. Second centrifugation was undertaken for 20 mins at 13,000 rpm at 4°C (Beckman microfuge 22R, rotor F241.5P). Finally, the supernatant containing the whole cell extract (WCE) was collected and snap frozen with liquid nitrogen.

2.9.2 Checking the chromatin fragments in a non denaturing agarose gel

After the sonication, sheared chromatin fragments were checked in a non-denaturing agarose gel. The procedure was as follows:

1) 20 µl of the WCE for each sample were deproteinized by adding 80 µl 1xTE, 25 µl 5x pronase buffer (125 mM tris pH 7.5, 25 mM EDTA and 2.5% SDS) and pronase (1 mg/ml final concentration). The samples were incubated over night at 65°C. After, RNase (0.16 mg/ml final concentration) was added to allow the degradation of RNA and the samples were incubated at 37°C for 1 h.

2) To purify the DNA a Qiagen PCR purification kit was used and the DNA was eluted in 20 µl 1xTE.

3) Afterwards, the size of the fragments was checked in a 1.5% non-denaturing agarose gel, where 5 µl sample, 5 µl water and 5 µl 10x loading buffer were loaded in each well followed by the separation of the fragment electrophoretically at 40 V for

15 mins (Bio-Rad, Wide Mini Sub Cell GT Cell with 7x10 cm tray). Fragments should be between 100 bp to 1000 bp with an average length of 400 bp to 500 bp.

2.9.3 Immunoprecipitation

In this step the WCE was incubated with a specific antibody (anti-acetyl-histone H4 (Lys16) and anti-acetyl-histone H3 (Lys9), H3 (Lys14), Upstate) to precipitate the fragment containing the protein (antigen). An input control was also carried out for each immunoprecipitated chromatin sample, and this was not treated with the antibodies. The procedure was as follows:

1) To 100 µl WCE, 900 µl FA/SDS (+PMSF) buffer and 3 µl antibody were added. This was incubated by rotation overnight at 4°C. Subsequently, ~30 µl beads were added to each sample and the samples were washed three times with FA/SDS (50 mM HEPES KOH pH 7.5, 150 mM NaCl, 1 mM EDTA, triton X-100). The supernatant was removed each time by aspiration and finally was equilibrated with 0.1% BSA and 400 µg/ml single stranded salmon sperm in FA/SDS and incubated for 1 h. After the incubation, the beads were again washed three times with FA/SDS and then an appropriate volume of FA/SDS was added to transfer 50 µl of the beads solution to the over night immunoprecipitated tubes. The immunoprecipitated DNA was incubated with the beads by rotation at 4°C for 2~3 hrs.

2) After this incubation, the samples were spun down at 4,000 rpm (Eppendorf 5415D centrifuge, rotor F45-24-11) and the supernatant was removed by aspiration. Then, the samples were washed with several solutions in the following order: FA/SDS, FA/SDS with 500 mM NaCl, LiCl solution (10 mM Tris-HCl, 250 mM LiCl, 1 mM EDTA, 0.5% Igapel CA-630, 0.5% Sodium deoxycholate) and finally with 1xTE buffer. The samples were rotated for 10 mins at 4°C in these solutions followed by a spun at 4,000 rpm (Eppendorf 5415D centrifuge, rotor F45-24-11).

3) Subsequently, 125 µl of pronase buffer was added to the samples and incubated at 65°C for 20 mins in a thermomixer (Eppendorf, UK limited) to allow the separation of the precipitated chromatin from the beads. Afterwards, the samples were centrifuged at 4,000 rpm for 1 min (Eppendorf 5415D centrifuge, rotor F45-24-11) and the supernatant was transferred to a new tube where pronase was added (1 mg/ml final concentration) for deproteinisation. The samples were incubated over night at 65°C. Finally, the DNA was purified using Qiagen PCR purification kits. The resulting DNA was eluted in 20 µl 1xTE.

4) The input samples were treated as previously described in section 2.9.2 steps 1 and 2.

2.9.4 Quantification by quantitative PCR (qPCR)

Quantitative PCR (qPCR) allows the quantification of precipitated DNA with a specific antibody. The precipitated DNA was amplified by PCR using the iQTM SYBR®Green supermix (Bio-Rad) and was analysed using the iCycler iQ real-time PCR detection system (Bio-Rad).

The SYBR®Green dye is able to bind to dsDNA emitting fluorescence which is proportional to the PCR product obtained by amplification. During each PCR cycle, the fluorescence signal was collected at the exponential phase of PCR amplification via a camera. After PCR, data were analysed using the iCycler software (Bio-Rad). The reference standard dilution of a known sample can be used to determine the amplified dsDNA in the PCR, giving the fraction or ratio of the sample relative to the standard. All the steps were undertaken as follows:

1) The iCycler iQ real-time PCR detection system (Bio-Rad) apparatus was switched on at least 30 mins before to enable the stabilisation of the laser lamp.

2) Immunoprecipitated and input samples were diluted appropriately to obtain the unknown Ct numbers (the cycle number at which the fluorescence from the sample crosses the threshold) between the Ct numbers of the reference standard dilutions or standard curve.

3) Subsequently, the qPCR components were added to each PCR reaction and PCR was carried out in triplicate. For each DNA sample: 9.6 µl iQTM SYBR®Green Supermix (Bio-Rad), 10 µl diluted DNA in water, 1 µM each primer.

4) The PCR was undertaken using a 96-well plate from Bio-Rad and covered with a sealing plastic (Bio-Rad). Then, the PCR reactions were vortex carefully with a final centrifugation at 2,000 rpm for 2 mins (Eppendorf 518, rotor A-4-62 MTP).

5) The program used for the qPCR was: 95°C for 3 mins, 95°C for 15 secs, 52°C for 20 secs*, 52°C for 10 secs, Steps 2-4 repeated 45 times, 95°C for 1 min, 55°C for 30 secs*. The last step was repeated 41 times, increased by 1°C with each repeat. Fluorescence data was collected (*) during step 4 and after step 7.

6) When the reaction was completed, the analysis of the data was carried out using the iCycler software (Bio-Rad). Ct is inversely proportional to the copy number of the target template, therefore, a low Ct value represents a high template concentration and

vice versa. The amount of DNA is determined by comparing the results to the standard curve produced with a serial dilution of known DNA.

Chapter III

STRAIN CONSTRUCTION AND URA3 EXPRESSION LEVELS

3.1 Introduction

3.1.1 Strain construction

In this chapter, construction of the strains employed for the research undertaken and the subtelomeric expression of *URA3* when at different chromosome ends are described.

As stated in Chapter II, the original strains were kindly provided by Professor Edward Louis. In these strains, the *URA3* gene is inserted 1.75 Kb centromere proximal to the $TG_{1\text{-}3}$ telomeric consensus sequence and 1 Kb centromere proximal to Core X-ACS at two chromosome ends in two different strains by a method for direct deletion in budding yeast (described by Baudin et al., 1993). The method consists of a single PCR amplification whereby each primer contains two complementary regions; one region (44 bp long) allows homologous recombination to occur between the flanking region in the genome where *URA3* should be inserted and the other region is ~20 bp long which is homologous to the plasmidic *URA3* gene. The primers used are described in figure 3.1. After the PCR amplification, this crude PCR mix was used to transform yeast cells so the DNA fragment could be inserted into the precise subtelomeric position by homologous recombination (Pryde and Louis, 1999).

S1ATATTAAGGAACTTTAAGTTAATGATACCATGATAGTATTAAGACgcttttcaattcaattca
S2AAATATTCTATTCTTCAACCATAATACATAAACACACTTAATTGCaaatcattacgaccgagatt

Figure 3.1 *Primers used for the insertion of URA3 at different subtelomeric regions.* Lower case is the fragment homologous to *URA3*. S1 is the centromere proximal site and S2 is the distal side of the site of insertion (Pryde and Louis, 1999).

These strains are also mutated at the endogenous *URA3,* (*URA3-52*) by inserting a Ty transposon into the *URA3* open reading frame. This enabled the selection of transformants (Rose and Winston, 1984) which had *URA3* inserted in the subtelomeric region.

However, for the purpose of the work presented in this thesis, a single copy of the *URA3* sequence is needed to study CPD incidence, repair, and the DNA sensitivity to MNase since the high resolution technology probes required a specific and unique DNA sequence. Therefore, I deleted the endogenous *URA3-52* from the original strains. As a result the designed primers and probes for the following experiments could only anneal to the unique subtelomeric *URA3* sequence.

3.1.2 Silencing of the subtelomeric *URA3* gene

As previously described in Chapter I (page 38), telomeres adopt a repressed or silenced structure due to their chromatin conformation and via the involvement of proteins that contribute to silencing and chromatin organisation. For example, the SIR complex is involved in the silencing propagation along the telomere and subtelomere at each chromosome end (Auriche et al., 2008; Gottschling et al., 1990; Sandell and Zakian, 1992). High levels of silencing can reduce the binding of RNA Pol II and transcription factors at the telomere end. Thus, the expression levels of the *URA3* gene or the gene located nearby decreased (Aparicio and Gottschling, 1994; Chen and Widom, 2005). However, if the silencing or TPE levels are low, there is less of an influence of silencing and thus the expression of the *URA3* gene increases. Moreover, since there are differences in silencing levels, the subtelomeric *URA3* gene may be expressed in some cells and repressed in others and can switch repeatedly from transcriptionally active states to a transcriptionally repressed state. This switching between active and repressed transcription is due to epigenetic events (Gottschling et al., 1990; Mondoux et al., 2007; Pryde and Louis, 1999; Sandell and Zakian, 1992).

The expression of genes close to the chromosome ends are subject to TPE (the TPE phenomenon is described in Chapter I (page 38). For instance, when at its natural location the expression of *URA3* is inducible in response to uracil starvation (Flynn and Reece, 1999; Losson et al., 1983; Patzold and Lehming, 2001; Roy et al., 1990; Struhl, 1986). However, the regulation of *URA3* gene expression differs from that at its natural location at chromosome ends. In addition, previous studies show that the expression levels at different chromosome ends could vary due to differences in silencing (Mondoux et al., 2007; Pryde and Louis, 1999).

In this chapter I measured the expression levels of distinct *URA3* genes located equidistant at different chromosome ends. After, the expressions were compared to strains where *URA3* is at its natural location.

Silencing can be disrupted by *Δsir3* affecting repression and TPE at the subtelomeric region (McAinsh et al., 1999). Therefore, in the study presented in this thesis, the enzymatic component of the SIR complex (Sir2p) was abolished by replacing the *SIR2* gene with the *LEU2* gene to examine the effect of this enzyme in silencing and the consequence of this mutation in the subtelomeric *URA3* reporter gene expression at different chromosome ends.

3.2 Materials and methods

3.2.1 Yeast strains

The yeast strains employed in this chapter were FEP 178 *ura3-52Δ* (MAT a, *ura3-52, can1-1, ade2Δ, leu2Δ, URA3 at CHRIII-R*), FEP 100-10 *ura3-52Δ* (MAT a, *ura3-52, can1-1, ade2Δ, leu2Δ URA3 at CHRXI-L*), FEP 100-10 (MAT a, *ura3-52::KanMX can1-1, ade2Δ, leu2Δ URA3 at CHRXI-L*), FEP 178 (MAT a, *ura3-52::KanMX can1-1, ade2Δ, leu2Δ URA3 at CHRIII-R*), FEP178*sir2** (same as FEP178, except *sir2::LEU2*) and FEP100-10*sir2** (same as FEP100-10, except *sir2::LEU2*).

3.2.2 *KanMX* amplification

The PCR reaction was carried out as follows: 1 µl of pUG6 DNA (10 ng), Buffer 10X (to a final concentration of 1X), 0.4 µM of each primer, 1.5 mM of $MgCl_2$, 200 µM of each dNTP and distilled water to a 50 µl final volume. The PCR program used was as follows: initial incubation at 96ºC for 90 secs and 29 cycles with the denaturing step at 96ºC for 30 secs, 55ºC for 50 secs, 68ºC for 90 secs and final extension of 68ºC for 10 mins. The PCR product obtained was 775 bp and contained the amplified loxP-KanMX-loxP fragment.

3.2.3 Amplification of the endogenous *URA3-52* flanking sequences

The reaction mix was undertaken as follows: 1 µl of genomic DNA (20 ng), Buffer 10X (to a final concentration of 1X), 0.4 µM of each primer, 1.5 mM of $MgCl_2$, 200 µM of each dNTP and distilled water to 50 µl. The PCR program employed was as follows: initial incubation of 96ºC for 1 min 30 secs and 29 cycles at 96ºC for 30 secs, at 55ºC for 50 secs, 68ºC for 90 secs and a final extension of 68ºC for 10 mins. Afterwards, the products obtained were checked in a non-denaturing agarose gel.

3.3 Results

3.3.1 Strain construction

3.3.1.1 Replacement of the endogenous mutated *URA3* by *KanMX*

Replacement of the endogenous *URA3-52* gene was undertaken by PCR amplification and subsequent transformation. The endogenous *URA3-52* is 830 bp and located on chromosome V. For the replacement of this fragment, three PCR reactions were carried out separately, two to amplify the flanking regions of endogenous *URA3-52* and the third one to amplify the gene (*KanMX*) which would replace the endogenous *URA3-52* gene. Afterwards, the three PCR products were fused by two PCR reactions. Finally, the obtained PCR product (*KanMX* with *URA-52* flanking sequence) was transformed into the original strain using the lithium acetate method (described by Gietz et al., 1992). The endogenous *URA3* was replaced by *KanMX* via homologous recombination with the flanking sequence of *URA3-52*. The procedure is described below in more detail.

***KanMX* amplification**

The amplification of *KanMX*, located in the pUG6 (Euroscarf) plasmid was undertaken using PCR (Gueldener et al., 2002; Guldener et al., 1996). The primers employed in this reaction (Appendix I: URA3-*KanMX*-F and URA3-*KanMX*-R) had two regions, one region was homologous to the endogenous *URA3* flanking sequence (~40 bp) and the other is homologous to the loxP-*KanMX*-loxP (figure 3.3).

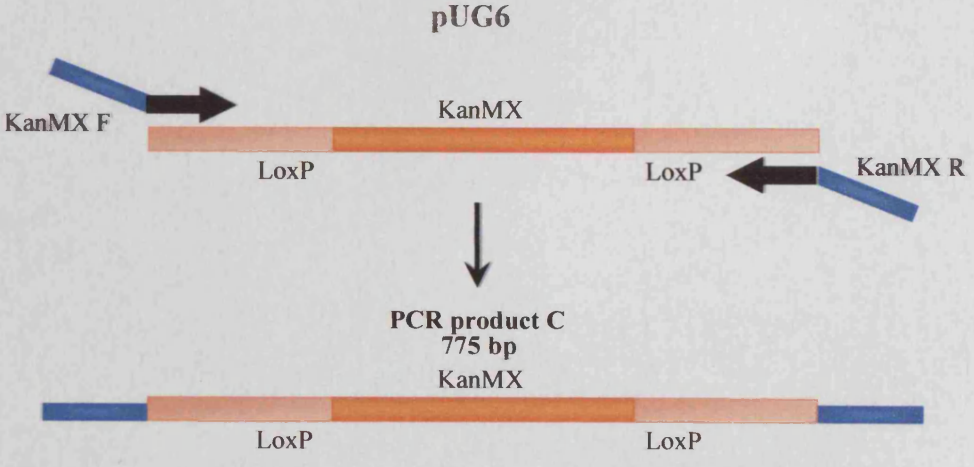

Figure 3.3 *Amplification of loxP-KanMX-loxP located on plasmid pUG6.* The black region of the primer is homologous to the loxP-*KanMX*-loxP sequence in the plasmid and the blue region is homologous to the flanking region of the endogenous *URA3* gene.

Amplification of the endogenous *URA3-52* flanking sequences

Both flanking sequences of the endogenous *URA3-52* were amplified using genomic DNA as a template (figure 3.4). After PCR, the generated products were 394 bp (flanking sequence upstream of *URA3-52*) and 475bp (flanking sequence downstream of *URA3-52*). The primers used were termed *URA3*-1 and *URA3*-2 for the 394 bp PCR product, whereas, for the 475 bp PCR product the primers used were *URA3*-3 and *URA3*-4 (see Appendix I for primers details).

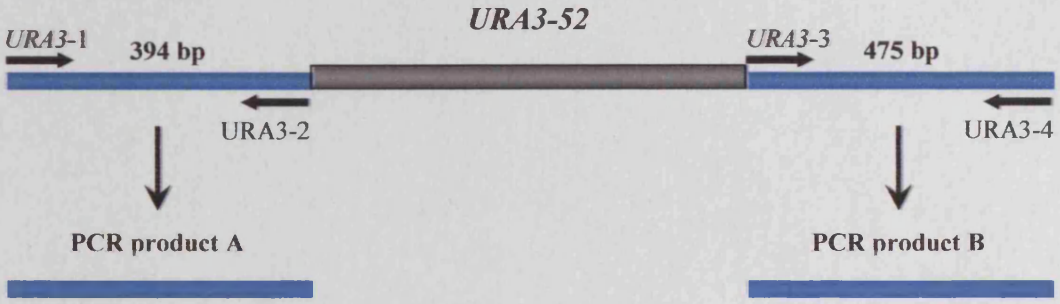

Figure 3.4 *Amplification of the endogenous URA3-52 flanking sequence at the genomic DNA.* The primers used were homologous to the flanking sequence of *URA3-52* in the genomic DNA.

Fusion of the PCR products

The PCR products obtained were purified with a PCR purification kit (Qiagen) and fused by two PCR (figure 3.5). In the first fusion PCR, the 394 bp fragment and loxP-*KanMX*-loxP fragments were fused and in the second fusion PCR, the PCR product obtained from the first fusion PCR was fused with the 475 bp long fragments. Both reactions were undertaken using the expand high fidelity PCR system (Roche diagnostic). Before the fusion PCR, the three purified PCR products were diluted 2000x and mixed. Thus, for the first fusion PCR 394 bp and loxP-*KanMX*-loxP fragments were diluted 2000x and mixed together, whereas, for the second fusion PCR the obtained PCR product in the first fusion PCR and the 475 bp fragment were diluted and mixed together. Afterwards, for each fusion PCR, 2 µl of the mixed DNA were used. The programs employed were as follows: initial incubation at 94°C for 4 mins and then 4 cycles of 94°C for 15 secs, 52°C for 3 mins and 68°C for 4 mins with a final extension of cycle at 68°C for 10 mins. This PCR program was followed by a second PCR program with initial incubation at 94°C for 1 min and them 29 cycles of 94°C for 15 secs, 51°C for 30 secs and 68°C for 2 mins and a final extension of 68°C for 10 mins.

3.3.1.2 Transformation and DNA extraction

The fused PCR product was transformed into the original strain by the lithium acetate method (described by Gietz et al., 1992) where the transformed PCR product replaced the endogenous *URA3-52* by homologous recombination with the flanking sequence of the endogenous *URA3-52*, replacing the endogenous *URA3-52* with *KanMX*. The DNA of the transformed colonies was extracted using glass beads as (described by Hoffman and Winston, 1987). Transformed colonies were analysed by PCR with *URA3*-outside-F and *URA3*-outside-R primers (Appendix I) to select for positive colonies. Afterwards, the obtained PCR products were analysed via an agarose gel (figure 3.6). The new strains obtained were named FEP 178*ura3-52Δ* and FEP100-10*ura3-52Δ*.

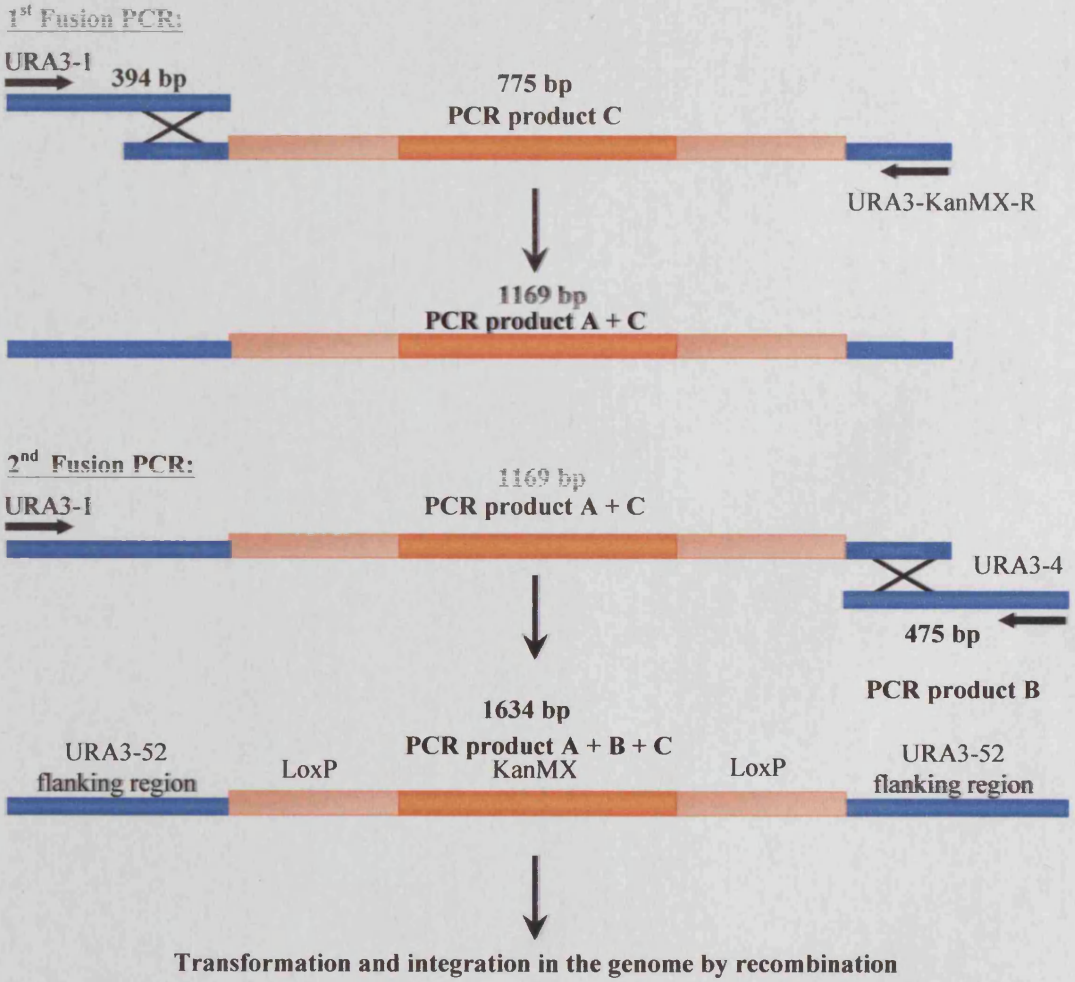

Figure 3.5 *Fusion of three PCR products*. The first fusion PCR was undertaken with URA3-1 and URA3-KanMX-R primers and as templates *KanMX* amplification product and 394 bp length PCR product. The obtained PCR product (PCR product A+C) was 1169 bp. The second fusion PCR was carried out with URA3-1 and URA3-

4 primers. As templates the first fusion PCR product (PCR product A+C) and 475 bp length *URA3* flanking sequence PCR product were used. The final product was 1634 bp (PCR product A+B+C) and it was transformed into yeast strains so it could integrate in the genome by recombination.

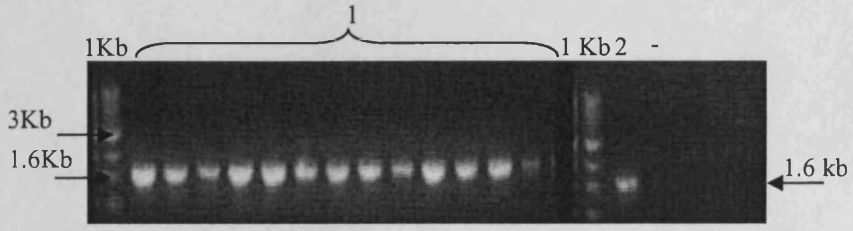

Figure 3.6 *DNA from the transformant colonies with endogenous URA3-52 replaced with KanMX.* The transformants obtained from the FEP100-10 strain are represented as 1 and the transformant obtained from the FEP178 strain is represented as 2 following by the genomic negative control.

3.3.1.3 Replacement of the endogenous *SIR2* gene with *LEU2*

The *SIR2* gene is located at chromosome IV and is 1689 bp long. The replacement was undertaken with an amplification of the *LEU2* gene (1128 bp), [from the pUG73 plasmid (Euroscarf) with *LEU2*R and *LEU2*F primers (see Appendix I)]. The primers used for *LEU2* amplification contain two regions, one of them homologous to the *SIR2* flanking sequence (5'side of the primer) and the other region is homologous to the plasmidic *LEU2* (3'side of the primer) (figure 3.7). The PCR was undertaken as previously described in this chapter (section 3.3.1.1).

The transformation followed by DNA extraction was then conducted as described in this chapter, (section 3.3.1.2) and the positive colonies were checked by PCR with *SIR2*F2 and *SIR2*R(2) primers (Appendix I). The obtained PCR amplicon was analysed in an agarose gel (figure 3.8) and the generated strains were called FEP178*sir2** and FEP100-10*sir2**.

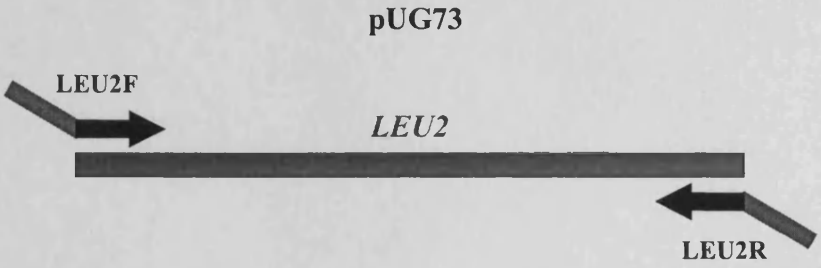

Figure 3.7 *Amplification of LEU2 located in the pUG73 plasmid.* The black region of the primer is homologous to the *LEU2* in the plasmid and the purple region is homologous to the flanking region of endogenous *SIR2* in the genome.

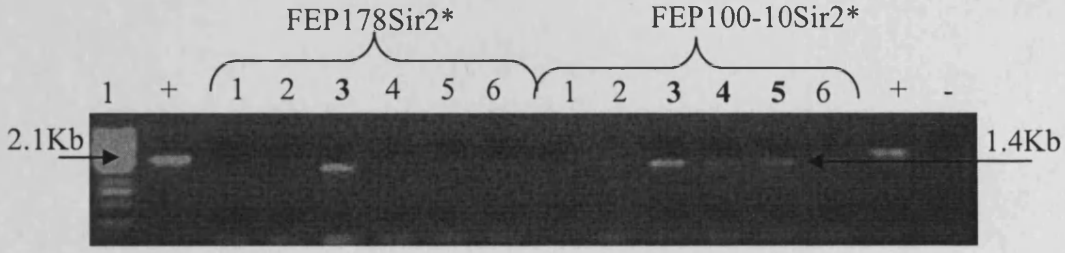

Figure 3.8 *DNA from transformant colonies with endogenous SIR2 replaced by LEU2 gene.* The positive control with the FEP178*ura3-52::KanMX* genomic DNA followed by the transformant colonies from FEP178*ura3-52::KanMX* and from FEP100-10 *ura3-52::KanMX* strains. The positive clones are illustrated in bold.

3.3.2 Subtelomeric *URA3* expression in the constructed strains

The expression of the subtelomeric *URA3* gene was measured to determine whether there were differences in silencing levels between different native chromosomes ends, and expression was compared to that of the endogenous *URA3* gene. *URA3* gene expression was also measured in the *SIR2* deleted strains to examine whether the deletion of *SIR2* could affect the silencing and the expression of *URA3*. The expression of *URA3* was determined by measuring the fraction of cells that were able to grow on plates containing 5-Fluoroorotic acid (5-FOA) *versus* the colonies able to grow on plates without 5-FOA. As mentioned before, 5-FOA is only toxic when the *URA3* gene product is present in the cell. Cells expressing *URA3* are unable to grow on 5-FOA and cells that do not express *URA3* become 5-FOA resistant and therefore can form colonies.

The results are summarised in figure 3.9 and in Appendix II. The figure shows the percentage of surviving colonies in each medium. When *URA3* is inserted in the XI-L (FEP100-10ura3-52Δ), there is no difference in the number of surviving colonies in the presence or absence of uracil in the different growth media, 54.8±8 % surviving colonies on plates with uracil and 49.1±18.9 % on plates without uracil. When *URA3* is inserted at III-R (FEP178) the number of surviving colonies is reduced by 20-fold in media with uracil (5.2±6.5 %) and 220-fold in media without uracil (2.5±0.57 %). When the *SIR2* gene is deleted, the survival of both strains was below 0.01 % irrespective of uracil status. As a control, the expression of the endogenous *URA3* was also analysed. The results were as expected; when *URA3* is at its natural location it is only expressed in the absence of uracil or starvation conditions (0.2±0.3 %) but not in the presence of uracil (94.6±57 %).

This experiment showed that the level of *URA3* expression differs when it is located at different chromosome ends; when the *URA3* gene is inserted into the III-R (FEP178) chromosome, the level of repression is very low. In contrast, when *URA3* is inserted at the XI-L (FEP100-10) chromosome end, the level of repression is much higher. When the *SIR2* gene is deleted the *URA3* is expressed at the same level at both chromosome ends. The regulation of the expression at the different chromosome ends also differs from that of the endogenous *URA3* gene. This confirms that the different chromosome ends have a distinct grade of silencing as previously (reported in Pryde and Louis, 1999). They analysed the expression of inserted *URA3* at different subtelomeric regions and at different chromosome ends.

The results shown in this thesis additionally suggest that repression at the subtelomeres is due to the spreading of silencing since when silencing is disrupted via deletion of the *SIR2* gene, the *URA3* gene at both subtelomeric regions is expressed.

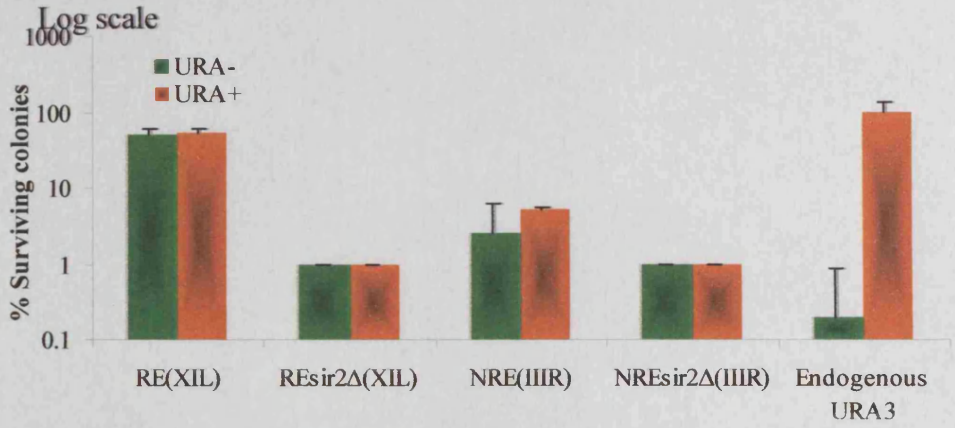

Figure 3.9 *Expression of the URA3 gene for all strains employed.* Colonies grown in minimal medium with uracil are indicated in orange. Colonies grown in minimal medium without uracil are represented in green. The strains used were NRE (*URA3* inserted at III-R), NRE*sir2*Δ (*URA3* inserted at III-R and deletion of *SIR2*), RE (*URA3* inserted at XI-L), RE*sir2*Δ (*URA3* inserted at XI-L and deletion of *SIR2*).

In order to simplify nomenclature, the strain where *URA3* is inserted in the III-R was termed the non repressive end (NRE) and the strain where *URA3* is inserted in the XI-L was termed the repressive end (RE) throughout this thesis. When *SIR2* was deleted the strains where called NRE*sir2*Δ and RE*sir*2Δ.

3.4 Discussion

3.4.1 Expression of the subtelomeric *URA3* gene at different chromosome ends and the influence of *SIR2*

As expected, when at its natural location the expression of *URA3* is only inducible in response to uracil starvation. The *URA3* transcriptional activator Ppr1p (pyrimidine pathway regulator 1) is regulated by intermediates of the pyrimidine biosynthesis pathway such as DHO (dihydroorotic acid) and OA (orotic acid) or by the product of the regulatory gene. When the levels of OA and DHO increase in the cell, Ppr1p enhances *URA3* expression. However, when there are enough *URA3* products, the expression of the gene decreases. Therefore, endogenous *URA3* expression increases in medium lacking uracil compared to medium with uracil (Flynn and Reece, 1999; Losson et al., 1983; Patzold and Lehming, 2001). In addition, it has been reported that as with the *HIS3* promoter, the *URA3* promoter region has at least four different regulatory elements and they are divided into two categories; elements involved in the basal transcription such as poly (dA-dT) tracts and those involved in the induced level such as the uracil-controlled upstream activating site (UAS_{URA}). Ppr1p binds to the UAS_{URA} and with the addition of DHO or OA the Ppr1p transcription factor becomes active (Roy et al., 1990; Struhl, 1986).

However, regulation of the subtelomeric *URA3* expression differs from that of the endogenous *URA3*. My results show different levels of expression for the subtelomeric *URA3* gene at the two distinct chromosome ends. The expression of *URA3* is low when it is at XI-L (RE); yet, *URA3* is more highly expressed when it is inserted at III-R (NRE). This is consistent with a previous report where expression levels of a reporter gene at different chromosome ends vary due to variation in silencing at chromosome ends and it is not dependent on Ppr1p. Consequently, they suggest that *S. cerevisiae*, chromosome ends are divided into subgroups because of differences in the levels of silencing or TPE (Pryde and Louis, 1999).

Although, it is not known why different chromosomes display different levels of silencing, several studies suggest that changes in telomere length influences TPE. The length of the telomeres is dependent on Rif proteins (Rif1p and Rif2p) (Auriche et al., 2008). Rif2p together with Rif1p are involved in the regulation of telomere length and both of these interact together and with Rap1p carboxyl terminus. If there is a failure in the Rif1p-Rap1p interaction or *RIF1* is mutated, then the telomere length increases and silencing is affected because Sir proteins are also recruited by Rap1p

carboxyl terminus to the telomere. Therefore, in longer telomeres there are more Rap1p binding sites and more Sir proteins can be recruited to the telomere, increasing the silencing levels (Tham and Zakian, 2002). Additionally, it has been shown that when both, Rif1p and Rif2p are mutated, the silencing and TPE is increased as more Sirp can also bind to Rap1p (Levy and Blackburn, 2004; Wotton and Shore, 1997) because there are no free Rif1p and Rif2p to compete with Sir proteins and the telomeres became longer (Hardy et al., 1992; Kyrion et al., 1993).

It has also been reported that mutations of *SIR3* and *SIR4* result in slight telomere shortening (Palladino et al., 1993). The length of the telomere can therefore also be regulated by Sir proteins that bind to Rap1p. So the proteins directly involved in silencing (Sir3p and Si4p) and proteins directly involved in telomere length (Rif1p and Rif2p) compete to bind to the Rap1 carboxyl terminus (figure 3.10). In other words, telomere length and silencing are inter-related; proteins involved in telomere length such as Rif can influence silencing levels and *vice versa*.

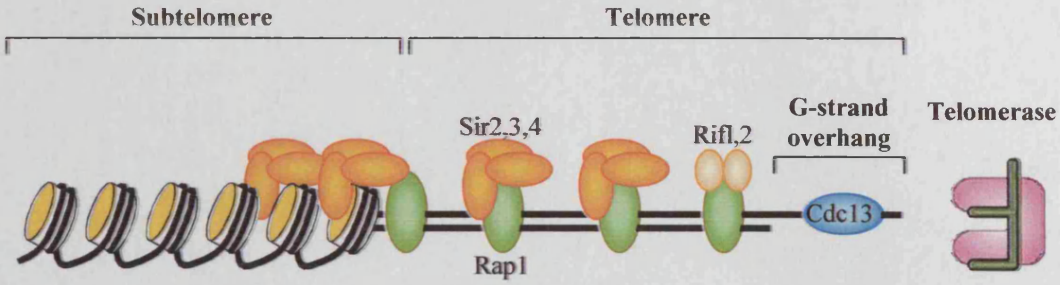

Figure 3.10 *Regulation of telomere length and silencing at chromosome ends.* The Carboxy terminal domain of Rap1p can recruit Sir proteins and Rif proteins, creating competition between the telomere length and silencing activity {adapted from \Blasco, 2007 #368}.

For that reason, the result in this chapter suggests that the III-R telomere is shorter than XI-L, so the *URA3* expression is affected by silencing at XI-L but not at III-R.

It has been shown that the decreased binding of Rap1p per nucleotide causes telomere elongation (Ji et al., 2008). Additionally, silencing can be also affected by the binding reduction of Rap1p to the telomere, decreasing the TPE and silencing. Consequently, it can be suggested that the efficiency of Rap1 in recruiting Sir proteins can modulate the TPE in each chromosome end.

The TPE can also be modified by the connection between localisation of the telomeres in the nuclear envelope and the level of TPE, although this correlation it is not clear. There is evidence that telomeres with the highest levels of TPE are often found at the nuclear envelope and this is mainly due to the fact that the Rap1p foci are located at the nuclear envelope, and are important for TPE. The number of Rap1p foci per cell correlates with the TPE level and when the silencing is abrogated the number of Rap1p foci decreases in a cell (Mondoux et al., 2007). A cluster of telomeres located at Rap1p foci creates a high concentration of silencing proteins, which facilitates TPE. However, the location of a telomere in a cell can differ between cells. Moreover, the fraction of telomeres localised to the periphery varies between telomeres and with position in the cell cycle (Bourgeois et al., 1985; Kosak and Groudine, 2004; Zink et al., 2004). The *URA3* expression results suggest that the XI-L chromosome end is probably located near Rap1p foci or that it is clustered in a Rap1p focus.

The spreading of Sirps might also differ between telomeres, creating a variation in gene repression. For instance, when Sir1p, Sir2p, Sir3p or Sir4p are mutated, silencing is disrupted. In contrast, when Sir3p is over expressed silencing and TPE are increased (Pryde and Louis, 1999). These differences in spreading can be linked with the differences in silencing protein concentration at each chromosome end. For example Sas2p, a catalytic subunit of the Sas complex, prevents the spreading of Sir proteins into subtelomeric regions, i.e. it has a crucial role in maintaining the euchromatin-heterochromatin boundaries. In similar way, Sir2p determines the spreading of Sirp and therefore, the spreading of TPE at the chromosome ends (Kimura et al., 2002; Shia et al., 2006; Suka et al., 2002). Both Sir2p and Sas2p establish a gradient generating different equilibrium between them at distinct chromosome ends. The results presented in this chapter suggest that at the RE, there are more Sirp recruited than at the NRE. Thus, the silencing levels at the RE are higher; and therefore the expression of *URA3* at the RE is subjected to TPE, whereas at the NRE, the *URA3* expression is not affected by silencing. In other words, it is also possible that the local concentration of Sirp varies between subtelomeres and in the RE there is a higher concentration of Sirp compared with the NRE at the subtelomeric *URA3* gene.

The TPE can also be modified by homologues of sir2 proteins (Hsts proteins). For instance, over-expression of *HST1* can restore silencing in cells where *SIR2* is

mutated (Brachmann et al., 1995). Therefore, it is possible that consequently there are different concentrations of *trans*-acting elements involved in TPE at the RE and NRE.

In addition, subtelomeric elements can influence the silencing at telomeres. All telomeres exhibit different subtelomeric structures. For instance, the X element can be from ~300bp to 3Kb and the only element found in all X elements is the Core-X repeat. Most of the X-elements contain antisilencing X-combinatorial repeats (XCRs) apart from Tbf1p to avoid the spreading of silencing to the internal part of the chromosomes. These can vary in number and organisation between chromosome ends (Mondoux et al., 2007). The Y' element is only found in some of the telomeres and it is distal to the element X (Chan and Tye, 1983). Therefore, different *trans*-acting factors involved in silencing can be recruited to individual subtelomeres because of the differences in the subtelomeric structure between chromosome ends. It is likely that the subtelomeric regions of III-R and XI-L are different so the regulation of the silencing via *trans*-acting elements varies between these chromosomes.

As reported in Chapter I (page 38), there are at least six proteins essential for the TPE in yeast: Rap1p, Sir2p, Sir3p, Sir4p and the Ku heterodimeric complex (yKu70p and yKu80p). From the sequence specific proteins that recognise telomeric TG naked repeats, only Rap1p is essential for silencing. The Ku heterodimer also binds to the telomere contributing to silencing by recruiting Sir4p to the telomere and by binding the telomere to the nuclear envelope. Silencing at telomeres can be spread throughout the telomere and subtelomere with the help of the Sir complex (Sir2p, Sir3p and Sir4p) (Aparicio et al., 1991; Gasser and Cockell, 2001; Hickman et al., 2007; Kaeberlein and Powers, 2007; Perrod and Gasser, 2003; Pryde and Louis, 1999). When the gene *SIR2* which encodes Sir2p histone deacetyltransferase is deleted, transcriptional silencing of the *URA3* subtelomeric gene is disrupted at both, NRE and RE, therefore the *URA3* gene is expressed at the same level.

This result is consistent with previous results whereby mutations in Sir proteins abolished the TPE. As it is already known, TPE is at the level of transcription, therefore, Sirps are crucial to maintain transcriptional repression at telomeres and the repression of a reporter gene in a subtelomeric region is dependent of its location but not on its promoter (Perrod and Gasser, 2003; Pryde and Louis, 1999).

To conclude, in Chapter III I have shown that the repressed state at a specific subtelomeric location in different chromosome ends can vary and the repression is abrogated by deletion of *SIR2*. It has been suggested that the chromatin structure may

be mechanistically linked to silencing or the repressed state in a reporter gene at the telomere (Gottschling, 1992). When subtelomeric *URA3* is repressed the TATA sequence at the promoter region is inaccessible due to the chromatin conformation. Further evidence is that the induction of telomeric transcription after deletion of *SIR3* changes the telomeric chromatin and the DNA at the chromosome end becomes more accessible (de Bruin et al., 2000). Expression of the subtelomeric *URA3* is not regulated as when at its natural location, suggesting that the differences in the chromatin environment play a major role in the expression of the genes. Thus, the experiments in the next chapter examined the accessibility of the DNA in chromatin to MNase in order to determine whether the variation in repression at the distinct chromosome ends is due to detectable differences in chromatin structure, and whether the absence of *SIR2* which disrupts silencing also influences the chromatin structure.

Due to the fact that Rap1p foci are dispersed when the DNA damage occurs to allow repair (McAinsh et al., 1999), it is possible that when the chromatin is more accessible or the silencing is abolished, then the repair of DNA damage may be more efficient. Therefore, the differences in DNA repair of UV induced CPDs were analysed in Chapter V.

Chapter IV

CHROMATIN ACCESSIBILTY OF URA3 *AT DIFFERENT SUBTELOMERES*

4.1 Introduction

4.1.1 Chromatin environment

As previously discussed in Chapter I, to fit in the nucleus the DNA is packaged as chromatin. This packaging can occur at different levels; the lowest level of chromatin organisation is where 146 bp of DNA is wrapped around a nucleosome and this basic element is repeated along the DNA. The nucleosome is composed of four pairs of histone (H2A, H2B, H4 and H3), each of them associated as homodimers, forming a histone octamer. In eukaryotes, nucleosomes occupy 80% of the genome and this structure can condense further, into 30 nm or more fibre, forming the highest level of condensation called heterochromatin in higher eukaryotes (Kornberg and Lorch, 1999). In budding yeast, the chromatin structure similar to heterochromatin is called silenced chromatin, and it is located at the rDNA, the *HML* and *HMR* mating type loci and telomeres (Rusche et al., 2003).

Nucleosomes are not homogeneously distributed in the eukaryotic genome. In some regions of the genome, several determined nucleosomes organisations (or arrays) dominate, whereas in other regions a single nucleosome organisation can dominate and in other regions there is no particular organisation of the nucleosomes. Moreover, the nucleosomes at highly expressed genes are delocalised, probably allowing the occupancy of RNA polymerases and transcription factors in the DNA. Indeed, it has been reported that most of the nucleosome free regions are found ~200 bp upstream of many coding sequences. These regions were identified as transcriptional start sites or promoters, especially in transcriptionally active genes, and they are related to the localisation of Poly dA-dT sequences (Segal and Widom, 2009; Sekinger et al., 2005; Yuan et al., 2005).

Thus, one factor determining the position of the nucleosomes is the DNA sequence since some sequences are more likely to have nucleosomes than others. Overall, most nucleosomes are located at the intergenic sequences and coding regions; whereas, the sequences associated with transcription factors are depleted of

nucleosomes. For example, using *in vivo* UV footprinting and DNA repair by photolyase, it has been confirmed that poly dA-dT sequences are mostly free of nucleosomes (Suter et al., 2000) due to the rigidity of the poly dA-dT sequence (Anderson and Widom, 2001; Field et al., 2008; Segal et al., 2006; Struhl, 1985; Yuan et al., 2005). Nucleosome free regions, such as Poly dA-dT sequences, are important for the transcription levels as that it can alter the chromatin structure (Field *et al.*, 2008; Struhl, 1985). However, there are exceptions and sometimes nucleosomes can occupy unfavourable sites such as poly dA-dT regions, altering the chromatin structure and gene expression (Losa et al., 1990). In addition, in some regions nucleosomes have a strong affinity for transcription factor binding sites, making those sites inaccessible. Therefore, nucleosomes can also have a regulatory role (Segal et al., 2006), and nucleosome position and chromatin remodellers can regulate metabolic processes in the cell (Altaf et al., 2007; Ehrenhofer-Murray, 2004; Verger and Crossley, 2004).

Chromatin alterations are undertaken mainly by chromatin remodelling complexes such as SWI/SNF family (Racki and Narlikar, 2008; Skiniotis et al., 2007), histone post-translational modifications such as acetylation (Millar and Grunstein, 2006) and histone variants (Jin et al., 2005). For example, the Isw2 chromatin remodeller can shift a nucleosome into a Poly dA-dT promoter sequence, however, when Isw2 is lost, this nucleosome is displaced. The changes made by Isw2 can be related to transcription and in this case the chromatin remodeller acts as a repressor (Whitehouse and Tsukiyama, 2006). Different nucleosomal conformations can exist in equilibrium and move throughout the genome. Thus, nucleosomes have dynamic properties which can consequently facilitate the recognition of a DNA sequence by other proteins or occlude some protein binding sites to inhibit particular activities.

Thus, under the influence of a chromatin remodeller, nucleosomes can unfold, dissociate or change position. Currently, there are three models to explain nucleosome movement throughout DNA.

In the partial unwrapping of the nucleosomal model, the H2A-H2B dimer at the ends of the nucleosomal DNA can dissociate from the nucleosome, making the nucleosomal DNA more accessible to proteins (Geraghty et al., 1998). The unfolding, or unwrapping, of the nucleosomal DNA due to the dissociation of the H2A-H2B generates a protuberance which can diffuse throughout the nucleosome (Kunkel and Erie, 2005).

The second model is the nucleosome sliding, where the nucleosome changes position without dissociation or reassembly. Nucleosome sliding can generate an over or under-twisting of the DNA. This torsion can be diffused through the nucleosome changing its position in the genome (Lomvardas and Thanos, 2001). As mentioned above, nucleosomes can have dominant positions. However, around dominant positions are also found minor positions, probably less energetically favourable and nucleosomes occupy them by sliding through the genome (Whitehouse and Tsukiyama, 2006). It has been reported that nucleosome positions can be changed by the sliding model with the insertion or deletion of a DNA sequence into specific chromatin regions (Becker, 2002; Mollazadeh-Beidokhti et al., 2009; Tanaka et al., 1996; Thoma, 1986).

The final model concerns the dissociation of the whole nucleosome octamer followed by reassembly (Cavalli and Thoma, 1993). In this case, total disruption of the DNA-histone interactions is needed.

The most likely models are the unwrapping and the sliding ones, since they only require a partial disruption of the nucleosomes. Thus, the first and the second model described here are energetically more favourable than the dissociation model. Figure 4.1 illustrates all the described models.

As shown in Chapter III, the silencing at different chromosome ends varies, so the accessibility of the DNA to TFs may differ. Consequently, this chapter describes experiments designed to study the MNase accessibility to DNA in different chromosome ends.

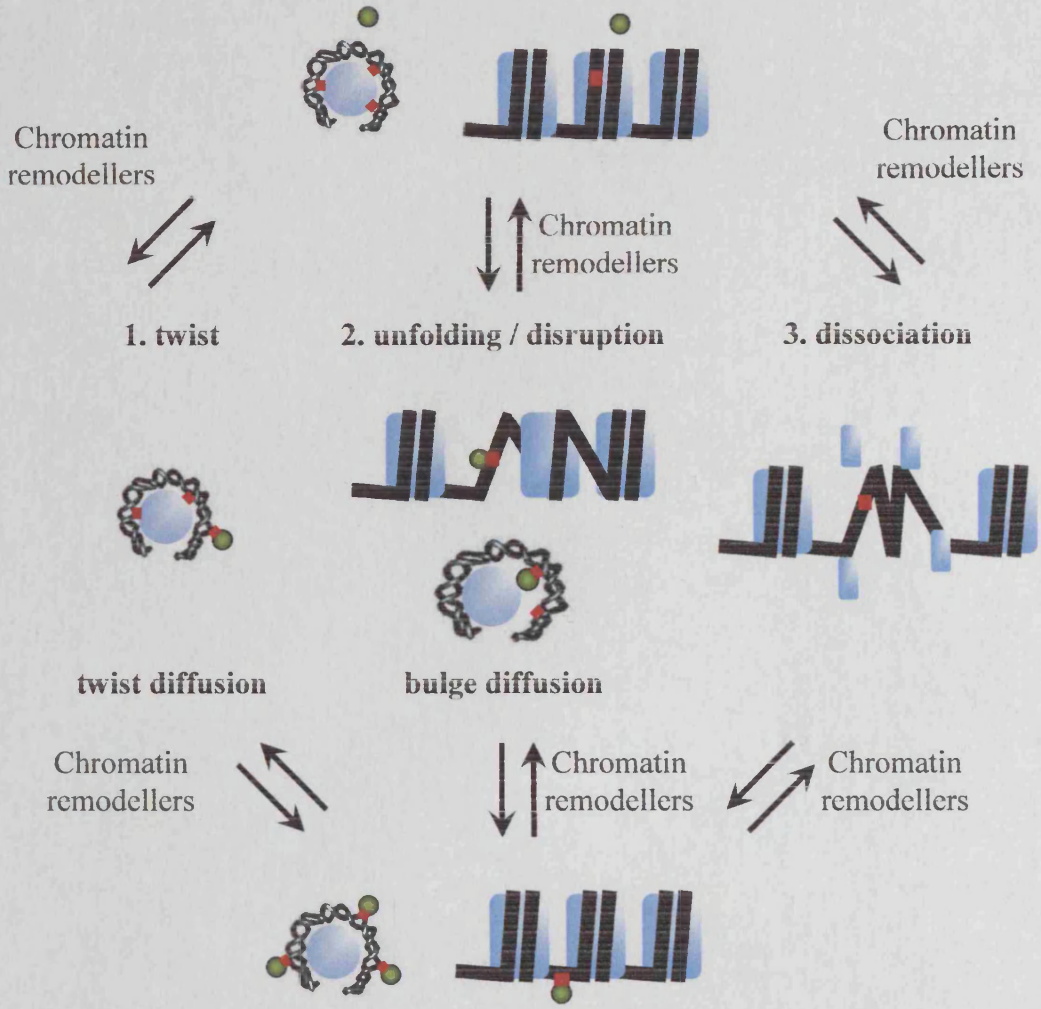

Figure 4.1 *Models explaining nucleosomes mobility in the genome.* Nucleosomes can unfold (1) generating a protuberance which can diffuse throughout the nucleosome. (2) Dissociate or shift (twist diffusion), generating the changes in the position of the nucleosome. (3) Finally, ,the whole nucleosome can dissociate. Nucleosomes dynamic properties allow the recognition of binding sites or DNA lesions (green sphere) by proteins such as TFs and proteins involved in DNA repair (red square) (adapted from Thoma, 2005).

4.1.2 MNase accessibility at subtelomeric *URA3* in the RE and NRE

In budding yeast, the telomeric chromatin is highly condensed and is named silenced chromatin since it is transcriptionally inactive and the silencing may be extended to subtelomeric regions.

Telomeres contain a 3´overhang to enable end replication. This can be recognised as a DSB by the DNA repair machinery. Therefore, telomeres have evolved specialised structures which DNA repair machinery distinguished from the

DSB. For example, several proteins are confined to the single-stranded 3' overhang and they have a dual role:

(i) Single-stranded proteins form a structure to protect the telomeres from degradation, fusion or being recognized as damaged DNA.

(ii) These proteins also permit the telomerase activity to take place (reviewed by Auriche et al., 2008). For instance, Cdc13p interact with Estp delivering the catalytic core telomerase to the telomeres and also with other capping proteins such as Stn1p and Ten1p conferring protection to the telomere ends (reviewed by Auriche et al., 2008; Grandin et al., 2001; Grandin et al., 1997; Puglisi et al., 2008).

There are proteins that specifically recognize the double-strand, such as Rap1p in *S. cerevisiae* (Grossi et al., 2001; Longtine et al., 1989), the homologue in humans are TRF1 and TRF2 (Bilaud et al., 1997; Chong et al., 1995). For example, Rap1p can recruit Sir Proteins to the telomere (described in Chapter III). Ku heterodimer (Ku70/Ku80) is located at the end of the double-stranded region (Fisher and Zakian, 2005). These proteins, together with the subtelomeric nucleosomes form a silenced chromatin organisation complex (described in Chapter I). The silencing can spread to the subtelomeric region forming the TPE phenomenon. The binding of the telomere to the nuclear envelope and the folding back stabilize the telomeric chromatin and silencing.

Digestion with MNase, an enzyme which cut in the DNA linker regions between nucleosomes, shows that contrary to human telomeres, the short telomeres in budding yeast are not organized with nucleosomes (Wright et al., 1992). However, MNase digestion also revealed that there are nucleosomes at the subtelomeric region of the chromosome ends (Y' and X elements), conferring protection to the telomere and which together with the silencing proteins gives a highly specialized chromatin structure (Gotta et al., 1997; Martino et al., 2009). This difference between yeast and humans is probably due to telomeres in budding yeast are not long enough (200 bp to 300 bp) to contain nucleosomes, whereas, in humans the telomeres are longer (2 to 20 Kb) (Tommerup et al., 1994; Wright et al., 1992).

To summarise, nucleosome occupancy varies across chromosomal regions, some regions having characteristic nucleosome occupancy. For example, telomeres and active rDNA exhibit low levels of nucleosome occupancy (Segal et al., 2006).

As previously reported in Chapter III, subtelomeric *URA3* gene expression varies depending on the chromosome ends, therefore, the structure of the chromatin

can also be different. This chapter describes the study of the chromatin structures of *URA3* at the repressive and non repressive ends on XIL and IIIR respectively.

It has been shown in chapter III that when *SIR2* is deleted the subtelomeric *URA3* gene is expressed in both subtelomeric regions at the same level (IIIR and XIL). One explanation for this result is that when *SIR2* is deleted, silencing is abolished and the complex chromatin structure becomes more relaxed at the RE, therefore facilitating access of the RNA polymerase II to the subtelomeric DNA. This is reinforced by findings from a previous report describing that the Ty5-1 retrotransposon, a subtelomeric transcriptional unit located at the in *S. cerevisiae* IIIL is silenced at the wild type strains but is derepressed in a *sir3* mutant (Vega-Palas et al., 1997). Other findings by the same group showed that the loss of Ty5-1 silencing was due to a reorganisation of the chromatin structure at the Ty5-1 in *Sir3* mutant (Vega-Palas et al., 1998). Evidences of the abrogation of silencing at the HM loci, telomeres and rDNA due to *sir2* mutation at the core sequence have been also reported (Sherman et al., 1999).

4.1.3 Chromatin studies undertaken at *URA3* gene

Numerous chromatin studies have been carried out with the *URA3* gene. For instance, low resolution studies of the nucleosome positions at the *URA3* gene when integrated in a minichromosome (YRpTRURAP) have been examined using MNase and *DNaseI* (Thoma, 1986). This was followed by high resolution nucleosome position with *URA3* gene at its natural location (Tanaka et al., 1996). In both instances, nucleosomes at the *URA3* gene adopt a similar position. Six positioned nuclesosomes were described in the gene and thus chromatin organisation correlated with the low expression of the gene. In the 5' and 3' *URA3* flanking regions, the chromatin is packaged via positioned nucleosomes. In the promoter region there is a dominant position for a nucleosome located at the edge of the TATA box. However, there also are alternative positions for this nucleosome in which the TATA box is included in a nucleosome. Therefore, in the case of *URA3*, the nucleosome arrangement may influence the gene expression (Tanaka et al., 1996; Thoma, 1986).

4.2 Results

4.2.1 *URA3* chromatin is more sensitive to MNase in the NRE

In order to later study the influence of chromatin on NER and *URA3* expression, the accessibility of the DNA was first analysed by the ability of nucleosomes and silencing proteins to protect DNA from MNase digestion.

The region selected was the *Mse*I restriction fragment located in the coding region of the subtelomeric *URA3* gene and is 640 bp in length (from +221 to +861 bp). The NRE and RE strains were grown in complete medium and the chromatin treated with increasing amount of MNase. As control, naked DNA was also treated with increasing amount of MNase. Figure 4.2 shows gels for DNA mapping MNase sensitive sites in the TS and NTS of the *Mse*I fragment of the *URA3* coding region at the RE and NRE. The relative intensity of each band is represented graphically in figure 4.3, where the higher the band peak, the higher the accessibility of the DNA to MNase. When the fragment is not treated with MNase, there is a strong band at the top of the gel which indicates the full length fragment and smaller fragments in untreated samples are due to unspecific labeling or spontaneous breakage.

The results indicate that overall, the sequence in chromatin at the RE is more protected from MNase cleavage than when at the NRE. A region protected from MNase digestion when *URA3* is at the RE is indicated as A on the gel (figure 4.2). This protected region is also indicated as A in the NTS (region from 540 to 722 bp) in figure 4.3. Thus, the protected region in the NTS is from +540 to +722 bp (182 pb length). However in the TS, the protected region probably extends to +861 bp (321 bp length).

Clearly, there is a difference in MNase accessibility at *URA3* between the NRE and RE strains. These differences correlate with *URA3* expression as described in Chapter III. When *URA3* is at the RE, the gene is not expressed, and the chromatin adopts a closed conformation; whereas when it is at the NRE, the *URA3* gene is expressed and the chromatin has a more relaxed structure.

Figure 4.2 *A Typical footprinting autoradiograph to analyse* MNase *sensitivity sites at high resolution for Mse*I *fragment of* URA3 *when at the NRE and RE.* In these gels the NTS and TS for the repressive and non repressive ends were studied. The Sanger sequence of the *URA3 Mse*I fragment is shown on the left hand side in the combinations of A and G, C and T. Chromatin protected region at the repressive end are indicated by A and a bracket. DNA and chromatin samples from each strain were treated with increasing amount of MNase. For each set of chromatin samples the concentrations used were untreated, 10 U/ml, 20 U/ml, 40 U/ml and 45 U/ml from left to right. The naked DNA was untreated or treated with 10 U/ml, 20 U/ml and 30 U/ml of MNase from left to right.

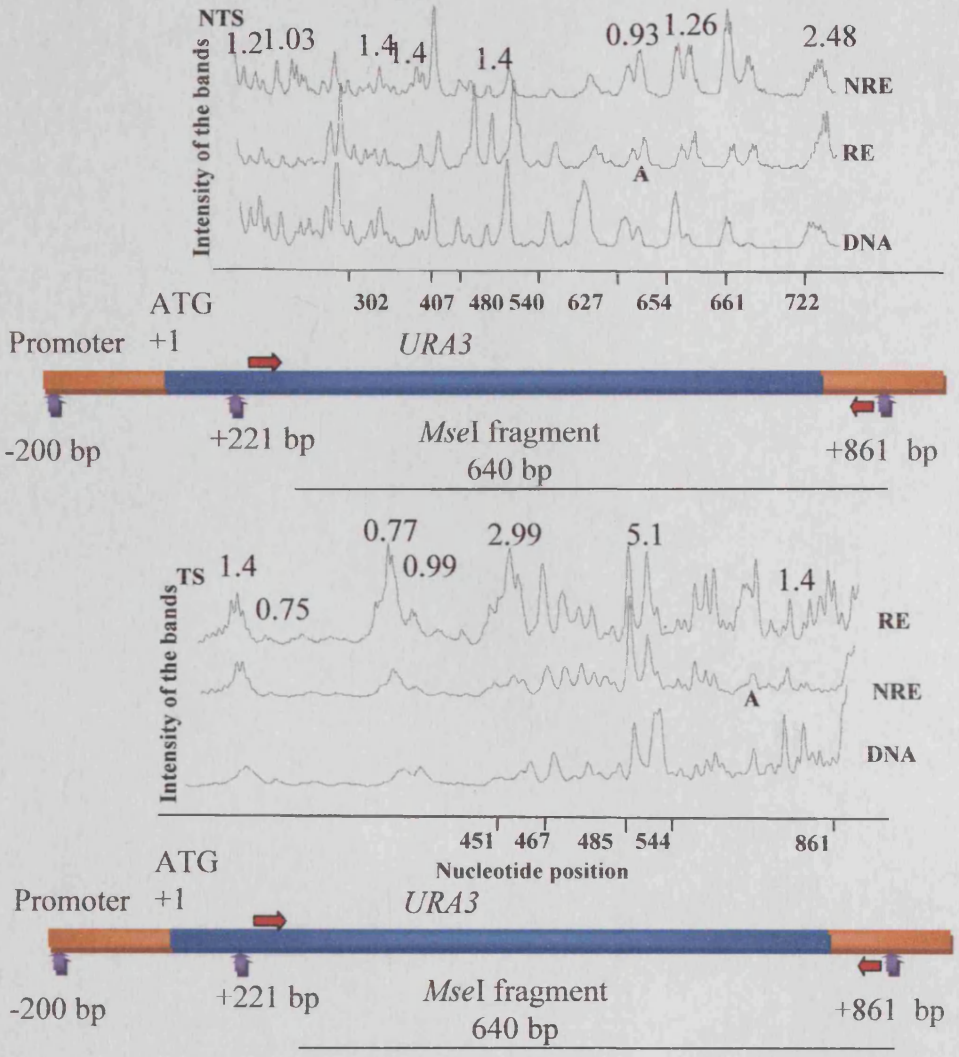

Figure 4.3 *Graphs showing* MNase *sensitive patterns of the* URA3 *MseI fragment at NRE and RE.* After scanning the gel, the relative MNase accessibility is plotted graphically. The orange boxes indicate the regions in the chromatin where the DNA is less accessible to MNase. The numbers above the curves indicate the ratio (peaks intensity) between NRE and RE (NRE*vs* RE).

4.2.2 The MNase sensitive patterns between the NRE and RE are similar in *SIR2* mutants

MNase accessibility was also examined in the strains where *SIR2* is deleted to determine whether the disruption of silencing can affect the chromatin structure.

The MNase cleavage sites on the *Mse*I restriction fragment were mapped at high resolution. Figure 4.4 shows typical gels for the TS and NTS of the *URA3 Mse*I restriction fragment digested with increasing amount of MNase at NRE*sir2Δ* and RE*sir2Δ*. The graphs represented in figure 4.5 are the analysis of such gels, where higher the peaks represent higher accessibility of the DNA to the MNase. MNase

sensitivity was shown to be similar in NRE*sir2Δ* and RE*sir2Δ*. Only the region from +503 to +540 bp showed a difference between them, this being more prone to MNase cleavage in the RE*sir2Δ*, where *URA3* is at the repressive end. The inaccessibility at the NRE could be caused by the binding of TFs to the DNA.

Three biological repeats were undertaken with the experiments presented in this chapter and the band patterns were similar between repeats.

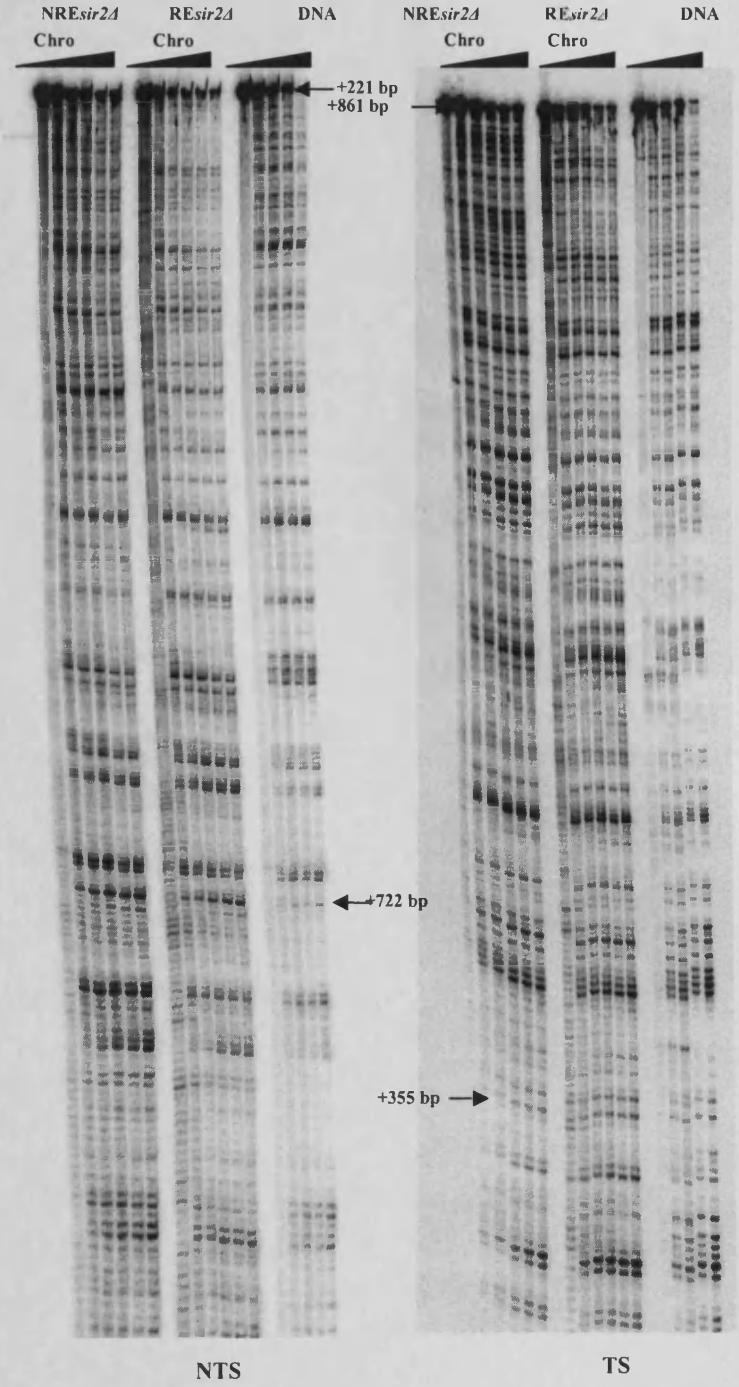

Figure 4.4 *A Typical footprinting autoradiograph to analyse* MNase *sensitive sites at high resolution in the Mse*I *fragment of the subtelomeric URA3 gene for the NREsir2Δ and REsir2Δ.* These gels represent the NTS and TS for the repressive and non-repressive ends in *sir2Δ*. DNA and chromatin samples from each strain were treated with an increasing amount of MNase. For each set of chromatin samples the concentrations used were untreated, 10 U/ml, 20 U/ml, 40 U/ml and 45 U/ml from left to right. Naked DNA was untreated or treated with, 10 U/ml, 20 U/ml and 30 U/ml of MNase from left to right.

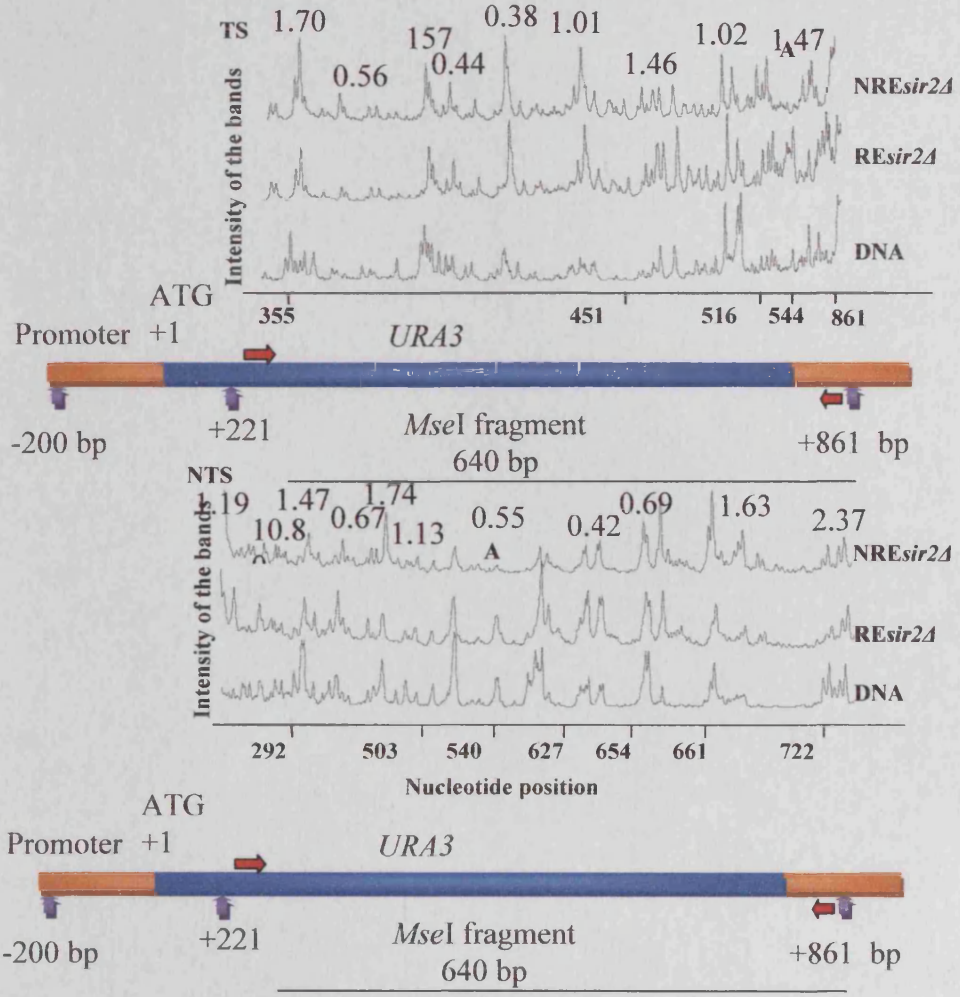

Figure 4.5 *The Graph represents the* MNase *sensitivity in the URA3-containing Mse*I *restriction fragment for the NREsir2Δ and REsir2Δ strains.* A chromatin region protected from digestion at the repressive end is indicated by A. DNA and chromatin samples from each strain were treated with an increasing amount of MNase. For each set of chromatin samples the concentrations were untreated, 10 U/ml, 20 U/ml, 40 U/ml and 45 U/ml from left to right. The naked DNA was untreated or treated with 10 U/ml, 20 U/ml and 30 U/ml of MNase from left to right. The numbers above the curves indicate the ratio (peaks intensity) between NRE and RE (NRE*sir2Δ vs* RE*sir2Δ*).

4.3 Discussion

In this chapter the accessibility of the MNase to different subtelomeric regions is described but not the nucleosome locations since the study was undertaken at high resolution and bands do not correlate with the linker regions in the chromatin. These extra bands could be generated since the MNase enzyme not only digests the linker regions, but also the single-stranded DNA. Therefore, the findings presented here only reflect the chromatin status not the nucleosome locations.

4.3.1 The subtelomeric *URA3* chromatin is more sensitive to MNase when it is in the NRE strain

In summary, the findings correlate well with the formulated hypothesis that chromatin differs at both chromosome end, NRE and RE. Moreover, DNA accessibility correlates with the subtelomeric *URA3* expression. The main changes in MNase accessibility at the *URA3* between RE and NRE are found in the terminal region of the coding sequence where in the NRE the DNA is more accessible to the MNase than when at the RE. Essentially, from +540 to +722 bp (182 bp long) the DNA is more accessible when at the NRE. The other region that is more accessible at the NRE is from +355 to +485 bp and this fragment is 130 bp long. This result is in agreement with a previous report where the transcriptional status of a gene and the accessibility to the DNA are associated; the higher the transcription the more accessible is the chromatin to restriction enzymes (de Bruin et al., 2000). Thus, given the chromatin structure in this region influence the accessibility of transcription factors, the NER machinery may also have a reduced access. Previous studies in chromatin structure and repair rate enforce this suggestion (reviewed by Nag and Smerdon, 2009).

This variation in chromatin structure is likely to be due to the difference of silencing between these chromosome ends. Indeed differences in concentration of Sir proteins between chromosome ends (Mondoux and Zakian, 2007; Pryde and Louis, 1999) may influence the organisation of the chromatin.

Telomere length may be another factor which could affect chromatin organisation, as well as the differences in the subtelomeric sequences, and the differences in the spreading of silencing elements (explained in Chapter III). Thus, the causes of the variation in the subtelomeric *URA3* gene expression could be the causes of different chromatin structure at both chromosome ends.

As mentioned before, the results suggest that the chromatin organisation differ between chromosome ends being more relaxed at the NRE than at the RE. This implies that chromatin structure influences the transcription of the subtelomeric *URA3* gene. How silenced chromatin represses gene transcription is poorly understood. However, it has been reported that transcriptional repression can be undertaken at different steps in transcription and several models have been proposed to explain this repression. For example, the steric hindrance model where there is an inhibition of the accessibility of sequence specific proteins to the DNA (Gao and Gross, 2006; Rusche et al., 2003), or the downstream inhibition model where the pre-initiation complex (PIC) can be recruited to the DNA but transcription is blocked downstream of an activator binding in a SIR-dependent manner (Gao and Gross, 2008; Lee et al., 1993; Sekinger and Gross, 2001). Recently, the PIC interference model has been described, where the gene specific activator is recruited to its binding site but the recruitment of PIC to the promoter is blocked (Chen and Widom, 2005).

Evidence of chromatin organisation acting as a transcriptional regulator in humans has been reported. For example, the human granulocyte-macrophage colony-stimulating factor enhancer forms several tissue specific enhanceosome-like complexes that replace nucleosomes. Thus, this enhancer is divided in modules that are differentially regulated and adopts a different nucleosomal architecture in different tissues or cell types (Bert et al., 2007). In *Bombix mori* the transcription of *tRNA* genes can also be regulated by chromatin or nucleosome organisation (Parthasarthy and Gopinathan, 2005).

However, when transcription is activated it does not always lead to nucleosome loss. For instance, in galactose regulated yeast genes, there is chromatin reorganisation during activation and repression. Thus, there is no significant nucleosome loss due to transcription, and the inactive chromatin structure is restored when the gene becomes repressed (Cavalli and Thoma, 1993). On the contrary, for other transcriptionally active genes, there is nucleosome loss. It is possible that structural perturbation occurs during transcriptional activation and that the regeneration of the inactive chromatin structure can be gene specific. Thus, reorganisation of the inactive chromatin can be dependent on several factors such as a different affinity of the DNA sequence for the nucleosome and transcription rate.

4.3.2 The chromatin organisation is similar in the RE*sir2Δ* and NRE*sir2Δ*

The accessibility to MNase of the *URA3* sequence in both chromatin environments became similar and only the region from +503 to +540 bp ~ shows a difference between both chromosome ends. This is more prone to MNase cleavage at the RE*sir2Δ* than at the NRE*sir2Δ*, where *URA3* is at the repressive end. This 37 bp region may be occupied by transcription factors and proteins involved in the expression of the gene since this result correlated with the subtelomeric *URA3* expression in the *SIR2* mutated strains.

Like mutations in *SIR3* and *SIR4*, the mutation in *SIR2* eliminates transcriptional silencing in HM and the subtelomere (Aparicio et al., 1991). Moreover, when *SIR2* is mutated, Rap1p, Sir3p and Sir4p are not found in telomeric foci (Gotta et al., 1997). At the transcriptional silencing cryptic mating type loci, HMR and HML, deletion of *SIR2* or *SIR4* lead to a failure in the recruitment of *SIR3* protein. Thus, the highly organised chromatin structure is dissociated in the *SIR2* mutant and the chromatin becomes more open, so facilitating the expression of genes previously silenced by silent chromatin (Fritze et al., 1997; Gao and Gross, 2008).

SIR2 also reduces the accessibility of the sequences by regulating the chromatin structure at the rDNA. This affects transcriptional silencing and suppresses recombination at the rDNA. Furthermore, when *SIR2* is over-expressed, rDNA gene expression is reduced (Fritze et al., 1997). For example, the rDNA is encoded by RND1 which the chromatin has heterochromatin characteristics. Ty1 retrotransposons are frequently integrated in these regions, becoming transcriptionally silenced. However, when *SIR2* is disrupted the transcription of Ty1 becomes active (Bryk et al., 1997; Smith and Boeke, 1997). Evidence of the association *in vivo* of *SIR2* product with the rDNA has also been reported, however, in the contrary to telomeres this association does not required other Sir proteins (Gotta et al., 1997).

In this chapter, after disruption of silencing, the *URA3* gene is expressed at both chromosome ends and the DNA accessibility become comparable at the RE and NRE. These results suggest that proteins involved in silencing can stabilize the chromatin and when the silencing is interrupted, the chromatin can mobilize and the DNA becomes more accessible to processes such as repair and transcription.

In summary, the results strongly suggest that the expression of the silenced or repressed subtelomeric *URA3* (Chapter III) is regulated by chromatin structure,

because mutations that disrupt silencing produce a more open chromatin structure at the repressed gene (figure 4.6).

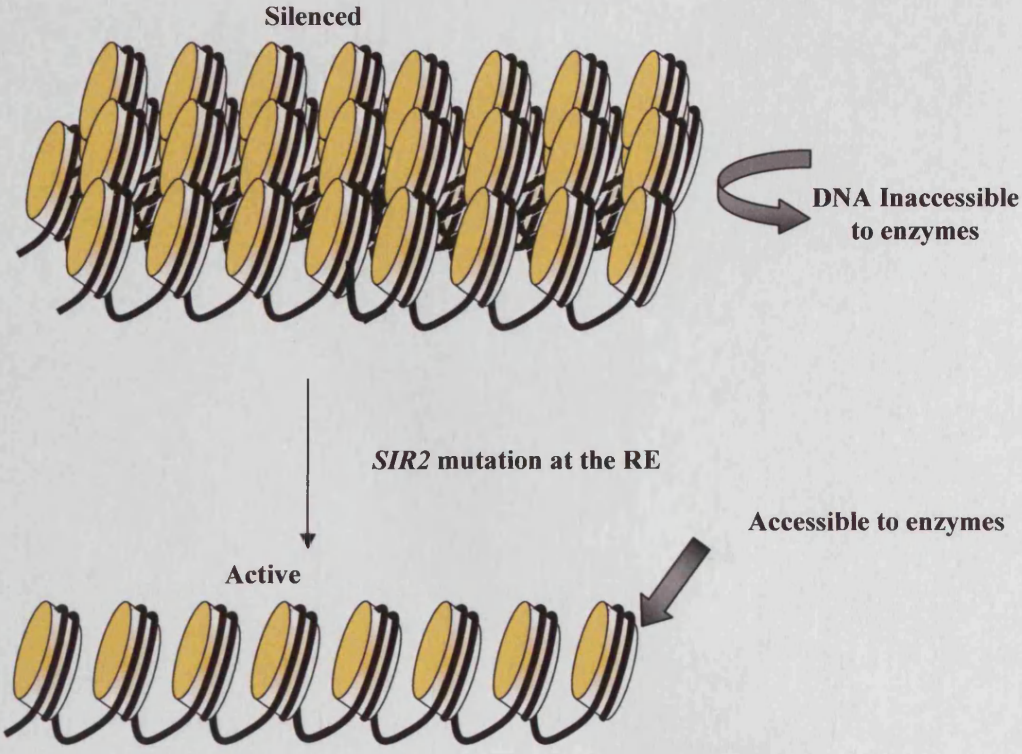

Figure 4.6 *The possible influence of the SIR2 deletion in the chromatin structure of the RE strain.* The silenced chromatin acts as a barrier for metabolic processes. After the mutation of *SIR2* the highly compacted chromatin change to more relax chromatin structure so the genes located there can be active transcriptionaly and accessibility to enzymes involved in DNA repair increase.

4.3.3 The NER rate and the chromatin structure

There are several studies undertaken by our group in *MET16* and *MET17* in addition to others which suggest that chromatin structure can also influence the DNA repair rate as well as gene expression (Bedoyan et al., 1992; Bi et al., 1999; Ferreiro et al., 2004; Powell et al., 2003) . For the cellular *MFA2α* gene when *GCN5* (HAT) is mutated, the repair rate is slower (Teng et al., 2002; Vetting et al., 2005). In the next chapter the NER repair rate for *URA3* at the NRE, RE in wild type and the *sir2Δ* strain was determined to see whether the chromatin structure and the abrogation of silencing have an effect on NER rate.

Chapter V

ANALYSIS OF DNA REPAIR EFFICIENCY IN THE RE AND NRE

5.1 Introduction

Cells have to maintain genome integrity. Therefore, the efficient repair of DNA damage from extracellular and intracellular agents is vital. One of the repair mechanisms is NER; this is a highly conserved repair mechanism that removes bulky DNA lesions including UV induced CPDs, (6-4) PPs and other chemical adducts (de Laat et al., 1999; Prakash and Prakash, 2000). Eukaryotic NER requires approximately 30 proteins to remove damage from naked DNA. As mentioned in Chapter I (page 16) the mechanism is divided into two subpathways; TC-NER, repairs the TS of transcriptionally active genes and GG-NER repairs the NTS of transcriptionally active genes and both strands of transcriptionally inactive genes. The TC-NER subpathway tends to repair damage faster than GG-NER as restoring the ability to transcribe appears to be a priority. This faster repair is probably due to the recognition of the damage undertaken by the stalled RNA polymerase II at the DNA lesion and other proteins that are shared between transcription and TC-NER (Coin et al., 2008; Li et al., 2006; Prakash and Prakash, 2000).

The core NER mechanism operation on naked DNA was first determined (Aboussekhra et al., 1995; Guzder et al., 1995) and afterwards, the NER efficiency was studied in a chromatin environment (reviewed by Teng et al., 2008; Waters and Smerdon, 2005). *In vitro* studies, using reconstituted nucleosome as templates showed that nucleosomes exert an inhibitory effect on NER since the packaging of DNA into nucleosomes in living cells and chromatin provides a completely different template from naked DNA. Thus, the overall repair of DNA damage by NER is less efficient in nucleosomes than in naked DNA (Wang et al., 1991).

Interactions between nucleosomes and NER have been long documented, and they reflect the influence of the static and dynamic aspects of nucleosomes on the process (Ferreiro et al., 2004; Livingstone-Zatchej et al., 2003). The chromatin organisation within the location of a particular DNA damage significantly affects the efficiency of NER. For instance, high resolution mapping of CPD repair by NER revealed a faster repair of lesions in linker DNA and towards the 5' end of positioned

nucleosomes and a slower repair in the centre or in the "internal protected region"of the nucleosomes. However, this modulation was only found in the NTS of active genes and in both strands of inactive genes in several *S. cerevisiae* loci (Ferreiro et al., 2004; Li and Smerdon, 2002; Tijsterman et al., 1999; Wellinger and Thoma, 1997). In other words, repair modulation was found in the strands where the location of the nucleosomes and the chromatin is more stable or compact. Some examples where repair efficiency is regulated by the chromatin are at the *URA3* gene (Tijsterman et al., 1999; Wellinger and Thoma, 1997), the *GAL1-10* promoter (Allinen, 2002) and the *MET16* (Ferreiro et al., 2004).

On the contrary, for the TS of active genes the repair rate is more homogeneous since the chromatin is more relaxed possibly leading to an easier access of the NER machinery. This also suggests that chromatin structure is a factor which can modulate the repair efficiency. Another evidence of the chromatin structure influence in NER is the work described by Ferreiro et al. (2004) where they examined the repair of *MET16* to clarify the relationship between chromatin, transcription and repair. In the *MET16* gene, the Cbf1p and the grown media can modulate the chromatin structure, transcription and repair. For example, the transcription of *MET16* is repressed when a *cbf1Δ* strain is grown in minimal medium. In this case, the MNase digestion pattern of chromatin reveals a more compact region, mainly around the TATA box. However, in the wild type strain, the chromatin is more MNase sensitive at the TATA box. This modulation of the chromatin structure influenced transcription which is induced in minimal medium (derepressing conditions) in the *CBF1* wild type cells, but not in the mutant strain. When DNA repair rate was studied at *MET16*, a general influence of Cbf1p on the CPD repair rate was found; repair was less efficient in the *cbf1Δ* compared to the wild type strain. Moreover, under the derepressing and repressing conditions, with both the wild type and mutant strains, the repair rate pattern for *MET16* is not homogeneous showing the nucleosome positions in the chromatin at the NTS. It is worthy to note that in the *cbf1Δ* strain, *MET16* under derepressing and repressing conditions is lowly transcribed. On the contrary, in the wild type strain, under derepressing condition *MET16* is highly transcribed and under repressing conditions is lowly transcribed. Repair trends may thus vary for genes with different status of transcription and different chromatin structure.

Chromatin remodellers have been implicated in the modulation of the chromatin structure and they are linked to permit transcription and repair processes. Evidence of

this is the Rad16p, a protein involved in the damage recognition during yeast GG-NER. This protein can modify the chromatin to allow damage recognition for the repair machinery. Furthermore, it has been proposed that Rad16p might be a chromatin remodeller from the SWI/SNIF family due to the fact that it shares homology with Snf2p, the catalytic subunits of SWI/SNF, and alters the chromatin environment leading to the recognition of the lesion (Bang et al., 1992; Bi et al., 2004; Teng et al., 2008).

Other examples of chromatin remodellers which are involved in modulating the chromatin to allow repair by the NER are the subunits Snf5p and Snf6p of the yeast chromatin remodelling complex SWI/SNF. These subunits can be co-purified with Rad4p and Rad23p, which are factors involved in early damage recognition in NER (Gong et al., 2006). A SWI/SNF remodeller complex has been reported to stimulate NER both *in vivo* and in reconstituted nucleosomes (Gong et al., 2006; Hara and Sancar, 2002), possibly by facilitating access of the Rad4p and Rad23p which triggers the recognition step of NER to the DNA lesion. Swi2p, another component of SWI/SNF complex, is involved in remodelling the chromatin structure after UV irradiation facilitating the DNA accessibility in the chromatin at the *MFA2* promoter region (Yu et al., 2005).

Results shown in Chapter III and chapter IV strongly suggest that the chromatin environment is related to the subtelomeric *URA3* expression. Thus, at the NRE the DNA is more accessible to MNase and the gene is expressed. On the contrary, at the RE, the DNA is less accessible to MNase and thus the gene is not expressed.

When the *SIR2* gene was deleted, the chromatin structure and the expression of the *URA3* gene were affected. The MNase sensitivity and the expression of the gene become similar at both, the RE and NRE. The influence of the *SIR2* deletion was more dramatic at the RE than at the NRE. These results suggest that *SIR2* negatively affects gene transcription and chromatin organisation. In addition, the NER rate may also be affected as a result of these chromatin organisations. In this chapter the repair efficiency of CPD removal at the sequence level of the *URA3* gene is described. Once again, the strains for this study were RE, NRE, NRE*sir2Δ* and RE*sir2Δ*.

This system hopefully would enable a better understanding of the correlations between chromatin structure and NER since the same sequence can be studied in different chromatin environments.

5.2. Results

5.2.1 Quality of DNA

Yeast cells were UV treated and allowed to recover in complete medium for 0, 1, 2, 3 or 4 repair hours. DNA from each sample was then extracted and the quality of the extracted DNA was analysed in agarose gels. Figure 5.1 shows typical gels to determine the quality of the extracted DNA for the NRE and RE strains. Figure 5.2 shows the typical quality of the extracted DNA for the NRE*sir2Δ* and RE*sir2Δ* strains.

Sharp bright bands of DNA are observed in all of the gels (figure 5.1 and figure 5.2) indicating high quality DNA for all of the samples. Therefore, the analysis of CPD repair rate was undertaken with the DNA of samples such as shown below.

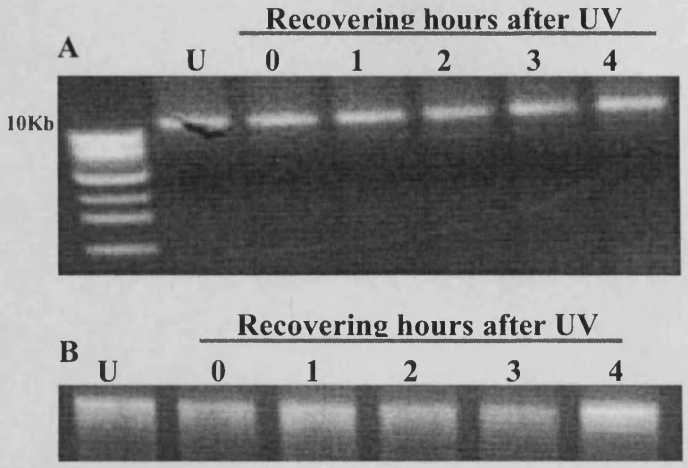

Figure 5.1 *Quality of the extracted DNA from the NRE and RE strains.* (U) Represent the sample taken before the UV and (0, 1, 2, 3, 4) represents the samples taken 0, 1, 2, 3, 4, hours after UV (**A**) shows the DNA from the NRE strains (**B**) shows the DNA from the RE strains.

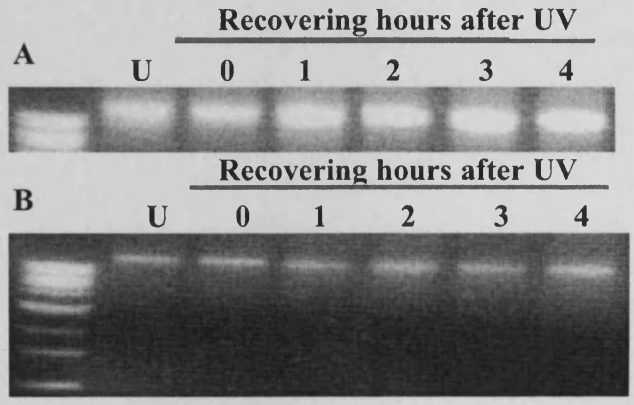

Figure 5.2 *Quality of extracted DNA from NREsir2Δ and REsir2Δ strains.* (U) Represent the sample taken before the UV and (0, 1, 2, 3, 4) represents the samples taken 0, 1, 2, 3, 4, hours after UV (**A**) shows the DNA from the NRE*sir2Δ* strains (**B**) shows the DNA from the RE*sir2Δ* strains.

Next, good quality intact DNA was digested with the *Mse*I restriction endonuclease and the digestion was analysed via another agarose gel. As an example, figure 5.3 illustrates digested DNA from the wild type NRE strain with the samples collected before and after UV.

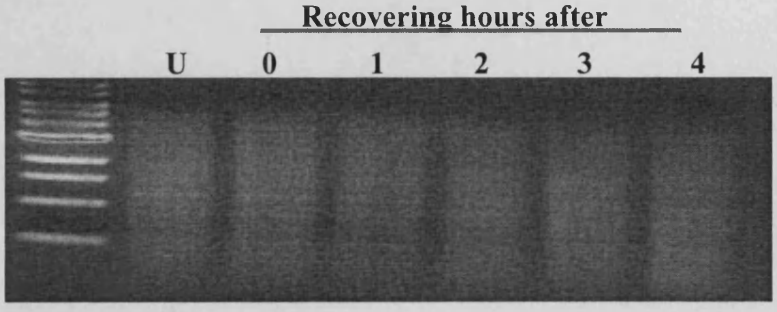

Figure 5.3 *Genomic DNA digested with Mse*I *restriction enzyme.* A smear indicates a good digestion of the DNA. (U) Represent the sample taken before the UV and (0, 1, 2, 3, 4) represents the samples taken 0, 1, 2, 3, 4, hours after UV.

5.2.2 The NER efficiency in the NRE and RE strains

The NER of CPDs in the *URA3* gene at the NRE or the RE was investigated at the sequence level. After the digestion with *Mse*I, the DNA was treated with a crude extract of *M. luteus* containing an endonuclease V, an enzyme which cuts where the CPDs are produced in the DNA. The fragments were labeled and ran on a polyacrylamide gel (described by Teng et al., 1997). Figure 5.4 shows DNA sequencing gels from the subtelomeric *URA3 Mse*I restriction fragment for the TS and NTS at both strains. Each band represents a specific position in the DNA where CPDs occur. The intensity of the bands indicates the extent of damage at particular positions

within the sequence. The non-radiated sample (U) provided a unique top strong band indicating the full-length fragment. UV-irradiated samples were taken either immediately after 150 J/m^2 of UV (0 repair hour) or at various times after UV (1, 2, 3, 4 repair hours) to determine repair efficiency. These samples resulted in multiple fragments on the sequencing gel. Full size fragments indicate molecules where no damage was induced. The size of these fragments is smaller than the intact fragment and it represent the location of the DNA damage. Positions are determined by the Sanger sequence represented in the gel. The decrease in intensity of a particular band with increasing repair time indicates that the damage is repaired. The gels were quantified as described in Chapter II (page 54). CPD repair rates at the *Mse*I fragment are summarized in figure 5.5. This shows the average time (in hours) needed to repair 50% of the initial amount of the lesion (at 0 hours) ($T_{50\%}$) of three independent experiments at each CPD site.

When the differences in repair of this sequence at the RE and NRE are compared, it is clear that NER is much faster when *URA3* is at the NRE for both the NTS ($P<0.0001$, Mann Whitney test) and the TS ($P<0.0001$, Mann Whitney test). The differences in the repair between the TS and the NTS of *URA3* at the RE with the average $T_{50\%}$ for the entire fragment are smaller than at the NRE being 7.77 hrs and 8.18 hrs respectively. However, the repair is faster for the TS compared to NTS when *URA3* is at the NRE, with average $T_{50\%}$ of 2.85 hrs and 4.03 hrs respectively. This faster repair of CPDs in the TS as opposed to the NTS suggests that a TCNER subpathway is involved in the TS repair and the GGNER is involved in the NTS repair.

To conclude, the repair results obtained here correlate well with the MNase sensitivity pattern previously described. When *URA3* is at the RE the chromatin is less accessible to MNase, and the repair of CPDs is slower. For instance, in the TS, the repair at the RE is markedly slower than at the NRE ($P<0.0001$, Mann Whitney test). One of the maximum differences for individual repair of CPDs between both strains (NRE and RE) in the TS was obtained around +561bp, +554/TTTCTCT/+562 (3-fold difference) and one of the minimum differences were found around +478bp, +477/TC/+480 (2-fold difference). At both repair locations, the repair data correlates with the MNase sensitivity. In the RE strain both repair points are a MNase protected region yet are non MNase protected at the NRE.

Figure 5.5 illustrates the differences in DNA repair efficiency of the *URA3* sequence between the NRE and RE at the TS and NTS.

In the NTS repair was also slower at the RE than at the NRE ($P<0.0001$, figure 5.5). One of the maximum differences in repair efficiency of individual CPDs in the NTS between these *SIR2* wild type strains was obtained around +654 bp, +655/CC/+658 (3.47-fold difference) and the minimal differences were around +407 bp, +395/TTT/+399 (1.14-fold difference). Here, once again both individual repair rates correlate with MNase sensitivity where chromatin was protected from MNase at the RE and sensitive at the NRE (figure 5.5).

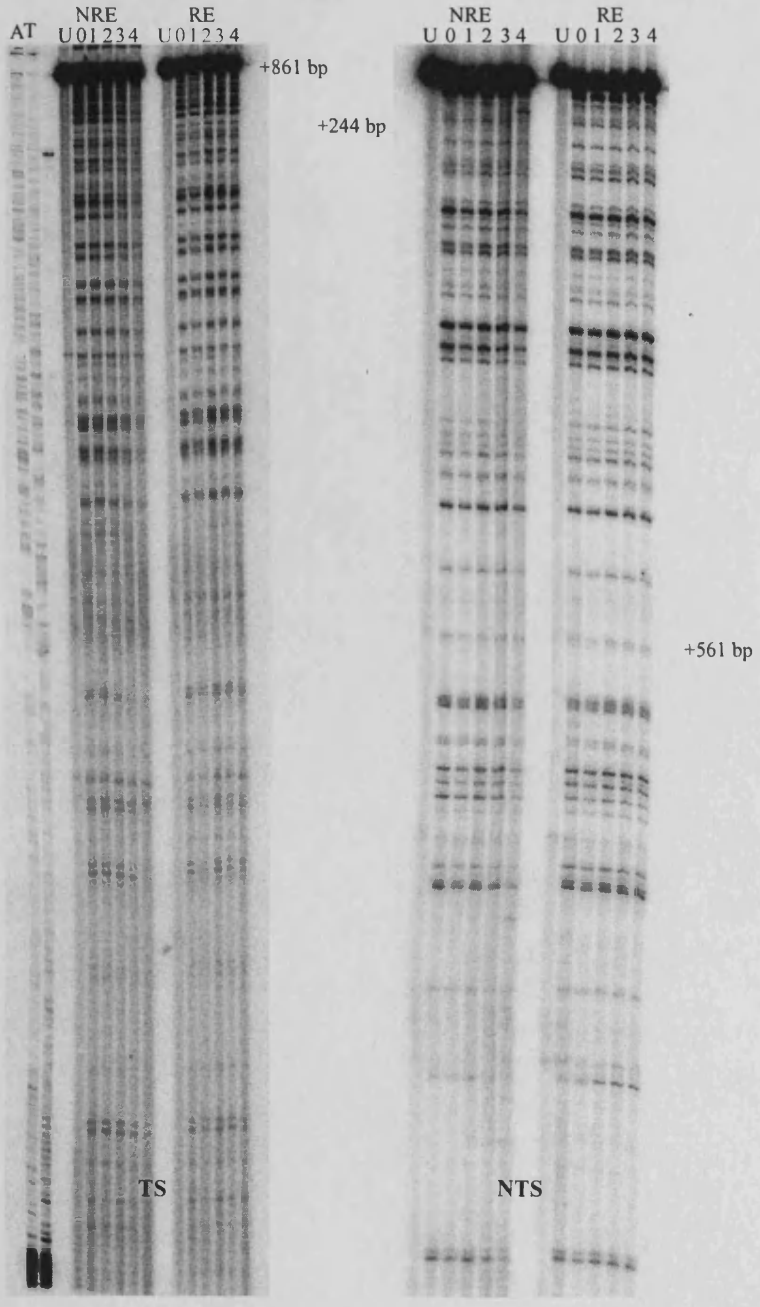

Figure 5.4 *A Representative autoradiograph at nucleotide resolution showing CPDs for the TS and NTS of URA3 at the NRE and RE.* The resolved fragment was the *Mse*I fragment of *URA3*. A Sanger sequence called A and T, containing A+G and C+T respectively, was included to determine the nucleotide position where the damage occurs. U corresponds to untreated cells. Cells were UV treated and allowed to repair the damage for 0, 1, 2, 3 and 4 hours (0, 1, 2, 3, and 4). The intense top bands represent the undamaged *Mse*I fragment of *URA3*, the bands below represent the fragments were the CPD lesion have occurred which were cut with the CPD specific UV-endonuclease.

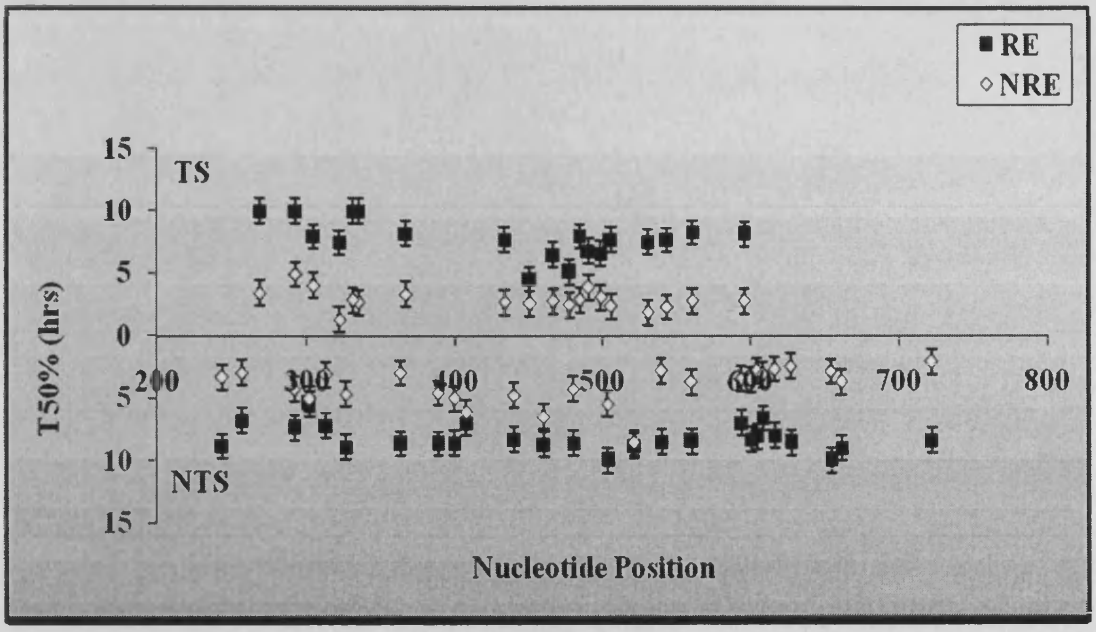

Figure 5.5 *DNA repair efficiency analysis for CPDs in the TS and NTS of URA3 at the RE and NRE.* The graph represents the repair rate for each CPD *versus* the nucleotide position. The rate of DNA repair for the NRE (white diamonds) and RE (black squares) is expressed as the $T_{50\%}$ for CPDs in the TS (top) and NTS (bottom).

5.3.3 DNA repair efficiency when *SIR2* is deleted in the RE and NRE strains

The strains used for the repair analysis were NRE*sir2Δ* and RE*sir2Δ* and the fragment examined was the same *Mse*I restriction fragment of the *URA3* gene as above. The result shows that for the TS, there were still significant differences in the repair rates between the NRE and RE strains when *SIR2* was deleted ($P<0.0001$, Mann Whitney test) (figure 5.6 and figure 5.7). However, this difference in the TS average repair was slightly higher between wild type strains (NRE and RE) than between the NRE*sir2Δ* and RE*sir2Δ* strains (figure 5.8). In the NTS, there were not statistical difference in repair efficiency between the NRE*sir2Δ* and RE*sir2Δ* ($P>0.05$, Mann Whitney test), thus, the differences in the NTS between NRE and RE when *SIR2* is deleted are smaller than between RE and NRE strains (figure 5.8).

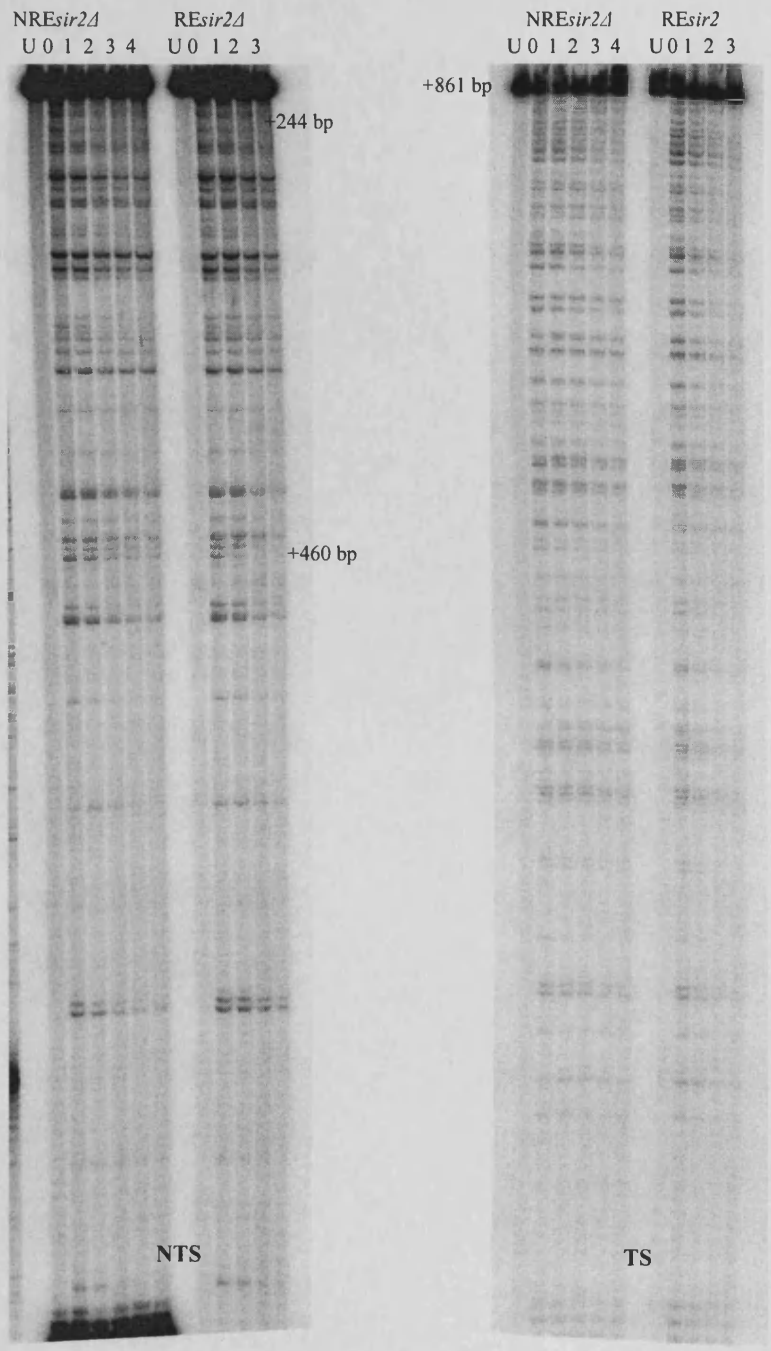

Figure 5.6 *A Representative autoradiograph at nucleotide resolution showing CPDs for the TS and NTS of URA3 at the NREsir2Δ and REsir2Δ.* The resolved fragment was the *Mse*I fragment of *URA3*. U corresponds to untreated cells. Cells were UV treated and allowed to repair the damage for 0, 1, 2, 3 and 4 hours (0, 1, 2, 3, and 4). The intense top bands represent the undamaged *Mse*I fragment of *URA3*, the bands below represent the fragments were the CPD lesion have occurred which were cut with the CPD specific UV-endonuclease.

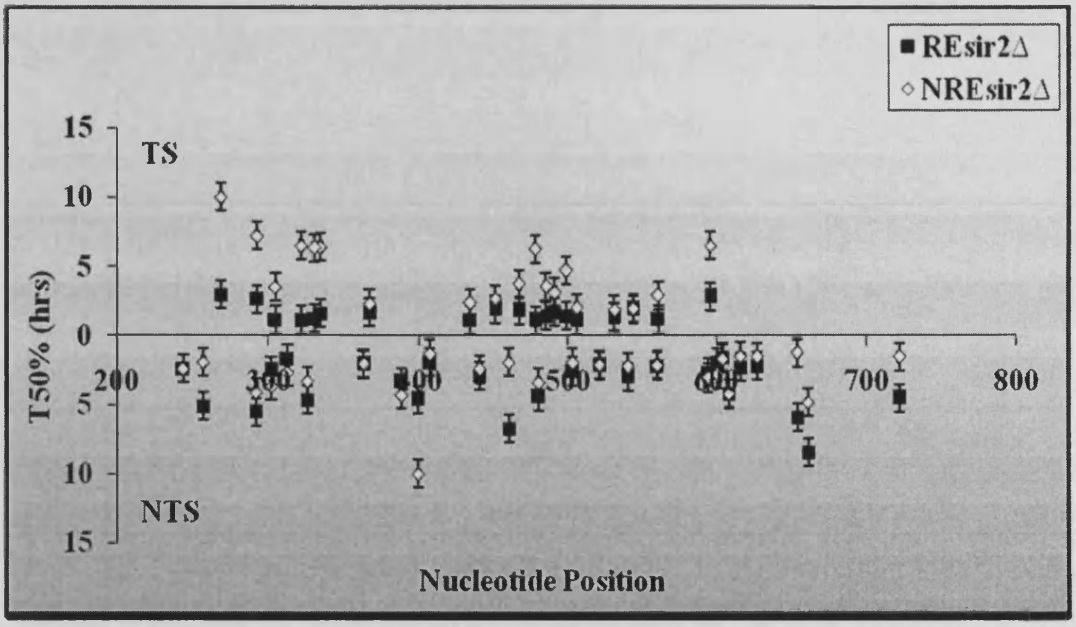

Figure 5.7 *DNA repair efficiency analysis for CPDs in the TS and NTS of URA3 in the NREsir2Δ and REsir2Δ strains*. The graph represents the repair rate for each CPD *versus* the nucleotide position. The rate of DNA repair for the NRE*sir2Δ* (white diamonds) and RE*sir2Δ* (black squares) is expressed as the $T_{50\%}$ for CPDs at the TS (top) and NTS (bottom).

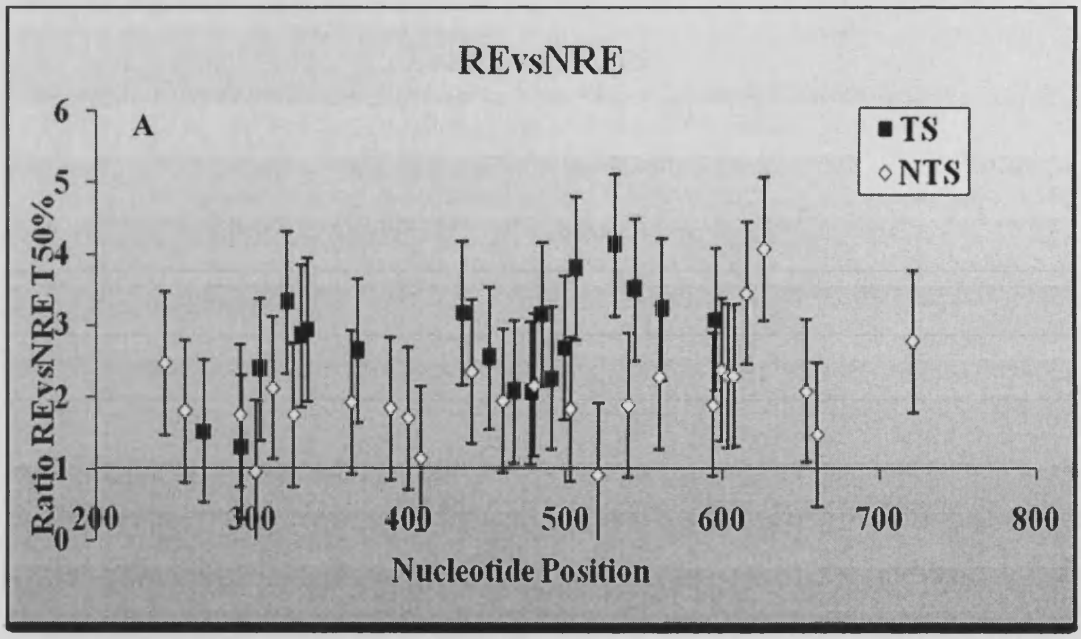

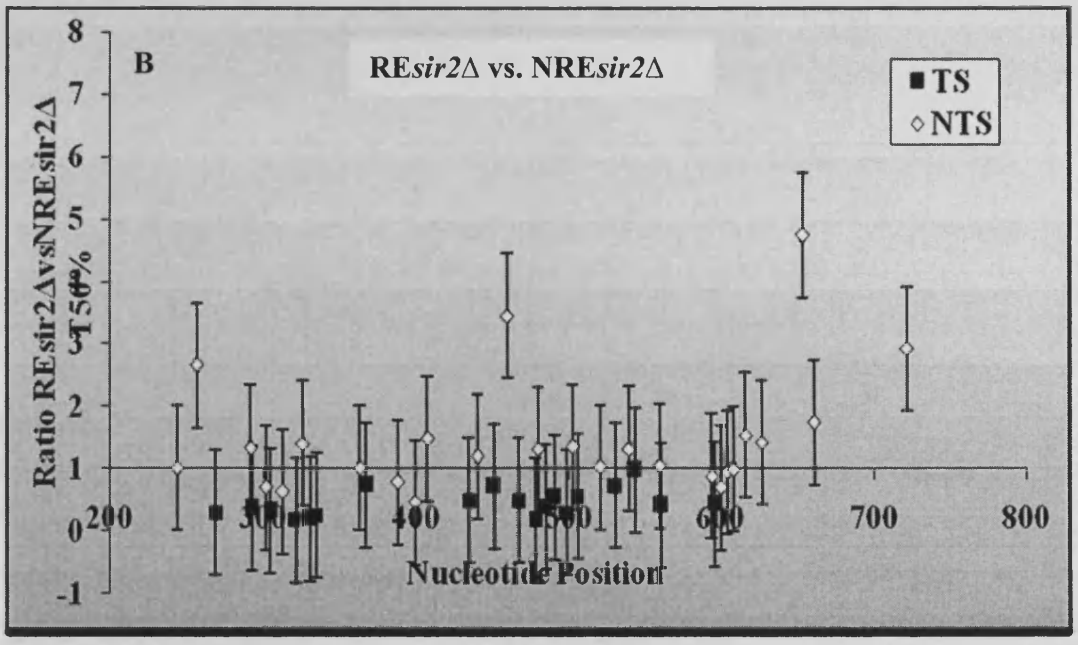

Figure 5.8 *The relative repair ratios of* $T_{50\%}$. **(A)** Shows the repair rate ratio for the RE *versus* NRE. Values above 1 indicate faster repair in the NRE **(B)** shows the repair rate ratio for the RE*sir2Δ versus* the NRE*sir2*Δ strain. The values above 1 indicate faster repair in the NRE*sir2*Δ strain and less than one indicate slower repair in this strain.

The tables presented below are a summary of the differences (Table 5.1) and the statistical significance (Table 5.2) in DNA repair efficiency between the strains.

Table 5.1 *Differences in the average DNA repair efficiency between the strains.* The average has been calculated as the average needed to repair 50% of the lesion.

Fold differences (hours)		
NTS	**TS**	strains
1.41	1.53	NRE vs NRE*sir2Δ*
2.32	4.72	RE vs RE*sir2Δ*
2.02	2.71	RE vsNRE
1.23	2.68	RE*sir2Δ*vs NRE*sir2Δ*

Table 5.2 *Statistical differences in the average DNA repair efficiency between the strains.* The average has been calculated as time needed to repair 50% of the lesions. The statistical analysis has been undertaken using the Mann Whitney test.

Statistical differences		
NTS	**TS**	**strains**
P < 0.05	P >0.05	**NRE vs NRE*sir2Δ***
P<0.0001	P<0.0001	**RE vs RE*sir2Δ***
P<0.0001	P<0.0001	**NRE vsRE**
P > 0.05	P<0.0001	**NRE*sir2Δ*vs RE*sir2Δ***

Further analysis of the data, showed significant differences in the repair rate between the wild type RE and the mutant RE*sir2Δ* for both, the TS and the NTS, repair being faster when the *SIR2* gene is deleted (P<0.0001, Mann Whitney test, figure 5.9). Although the differences were not as big as between RE and *REsir2Δ,* there are also statistical differences in the repair rate between NRE and NRE*sir2Δ* in the NTS (P<0.05, Mann Whitney test, figure 5.9). However, there were not statistical differences in the TS between NRE and NRE*sir2*Δ (P>0.05, Mann Whitney test, figure 5.9). Indeed, in general the difference in repair efficiency between NRE and NRE*sir2Δ* is much smaller than between RE and RE*sir2Δ* (figure 5.9). Thus, the difference in the average repair efficiency between RE and RE*sir2Δ* is 2.32-fold for the NTS and 4.72-fold for the TS. In contrast, the difference in average DNA repair rate between NRE*Sir2Δ* and NRE TS is 1.53-fold for the TS and 1.41-fold for the NTS..

In the RE*sir2*Δ and NRE*sir2*Δ strains, the MNase sensitivity does not correlate with the repair efficiency. For instance, in the NTS the maximum difference in repairing individual CPDs between RE*sir2*Δ and NRE*sir2* is around +654 bp, +655/CC/+658. In this region, the NRE*sir2Δ* is MNase sensitive and the repair is 4.74-fold faster than in the RE*sir2Δ* which is also MNase sensitive region. Another big difference between both strains is found around +460 bp +460/TC/+463, in this case, this region is also MNase sensitive in both strains and the fold difference is 3.40. The minimum difference between RE*sir2*Δ and NRE*sir2*Δ strains is around +363 bp, +353/TT/+355 (1-fold) and in +604 bp +603/CCC/+607 (1-fold) where the chromatin is equally sensitive to MNase in both strains.

In the TS, one of the maximum difference between the RE*sir2Δ* and NRE*sir2Δ* strain in repairing CPDs is around +478 bp, +477/TC/+480, (5.68-fold difference). Another maximum difference is at +331 bp, +331/TCTT/+336 (5.08-fold), whereas one of the minimum is at the +367 bp, +367/CC/+370 (1.3-fold). In this case also, the chromatin of both strains is sensitive to MNase.

To summarize, the repair became faster when *SIR2* is deleted no matter whether *URA3* is in the NRE or the RE, and the rate in these two ends is more comparable. The results imply that the repair is influenced by the chromatin structure and that *SIR2* has a strong effect at the RE but not so much at the NRE. This correlates well with the role of Sir2p in chromatin organisation, silencing or gene expression.

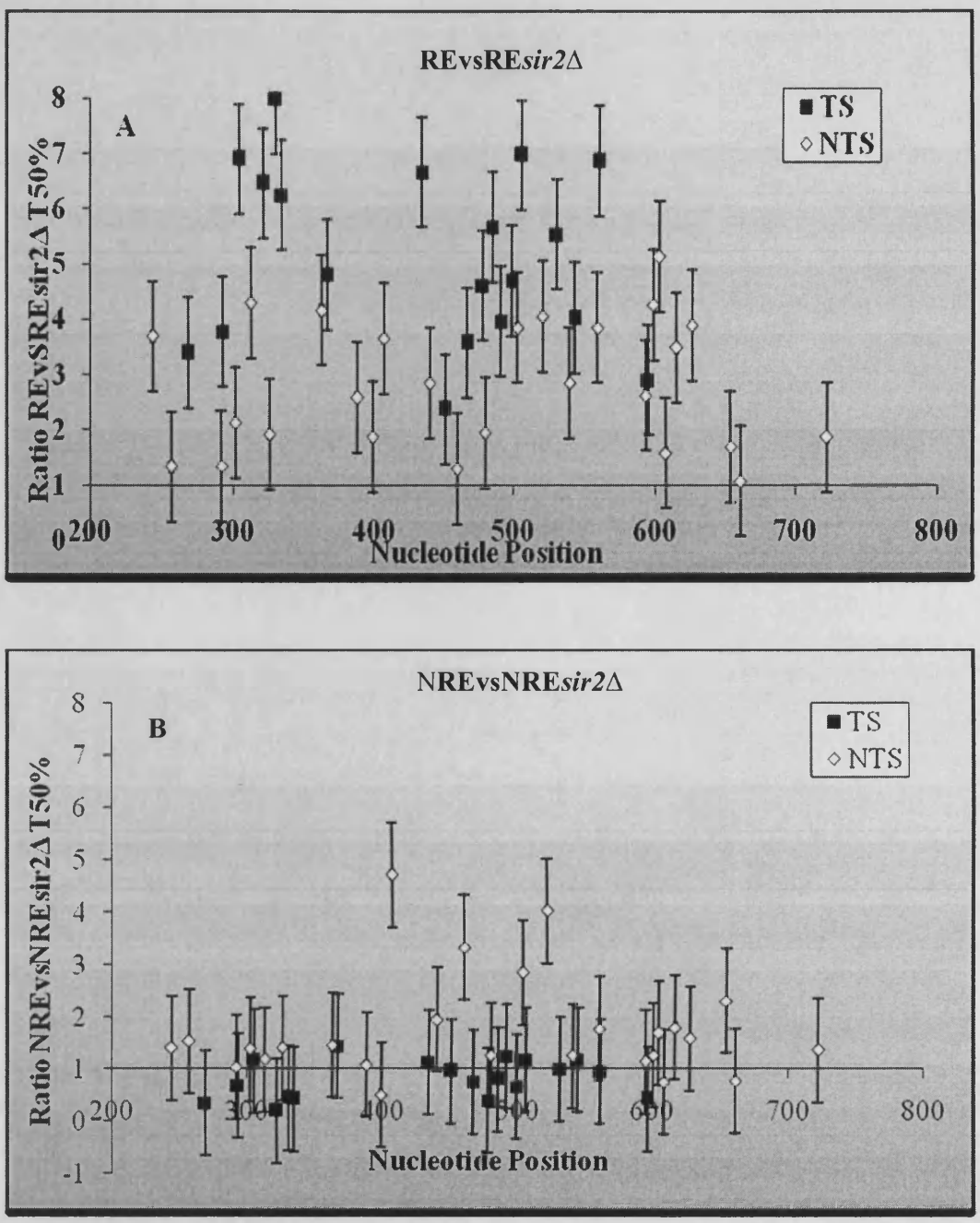

Figure 5.9 *The relative repair rate ratios of* $T_{50\%}$. (A) Shows the repair rate ratio RE *versus* RE*sir2*Δ.Values above 1 indicate faster in RE*sir2*Δ (B) shows the repair rate ratio for the NRE *versus* NRE*sir2*Δ strain. Values above 1 indicate faster repair in NRE*sir2*Δ.

5.4 DISCUSSION

The results presented here show that when *URA3* is at the NRE, the repair efficiency is higher. This correlates with the MNase sensitivity and the expression of the gene which is also higher when *URA3* is at the NRE than at the RE. Thus, the silencing varies between chromosomes ends and the repair efficiency also differs. In general, when *SIR2* is deleted the repair effectiveness increases at the RE and becomes comparable to the repair at the NRE since the chromatin changes and the repression of the *URA3* is being relieved. In the RE*sir2Δ*, the subtelomeric *URA3* is expressed at the same levels as in the NRE*sir2Δ* and the chromatin accessibility to MNase became similar. Thus, these studies suggest that Sir2p and thus, silencing, affects NER efficiency.

5.4.1 NER is faster in the NRE than in the RE strains

It appears that, silencing grades influence the repair efficiency. The simplest explanation is that the chromatin is more compact in the RE, therefore the recognition of the DNA lesions for the repair is inhibited, perhaps because the repair machinery cannot access the DNA damage. To facilitate NER at the RE, the chromatin must change. This is possible because chromatin is dynamic. After the modulation of the chromatin, the nucleosomes become free and can mobilise, permitting the access of NER proteins to the DNA.

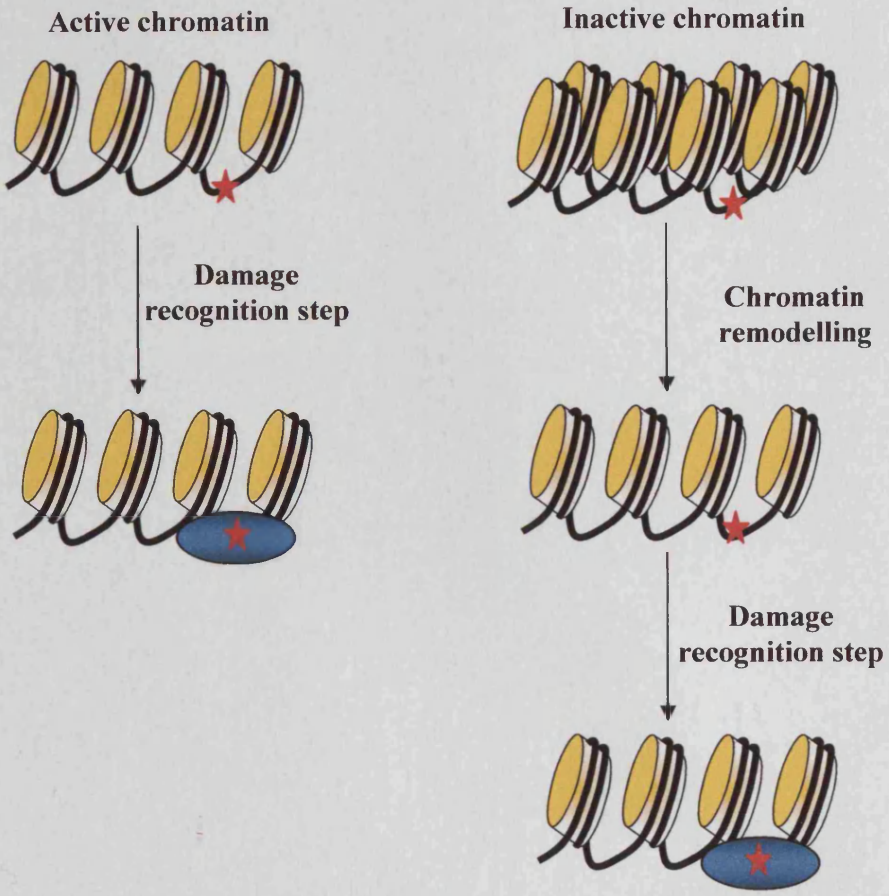

Figure 5.10 *Nucleotide excision repair in different chromatin environment.* The repair at the transcriptionally active chromatin structure does not require the remodelling since the DNA lesion is already accessible for the repair machinery. In contrast, in the inactive chromatin environment, this additional step is needed for the recognition of the lesion.

It is likely that at the NRE the remodelling of the chromatin is not needed to the same extent since it is already modified for gene expression; therefore the repair is faster.

Figure 5.10 shows a hypothetical model (described by Smerdon, 1991) called "the access-repair-restore" model. In this model, after the repair, the chromatin structure is restored. For compacted or inactive chromatin, cells need to remodel the chromatin to access and repair potentially lethal DNA lesions. The remodelling of the chromatin likely requires the operation of ATP-chromatin remodelling complexes and histone tails modifiers. As a result, the nucleosomes become more dynamic and unfold, disrupt or dissociate facilitating the NER. Thus, coordination between chromatin dynamics and repair is required to ensure maintenance of the genetic and epigenetic information. After NER, protein complexes such as chromatin assembly factor-1 (CAF-1) are involved in chromatin restoration.

This hypothesis can explain the results I obtained in this chapter. At the RE, chromatin remodelling is the extra step needed for the repair but not at the NRE, as a result, the NER rate is slower than at the NRE. When *SIR2* is deleted, silencing in the RE strain is abolished and the chromatin structure becomes similar to that of the NRE. This is further described in Chapter IV (page 86 and 91). Consequently, the same extent of chromatin remodelling is not needed before repair. Therefore, the NER rate as well as the expression of the gene becomes similar in the NRE*sir2Δ* and RE*sir2Δ* strains.

Previous experiments have shown that the NER of various DNA damages in the TS of transcriptionally active genes is faster than in the NTS and other non-transcribed regions (Friedberg, 1996). Thus, the results presented in this chapter also show this difference in repair efficiency at the NRE between TS and NTS. On the contrary, at the RE, the repair is more similar in the TS and NTS. However, here the role of the TC-NER sub pathway at the TS of NRE can only be suggested and the unequivocal role of the TC-NER can simply be demonstrated via *rad26Δ* while TC-NER is defective.

As mentioned in the introduction, previous work has been reported showing that repair is not homogeneous in the TS and NTS of transcriptionally inactive genes and in the NTS of active genes. Conversely, NER is faster at the linker regions and slower at the internal protected region of the nucleosome (Allinen, 2002; Ferreiro et al., 2004; Powell et al., 2003; Teng et al., 2002; Wellinger and Thoma, 1997). However, in this study heterogeneity in repair efficiency was not observed. It is possible that the silenced chromatin is so compact that the linker region of the chromatin is also occluded so there are no differences in NER between these regions and the internal protected region of the nucleosomes.

5.4.2 The influence of a *SIR2* deletion on DNA repair efficiency in the RE and NRE strain

When *SIR2* is deleted in the RE strain, there is an elevation in the number of 5-FOA surviving colonies and clear differences in repair efficiency are also observed. The disruption of silencing due to *SIR2* deletion, led to the CPD repair in the NTS becoming similar in the RE*sir2Δ* and NRE*sir2Δ* strains. Surprisingly the repair of the TS is slightly faster in the RE*sir2Δ* than in the NRE*sir2Δ* strain suggesting that the loss of *SIR2* has had more effect at the RE than at NRE. Furthermore, in the

NRE*sir2Δ* strain, there are no significant differences between NRE and NRE*sir2Δ* repair of the TS. The only changes in DNA repair rate occur at the NTS of the NRE*sir2Δ* strain, it being much faster than in the NRE. However, this differences in the NTS are smaller than between RE and *REsir2Δ*. Therefore, it is likely that at the NRE, there is little modification on the chromatin organisation at the NTS caused by *SIR2* deletion. Hence, there are no dramatic effects on the CPD repair efficiency. Thus, there are more differences in repair between the RE and RE*sir2Δ* strains than between the NRE and NRE*sir2Δ* strains.

Unexpectedly, when *SIR2* is deleted the differences in repair rate are still homogeneous at the RE or NRE. In the RE*sir2Δ* and NRE*sir2Δ* strain the chromatin was more similar in terms of accessibility to MNase, so the repair was also similar in both strains. It is likely that the chromatin was more relaxed so the repair was more efficient at the RE*sir2Δ* compared to RE because the differences in repair are greater between RE and RE*sir2Δ* than between NRE and NRE*sir2Δ*. On the contrary, it is likely that at the NRE there are not many differences in MNase accessibility between the wild type and *sir2Δ* strain.

Therefore, the deletion of *SIR2* influenced the elevation in 5-FOA surviving colonies and NER. This correlates with previous work where the dosage of proteins involved in silencing affect DNA repair (Benbow and Dubois, 2008). Additionally, the chromatin structure influences the repair rate and could also influence the transcriptional status (Bedoyan et al., 1992; Bi et al., 1999; Ferreiro et al., 2004; Powell et al., 2003; Vetting et al., 2005).

5.4.3 Acetylation and the role in chromatin structure

It has been reported that histone-tail acetylation destabilises the higher order structures of chromatin (Shogren-Knaak et al., 2006). In addition, there is evidence where acetylation levels can increase in response to UV. For instance, when cells with transcriptionally inactive *MFA2* are treated with UV, the acetylation level at H3 increases thirty minutes after UV treatment allowing DNA repair to take place (Vetting et al., 2005).

As mentioned in Chapter I (page 32), *SIR2* is a histone deacetyltransferase involved in the deacetylation of H4K16. Sir3p has an affinity for H4K16 hypoacetylated histones. Therefore, after the deacetylation of H4K16, Sir3p and Sir4p bind to the H4 spreading the silencing of chromatin from the telomere towards the

centromere. This is explained further in Chapter I (page 38). Thus, H4K16 deacetylation is related to the silencing of the chromatin in telomeres. Sir2p is not only involved in the deacetylation of H4K16 but also in the deacetylation of H3K (9, 14), although to a minor extent (Imai et al., 2000; Tanny et al., 2004).

Therefore, in the next chapter the histone acetylation levels at the NRE and RE will be measured to examine whether there are changes in response to UV.

Chapter VI

ACETYLATION LEVELS FOR URA3 IN THE NRE AND RE STRAINS

6.1 Introduction

Chromatin structure is modulated by ATP-dependent chromatin remodellers, histone modifications (e.g. acetylation, methylation) and histone variants. Generally in nucleosomes, after the action of histone modifiers (e.g. HATs, HDACTs), ATP-dependent chromatin remodellers are recruited to the chromatin and chromatin reorganisation is undertaken.

However, sometimes histone modifiers are directly involved in the remodelling of the chromatin. The most well-studied histone tail modifications are acetylation and deacetylation of histone tails (Kouzarides, 2007) known to regulate functions such as replication, transcription and DNA repair (Altaf et al., 2007; Ehrenhofer-Murray, 2004; Verger and Crossley, 2004). Overall, the acetylation state of histone tails is associated with transcriptionally active regions and the deacetylation state with repressive or silenced regions (Fukuda et al., 2006).

It has been reported that acetylation at different histones results in diverse effects in the nucleosomal organisation and chromatin structure. For instance, acetylation at histone H2B and H4 tail domains results in the abrogation of the tertiary chromatin structure since it causes the reduction of self association to form nucleosomal arrays, whilst the acetylation of the histone H3 tail domain confers instability to the DNA located at the edge of the nucleosome (Kou et al., 2008).

Recently, it has been suggested that a combination of modifications may regulate downstream specific processes such as repair, transcription and replication at a particular region in the genome. This suggestion is termed the histone code hypothesis. Here, histone amino-terminal tails modifications occur at selected residues to make specific patterns which are related to a particular metabolic process. For example, it has been recently reported that in human colon cancer cells, H4K12 acetylation and the histone deacetylase 2 expression (HDAC2) is informative as to the tumour stage in the colon, however, H3K18 acetylation levels are not (Ashktorab et al., 2008).

In budding yeast different H3 and H4 histone modifications act sequentially or in combination to regulate a specific process. In addition, it has been reported that amino and carboxyl terminal tails of the histone H2A are involved in maintaining the silencing levels at telomeres, more specifically, at H2AK (4, 7, 21) (Wyatt et al., 2003). Figure 6.1 shows several examples of specific histone codes and how a combination of modifications at H3 and H4 histones can regulate different biological functions (Downs et al., 2007; Jenuwein and Allis, 2001; Turner, 2000).

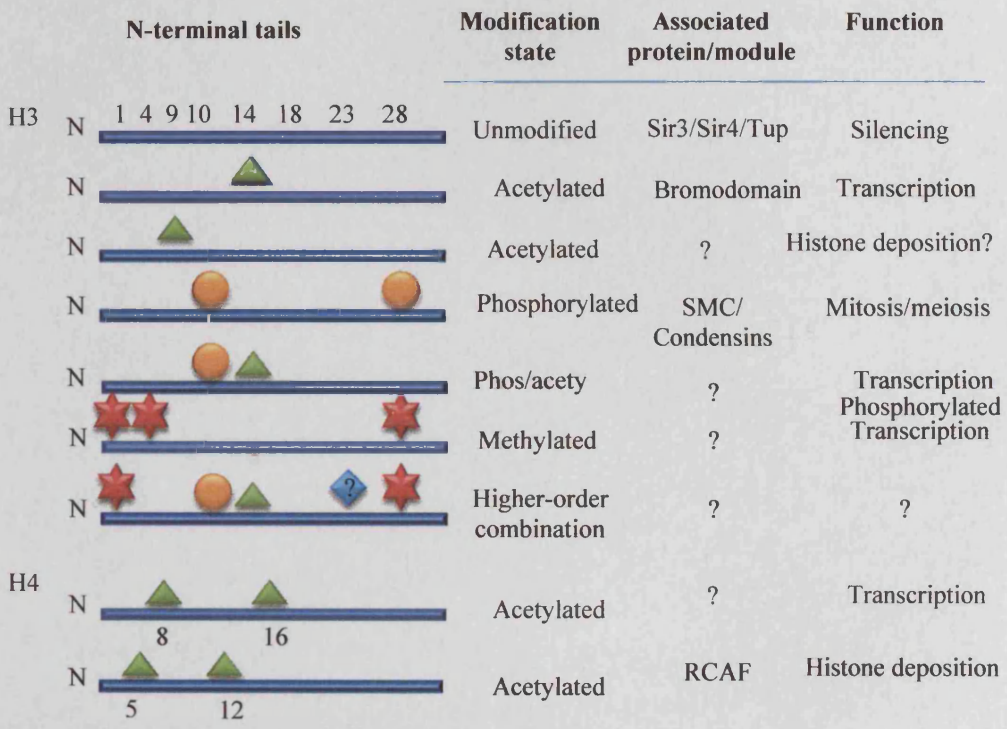

Figure 6.1 *Several examples of the histone code.* There are several histone modifications at the H3 and H4 histone tails residues. The numbers indicate the position where the modification is in the H3 or H4 histones. The green triangle indicates the acetylation modification, the orange sphere indicates the phosphorylation modification, the red star indicates methylation modification and the blue diamond indicate an unknown modification. H4K (5, 8, 12, 16) and H3K (4, 9, 14) are lysines. H3K (10, 28, 23) are serines and H3K1 is an alanine. Each specific combination of modifications can modulate a particular function and/or organise a specific chromatin structure (adapted from Strahl and Allis, 2000).

These modifications not only occur at the histone tails, but also at the globular domain of histones. For example, the acetylation of H3K56 is likely involved in the regulation of transcription since it is found to be acetylated at some active genes. The acetylation of H3K56 is required for the binding of Snf5p to allow the remodelling of the chromatin (Xu et al., 2005).

Acetylation of the H3K56 position is also involved in the repair of DNA breaks produced by bleomycin and camptothecin (CPT). Acetylation levels of H3K56 increase in response to DNA breaks and H3K56 mutations result in acute bleomycin and CPT sensitivity (Masumoto et al., 2005). Histone H3K56 also regulates a DNA damage response in *S. pombe*. Furthermore, deacetylation at this site is undertaken by Hst4p, a homologue of the Sir2p histone deacetyltransferase (Haldar and Kamakaka, 2008). In *S. cerevisiae*, Sir2p is involved in the regulation of acetylation levels at H3K56. Histone H3K56 acetylation levels influence silencing and chromatin structure at telomeres. The deacetylation of H3K56 condenses chromatin and prevents access to RNA polymerase thus inhibiting gene expression. Therefore, when H3K56 is mutated, telomeric DNA is more accessible. This relates to the finding that overall H3K56 is hypo-acetylated at telomeres and hyper-acetylated at active genes (Xu et al., 2007).

Another example where modifications at histone globular domains are related with biological processes is at histone H4K91. The deacetylation at this site is involved in the regulation of gene silencing since acetylation at H4K91 is related with the active region of the *S. cerevisiae* genome. The acetylation of H4K91 is also involved in the modulation of the chromatin structure as well as DNA repair (Cairns, 2005).

It has been recently shown that mutations at the H3K79 site change the number of survival cells after UV treatment and affect the CPD repair efficiency by NER. This is generated by a more inaccessible state of chromatin to MNase and thus to NER proteins. However, a single mutation at the H3K4 does not alter the CPD repair efficiency and the number of survival cells (Chaudhuri et al., 2009).

Eukaryotes have evolved specialized chromatin structures at chromosome ends to protect chromosomes. In *S. cerevisiae*, this complex chromatin structure is called silenced chromatin. One of the components forming the silenced chromatin at telomeres is the Sirp complex. As mentioned in previous chapters, the Sirp complex contains a structural component (Sir3p and Sir4p) and an enzymatic component (Sir2p). Silencing of chromatin at telomeres is regulated by Rap1p and the yKu70/yKu80 heterodimer which recruit silencing information regulators to this region. The Sir factors form heterodimers like Sir3p/Sir4p, Sir3p/Sir3p and Sir2p/Sir4p and they can spread to the subtelomeric regions (Gasser and Cockell, 2001; Laroche et al., 1998; Moazed, 2001). Thus, Sir3p and Sir4p can spread along

the telomere together with the silenced chromatin by an interaction with histone H4 and H3. This interaction between Sir3p and Sir4p and between histone H3 and H4 is strongly dependent on the hypoacetylation of H4K16 (Altaf et al., 2007; Suka et al., 2002). Thus, H4K16 is involved in the modulation of chromatin structure. Acetylation at this site abolishes the formation of higher order chromatin structure, therefore hypoacetylated H4K16 is required for the formation and spreading of the Sir complex. Indeed, hypoacetylation of H4K16 is common within telomeres and has been associated with silencing (Katan-Khaykovich and Struhl, 2005; Rusche et al., 2003; Suka et al., 2002; Vaquero et al., 2007). In addition, the boundaries of telomeric chromatin can be regulated by the hypoacetylation of H4K16 since they affect the Sirp proteins binding to the chromatin. As mentioned in previous chapters, the deacetylation of histone H3 and H4 is undertaken by Sir2p, particularly at H4K16 and H3K (9, 14) (Imai et al., 2000; Tanny and Moazed, 2001). This specificity in the acetylation site of histone H4 and H3 suggests that the silenced chromatin is modulated by the histone code phenomenon (Downs et al., 2007; Jenuwein and Allis, 2001).

It has been shown that loss of acetylation, but not methylation, has a role in the recruitment and the spreading of Sir proteins. Thus, loss of methylation at the H3K (4, 79) reflects intermediate events during the formation of silent chromatin and hypoacetylation of H4K16 is necessary and sufficient for the spreading of silencing (Yang et al., 2008).

Even if Sir2p is the main enzyme involved in the regulation of silencing at telomeres, the homologous proteins Hst3p and Hst4p have been recently reported to have a role in the deacetylation of H3K56 at telomeres in *S. cerevisiae* and *S. pombe* respectively. In mutant *hst3Δ* and *hst4Δ* cells, silencing is abolished at telomeres, yet this loss of silencing is independent of the recruitment of Sir2p or Sirp to the telomere (Yang et al., 2008).

As in budding yeast, it has been recently shown that in human fibroblasts the Sir2p family member Sirt6p has a role in maintaining functional telomeres. The NAD^+-dependent deacetylase Sirt6p is associated with the telomeres and specifically deacetylates the histone tail H3K9. Therefore, Sirt6p is required for the maintenance of the H3K9 hypoacetylation levels; the hyperacetylation of this specific site correlates with telomere dysfunction (Michishita et al., 2008).

In this chapter, the acetylation levels in response to UV light at H4K16 as well as H3K (9, 14) in the subtelomeric *URA3* at the NRE, RE, RE*sir2Δ* and NRE*sir2Δ* strains are analysed and discussed.

Firstly, comparisons of H4K16 acetylation levels between RE and RE*sir2Δ*, as well as between the NRE and NRE*sir2Δ* strains were undertaken to investigate whether the *SIR2* deletion could influence the acetylation levels after UV treatment.

Secondly, the acetylation levels at H3K (9, 14) were investigated and compared between these strains. This enabled me to determine whether the UV stimulus on the acetylation levels at the H3K (9, 14) mirrored those seen at genes such as *MFA2* (Yu et al., 2005) and whether they related to the H4 acetylation changes. This study also investigates whether acetylation levels correlated with NER efficiency in the subtelomeres (Chapter V) and whether the differences in acetylation levels between wild type and *SIR2* mutant strains can also be correlated with the differences in CPD repair efficiency between the strains described in Chapter V.

6.2 Materials and methods

The materials and methods for chromatin immunoprecipitation (ChIP) are described in Chapter II (page 55). UV treatment was undertaken as for the repair experiments described in chapter II (page 46); samples were taken at 30 and 90 mins after UV treatment along with an unirradiated sample.

6.2.1 Yeast strains

The yeast strains employed in this chapter were RE (MAT a, *ura3-52::KanMX can1-1 ade2Δ, leu2Δ, URA3 at CHRXI-L*), NRE (MAT a, *ura3-52::KanMX can1-1 ade2Δ, leu2Δ, URA3 at CHRIII-R*), NRE*sir2Δ* (same as NRE, except *sir2::LEU2*) and RE*sir2Δ* (same as RE, except *sir2::LEU2*).

6.2.2 Primers employed for the acetylation levels at H4K16 and H3K (9, 14)

The primers employed for the acetylation levels in reponse to UV in all the strains were named +222 A and +390 B for the +222 bp to +390 bp fragment (named 222 fragment). The primers used for the +540 bp to +669 bp fragment (named 540 fragment) are +540 A and +669 B. All the primers are listed in Appendix I.

6.3 Results

6.3.1 Quality and size verification of the sonicated chromatin

In order to generate a precise ChIP, chromatin must be sonicated to obtain fragments of around ~400 bp in size. After sonication, the DNA was resolved in agarose gels to determine size and quality. Figure 6.2 shows an example of sonicated DNA.

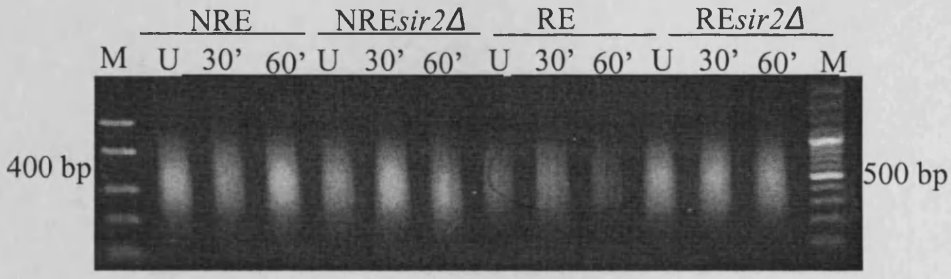

Figure 6.2 *Sonicated DNA samples for all the strains*. The smear shows that the size of DNA is around ~400bp. The samples were taken before (U) and after UV treatment (30' and 60'). M indicate the ladder or marker.

6.3.2 *SIR2* regulates the UV-induced histone H4K16 acetylation in the RE but not in the NRE strain

As previously mentioned, Sir2p contains coupled histone deacetylase and phosphoribosyltransferase activity (Imai et al., 2000; Landry et al., 2000; Mitchell, 2000; Sauve et al., 2001; Tanny and Moazed, 2001) and can deacetylate histone H4 K16 and H3 K(9, 14) (Johnson et al., 1990; Vaquero et al., 2007).

In this section the acetylation levels before and after UV treatment are described. The acetylation levels of H4K16 in response to UV in the coding region of the subtelomeric *URA3* gene were monitored in the *sir2Δ* and wild type ($SIR2^{+}$) strains by ChIP. Samples from all strains were collected before and after UV treatment (30 and 60 mins). The regions selected for the analysis of acetylation levels were fragments 222 and 540 (described in section 6.2.2) located in the coding region of the *URA3* gene.

The experiments were repeated three times (Appendix IV) and the results are shown in figure 6.3.

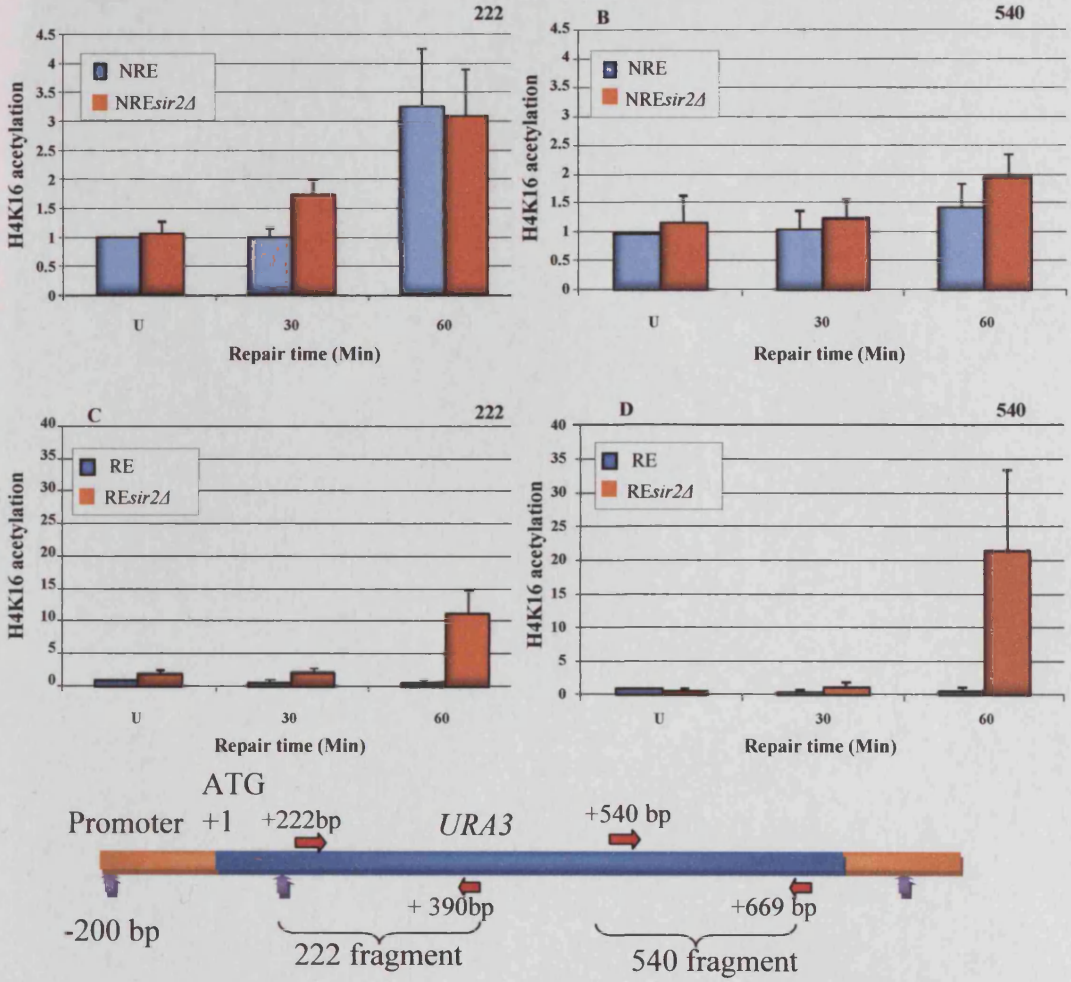

Figure 6.3 *H4K16 acetylation levels at the URA3 coding region in the 222 and 540 fragments of RE, REsir2Δ, NRE and NREsir2Δ strains in response to UV.* The H4K16 acetylation is represented as the relative level of acetylation to the untreated NRE or RE. (U) Represents cells not treated with UV; (30 and 60) represent cells irradiated with UV and allowed 30 and 60 mins repair. (**A, B**) comparison of H4K16 acetylation levels between the NRE and NRE*sir2*Δ strains for the 222(**A**) and 540 fragments (**B**). (**C, D**) comparison of H4K16 acetylation levels between the RE and RE*sir2Δ* strains for the 222 (**C**) and 540 fragment (**D**).

As indicated in figure 6.3 (A and B), when the *URA3* gene is in the NRE strain, histone H4K16 acetylation is stimulated by UV. There was an increase in acetylation levels in the wild type NRE strain. When the *SIR2* gene is deleted, the mutant strain responded in the same fashion as the *SIR2*$^{+}$ strain. Therefore, there are no differences in acetylation levels between NRE and NRE*sir2*Δ 60 mins after UV treatment. Moreover, there were no statistical differences in H4K16 acetylation levels after UV between NRE and NRE*sir2Δ* strains (Mann Whitney test). Table 6.1 illustrates the differences in H4K16 acetylation levels between untreated and 60 mins after UV in

the NRE and NRE*sir2Δ* strains together with the statistical differences in the acetylation levels after UV exposure between NRE and NRE*sir2Δ* strains.

Table 6.1 *Statistical differences in H4K16 acetylation levels between untreated and 60 mins after UV irradiation in the coding regions 222 and 540 in the NRE and NREsir2Δ strains.* There are no statistical differences or significant changes in acetylation levels between NRE and NRE*sir2Δ* strains after UV irradiation (Mann Whitney test).

Acetylation levels after UV	
REGION	P-values
222	0.94
540	0.79

In contrast to NRE, as shown in figure 6.3 C and D, when *URA3* is in the RE strain, there is no increase in the acetylation levels after UV. The acetylation level of H4K16 is relatively low, and remains low up to 60 mins after UV treatment. However, when *SIR2* is deleted there is increase in the acetylation of histone H4K16 at 222 and 540 fragments 60 mins after UV treatment. Moreover, there are statistical differences in H4K16 acetylation levels between RE and RE*sir2Δ* strains after UV (Mann Whitney test). Table 6.2 illustrates the differences in H4K16 acetylation levels between untreated and 60 mins after UV in the RE and RE*sir2Δ* strains together with the statistical differences in the acetylation levels after UV exposure between RE and RE*sir2Δ* strains.

Table 6.2 *Statistical differences in H4K16 acetylation level between untreated and 60 mins after UV irradiation in coding regions 222 and 540 in the RE and REsir2Δ strains.* There are statistical differences in acetylation levels between RE and RE*sir2Δ* strains after UV irradiation (Mann Whitney test).

Acetylation levels after UV	
REGION	P-values
222	<0.0001
540	<0.0001

Surprisingly, there were no differences in acetylation levels between untreated *SIR2*$^{+}$ and mutant strains in both, NRE and RE. The results indicate that Sir2p overrides the requirement of hyperacetylation in histone H4K16 following UV irradiation. Furthermore, it can be suggested that in the RE, Sir2p inhibits the increase

in acetylation since the acetylation levels increase dramatically 60 mins after UV when *SIR2* is deleted.

These findings are enforced by previous studies showing that UV irradiation stimulates histone H3 and H4 acetylation and this response varies between different regions of the genome (Vetting et al., 2005).

6.3.3 *SIR2* regulates the UV induced histone H3K (9, 14) acetylation in the RE but not in the NRE strain

Sir2p is also involved in the deacetylation of H3K (9, 14), therefore, the acetylation levels of H3K (9, 14) after UV were studied.

Cells were treated with UV and samples from all strains were collected before (U) and after UV treatment (30 and 60 mins). The regions selected for the analysis of acetylation levels were the same as for H4K16 acetylation; from +222 bp to +390 bp (222 region) and from +540 bp to +669 pb (540 region) in the coding region of the subtelomeric *URA3* gene.

The results showed that the UV-induced H3K (9, 14) acetylation follows the same pattern as for H4K16 acetylation, (figure 6.4, A and B). Thus, overall, in the RE strain there is no increase in acetylation levels after UV. Conversely, in the RE*sir2Δ* strain the H3 acetylation level increases dramatically by 60 mins after UV exposure. The data shows that the H3K (9, 14) acetylation levels after UV in the RE are also repressed by Sir2p.

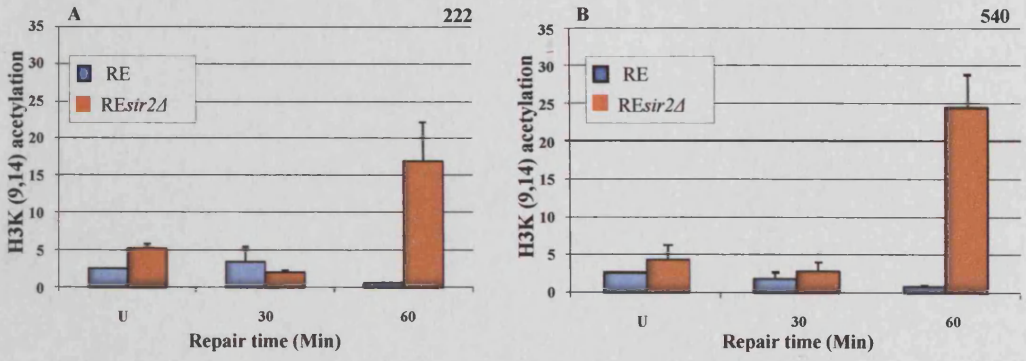

Figure 6.4 *H3K (9, 14) acetylation levels at the URA3 coding region for the RE and REsir2Δ strains in response to UV.* The H3K (9, 14) acetylation is represented as relative level of acetylation to the untreated RE. (U) represents cells that were not treated with UV; (30 and 60) represent cells that were irradiated with UV and allowed 30 and 60 mins repair. Acetylation levels were studied in the 222 (A) and the 540 fragments (B).

Table 6.3 illustrates the differences in the H3K (9, 14) acetylation levels in the RE and RE*sir2Δ* strains between untreated and 60 mins after UV, together with the statistical differences in the acetylation levels after UV exposure between RE and RE*sir2Δ* strains.

Table 6.3 *Statistical differences in H3K (9, 14) acetylation level between untreated and 60 mins after UV irradiation in coding regions 222 and 540 in the RE and REsir2Δ strains.* There are statistical differences in *H3K (9, 14)* acetylation levels between RE and RE*sir2Δ* strains after the UV irradiation (Mann Whitney test).

Acetylation levels after UV	
REGION	P-values
222	<0.0001
540	<0.0001

All the experiments were repeated three times and the data are presented in Appendix IV.

6.4 Discussion

6.4.1 Acetylation levels in response to UV for the H3K (9, 14) and H4K16 in the RE and RE*sir2Δ* strains.

In this chapter, it has been shown that after UV treatment in the RE strain, *URA3* coding region is hypoacetylated at H3K (9, 14) and H4K16, furthermore the acetylation levels in *SIR2*$^{+}$ cells do not change in response to UV. Therefore, the low acetylation level is linked to slow repair, chromatin inaccessibility and repression of genes as described in previous chapters (III, IV and V). In contrast, when *SIR2* is deleted, there is a significant increase in the acetylation levels only after UV damage. This increase in acetylation levels is related to fast repair in the RE*sir2Δ* strain.

The results presented here correlate with other reports suggesting that fast repair is associated with hyperacetylation, whereas, slow repair is associated with hypocacetylation (Chaudhuri et al., 2009). Moreover, the results shown here also suggest that at hypoacetylated regions, the NER machinery cannot operate without increasing the acetylation levels in the chromatin and thus, modifying chromatin structure.

Previous studies confirmed that histone acetylation and deacetylation can remodel the structure of the chromatin and therefore regulate and modulate the repair efficiency or transcription in some places of the genome (Teng et al., 2002; Yu et al., 2005; Yu and Waters, 2005). For example, Gcn5p is a histone acetyltransferase that acetylates the histone tails of nucleosomes, N-terminal lysines on H2B (K11 and K16) and H3 (K8, K18, K23, K27). It only acts on free histones, however, in association with HAT complexes, Gcn5p can acetylate histones found in nucleosomes (Grant et al., 1997; Ruiz-Garcia et al., 1997; Suka et al., 2001). It has been shown that the deletion of the *GCN5* gene reduces the NER efficiency in CPD repair at the actively transcribed *MFA2* gene, but has less effect in the *RPB2* gene and no effect in the entire genome, suggesting the local function of some HDAC such as Gcn5p which can remodel the chromatin around *MFA2* and affect NER (Teng et al., 2002). Thus, Gcn5p can act as a co-activator in transcriptional regulation affecting the repair efficiency. Furthermore, it is involved in the increment of the acetylation levels after UV, modulating the chromatin structure and increasing the repair efficiency at *MFA2* gene (Yu et al., 2005). In this work, they showed that, the acetylation levels of H3K (9, 14) increased after treating the cells with UV, however, the acetylation levels at H4K (5, 8, 12, 16) did not change. This increase reached a peak 30 mins after UV

treatment for histone H3 acetylation. However, there was little UV response in acetylation levels at histone H4, having the higher peak 10 mins after UV treatment (Yu et al., 2005).

It has been shown that the pre-UV acetylated regions in the genome can have efficient or fast NER independent of Rad16p (ATPase from SWI/SNF family required for NER) (Teng et al., 2008). These findings can also enforce the results I have obtained. Thus, it is possible that the increment in the acetylation after UV in the mutant cells can regulate directly the chromatin structure, generating suitable binding surface for NER machinery and as a consequence, faster DNA repair.

Surprisingly, there is no increase in the acetylation levels before UV in the RE and NRE strains when *SIR2* is deleted, suggesting that there might be other histones deacetylases homologues to Sir2p, such as Hst1p and Hst4p which could be involved in the deacetylation (Brachmann et al., 1995).

The results obtained here regarding the acetylation levels at the H4K16 and H3K (9, 14) in the untreated sample do not correlate with the loss of silencing in the RE*sir2*Δ and NRE*sir2*Δ strains. This result suggests that the increase in acetylation levels correlates only with NER and not with *URA3* expression. In other words, when *SIR2* is deleted the inhibitory role of Sir2p in NER is abrogated and probably histone acetyltransferases such as Sas2p can acetylate H4K16 and H3K (9, 14) after the treatment with UV.

Another evidence of the association between NER efficiency and acetylation is also found in the results presented in this chapter. In the RE*sir2Δ* strain, the acetylation levels are higher than in the NRE*sir2Δ*. Additionally the repair rate is slightly faster in the RE*sir2Δ* compared to NRE*sir2Δ*.

In summary, at the RE, *SIR2* is involved in inhibiting the increments of acetylation levels after UV treatment. This suggests that the grade of acetylation affect the repair efficiency and the *SIR2* deletion affect the chromatin structure at the XIL subtelomere. Previous data suggest that deacetylation by Sir2p is linked with chromatin organisation (Armstrong et al., 2002; Parsons et al., 2003) and the results obtained here and in previous chapters support this hypothesis.

6.4.2 Acetylation levels in response to UV for the H3K (9, 14) and H4K16 in the NRE and NRE*sir2Δ* strains

Sir2p does not regulate acetylation levels after UV in the NRE strain since the acetylation levels after UV between NRE and NRE*sir2Δ* were not significatively different.

It is possible that in the chromosome end where *URA3* is inserted at the IIIR, the chromatin is not repressed enough. This data can be enforced by the results obtained in previous chapters. For example, the NER efficiency data (Chapter V) also suggest that *SIR2* influence is stronger at the RE. Additionally, *SIR2* deletion might not affect silencing in the NRE strain as much as in the RE strain.

It has been shown that telomeric silencing is disrupted when damage is induced. Telomeric foci are dispersed when damage occur, suggesting that Sir proteins dissociate after treatment with damaging agents (McAinsh et al., 1999). This supports the results obtained for the NRE strain since in the NRE and NRE*sir2Δ*, there is a gradual increment in acetylation levels after the damage is produced, suggesting that the structure of the chromatin changes allowing NER.

However, there is no increase in acetylation levels in the NRE and NRE*sir2Δ* strains before UV treatment. This finding suggests that in the NRE as well as in the RE, the acetylation levels are not linked with *URA3* expression.

In summary, there is increase in acetylation levels after UV treatment along with efficient NER in the NRE, NRE*sir2Δ* and RE*sir2Δ* strains. However, there is no increase in acetylation level and the NER is slow in the RE strain.

6.4.3 Reorganisation of the chromatin after *SIR2* deletion in the RE and NRE strains

The results described here suggest a chromatin reorganisation in the RE and NRE strains after the deletion of *SIR2* gene when the strains are treated with UV. Figure 6.5 shows a hypothesis of the chromatin reorganisation in the RE and NRE strains after UV when *SIR2* is deleted.

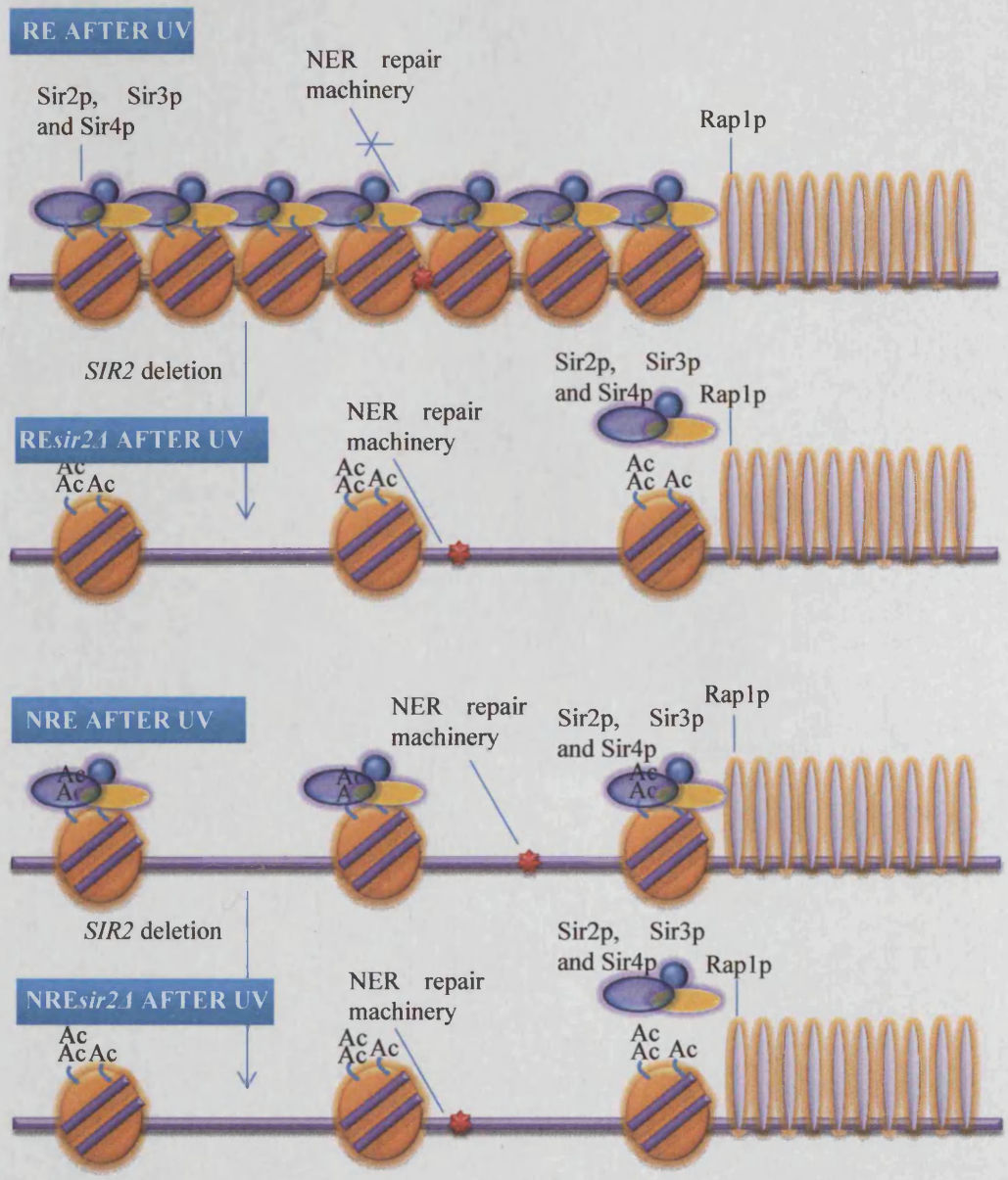

Figure 6.5 *Reorganisation of the chromatin in the NRE and RE strains when SIR2 is deleted and after UV exposure.* In the RE, chromatin has a compact structure due to hypoacetylation levels. When *SIR2* is deleted, the acetylation levels increase and the chromatin becomes more relax. In the NRE and NRE*sir2Δ* strains, the acetylation levels are similar however in NRE there are Sir proteins which can bind to some nucleosomes but cannot build a chromatin structure as complex as in RE. In the NRE*sir2Δ* strains there are no Sirp proteins that bind to nucleosomes.

After UV irradiation, the acetylation levels increase at histones H4K16 and H3K (9, 14) in the NRE strain. It is likely that in the NRE strain, the recruitment of the SIR complex is lower compared to the RE strain. Therefore, the Sir2p has a minor influences in this strain than in the RE strain and the acetylation levels do not change after UV irradiation when *SIR2* is deleted.

The results obtained in the RE suggest that chromatin structure does not change after UV stimuli. The chromatin is so compact that it cannot be remodelled to repair the UV lesion by NER. In this case, probably the integrity of the chromatin is more important than the efficiency of NER. Similar effect has been observed at the centromeres (Capiaghi et al., 2004). It is likely that at this subtelomere (XIL) the chromatin is very compact due to the amount of Sir proteins recruited. Consequently, some specific acetylation sites are not accessible to HATs.

It might be possible that the nucleosomal concentration and the H3 and H4 histone concentration are higher in the RE strain than in the NRE strain. Therefore, when *SIR2* is deleted the acetylation levels are also higher in the RE than in the NRE due to more histone H3 and H4, destabilizing more the chromatin structure.

Previous results observed and evaluated in chapter III, IV, V also suggest that the chromatin organisation, *URA3* expression and NER efficiency are more dependent on Sir2p in the RE strain than in the NRE strain.

Chapter VII

GENERAL CONCLUSION AND FUTURE WORK

7.1 Summary

S. cerevisiae is a unicellular eukaryote which can be used as a model to investigate NER since the mechanism is highly conserved throughout evolution.

The experiments described in this study aimed to explore the relationship between gene silencing at subtelomeres, chromatin structure and NER. This study also examined the role of Sir2p in NER and chromatin organisation, since Sir2p is a HDAC which has a role in compaction of the silenced chromatin. I employed two different subtelomeres regions, both located at the same distance from the telomeres. To minimize the effect of NER on sequence diversity, *URA3* was used as a reporter gene and was inserted at the subtelomere of both chromosome ends that were analysed.

The first part of this work (Chapter III) describes the construction of *sir2* mutant strains and investigates the expression of the yeast *URA3* gene at different subtelomeres. The effect of Sir2p in the *URA3* expression was also determined. The second part (Chapter IV) focuses on the analysis of the chromatin structure in subtelomeric *URA3* with two different grades of silencing and the role of Sir2p in chromatin organisation. The third part (Chapter V) describes the CPD repair efficiency in both subtelomeric *URA3* genes and the inhibitory effect that Sir2p has in repair efficiency. Finally, the acetylation levels at both subtelomeric *URA3* genes in response to UV light and the role of Sir2p deacetylase were studied (Chapter VI). These experiments were carried out to examine the correlation between chromatin structure, epigenetic histone codes, CPD repair efficiency and silencing. The overview of the aims and findings of this work are illustrated in figure 7.1.

As each aspect was discussed in detail within the relevant section; this chapter will focus primarily on the possible routes of further investigation to enhance the understanding of the roles of silenced chromatin and epigenetic changes in NER.

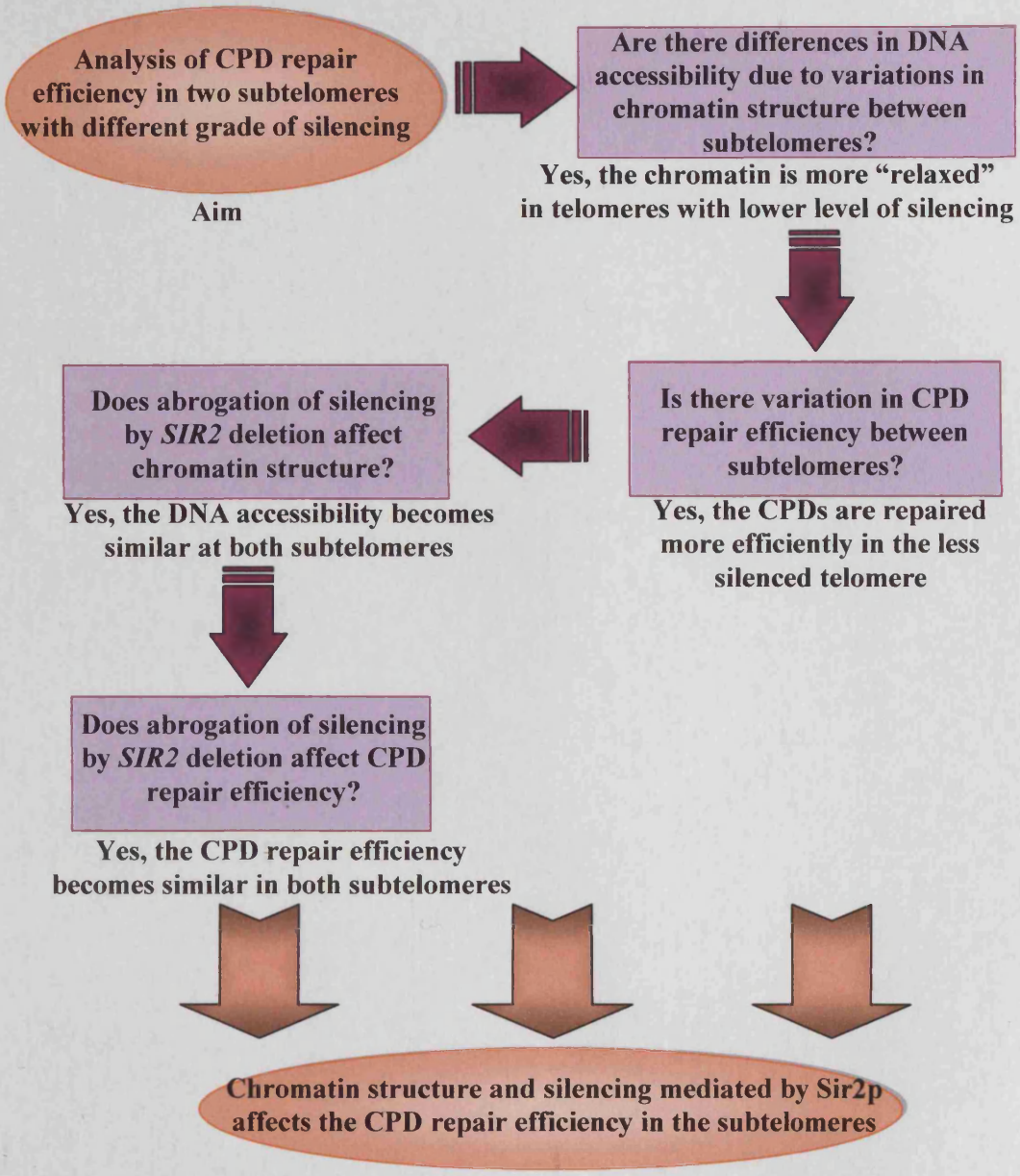

Figure 7.1 *Summary of the aims and outcomes of the work illustrated in the thesis.*

7.2 Silencing affects the CPD repair efficiency in the subtelomeres

There is a little doubt that chromatin organisation influences gene transcription and thus gene expression. Supporting this idea, there have been studies using *HIS3* in a plasmid environment (Kim et al., 2006). The expression of this gene can be regulated by amino acid starvation. The study showed that the chromatin of uninduced *HIS3* is protected from cleavage by restriction enzymes. In contrast, when the gene was induced, the chromatin became less compact and had increased sensitivity to restriction enzymes.

We have already shown exactly the same effects with respect to NER and nucleosomes at the repressed *MFA2* gene (Yu et al., 2005). Correlations have also been addressed between chromatin and NER at the *MET16* and *MET 17* loci (Ferreiro et al., 2004; Powell et al., 2003). Furthermore, recent work examining chromatin organisation and NER has been carried out in specialized chromosome regions (Capiaghi et al., 2004; Chaudhuri et al., 2009; Kaufman et al., 1997; Terleth et al., 1989) where in general, the authors implied that the more relaxed the chromatin, the more efficient the NER.

For example, in budding yeast centromeres, UV induced photoproducts do not disrupt the organisation of the chromatin and the repair by NER is inhibited. Here, the chromatin acquired a compact organisation and apparently maintaining the chromatin structure for the accurate segregation of chromosomes is more important than the repair of CPDs in the centromeric DNA. However, if the chromatin organisation in the kinetochore is severely disrupted by mutations, there is efficient repair of the UV lesions in these regions (Capiaghi et al., 2004).

At the mating type loci, influence on NER efficiency and the transcriptional status by the SIR complex has been well recognized (Chaudhuri et al., 2009; Terleth et al., 1989). The active *MATα* locus is repaired more rapidly than the inactive *HMLα*. However, in the *sir3* mutant due to derepression, both loci are active and the UV damage is repaired with a similar efficiency (Terleth et al., 1989). Another work had recently shown that the H3K79 mutants (a specific site for the methylation) are more sensitive to UV irradiation compared to the wild type. The chromatin is rendered more resistant to MNase digestion in the H3K79 mutants than in the wild type strains at the HMLα locus (Chaudhuri et al., 2009). However, when *SIR2* and *SIR3* are deleted in the wild type and H3K79 mutant strains, there is a significative increase in CPD removal at the HML locus (Chaudhuri et al., 2009). The rate of CPD removal at HML in both strains is comparable and the chromatin became more accessible to MNase. Therefore, the authors suggested that the decrease in CPD removal at the HML locus is due to enhance binding of the Sir protein complex.

CAF-I complex is essential for nucleosome assembly after replication since it forms nucleosomes for a short period after the DNA synthesis is stopped. In addition, this complex is implicated in nucleosome assembly after NER as this repair process involves DNA synthesis of the damage region. A defect in telomeric silencing is caused by a mutation in any of the genes encoding the three subunits termed

chromatin assembly complex (Cac1p, Cac2p, Cac3p) which form CAF-I. Such mutant cells become more sensitive to UV DNA damage, suggesting the importance of maintaining the local chromatin structure after the UV damage is repaired (Kaufman et al., 1997).

The insertion of *URA3* in subtelomeres is a good approach for the analysis of silencing, DNA repair efficiency and chromatin structure in the telomeric region as it eliminates variation of DNA sequence context. In a recent study, the *URA3* gene was inserted in the subtelomere approximately 2 Kb and 6 Kb away from the VR telomere (Livingstone-Zatchej et al., 2003). The authors demostrated that overall UV damage produced in the *URA3* gene is repaired slower via NER than via PR. This demonstrates that the accessibility to DNA due to chromatin structure impinges more on NER than PR. This is probably because NER is a multicomplex machinery and PR relies only in the activity of the photolyase enzyme. At 6 Kb away from the telomere the overall repair of the *URA3* was faster in the TS than in the NTS, however, when *URA3* was placed 2 Kb away from the telomere, the TS was repaired only slightly faster than the NTS, suggesting that differences in silencing influence the NER repair rate. The NER efficiency at the NTS was similar at both locations. When *SIR3* was deleted, disrupting the silencing, the TS were repaired more rapidly than the NTS at 2Kb away from the telomere. Thus, the deletion of *SIR3* enhanced NER efficiency. Contrarily, overexpression of Sir3p resulted in a more pronounced silencing levels and slower repair by NER machinery. The analysis of positioned nucleosomes when Sir3p is overexpressed also induced a closer chromatin organisation further inhibiting the accessibility of NER machinery to the *URA3* gene (Livingstone-Zatchej et al., 2003).

A study of telomeric silencing in *S. cerevisiae* has revealed differences in silencing levels between chromosome ends (Pryde and Louis, 1999). In that study *URA3* was inserted at different subtelomeric locations and the silenced levels were measured by growing the cells in the presence of 5-FOA. The results showed that the silencing can vary between chromosome ends, in the inserted *URA3* gene at the same distant from the telomere.

The work presented in this thesis examined the effect of silencing on NER at two chromosome ends with different levels of silencing. The study follows the above investigation (Livingstone-Zatchej et al., 2003) and the experiments described in my thesis provided a more thorough and detailed examination of the effect of telomeric

silencing on NER repair efficiency, chromatin structure and acetylation levels in response to UV damage. The main differences between the previous study and this work:

a. *URA3* was inserted in two chromosome ends with different levels of silencing at the same distance from the telomere, so the effect of silencing in the chromatin and NER repair efficiency can be physically separated.

b. The techniques utilized in this work are more detailed as NER and the chromatin structure were determined at the sequence level and not at low resolution or at the level of the gene as shown in (Livingstone-Zatchej et al., 2003). As a result, I could examine the NER rate of individual CPDs and compare the time needed to repair specific DNA lesion in the *URA3* sequence to the MNase accessibility of the DNA in chromatin. In the previously reported work by (Livingstone-Zatchej et al., 2003), they found that by analysing the chromatin at low resolution the mutation of *SIR3* does not alter the overall chromatin structure. Moreover, the reorganisations of the nucleosomes are only described in the promoter region and not in the coding region. However, the repair analysis of (Livingstone-Zatchej et al., 2003) suggested an enhance efficiency of NER at the *URA3* gene when *SIR3* is mutated. Probably the *SIR3* mutation induces changes in chromatin structure that it cannot be detected by the low resolution technique. This was consistent with the findings where Ty5-1 retrotransposon is located at the IIIL chromosome end and it is repressed in the wild type but not in the *sir3* mutant (Vega-Palas et al., 1998). Thus, the studies of (Livingstone-Zatchej et al., 2003) were limited in resolution and could not resolve differences in repair of linker DNA and core DNA, therefore, a high resolution approach was needed to clarify such issues.

c. The work presented in this thesis also addressed whether the disruption of silencing by *SIR2* deletion at different chromosome ends could influence NER, chromatin structure and acetylation levels of histones H3 and H4 in response to UV.

d. Finally, the work shown here described the role of the Sir2p histone deacetylase in NER efficiency. The acetylation data after UV exposure presented here, suggest an inhibitory role of Sir2p in NER.

7.3 Future work

NER efficiency

The NER rate indicates that at the highly silenced chromosome ends, the repair time in the NTS and TS is approximately similar and more than 8 hrs. However, in the chromosome end where the silencing levels are low, there are marked differences between strands, the repair being faster at the TS compared to NTS. This suggests a transcriptional activity of *URA3* and the participation of TC-NER in the repair of TS. Furthermore, *SIR2* deletion also impinges on NER efficiency, for example the NER efficiency was much faster at the TS of *URA3* gene at the highly repressed end when *SIR2* is deleted. The involvement of the TC-NER in the TS of the NRE strain could be tested by analysing the NER rate in the TS when *RAD26* is deleted or mutated.

Telomeres have an equilibrium between Sir2p and its counterpart Sas2p histone acetyltransferase which acetylates predominantly histone H4K16, thus, the positions that Sir2p deacetylates (Suka et al., 2002). In this thesis it has been observed that deletion of *SIR2* influences the chromatin structure and NER rate, therefore it is likely that the deletion or mutation of *SAS2* will impinge on NER efficiency and chromatin in subtelomeres.

Acetylation levels after UV and plasticity of the chromatin

NER efficiency depend on chromatin organisation since many studies have shown that at the NTS the repair rate is faster in the linker region and MNase accessible region compared to MNase resistant regions (Livingstone-Zatchej et al., 1997; Wellinger and Thoma, 1997). Nevertheless, the lesions in the protected regions might still be repaired due to nucleosome mobility (discussed in Chapter IV).

For example, chromatin studies have revealed the nucleosome positioning and MNase accessibility at the endogenous *URA3* and when *URA3* gene is inserted at a minichromosome. In both cases, the nucleosomal organisation is similar. This nucleosomal organisation at the *URA3* gene is correlated with other studies of the NER efficiency analysis at the NTS of *URA3* showing that the modulation of NER rate depends on the MNase accessibility (Tanaka et al., 1996; Thoma, 1986; Wellinger and Thoma, 1997).

In addition, the work presented here also suggests a correlation between the repair data and the MNase accessibility. For instance, in the RE, the MNase accessibility results suggest there is no regular nucleosome array, moreover, the repair

data provides evidence that the chromatin is probably highly compacted and even the linker regions are not accessible to the NER machinery. In the NRE, the chromatin is more accessible and NER efficiency is higher than at the RE strain; however the repair analysis and MNase accessibility at the NRE data also suggests that the chromatin follows an irregular pattern since there are no obvious changes in repair efficiency marking the linker regions or regions accessible to the NER machinery. Even when *SIR2* is deleted at both NRE and RE, the repair analysis and MNase analysis suggested an irregular chromatin organisation.

The high resolution analysis of MNase accessibility alone cannot determine the nucleosome position or the precise chromatin organisation. Consequently, the low resolution nucleosome mapping together with high resolution MNase accessibility analysis could determine this issue.

In the RE, there was no evidence of an increase in acetylation levels after UV irradiation, however, in RE*sir2*Δ, NRE and NRE*sir2*Δ an increase in acetylation levels was detected after UV treatment. Previous studies have correlated acetylation with an "open" chromatin structure and transcription (Teng et al., 2002). Therefore, it can be speculated that after treatment with UV, the chromatin is reorganized in the RE*sir2*Δ, NRE and NRE*sir2*Δ. To study this hypothesis, the accessibility of MNase to DNA after UV treatment could be examined. For example, in the RE*sir2*Δ strain, the MNase accessibility to DNA could be examined 60 mins after UV since the detected acetylation levels are the highest at that specific point.

Silenced regions and proteins

The *S. cerevisiae* genome has other silenced regions such as rDNA and HM loci. Therefore, NER can be also influenced in those regions and an analysis of them would broaden our knowledge of the silencing effect in NER.

There are other proteins, apart from Sir2p, that are involved in telomere silencing and each of them might influence NER differently. For example, a candidate protein could be Hdf1p, the homologous of mammalian Ku70p also known as Yku70p, as silencing is affected when it is mutated (Pryde and Louis, 1999). Other candidate proteins could be Sir3p, Sir4p and Sir1p proteins as each of them influence silencing differently. For example, in the subtelomeres, Sir2p and Sir4p completely abrogate silencing, Sir3p strongly reduces the level of silencing whereas Sir1p causes only slight derepression (Pryde and Louis, 1999).

In addition, as previously mentioned in Chapter III, proteins that are directly involved in telomere length (such as rif1p and rif2p) are indirectly involved in silencing suggesting that they are good candidates to study whether they influence NER repair and chromatin structure.

Aboussekhra, A. et al. 1995. Mammalian DNA nucleotide excision repair reconstituted with purified protein components. *Cell* 80(6), pp. 859-868.

Aboussekhra, A. and Thoma, F. 1998. Nucleotide excision repair and photolyase preferentially repair the nontranscribed strand of RNA polymerase III-transcribed genes in Saccharomyces cerevisiae. *Genes Dev* 12(3), pp. 411-421.

Alani, E. et al. 1987. A method for gene disruption that allows repeated use of URA3 selection in the construction of multiply disrupted yeast strains. *Genetics* 116(4), pp. 541-545.

Allinen, M. 2002. DNA damage response genes and chromosome 11q21-q24 candidate tumor suppressor genes in breast cancer. *Thesis*, pp. 1-79.

Altaf, M. et al. 2007. Histone modifications in response to DNA damage. *Mutat Res* 618(1-2), pp. 81-90.

Anderson, J. D. and Widom, J. 2001. Poly(dA-dT) promoter elements increase the equilibrium accessibility of nucleosomal DNA target sites. *Mol Cell Biol* 21(11), pp. 3830-3839.

Annunziato, A. T. and Hansen, J. C. 2000. Role of histone acetylation in the assembly and modulation of chromatin structures. *Gene Expr* 9(1-2), pp. 37-61.

Aparicio, O. M. et al. 1991. Modifiers of position effect are shared between telomeric and silent mating-type loci in S. cerevisiae. *Cell* 66(6), pp. 1279-1287.

Aparicio, O. M. and Gottschling, D. E. 1994. Overcoming telomeric silencing: a trans-activator competes to establish gene expression in a cell cycle-dependent way. *Genes Dev* 8(10), pp. 1133-1146.

Armstrong, C. M. et al. 2002. Mutations in Saccharomyces cerevisiae gene SIR2 can have differential effects on in vivo silencing phenotypes and in vitro histone deacetylation activity. *Mol Biol Cell* 13(4), pp. 1427-1438.

Ashktorab, H. et al. 2008. Global Histone H4 Acetylation and HDAC2 Expression in Colon Adenoma and Carcinoma. *Dig Dis Sci.*

Ataian, Y. and Krebs, J. E. 2006. Five repair pathways in one context: chromatin modification during DNA repair. *Biochem Cell Biol* 84(4), pp. 490-504.

Auriche, C. et al. 2008. Budding yeast with human telomeres: a puzzling structure. *Biochimie* 90(1), pp. 108-115.

Avvakumov, N. and Cote, J. 2007. The MYST family of histone acetyltransferases and their intimate links to cancer. *Oncogene* 26(37), pp. 5395-5407.

Axelrod, J. D. et al. 1993. GAL4 disrupts a repressing nucleosome during activation of GAL1 transcription in vivo. *Genes Dev* 7(5), pp. 857-869.

Aylon, Y. and Kupiec, M. 2004. DSB repair: the yeast paradigm. *DNA Repair (Amst)* 3(8-9), pp. 797-815.

Baer, M. and Sancar, G. B. 1989. Photolyases from Saccharomyces cerevisiae and Escherichia coli recognize common binding determinants in DNA containing pyrimidine dimers. *Mol Cell Biol* 9(11), pp. 4777-4788.

Bang, D. D. et al. 1992. Molecular cloning of RAD16, a gene involved in differential repair in Saccharomyces cerevisiae. *Nucleic Acids Res* 20(15), pp. 3925-3931.

Baudin, A. et al. 1993. A simple and efficient method for direct gene deletion in Saccharomyces cerevisiae. *Nucleic Acids Res* 21(14), pp. 3329-3330.

Becker, M. M. and Wang, J. C. 1984. Use of light for footprinting DNA in vivo. *Nature* 309(5970), pp. 682-687.

Becker, P. B. 2002. Nucleosome sliding: facts and fiction. *EMBO J* 21(18), pp. 4749-4753.

Becker, P. B. and Horz, W. 2002. ATP-dependent nucleosome remodeling. *Annu Rev Biochem* 71, pp. 247-273.

Bedoyan, J. et al. 1992. Transcription, nucleosome stability, and DNA repair in a yeast minichromosome. *J Biol Chem* 267(9), pp. 5996-6005.

Bell, S. D. et al. 2002. The interaction of Alba, a conserved archaeal chromatin protein, with Sir2 and its regulation by acetylation. *Science* 296(5565), pp. 148-151.

Benbow, S. Z. and Dubois, M. L. 2008. The dosage of chromatin proteins affects transcriptional silencing and DNA repair in Saccharomyces cerevisiae. *FEBS Lett* 582(4), pp. 497-502.

Bennett, R. A. et al. 1997. Interaction of human apurinic endonuclease and DNA polymerase beta in the base excision repair pathway. *Proc Natl Acad Sci U S A* 94(14), pp. 7166-7169.

Berger, S. L. 2007. The complex language of chromatin regulation during transcription. *Nature* 447(7143), pp. 407-412.

Bert, A. G. et al. 2007. A modular enhancer is differentially regulated by GATA and NFAT elements that direct different tissue-specific patterns of nucleosome positioning and inducible chromatin remodeling. *Mol Cell Biol* 27(8), pp. 2870-2885.

Bi, X. et al. 1999. The yeast HML I silencer defines a heterochromatin domain boundary by directional establishment of silencing. *Proc Natl Acad Sci U S A* 96(21), pp. 11934-11939.

Bi, X. et al. 2004. Regulation of transcriptional silencing in yeast by growth temperature. *J Mol Biol* 344(4), pp. 893-905.

Biddick, R. and Young, E. T. 2009. The disorderly study of ordered recruitment. *Yeast* 26(4), pp. 205-220.

Bilaud, T. et al. 1997. Telomeric localization of TRF2, a novel human telobox protein. *Nat Genet* 17(2), pp. 236-239.

Blander, G. and Guarente, L. 2004. The Sir2 family of protein deacetylases. *Annu Rev Biochem* 73, pp. 417-435.

Boeke, J. D. et al. 1984. A positive selection for mutants lacking orotidine-5'-phosphate decarboxylase activity in yeast: 5-fluoro-orotic acid resistance. *Mol Gen Genet* 197(2), pp. 345-346.

Boeke, J. D. et al. 1987. 5-Fluoroorotic acid as a selective agent in yeast molecular genetics. *Methods Enzymol* 154, pp. 164-175.

Boorstein, R. J. et al. 1990. Formation and stability of repairable pyrimidine photohydrates in DNA. *Biochemistry* 29(46), pp. 10455-10460.

Borra, M. T. et al. 2004. Substrate specificity and kinetic mechanism of the Sir2 family of NAD+-dependent histone/protein deacetylases. *Biochemistry* 43(30), pp. 9877-9887.

Boscheron, C. et al. 1996. Cooperation at a distance between silencers and proto-silencers at the yeast HML locus. *Embo J* 15(9), pp. 2184-2195.

Bourgeois, C. A. et al. 1985. New data on the in-situ position of the inactive X chromosome in the interphase nucleus of human fibroblasts. *Hum Genet* 69(2), pp. 122-129.

Brachmann, C. B. et al. 1995. The SIR2 gene family, conserved from bacteria to humans, functions in silencing, cell cycle progression, and chromosome stability. *Genes Dev* 9(23), pp. 2888-2902.

Braunstein, M. et al. 1993. Transcriptional silencing in yeast is associated with reduced nucleosome acetylation. *Genes Dev* 7(4), pp. 592-604.

Braunstein, M. et al. 1996. Efficient transcriptional silencing in Saccharomyces cerevisiae requires a heterochromatin histone acetylation pattern. *Mol Cell Biol* 16(8), pp. 4349-4356.

Brownell, J. E. and Allis, C. D. 1996. Special HATs for special occasions: linking histone acetylation to chromatin assembly and gene activation. *Curr Opin Genet Dev* 6(2), pp. 176-184.

Bryk, M. et al. 1997. Transcriptional silencing of Ty1 elements in the RDN1 locus of yeast. *Genes Dev* 11(2), pp. 255-269.

Buchman, A. R. et al. 1988. Two DNA-binding factors recognize specific sequences at silencers, upstream activating sequences, autonomously replicating sequences, and telomeres in Saccharomyces cerevisiae. *Mol Cell Biol* 8(1), pp. 210-225.

Buck, S. W. and Shore, D. 1995. Action of a RAP1 carboxy-terminal silencing domain reveals an underlying competition between HMR and telomeres in yeast. *Genes Dev* 9(3), pp. 370-384.

Bugreev, D. V. et al. 2006. Rad54 protein promotes branch migration of Holliday junctions. *Nature* 442(7102), pp. 590-593.

Cairns, B. R. 2005. Chromatin remodeling complexes: strength in diversity, precision through specialization. *Curr Opin Genet Dev* 15(2), pp. 185-190.

Capiaghi, C. et al. 2004. Kinetochores prevent repair of UV damage in Saccharomyces cerevisiae centromeres. *Mol Cell Biol* 24(16), pp. 6907-6918.

Carell, T. et al. 2001. The mechanism of action of DNA photolyases. *Curr Opin Chem Biol* 5(5), pp. 491-498.

Cavalli, G. and Thoma, F. 1993. Chromatin transitions during activation and repression of galactose-regulated genes in yeast. *EMBO J* 12(12), pp. 4603-4613.

Chan, C. S. and Tye, B. K. 1983. Organization of DNA sequences and replication origins at yeast telomeres. *Cell* 33(2), pp. 563-573.

Chaudhuri, S. et al. 2009. Histone H3 Lys79 methylation is required for efficient nucleotide excision repair in a silenced locus of Saccharomyces cerevisiae. *Nucleic Acids Res.*

Chen, L. and Widom, J. 2005. Mechanism of transcriptional silencing in yeast. *Cell* 120(1), pp. 37-48.

Chiani, F. et al. 2006. SIR2 modifies histone H4-K16 acetylation and affects superhelicity in the ARS region of plasmid chromatin in Saccharomyces cerevisiae. *Nucleic Acids Res* 34(19), pp. 5426-5437.

Chong, L. et al. 1995. A human telomeric protein. *Science* 270(5242), pp. 1663-1667.

Cline, S. D. and Hanawalt, P. C. 2003. Who's on first in the cellular response to DNA damage? *Nat Rev Mol Cell Biol* 4(5), pp. 361-372.

Cockell, M. et al. 1995. The carboxy termini of Sir4 and Rap1 affect Sir3 localization: evidence for a multicomponent complex required for yeast telomeric silencing. *J Cell Biol* 129(4), pp. 909-924.

Coin, F. et al. 2008. Nucleotide excision repair driven by the dissociation of CAK from TFIIH. *Mol Cell* 31(1), pp. 9-20.

Constantinou, A. et al. 2000. Werner's syndrome protein (WRN) migrates Holliday junctions and co-localizes with RPA upon replication arrest. *EMBO Rep* 1(1), pp. 80-84.

Cooke, M. S. et al. 2003. Oxidative DNA damage: mechanisms, mutation, and disease. *FASEB J* 17(10), pp. 1195-1214.

Dammann, R. et al. 1993. Chromatin structures and transcription of rDNA in yeast Saccharomyces cerevisiae. *Nucleic Acids Res* 21(10), pp. 2331-2338.

David, S. S. et al. 2007. Base-excision repair of oxidative DNA damage. *Nature* 447(7147), pp. 941-950.

de Boer, J. and Hoeijmakers, J. H. 2000. Nucleotide excision repair and human syndromes. *Carcinogenesis* 21(3), pp. 453-460.

de Bruin, D. et al. 2000. Telomere folding is required for the stable maintenance of telomere position effects in yeast. *Mol Cell Biol* 20(21), pp. 7991-8000.

de Laat, W. L. et al. 1999. Molecular mechanism of nucleotide excision repair. *Genes Dev* 13(7), pp. 768-785.

Deckert, J. and Struhl, K. 2002. Targeted recruitment of Rpd3 histone deacetylase represses transcription by inhibiting recruitment of Swi/Snf, SAGA, and TATA binding protein. *Mol Cell Biol* 22(18), pp. 6458-6470.

Demple, B. and Linn, S. 1982. 5,6-Saturated thymine lesions in DNA: production by ultraviolet light or hydrogen peroxide. *Nucleic Acids Res* 10(12), pp. 3781-3789.

Demple, B. and Sung, J. S. 2005. Molecular and biological roles of Ape1 protein in mammalian base excision repair. *DNA Repair (Amst)* 4(12), pp. 1442-1449.

Dhillon, N. and Kamakaka, R. T. 2000. A histone variant, Htz1p, and a Sir1p-like protein, Esc2p, mediate silencing at HMR. *Mol Cell* 6(4), pp. 769-780.

Dizdaroglu, M. 2005. Base-excision repair of oxidative DNA damage by DNA glycosylases. *Mutat Res* 591(1-2), pp. 45-59.

Downs, J. A. et al. 2003. Suppression of homologous recombination by the Saccharomyces cerevisiae linker histone. *Mol Cell* 11(6), pp. 1685-1692.

Downs, J. A. et al. 2007. Chromatin dynamics and the preservation of genetic information. *Nature* 447(7147), pp. 951-958.

Dror, V. and Winston, F. 2004. The Swi/Snf chromatin remodeling complex is required for ribosomal DNA and telomeric silencing in Saccharomyces cerevisiae. *Mol Cell Biol* 24(18), pp. 8227-8235.

Dzantiev, L. et al. 2004. A defined human system that supports bidirectional mismatch-provoked excision. *Mol Cell* 15(1), pp. 31-41.

Ehrenhofer-Murray, A. E. 2004. Chromatin dynamics at DNA replication, transcription and repair. *Eur J Biochem* 271(12), pp. 2335-2349.

Ferreiro, J. A. et al. 2004. Cbf1p modulates chromatin structure, transcription and repair at the Saccharomyces cerevisiae MET16 locus. *Nucleic Acids Res* 32(5), pp. 1617-1626.

Field, Y. et al. 2008. Distinct modes of regulation by chromatin encoded through nucleosome positioning signals. *PLoS Comput Biol* 4(11), p. e1000216.

Fillingham, J. et al. 2008. Chaperone control of the activity and specificity of the histone H3 acetyltransferase Rtt109. *Mol Cell Biol* 28(13), pp. 4342-4353.

Fisher, T. S. and Zakian, V. A. 2005. Ku: a multifunctional protein involved in telomere maintenance. *DNA Repair (Amst)* 4(11), pp. 1215-1226.

Flynn, P. J. and Reece, R. J. 1999. Activation of transcription by metabolic intermediates of the pyrimidine biosynthetic pathway. *Mol Cell Biol* 19(1), pp. 882-888.

Francois, F. et al. 2004. Development of an integrative transformation system for the opportunistic pathogenic yeast Candida lusitaniae using URA3 as a selection marker. *Yeast* 21(2), pp. 95-106.

Freeman-Cook, L. L. et al. 2005. Conserved locus-specific silencing functions of Schizosaccharomyces pombe sir2+. *Genetics* 169(3), pp. 1243-1260.

Friedberg, E. C. 1996. Relationships between DNA repair and transcription. *Annu Rev Biochem* 65, pp. 15-42.

Friedberg, E. C. 2003. DNA damage and repair. *Nature* 421(6921), pp. 436-440.

Friedberg, E. C. et al. 2005. *DNA repair and mutagenesis*. 2nd ed. Washington DC: ASM Press.

Fritze, C. E. et al. 1997. Direct evidence for SIR2 modulation of chromatin structure in yeast rDNA. *Embo J* 16(21), pp. 6495-6509.

Fukuda, H. et al. 2006. Simple histone acetylation plays a complex role in the regulation of gene expression. *Brief Funct Genomic Proteomic* 5(3), pp. 190-208.

Galvao, T. C. and de Lorenzo, V. 2005. Adaptation of the yeast URA3 selection system to gram-negative bacteria and generation of a {delta}betCDE Pseudomonas putida strain. *Appl Environ Microbiol* 71(2), pp. 883-892.

Gao, L. and Gross, D. S. 2006. Using genomics and proteomics to investigate mechanisms of transcriptional silencing in Saccharomyces cerevisiae. *Brief Funct Genomic Proteomic* 5(4), pp. 280-288.

Gao, L. and Gross, D. S. 2008. Sir2 silences gene transcription by targeting the transition between RNA polymerase II initiation and elongation. *Mol Cell Biol* 28(12), pp. 3979-3994.

Gardner, K. A. and Fox, C. A. 2001. The Sir1 protein's association with a silenced chromosome domain. *Genes Dev* 15(2), pp. 147-157.

Gasser, S. M. and Cockell, M. M. 2001. The molecular biology of the SIR proteins. *Gene* 279(1), pp. 1-16.

Georgel, P. T. and Hansen, J. C. 2001. Linker histone function in chromatin: dual mechanisms of action. *Biochem Cell Biol* 79(3), pp. 313-316.

Geraghty, D. S. et al. 1998. Evidence that partial unwrapping of DNA from nucleosomes facilitates the binding of heat shock factor following DNA replication in yeast. *J Biol Chem* 273(32), pp. 20463-20472.

Ghidelli, S. et al. 2001. Sir2p exists in two nucleosome-binding complexes with distinct deacetylase activities. *Embo J* 20(16), pp. 4522-4535.

Gietz, D. et al. 1992. Improved method for high efficiency transformation of intact yeast cells. *Nucleic Acids Res* 20(6), p. 1425.

Gong, F. et al. 2006. Rad4-Rad23 interaction with SWI/SNF links ATP-dependent chromatin remodeling with nucleotide excision repair. *Nat Struct Mol Biol* 13(10), pp. 902-907.

Gong, F. et al. 2005. Nucleotide excision repair in chromatin and the right of entry. *DNA Repair (Amst)* 4(8), pp. 884-896.

Gordon, L. K. and Haseltine, W. A. 1982. Quantitation of cyclobutane pyrimidine dimer formation in double- and single-stranded DNA fragments of defined sequence. *Radiat Res* 89(1), pp. 99-112.

Gotta, M. et al. 1997. Localization of Sir2p: the nucleolus as a compartment for silent information regulators. *EMBO J* 16(11), pp. 3243-3255.

Gottschling, D. E. 1992. Telomere-proximal DNA in Saccharomyces cerevisiae is refractory to methyltransferase activity in vivo. *Proc Natl Acad Sci U S A* 89(9), pp. 4062-4065.

Gottschling, D. E. et al. 1990. Position effect at S. cerevisiae telomeres: reversible repression of Pol II transcription. *Cell* 63(4), pp. 751-762.

Grandin, N. et al. 2001. Ten1 functions in telomere end protection and length regulation in association with Stn1 and Cdc13. *EMBO J* 20(5), pp. 1173-1183.

Grandin, N. et al. 1997. Stn1, a new Saccharomyces cerevisiae protein, is implicated in telomere size regulation in association with Cdc13. *Genes Dev* 11(4), pp. 512-527.

Grant, P. A. and Berger, S. L. 1999. Histone acetyltransferase complexes. *Semin Cell Dev Biol* 10(2), pp. 169-177.

Grant, P. A. et al. 1997. Yeast Gcn5 functions in two multisubunit complexes to acetylate nucleosomal histones: characterization of an Ada complex and the SAGA (Spt/Ada) complex. *Genes Dev* 11(13), pp. 1640-1650.

Green, C. M. and Almouzni, G. 2002. When repair meets chromatin. First in series on chromatin dynamics. *EMBO Rep* 3(1), pp. 28-33.

Gregoire, S. and Yang, X. J. 2005. Association with class IIa histone deacetylases upregulates the sumoylation of MEF2 transcription factors. *Mol Cell Biol* 25(6), pp. 2273-2287.

Grossi, S. et al. 2001. Telomere formation by rap1p binding site arrays reveals end-specific length regulation requirements and active telomeric recombination. *Mol Cell Biol* 21(23), pp. 8117-8128.

Grummt, I. and Pikaard, C. S. 2003. Epigenetic silencing of RNA polymerase I transcription. *Nat Rev Mol Cell Biol* 4(8), pp. 641-649.

Gueldener, U. et al. 2002. A second set of loxP marker cassettes for Cre-mediated multiple gene knockouts in budding yeast. *Nucleic Acids Res* 30(6), p. e23.

Guldener, U. et al. 1996. A new efficient gene disruption cassette for repeated use in budding yeast. *Nucleic Acids Res* 24(13), pp. 2519-2524.

Guzder, S. N. et al. 1995. Reconstitution of yeast nucleotide excision repair with purified Rad proteins, replication protein A, and transcription factor TFIIH. *J Biol Chem* 270(22), pp. 12973-12976.

Guzder, S. N. et al. 2006. Complex formation with damage recognition protein Rad14 is essential for Saccharomyces cerevisiae Rad1-Rad10 nuclease to perform its function in nucleotide excision repair in vivo. *Mol Cell Biol* 26(3), pp. 1135-1141.

Guzder, S. N. et al. 1999. Synergistic interaction between yeast nucleotide excision repair factors NEF2 and NEF4 in the binding of ultraviolet-damaged DNA. *J Biol Chem* 274(34), pp. 24257-24262.

Haber, J. E. 1998. Mating-type gene switching in Saccharomyces cerevisiae. *Annu Rev Genet* 32, pp. 561-599.

Haldar, D. and Kamakaka, R. T. 2008. Schizosaccharomyces pombe Hst4 functions in DNA damage response by regulating histone H3 K56 acetylation. *Eukaryot Cell* 7(5), pp. 800-813.

Hara, R. and Sancar, A. 2002. The SWI/SNF chromatin-remodeling factor stimulates repair by human excision nuclease in the mononucleosome core particle. *Mol Cell Biol* 22(19), pp. 6779-6787.

Hardy, C. F. et al. 1992. A RAP1-interacting protein involved in transcriptional silencing and telomere length regulation. *Genes Dev* 6(5), pp. 801-814.

Hecht, A. et al. 1995. Histone H3 and H4 N-termini interact with SIR3 and SIR4 proteins: a molecular model for the formation of heterochromatin in yeast. *Cell* 80(4), pp. 583-592.

Hefferin, M. L. and Tomkinson, A. E. 2005. Mechanism of DNA double-strand break repair by non-homologous end joining. *DNA Repair (Amst)* 4(6), pp. 639-648.

Hendrickson, E. A. 1997. Cell-cycle regulation of mammalian DNA double-strand-break repair. *Am J Hum Genet* 61(4), pp. 795-800.

Herrero, E. et al. 2008. Redox control and oxidative stress in yeast cells. *Biochim Biophys Acta* 1780(11), pp. 1217-1235.

Hickman, M. et al. 2007. Isolation and characterization of conditional alleles of the yeast SIR2 gene. *J Mol Biol* 367(5), pp. 1246-1257.

Hitomi, K. et al. 1997. Binding and catalytic properties of Xenopus (6-4) photolyase. *J Biol Chem* 272(51), pp. 32591-32598.

Hoeijmakers, J. H. 2001. Genome maintenance mechanisms for preventing cancer. *Nature* 411(6835), pp. 366-374.

Hoffman, C. S. and Winston, F. 1987. A ten-minute DNA preparation from yeast efficiently releases autonomous plasmids for transformation of Escherichia coli. *Gene* 57(2-3), pp. 267-272.

Imai, S. et al. 2000. Transcriptional silencing and longevity protein Sir2 is an NAD-dependent histone deacetylase. *Nature* 403(6771), pp. 795-800.

Jensen, K. A. and Smerdon, M. J. 1990. DNA repair within nucleosome cores of UV-irradiated human cells. *Biochemistry* 29(20), pp. 4773-4782.

Jenuwein, T. and Allis, C. D. 2001. Translating the histone code. *Science* 293(5532), pp. 1074-1080.

Ji, H. et al. 2008. Yeast Est2p affects telomere length by influencing association of Rap1p with telomeric chromatin. *Mol Cell Biol* 28(7), pp. 2380-2390.

Jin, J. et al. 2005. In and out: histone variant exchange in chromatin. *Trends Biochem Sci* 30(12), pp. 680-687.

Johnson, L. M. et al. 1990. Genetic evidence for an interaction between SIR3 and histone H4 in the repression of the silent mating loci in Saccharomyces cerevisiae. *Proc Natl Acad Sci U S A* 87(16), pp. 6286-6290.

Jones, M. E. 1992. Orotidylate decarboxylase of yeast and man. *Curr Top Cell Regul* 33, pp. 331-342.

Kaeberlein, M. and Powers, R. W., 3rd 2007. Sir2 and calorie restriction in yeast: a skeptical perspective. *Ageing Res Rev* 6(2), pp. 128-140.

Karow, J. K. et al. 2000. RecQ family helicases: roles in cancer and aging. *Curr Opin Genet Dev* 10(1), pp. 32-38.

Katan-Khaykovich, Y. and Struhl, K. 2005. Heterochromatin formation involves changes in histone modifications over multiple cell generations. *Embo J* 24(12), pp. 2138-2149.

Kaufman, P. D. et al. 1997. Ultraviolet radiation sensitivity and reduction of telomeric silencing in Saccharomyces cerevisiae cells lacking chromatin assembly factor-I. *Genes Dev* 11(3), pp. 345-357.

Kelly, T. J. et al. 2000. Type B histone acetyltransferase Hat1p participates in telomeric silencing. *Mol Cell Biol* 20(19), pp. 7051-7058.

Kim, Y. et al. 2006. Activation of Saccharomyces cerevisiae HIS3 results in Gcn4p-dependent, SWI/SNF-dependent mobilization of nucleosomes over the entire gene. *Mol Cell Biol* 26(22), pp. 8607-8622.

Kimura, A. et al. 2002. Chromosomal gradient of histone acetylation established by Sas2p and Sir2p functions as a shield against gene silencing. *Nat Genet* 32(3), pp. 370-377.

Kornberg, R. D. 1977. Structure of chromatin. *Annu Rev Biochem* 46, pp. 931-954.

Kornberg, R. D. and Lorch, Y. 1999. Twenty-five years of the nucleosome, fundamental particle of the eukaryote chromosome. *Cell* 98(3), pp. 285-294.

Kosak, S. T. and Groudine, M. 2004. Gene order and dynamic domains. *Science* 306(5696), pp. 644-647.

Kou, H. et al. 2008. Mms19 protein functions in nucleotide excision repair by sustaining an adequate cellular concentration of the TFIIH component Rad3. *Proc Natl Acad Sci U S A* 105(41), pp. 15714-15719.

Kouzarides, T. 2000. Acetylation: a regulatory modification to rival phosphorylation? *Embo J* 19(6), pp. 1176-1179.

Kouzarides, T. 2007. Chromatin modifications and their function. *Cell* 128(4), pp. 693-705.

Krokan, H. E. et al. 1997. DNA glycosylases in the base excision repair of DNA. *Biochem J* 325 (Pt 1), pp. 1-16.

Kunkel, T. A. and Erie, D. A. 2005. DNA mismatch repair. *Annu Rev Biochem* 74, pp. 681-710.

Kuo, M. H. et al. 1998. Histone acetyltransferase activity of yeast Gcn5p is required for the activation of target genes in vivo. *Genes Dev* 12(5), pp. 627-639.

Kusumoto, R. et al. 2001. Diversity of the damage recognition step in the global genomic nucleotide excision repair in vitro. *Mutat Res* 485(3), pp. 219-227.

Kyrion, G. et al. 1993. RAP1 and telomere structure regulate telomere position effects in Saccharomyces cerevisiae. *Genes Dev* 7(7A), pp. 1146-1159.

Lafon, A. et al. 2007. MYST opportunities for growth control: yeast genes illuminate human cancer gene functions. *Oncogene* 26(37), pp. 5373-5384.

Landry, J. et al. 2000. Role of NAD(+) in the deacetylase activity of the SIR2-like proteins. *Biochem Biophys Res Commun* 278(3), pp. 685-690.

Laroche, T. et al. 1998. Mutation of yeast Ku genes disrupts the subnuclear organization of telomeres. *Curr Biol* 8(11), pp. 653-656.

Lee, D. Y. et al. 1993. A positive role for histone acetylation in transcription factor access to nucleosomal DNA. *Cell* 72(1), pp. 73-84.

Lee, K. et al. 2004. Chromatin remodeling facilitates DNA incision in UV-damaged nucleosomes. *Mol Cells* 18(1), pp. 100-106.

Lee, S. D. and Alani, E. 2006. Analysis of interactions between mismatch repair initiation factors and the replication processivity factor PCNA. *J Mol Biol* 355(2), pp. 175-184.

Leibeling, D. et al. 2006. Nucleotide excision repair and cancer. *J Mol Histol* 37(5-7), pp. 225-238.

Lettieri, T. et al. 2008. Functionally distinct nucleosome-free regions in yeast require Rad7 and Rad16 for nucleotide excision repair. *DNA Repair (Amst)* 7(5), pp. 734-743.

Levy, D. L. and Blackburn, E. H. 2004. Counting of Rif1p and Rif2p on Saccharomyces cerevisiae telomeres regulates telomere length. *Mol Cell Biol* 24(24), pp. 10857-10867.

Li, S. et al. 2006. Modulation of Rad26- and Rpb9-mediated DNA repair by different promoter elements. *J Biol Chem* 281(48), pp. 36643-36651.

Li, S. and Smerdon, M. J. 2002. Nucleosome structure and repair of N-methylpurines in the GAL1-10 genes of Saccharomyces cerevisiae. *J Biol Chem* 277(47), pp. 44651-44659.

Liou, G. G. et al. 2005. Assembly of the SIR complex and its regulation by O-acetyl-ADP-ribose, a product of NAD-dependent histone deacetylation. *Cell* 121(4), pp. 515-527.

Livingstone-Zatchej, M. et al. 2003. Repair of UV lesions in silenced chromatin provides in vivo evidence for a compact chromatin structure. *J Biol Chem* 278(39), pp. 37471-37479.

Livingstone-Zatchej, M. et al. 1997. RNA polymerase II transcription inhibits DNA repair by photolyase in the transcribed strand of active yeast genes. *Nucleic Acids Res* 25(19), pp. 3795-3800.

Lomvardas, S. and Thanos, D. 2001. Nucleosome sliding via TBP DNA binding in vivo. *Cell* 106(6), pp. 685-696.

Longtine, M. S. et al. 1989. A yeast telomere binding activity binds to two related telomere sequence motifs and is indistinguishable from RAP1. *Curr Genet* 16(4), pp. 225-239.

Loo, S. et al. 1995. The origin recognition complex in silencing, cell cycle progression, and DNA replication. *Mol Biol Cell* 6(6), pp. 741-756.

Losa, R. et al. 1990. Poly(dA).poly(dT) rich sequences are not sufficient to exclude nucleosome formation in a constitutive yeast promoter. *Nucleic Acids Res* 18(12), pp. 3495-3502.

Losson, R. et al. 1983. In vivo transcription of a eukaryotic regulatory gene. *EMBO J* 2(12), pp. 2179-2184.

Luger, K. 2006. Dynamic nucleosomes. *Chromosome Res* 14(1), pp. 5-16.

Luger, K. et al. 1997. Crystal structure of the nucleosome core particle at 2.8 A resolution. *Nature* 389(6648), pp. 251-260.

Lustig, A. J. 1998. Mechanisms of silencing in Saccharomyces cerevisiae. *Curr Opin Genet Dev* 8(2), pp. 233-239.

Lydall, D. and Whitehall, S. 2005. Chromatin and the DNA damage response. *DNA Repair (Amst)* 4(10), pp. 1195-1207.

Madeo, F. et al. 2009. Caspase-dependent and caspase-independent cell death pathways in yeast. *Biochem Biophys Res Commun* 382(2), pp. 227-231.

Martino, F. et al. 2009. Reconstitution of yeast silent chromatin: multiple contact sites and O-AADPR binding load SIR complexes onto nucleosomes in vitro. *Mol Cell* 33(3), pp. 323-334.

Masumoto, H. et al. 2005. A role for cell-cycle-regulated histone H3 lysine 56 acetylation in the DNA damage response. *Nature* 436(7048), pp. 294-298.

Maynard, S. et al. 2009. Base excision repair of oxidative DNA damage and association with cancer and aging. *Carcinogenesis* 30(1), pp. 2-10.

McAinsh, A. D. et al. 1999. DNA damage triggers disruption of telomeric silencing and Mec1p-dependent relocation of Sir3p. *Curr Biol* 9(17), pp. 963-966.

Michishita, E. et al. 2008. SIRT6 is a histone H3 lysine 9 deacetylase that modulates telomeric chromatin. *Nature* 452(7186), pp. 492-496.

Millar, C. B. and Grunstein, M. 2006. Genome-wide patterns of histone modifications in yeast. *Nat Rev Mol Cell Biol* 7(9), pp. 657-666.

Mitchell, D. L. 2000. Effects of cytosine methylation on pyrimidine dimer formation in DNA. *Photochem Photobiol* 71(2), pp. 162-165.

Mitra, D. et al. 2006. SWI/SNF binding to the HO promoter requires histone acetylation and stimulates TATA-binding protein recruitment. *Mol Cell Biol* 26(11), pp. 4095-4110.

Moazed, D. 2001. Enzymatic activities of Sir2 and chromatin silencing. *Curr Opin Cell Biol* 13(2), pp. 232-238.

Moazed, D. et al. 2004. A model for step-wise assembly of heterochromatin in yeast. *Novartis Found Symp* 259, pp. 48-56; discussion 56-62, 163-169.

Moggs, J. G. and Almouzni, G. 1999. Chromatin rearrangements during nucleotide excision repair. *Biochimie* 81(1-2), pp. 45-52.

Mollazadeh-Beidokhti, L. et al. 2009. Stochastic model for nucleosome sliding under an external force. *Phys Rev E Stat Nonlin Soft Matter Phys* 79(3 Pt 1), p. 031922.

Mondoux, M. A. et al. 2007. Differential nuclear localization does not determine the silencing status of Saccharomyces cerevisiae telomeres. *Genetics* 177(4), pp. 2019-2029.

Mondoux, M. A. and Zakian, V. A. 2007. Subtelomeric elements influence but do not determine silencing levels at Saccharomyces cerevisiae telomeres. *Genetics* 177(4), pp. 2541-2546.

Moretti, P. et al. 1994. Evidence that a complex of SIR proteins interacts with the silencer and telomere-binding protein RAP1. *Genes Dev* 8(19), pp. 2257-2269.

Morrison, A. J. and Shen, X. 2005. DNA repair in the context of chromatin. *Cell Cycle* 4(4), pp. 568-571.

Morrison, A. J. and Shen, X. 2009. Chromatin remodelling beyond transcription: the INO80 and SWR1 complexes. *Nat Rev Mol Cell Biol.*

Moss, T. 2004. At the crossroads of growth control; making ribosomal RNA. *Curr Opin Genet Dev* 14(2), pp. 210-217.

Nag, R. and Smerdon, M. J. 2009. Altering the chromatin landscape for nucleotide excision repair. *Mutat Res.*

Newman, B. L. et al. 2002. A Drosophila homologue of Sir2 modifies position-effect variegation but does not affect life span. *Genetics* 162(4), pp. 1675-1685.

Nomura, M. 2001. Ribosomal RNA genes, RNA polymerases, nucleolar structures, and synthesis of rRNA in the yeast Saccharomyces cerevisiae. *Cold Spring Harb Symp Quant Biol* 66, pp. 555-565.

Nusinzon, I. and Horvath, C. M. 2005. Histone deacetylases as transcriptional activators? Role reversal in inducible gene regulation. *Sci STKE* 2005(296), p. re11.

Nusinzon, I. and Horvath, C. M. 2006. Positive and negative regulation of the innate antiviral response and beta interferon gene expression by deacetylation. *Mol Cell Biol* 26(8), pp. 3106-3113.

Palladino, F. et al. 1993. SIR3 and SIR4 proteins are required for the positioning and integrity of yeast telomeres. *Cell* 75(3), pp. 543-555.

Parsons, X. H. et al. 2003. Histone deacetylation by Sir2 generates a transcriptionally repressed nucleoprotein complex. *Proc Natl Acad Sci U S A* 100(4), pp. 1609-1614.

Parthasarthy, A. and Gopinathan, K. P. 2005. Modulation of differential transcription of tRNA genes through chromatin organization. *Biochem J* 391(Pt 2), pp. 371-381.

Patzold, A. J. and Lehming, N. 2001. Why Ppr1p is a weak activator of transcription. *FEBS Lett* 494(1-2), pp. 64-68.

Perrod, S. et al. 2001. A cytosolic NAD-dependent deacetylase, Hst2p, can modulate nucleolar and telomeric silencing in yeast. *Embo J* 20(1-2), pp. 197-209.

Perrod, S. and Gasser, S. M. 2003. Long-range silencing and position effects at telomeres and centromeres: parallels and differences. *Cell Mol Life Sci* 60(11), pp. 2303-2318.

Peterson, C. L. and Cote, J. 2004. Cellular machineries for chromosomal DNA repair. *Genes Dev* 18(6), pp. 602-616.

Petit, C. and Sancar, A. 1999. Nucleotide excision repair: from E. coli to man. *Biochimie* 81(1-2), pp. 15-25.

Pfeifer, G. P. et al. 1992. Binding of transcription factors creates hot spots for UV photoproducts in vivo. *Mol Cell Biol* 12(4), pp. 1798-1804.

Pillus, L. and Rine, J. 1989. Epigenetic inheritance of transcriptional states in S. cerevisiae. *Cell* 59(4), pp. 637-647.

Planta, R. J. and Raue, H. A. 1988. Control of ribosome biogenesis in yeast. *Trends Genet* 4(3), pp. 64-68.

Plosky, B. S. and Woodgate, R. 2004. Switching from high-fidelity replicases to low-fidelity lesion-bypass polymerases. *Curr Opin Genet Dev* 14(2), pp. 113-119.

Powell, N. G. et al. 2003. Transcription, nucleosome positioning and protein binding modulate nucleotide excision repair of the Saccharomyces cerevisiae MET17 promoter. *DNA Repair (Amst)* 2(4), pp. 375-386.

Prakash, S. and Prakash, L. 2000. Nucleotide excision repair in yeast. *Mutat Res* 451(1-2), pp. 13-24.

Pryde, F. E. and Louis, E. J. 1999. Limitations of silencing at native yeast telomeres. *EMBO J* 18(9), pp. 2538-2550.

Puglisi, A. et al. 2008. Distinct roles for yeast Stn1 in telomere capping and telomerase inhibition. *EMBO J* 27(17), pp. 2328-2339.

Racki, L. R. and Narlikar, G. J. 2008. ATP-dependent chromatin remodeling enzymes: two heads are not better, just different. *Curr Opin Genet Dev* 18(2), pp. 137-144.

Rasouli-Nia, A. et al. 2004. Stable down-regulation of human polynucleotide kinase enhances spontaneous mutation frequency and sensitizes cells to genotoxic agents. *Proc Natl Acad Sci U S A* 101(18), pp. 6905-6910.

Raynard, S. et al. 2006. A double Holliday junction dissolvasome comprising BLM, topoisomerase IIIalpha, and BLAP75. *J Biol Chem* 281(20), pp. 13861-13864.

Reed, S. H. 2005. Nucleotide excision repair in chromatin: the shape of things to come. *DNA Repair (Amst)* 4(8), pp. 909-918.

Richardson, C. et al. 1998. Double-strand break repair by interchromosomal recombination: suppression of chromosomal translocations. *Genes Dev* 12(24), pp. 3831-3842.

Rine, J. and Herskowitz, I. 1987. Four genes responsible for a position effect on expression from HML and HMR in Saccharomyces cerevisiae. *Genetics* 116(1), pp. 9-22.

Rivier, D. H. et al. 1999. HMR-I is an origin of replication and a silencer in Saccharomyces cerevisiae. *Genetics* 151(2), pp. 521-529.

Rose, M. and Winston, F. 1984. Identification of a Ty insertion within the coding sequence of the S. cerevisiae URA3 gene. *Mol Gen Genet* 193(3), pp. 557-560.

Rosenberg, M. I. and Parkhurst, S. M. 2002. Drosophila Sir2 is required for heterochromatic silencing and by euchromatic Hairy/E(Spl) bHLH repressors in segmentation and sex determination. *Cell* 109(4), pp. 447-458.

Roth, S. Y. et al. 2001. Histone acetyltransferases. *Annu Rev Biochem* 70, pp. 81-120.

Roy, A. et al. 1990. cis- and trans-acting regulatory elements of the yeast URA3 promoter. *Mol Cell Biol* 10(10), pp. 5257-5270.

Ruiz-Garcia, A. B. et al. 1997. Gcn5p is involved in the acetylation of histone H3 in nucleosomes. *FEBS Lett* 403(2), pp. 186-190.

Runger, T. M. and Kappes, U. P. 2008. Mechanisms of mutation formation with long-wave ultraviolet light (UVA). *Photodermatol Photoimmunol Photomed* 24(1), pp. 2-10.

Rusche, L. N. et al. 2003. The establishment, inheritance, and function of silenced chromatin in Saccharomyces cerevisiae. *Annu Rev Biochem* 72, pp. 481-516.

Saha, A. et al. 2006. Chromatin remodelling: the industrial revolution of DNA around histones. *Nat Rev Mol Cell Biol* 7(6), pp. 437-447.

San Filippo, J. et al. 2008. Mechanism of eukaryotic homologous recombination. *Annu Rev Biochem* 77, pp. 229-257.

Sancar, A. 1994. Structure and function of DNA photolyase. *Biochemistry* 33(1), pp. 2-9.

Sancar, A. et al. 2004. Molecular mechanisms of mammalian DNA repair and the DNA damage checkpoints. *Annu Rev Biochem* 73, pp. 39-85.

Sancar, G. B. 1990. DNA photolyases: physical properties, action mechanism, and roles in dark repair. *Mutat Res* 236(2-3), pp. 147-160.

Sancar, G. B. 2000. Enzymatic photoreactivation: 50 years and counting. *Mutat Res* 451(1-2), pp. 25-37.

Sandell, L. L. et al. 1994. Transcription of a yeast telomere alleviates telomere position effect without affecting chromosome stability. *Proc Natl Acad Sci U S A* 91(25), pp. 12061-12065.

Sandell, L. L. and Zakian, V. A. 1992. Telomeric position effect in yeast. *Trends Cell Biol* 2(1), pp. 10-14.

Sandmeier, J. J. et al. 2002. RPD3 is required for the inactivation of yeast ribosomal DNA genes in stationary phase. *Embo J* 21(18), pp. 4959-4968.

Santoro, R. 2005. The silence of the ribosomal RNA genes. *Cell Mol Life Sci* 62(18), pp. 2067-2079.

Sauve, A. A. et al. 2001. Chemistry of gene silencing: the mechanism of NAD+-dependent deacetylation reactions. *Biochemistry* 40(51), pp. 15456-15463.

Schieferstein, U. and Thoma, F. 1996. Modulation of cyclobutane pyrimidine dimer formation in a positioned nucleosome containing poly(dA.dT) tracts. *Biochemistry* 35(24), pp. 7705-7714.

Scott, A. D. et al. 1999. Spontaneous mutation, oxidative DNA damage, and the roles of base and nucleotide excision repair in the yeast Saccharomyces cerevisiae. *Yeast* 15(3), pp. 205-218.

Segal, E. et al. 2006. A genomic code for nucleosome positioning. *Nature* 442(7104), pp. 772-778.

Segal, E. and Widom, J. 2009. Poly(dA:dT) tracts: major determinants of nucleosome organization. *Curr Opin Struct Biol* 19(1), pp. 65-71.

Sekinger, E. A. and Gross, D. S. 2001. Silenced chromatin is permissive to activator binding and PIC recruitment. *Cell* 105(3), pp. 403-414.

Sekinger, E. A. et al. 2005. Intrinsic histone-DNA interactions and low nucleosome density are important for preferential accessibility of promoter regions in yeast. *Mol Cell* 18(6), pp. 735-748.

Selleck, S. B. and Majors, J. 1987. Photofootprinting in vivo detects transcription-dependent changes in yeast TATA boxes. *Nature* 325(7000), pp. 173-177.

Shampay, J. et al. 1984. DNA sequences of telomeres maintained in yeast. *Nature* 310(5973), pp. 154-157.

Shankaranarayana, G. D. et al. 2003. Sir2 regulates histone H3 lysine 9 methylation and heterochromatin assembly in fission yeast. *Curr Biol* 13(14), pp. 1240-1246.

Shei, G. J. and Broach, J. R. 1995. Yeast silencers can act as orientation-dependent gene inactivation centers that respond to environmental signals. *Mol Cell Biol* 15(7), pp. 3496-3506.

Sherman, J. M. et al. 1999. The conserved core of a human SIR2 homologue functions in yeast silencing. *Mol Biol Cell* 10(9), pp. 3045-3059.

Shia, W. J. et al. 2006. SAS-mediated acetylation of histone H4 Lys 16 is required for H2A.Z incorporation at subtelomeric regions in Saccharomyces cerevisiae. *Genes Dev* 20(18), pp. 2507-2512.

Shimizu, M. et al. 2000. Destabilization of nucleosomes by an unusual DNA conformation adopted by poly(dA) small middle dotpoly(dT) tracts in vivo. *EMBO J* 19(13), pp. 3358-3365.

Shogren-Knaak, M. et al. 2006. Histone H4-K16 acetylation controls chromatin structure and protein interactions. *Science* 311(5762), pp. 844-847.

Skiniotis, G. et al. 2007. Acetylated histone tail peptides induce structural rearrangements in the RSC chromatin remodeling complex. *J Biol Chem* 282(29), pp. 20804-20808.

Slieman, T. A. et al. 2000. Spore photoproduct (SP) lyase from Bacillus subtilis specifically binds to and cleaves SP (5-thyminyl-5,6-dihydrothymine) but not cyclobutane pyrimidine dimers in UV-irradiated DNA. *J Bacteriol* 182(22), pp. 6412-6417.

Smerdon, M. J. 1991. DNA repair and the role of chromatin structure. *Curr Opin Cell Biol* 3(3), pp. 422-428.

Smerdon, M. J. and Conconi, A. 1999. Modulation of DNA damage and DNA repair in chromatin. *Prog Nucleic Acid Res Mol Biol* 62, pp. 227-255.

Smerdon, M. J. and Lieberman, M. W. 1978. Nucleosome rearrangement in human chromatin during UV-induced DNA- reapir synthesis. *Proc Natl Acad Sci U S A* 75(9), pp. 4238-4241.

Smerdon, M. J. and Lieberman, M. W. 1980. Distribution within chromatin of deoxyribonucleic acid repair synthesis occurring at different times after ultraviolet radiation. *Biochemistry* 19(13), pp. 2992-3000.

Smith, J. S. and Boeke, J. D. 1997. An unusual form of transcriptional silencing in yeast ribosomal DNA. *Genes Dev* 11(2), pp. 241-254.

Starai, V. J. et al. 2002. Sir2-dependent activation of acetyl-CoA synthetase by deacetylation of active lysine. *Science* 298(5602), pp. 2390-2392.

Strahl, B. D. and Allis, C. D. 2000. The language of covalent histone modifications. *Nature* 403(6765), pp. 41-45.

Struhl, K. 1985. Naturally occurring poly(dA-dT) sequences are upstream promoter elements for constitutive transcription in yeast. *Proc Natl Acad Sci U S A* 82(24), pp. 8419-8423.

Struhl, K. 1986. Constitutive and inducible Saccharomyces cerevisiae promoters: evidence for two distinct molecular mechanisms. *Mol Cell Biol* 6(11), pp. 3847-3853.

Suka, N. et al. 2002. Sir2p and Sas2p opposingly regulate acetylation of yeast histone H4 lysine16 and spreading of heterochromatin. *Nat Genet* 32(3), pp. 378-383.

Suka, N. et al. 2001. Highly specific antibodies determine histone acetylation site usage in yeast heterochromatin and euchromatin. *Mol Cell* 8(2), pp. 473-479.

Suter, B. et al. 2000. Poly(dA.dT) sequences exist as rigid DNA structures in nucleosome-free yeast promoters in vivo. *Nucleic Acids Res* 28(21), pp. 4083-4089.

Tanaka, S. et al. 1996. Chromatin structure of the yeast URA3 gene at high resolution provides insight into structure and positioning of nucleosomes in the chromosomal context. *J Mol Biol* 257(5), pp. 919-934.

Tanny, J. C. et al. 2004. Budding yeast silencing complexes and regulation of Sir2 activity by protein-protein interactions. *Mol Cell Biol* 24(16), pp. 6931-6946.

Tanny, J. C. and Moazed, D. 2001. Coupling of histone deacetylation to NAD breakdown by the yeast silencing protein Sir2: Evidence for acetyl transfer from substrate to an NAD breakdown product. *Proc Natl Acad Sci U S A* 98(2), pp. 415-420.

Teng, Y. et al. 1997. Excision repair at the level of the nucleotide in the Saccharomyces cerevisiae MFA2 gene: mapping of where enhanced repair in the transcribed strand begins or ends and identification of only a partial rad16 requisite for repairing upstream control sequences. *J Mol Biol* 267(2), pp. 324-337.

Teng, Y. et al. 2008. Saccharomyces cerevisiae Rad16 mediates ultraviolet-dependent histone H3 acetylation required for efficient global genome nucleotide-excision repair. *EMBO Rep* 9(1), pp. 97-102.

Teng, Y. and Waters, R. 2000. Excision repair at the level of the nucleotide in the upstream control region, the coding sequence and in the region where transcription terminates of the Saccharomyces cerevisiae MFA2 gene and the role of RAD26. *Nucleic Acids Res* 28(5), pp. 1114-1119.

Teng, Y. et al. 2002. The Saccharomyces cerevisiae histone acetyltransferase Gcn5 has a role in the photoreactivation and nucleotide excision repair of UV-induced cyclobutane pyrimidine dimers in the MFA2 gene. *J Mol Biol* 316(3), pp. 489-499.

Terleth, C. et al. 1989. Differential repair of UV damage in Saccharomyces cerevisiae. *Nucleic Acids Res* 17(12), pp. 4433-4439.

Tham, W. H. and Zakian, V. A. 2002. Transcriptional silencing at Saccharomyces telomeres: implications for other organisms. *Oncogene* 21(4), pp. 512-521.

Thoma, F. 1986. Protein-DNA interactions and nuclease-sensitive regions determine nucleosome positions on yeast plasmid chromatin. *J Mol Biol* 190(2), pp. 177-190.

Thoma, F. 1999. Light and dark in chromatin repair: repair of UV-induced DNA lesions by photolyase and nucleotide excision repair. *EMBO J* 18(23), pp. 6585-6598.

Tijsterman, M. et al. 1999. RNA polymerase II transcription suppresses nucleosomal modulation of UV-induced (6-4) photoproduct and cyclobutane pyrimidine dimer repair in yeast. *Mol Cell Biol* 19(1), pp. 934-940.

Todo, T. et al. 1996. Similarity among the Drosophila (6-4)photolyase, a human photolyase homolog, and the DNA photolyase-blue-light photoreceptor family. *Science* 272(5258), pp. 109-112.

Todo, T. et al. 1993. A new photoreactivating enzyme that specifically repairs ultraviolet light-induced (6-4)photoproducts. *Nature* 361(6410), pp. 371-374.

Tommerup, H. et al. 1994. Unusual chromatin in human telomeres. *Mol Cell Biol* 14(9), pp. 5777-5785.

Tong, J. K. et al. 1998. Chromatin deacetylation by an ATP-dependent nucleosome remodelling complex. *Nature* 395(6705), pp. 917-921.

Tornaletti, S. and Pfeifer, G. P. 1995. UV light as a footprinting agent: modulation of UV-induced DNA damage by transcription factors bound at the promoters of three human genes. *J Mol Biol* 249(4), pp. 714-728.

Tremblay, M. et al. 2008. Complementary roles of yeast Rad4p and Rad34p in nucleotide excision repair of active and inactive rRNA gene chromatin. *Mol Cell Biol* 28(24), pp. 7504-7513.

Triolo, T. and Sternglanz, R. 1996. Role of interactions between the origin recognition complex and SIR1 in transcriptional silencing. *Nature* 381(6579), pp. 251-253.

Tsuzuki, T. et al. 2007. Significance of error-avoiding mechanisms for oxidative DNA damage in carcinogenesis. *Cancer Sci* 98(4), pp. 465-470.

Turner, B. M. 2000. Histone acetylation and an epigenetic code. *Bioessays* 22(9), pp. 836-845.

Tuteja, N. et al. 2009. Genotoxic stress in plants: shedding light on DNA damage, repair and DNA repair helicases. *Mutat Res* 681(2-3), pp. 134-149.

Ulrich, H. D. 2007. Conservation of DNA damage tolerance pathways from yeast to humans. *Biochem Soc Trans* 35(Pt 5), pp. 1334-1337.

van Gool, A. J. et al. 1994. RAD26, the functional S. cerevisiae homolog of the Cockayne syndrome B gene ERCC6. *EMBO J* 13(22), pp. 5361-5369.

Vaquero, A. 2009. The conserved role of sirtuins in chromatin regulation. *Int J Dev Biol* 53(2-3), pp. 303-322.

Vaquero, A. et al. 2007. NAD+-dependent deacetylation of H4 lysine 16 by class III HDACs. *Oncogene* 26(37), pp. 5505-5520.

Varghese, A. J. 1970. 5-Thyminyl-5,6-dihydrothymine from DNA irradiated with ultraviolet light. *Biochem Biophys Res Commun* 38(3), pp. 484-490.

Vega-Palas, M. A. et al. 1997. Telomeric transcriptional silencing in a natural context. *Nat Genet* 15(3), pp. 232-233.

Vega-Palas, M. A. et al. 1998. Heterochromatin organization of a natural yeast telomere. Changes of nucleosome distribution driven by the absence of Sir3p. *J Biol Chem* 273(16), pp. 9388-9392.

Verger, A. and Crossley, M. 2004. Chromatin modifiers in transcription and DNA repair. *Cell Mol Life Sci* 61(17), pp. 2154-2162.

Verhage, R. et al. 1994. The RAD7 and RAD16 genes, which are essential for pyrimidine dimer removal from the silent mating type loci, are also required for repair of the nontranscribed strand of an active gene in Saccharomyces cerevisiae. *Mol Cell Biol* 14(9), pp. 6135-6142.

Veron, M. et al. 2006. Histone H1 of Saccharomyces cerevisiae inhibits transcriptional silencing. *Genetics* 173(2), pp. 579-587.

Vettese-Dadey, M. et al. 1996. Acetylation of histone H4 plays a primary role in enhancing transcription factor binding to nucleosomal DNA in vitro. *Embo J* 15(10), pp. 2508-2518.

Vetting, M. W. et al. 2005. Structure and functions of the GNAT superfamily of acetyltransferases. *Arch Biochem Biophys* 433(1), pp. 212-226.

Wade, P. A. 2001. Transcriptional control at regulatory checkpoints by histone deacetylases: molecular connections between cancer and chromatin. *Hum Mol Genet* 10(7), pp. 693-698.

Wang, A. et al. 2002. Requirement of Hos2 histone deacetylase for gene activity in yeast. *Science* 298(5597), pp. 1412-1414.

Wang, Z. et al. 1995. The yeast TFB1 and SSL1 genes, which encode subunits of transcription factor IIH, are required for nucleotide excision repair and RNA polymerase II transcription. *Mol Cell Biol* 15(4), pp. 2288-2293.

Wang, Z. et al. 1997. The RAD7, RAD16, and RAD23 genes of Saccharomyces cerevisiae: requirement for transcription-independent nucleotide excision repair in vitro and interactions between the gene products. *Mol Cell Biol* 17(2), pp. 635-643.

Wang, Z. G. et al. 1991. Nucleotide excision repair of DNA by human cell extracts is suppressed in reconstituted nucleosomes. *J Biol Chem* 266(33), pp. 22472-22478.

Warner, J. R. 1989. Synthesis of ribosomes in Saccharomyces cerevisiae. *Microbiol Rev* 53(2), pp. 256-271.

Waters, R. and Smerdon, M. J. 2005. Preface. *DNA Repair (Amst)* 4(8), pp. 853-854.

Waters, R. et al. 2009. Tilting at windmills? The nucleotide excision repair of chromosomal DNA. *DNA Repair (Amst)* 8(2), pp. 146-152.

Wellinger, R. E. and Thoma, F. 1997. Nucleosome structure and positioning modulate nucleotide excision repair in the non-transcribed strand of an active gene. *EMBO J* 16(16), pp. 5046-5056.

Whitehouse, I. and Tsukiyama, T. 2006. Antagonistic forces that position nucleosomes in vivo. *Nat Struct Mol Biol* 13(7), pp. 633-640.

Widom, J. 1998. Structure, dynamics, and function of chromatin in vitro. *Annu Rev Biophys Biomol Struct* 27, pp. 285-327.

Wiederhold, L. et al. 2004. AP endonuclease-independent DNA base excision repair in human cells. *Mol Cell* 15(2), pp. 209-220.

Wilson, D. M., 3rd and Barsky, D. 2001. The major human abasic endonuclease: formation, consequences and repair of abasic lesions in DNA. *Mutat Res* 485(4), pp. 283-307.

Wilson, D. M., 3rd and Bohr, V. A. 2007. The mechanics of base excision repair, and its relationship to aging and disease. *DNA Repair (Amst)* 6(4), pp. 544-559.

Wilson, S. H. 1998. Mammalian base excision repair and DNA polymerase beta. *Mutat Res* 407(3), pp. 203-215.

Witt, O. et al. 2009. HDAC family: What are the cancer relevant targets? *Cancer Lett* 277(1), pp. 8-21.

Workman, J. L. and Kingston, R. E. 1998. Alteration of nucleosome structure as a mechanism of transcriptional regulation. *Annu Rev Biochem* 67, pp. 545-579.

Wotton, D. and Shore, D. 1997. A novel Rap1p-interacting factor, Rif2p, cooperates with Rif1p to regulate telomere length in Saccharomyces cerevisiae. *Genes Dev* 11(6), pp. 748-760.

Wright, J. H. et al. 1992. Saccharomyces telomeres assume a non-nucleosomal chromatin structure. *Genes Dev* 6(2), pp. 197-210.

Wyatt, H. R. et al. 2003. Multiple roles for Saccharomyces cerevisiae histone H2A in telomere position effect, Spt phenotypes and double-strand-break repair. *Genetics* 164(1), pp. 47-64.

Xie, J. et al. 1999. Sum1 and Hst1 repress middle sporulation-specific gene expression during mitosis in Saccharomyces cerevisiae. *Embo J* 18(22), pp. 6448-6454.

Xu, F. et al. 2005. Acetylation in histone H3 globular domain regulates gene expression in yeast. *Cell* 121(3), pp. 375-385.

Xu, F. et al. 2007. Sir2 deacetylates histone H3 lysine 56 to regulate telomeric heterochromatin structure in yeast. *Mol Cell* 27(6), pp. 890-900.

Yang, B. et al. 2008. Insights into the impact of histone acetylation and methylation on Sir protein recruitment, spreading, and silencing in Saccharomyces cerevisiae. *J Mol Biol* 381(4), pp. 826-844.

Yang, X. J. and Seto, E. 2003. Collaborative spirit of histone deacetylases in regulating chromatin structure and gene expression. *Curr Opin Genet Dev* 13(2), pp. 143-153.

You, Y. H. et al. 2001. Cyclobutane pyrimidine dimers are responsible for the vast majority of mutations induced by UVB irradiation in mammalian cells. *J Biol Chem* 276(48), pp. 44688-44694.

Yu, S. et al. 2004. The yeast Rad7/Rad16/Abf1 complex generates superhelical torsion in DNA that is required for nucleotide excision repair. *DNA Repair (Amst)* 3(3), pp. 277-287.

Yu, S. et al. 2009. ABF1-binding sites promote efficient global genome nucleotide excision repair. *J Biol Chem* 284(2), pp. 966-973.

Yu, Y. et al. 2005. UV irradiation stimulates histone acetylation and chromatin remodeling at a repressed yeast locus. *Proc Natl Acad Sci U S A* 102(24), pp. 8650-8655.

Yu, Y. and Waters, R. 2005. Histone acetylation, chromatin remodelling and nucleotide excision repair: hint from the study on MFA2 in Saccharomyces cerevisiae. *Cell Cycle* 4(8), pp. 1043-1045.

Yuan, G. C. et al. 2005. Genome-scale identification of nucleosome positions in S. cerevisiae. *Science* 309(5734), pp. 626-630.

Yuan, L. W. and Giordano, A. 2002. Acetyltransferase machinery conserved in p300/CBP-family proteins. *Oncogene* 21(14), pp. 2253-2260.

Zhao, X. et al. 1997. Reaction mechanism of (6-4) photolyase. *J Biol Chem* 272(51), pp. 32580-32590.

Zink, D. et al. 2004. Transcription-dependent spatial arrangements of CFTR and adjacent genes in human cell nuclei. *J Cell Biol* 166(6), pp. 815-825.

Appendix I
Growth media, solutions, buffers, primers and probes

AI.1 Growth media

All media listed require sterilisation using an autoclave for 20-30 minutes at 15 psi.

YNBD minimal medium	**200 ml**
Yeast nitrogen base w/o amino acids	1.4 g
Glucose	4 g
Agar (to make YNBD plates)	4 g
H_2O	200 ml

Cool media to 50°C after sterilisation before the addition of any required amino acids.

YPD medium	**1000 ml**
1% Yeast extract	10 g
2% Bacto peptone	20 g
2% Glucose	100 ml of 20 % solution
H_2O to final volume	900 ml

YPD plates	**400 ml**
1% Yeast extract	4 g
2% Bacto peptone	8 g
2% Glucose	40 ml of 20 % solution
2% Bacto agar	8 ml
H_2O to final volume	360 ml

LB Medium (plates)	**1 litre**
0.5% Yeast extract	5 g
1% Bacto tryptone	10 g
1% NaCl	10 g
2% Bacto agar (to make LB plates)	8 ml
Deionised H_2O to 1 litre	360 ml

Adjust the pH to 7.0 using 5M NaOH

AI.2 Stock solutions and buffers

All stock solutions are prepared in 1 litre and are sterilized by autoclaving unless otherwise stated.

1 M DTT (Dithiothreitol)

DTT	3.09 g

Dissolve in 20 ml of 0.01 M sodium acetate (pH 5.2). Sterilise by filtration. Do not autoclave DTT or solution containing DTT.

0.5 M EDTA (ethylenediaminetetraacetic acid)

$EDTA.NA_2.2H_2O$	186.7 g
H_2O	800 ml

Stir vigorously on a magnetic stirrer. Adjust the pH to 8.0 with ~20 g of NaOH pellets. Add H_2O to make up to 1 litre.

5 M NaCl (Sodium chloride)

NaCl	292.2 g
H_2O	up to 1 litre

PBS (Phosphate Buffered Saline)

NaCl	8 g
KCl	0.2 g
$Na_2HPO4.2H_2O$	1.44 g
KH_2PO4	0.24 g
H_2O	800 ml

1 M Phosphate solution

Na_2HPO_4	71 g
H_3PO_4 (85%)	4 ml
H_2O	up to 1000 ml

10% SDS (Sodium dodecyl sulfate)

SDS (electrophoresis grade)	100 g
H_2O	900 ml

Heat the solution to 68°C to assist dissolution. Adjust the pH to 7.2 by adding a few drops of concentrated HCl. Make up the volume to 1 litre with H_2O.

3 M Na Ac (Sodium acetate), (pH 5.2)

Sodium acetate·$3H_2O$	408.1 g
H_2O	800 ml

Adjust the pH to 5.2 with glacial acetic acid. Add H_2O to make 1 litre.

20 × SSC

NaCl (3 M)	175.3 g
Sodium citrate dihydrate (0.3 M)	88.2 g
H_2O	800 ml

Adjust the pH to 7.0 with HCl. Make up the volume to 1 litre with H_2O.

1xTE (Tris-EDTA) Buffer

10 mM Tris-HCl (pH 7.5)
1 mM EDTA (pH 8.0)
Add H_20 to make up to 1 litre

pH	**HCl**
7.4	70 ml
7.6	60 ml
8.0	42 ml

1 M Tris

Tris base	121.1 g
H_2O	800 ml

Adjust the pH accordingly by adding concentrated HCl. Add H_20 to make up to 1 litre.

pH	HCl
7.4	70 ml
7.6	60 ml
8.0	42 ml

AI.3 DNA Extraction solutions

DNA Lysis Buffer

Urea	4 M
NaCl	200 mM
Tris-HCl (pH 8.0)	100 mM
EDTA	10 mM
n- Lauroyl Sarcosine	0.5 % (w/v)

Sorbitol-TE solution

Sorbitol	0.9 M
Tris-HCl (pH 8.0)	100 mM
EDTA	100 mM

AI.4 Solutions for gel electrophoresis

Solutions are prepared in 1litre unless otherwise specified

50xTAE (Tris-acetate-EDTA, 1 litre)

2 M Tris base	242 g
1 M Sodium Acetate.$3H_2O$	136 g
50 mM EDTA.Na2.$2H_2O$	19 g

Adjust the pH to 7.2 with glacial acetic acid. Add H_2O to make 1 litre.
Diluted 50X for use in preparation of gels and running buffers.

10×TBE (Tris-borate- EDTA, 1 litre)

Tris base	108 g
Boric acid	55 g
$Na_2EDTA{\cdot}2H_2O$	9.3 g

Add H_2O to 1 litre.

Denaturing running buffer

NaOH	36 mM
EDTA	1 mM

Non-denaturing loading buffer

Ficoll	10 %
SDS	0.5 %
Bromophenol Blue	0.06 %

Made up in 1xTAE

Denaturing loading buffer

NaOH	50 mM
EDTA	1 mM
Ficoll	2.5 %
Bromophenol blue	0.025 %

Sequencing gel-loading buffer

Deionized formamide	95 %
EDTA (pH 8.0)	20 mM
Xylene cyanol FF	0.05 %
Bromophenol blue	0.05 %

2×Dynabead Washing and Binding Buffer (2 × BW)

NaCl	2 M
Tris-HCl (pH 8.0)	10 mM
EDTA	1 mM

AI.5 Enzyme digestion buffers

ML (*M. luteus* enzyme) stock buffer

Tris (pH 7.5)	10 mM
Ethylene glycol	10 %
2-Mercaptoethanol	1 mM

T4 endo V working buffer (10 X concentration)

Phosphate buffer (pH 6.4)	500 mM
EDTA	100 mM
2-Mercaptoethanol	10 mM

AI.6 Solutions for ChIP (chromatin immunoprecipitation)

FA/SDS (ChIP Lysis analysis)

HEPES-KOH	50 mM
NaCl	150 mM
EDTA	1 mM
Triton X-100	1 %
Sodium deoxycholate	0.1 %
SDS 10%	0.1 %

LiCl (Lithium chloride)

Tris-HCl	10 mM
LiCl	250 mM
EDTA	1 mM
Igapel CA-630	0.5 %
Sodium deoxycholate	0.5 %

5 X Pronase Buffer

Tris pH7.5	125 mM
EDTA	25 mM
SDS	2.5 %
Pronase	1 mg/ml

Elution Buffer

SDS	1 %
$NaHCO_3$	0.1 M

AI.7 Probes and primers

Names	Sequences and modifications	
AntoTSMseIb	5'GATAGCTTTTTTAGCCGCTAAAGGCATTATCCGCCAAGTACA3'	5'Biotin
AntoNTSMseIb	5'GATAGCTTTTTTAATTGAAGCTCTAATTTGTGAGTTTAGTATAC3'	5'Biotin
AntoTSMseI	5'GATAGCAGCCGCTAAAGGCATTATCCGCCAAGTACA3'	NO
AntoNTSMseI	5'GATAGCAATTGAAGCTCTAATTTGTGAGTTTAGTATAC3'	NO
URA3kanMXF	5'AAGGATAAGTTTTGACCATCAAAGAAGGTTAATGTGGCTGCAGCTGAAGCTTCG3'	NO
URA3kanMXR	5'CGAGGTATTGGATAGTTCCTTTTTATAAAGGCCATGAAGCCGCATAGGCCACTAGTGGA3'	NO
URA3-1	5'GAAACTAGGGAAGACAAGCAA3'	NO
URA3-2	5'CGTACGAAGCTTCAGCTGCAGCCACATTAACCTTCTTTGATGGTC3'	NO
URA3-3	5'CCACTAGTGGCCTATGCGGCTTCATGGCCTTTATAAAAAGGAAC3'	NO
URA3-4	5'GAATTTTGTTTGGATTTGGTTA3'	NO
URA3outsideF	5'CAGACGATGATAACAAACCG3'	NO
URA3outsideR	5'CGTCCATCTTTACAGTCCTG3'	NO
SIR2F2	5'GGCCGCCAGTTGCGGTAAAA3'	NO
SIR2R(2)	5'CACCACCTCCTTTCTTTGACCC3'	NO
LEU2 F	5'AGACACATTCAAACCATTTTTCCCTCATCGGCACATTAAAGCTGGATGTCTAAGAATATCGTTGTCC3'	NO
LEU2R	5'ATTGATATTAATTTGGCACTTTTAAATTATTAAATTGCCTTCTACCTCTTTAAGCCAAGATTTCCTT3'	NO
+ 222 A	5'TAAGCCGCTAAAGGCATTAT	NO
+ 390 B	5'ACCGTGTGCATTCGTAA3'	NO
+ 540 A	5'GGCTTTATTGCTCAAAGAGAC	NO
+ 669 B	5'CTTGTCATCTAAACCCAC3'	NO

AI.8 Solutions for nucleosome mapping

Lysis solution per 1g cells

Sorbitol	1 M
β - mercaptoethanol	5 mM
Zymolase	25 mg

Ficoll solution

Ficoll	18 % w/v
KH_2PO_4 (pH 6.8)	20 mM
$MgCl_2$	1 mM
EGTA	0.25 mM
EDTA	0.25 mM

Stop solution (final concentration)

SDS	1 %
EDTA	5 ml

MNase digestion buffer

Tris-HCl	15 mM
NaCl	75 mM
$MgCl_2$	3 mM
$CaCl_2$	1.5 mM
2-mercaptoethanol	1 mM

Appendix II

Data from chapter III

AII.1 Average of the surviving colonies for the FEP100-10ura3-52Δ, FEP178ura3-52Δ, FEP178sir2*, and FEP100-10sir2*strains

The tables below summarize the number of colonies obtained in 3 independent experiments for the FEP100-10ura3-52Δ, FEP100-10sir2*,FEP178ura3-52Δ and FEP178sir2* strains.

	FEP100-10ura3-52Δ				FEP100-10sir2*				FEP178ura3-52Δ				FEP178sir2*				Control strain			
	- URA		+URA		- URA		+ URA		-URA		+ URA		- URA		+ URA		- URA		+ URA	
	+ FOA	- FOA	+ FOA	- FOA	+ FOA	- FOA	+ FOA	- FOA	+ FOA	- FOA	+ FOA	- FOA	+ FOA	- FOA	+ FOA	- FOA	+ FOA	- FOA	+ FOA	- FOA
Exp 1	51	149	72	128	0	116	0	81	6	628	8	156	0	152	0	77	0	320	115	119
Exp 2	86	120	64	126	0	130	0	42	14	360	9	166	0	156	0	91	0	328	69	125
Exp 3	56	124	80	140	0	120	0	60	19	594	9	174	0	128	0	69	2	384	184	145

The strain where *URA3* is inserted at natural location was used as a control strain.

AII.2 The percentage of the surviving colonies and standard error for the FEP100 -10ura3-52Δ, FEP178ura3-52Δ, FEP178sir2*, and FEP100-10sir2*strains

The % of the surviving colonies and the standard error were calculated. In the table below the statistical analysis for the FEP100-10ura3-52Δ, FEP178ura3-52Δ, FEP178sir2*, and FEP100-10sir2*strains is indicated. The expression of *URA3* was determined by measuring the fraction of cells that were able to grow on plates containing 5-Fluoroorotic acid (5-FOA) *versus* the colonies able to grow on plates without 5-FOA.

		FEP100-10ura3-52Δ	FEP100-10sir2*	FEP178ura3-52Δ	FEP178sir2*	Endogenous *URA3*
%	URA-	49.1	0.0	2.5	0.0	0.2
	URA+	54.8	0.0	5.2	0.0	94.6
St. E	URA-	10.9	0.0	3.8	0.0	0.7
	URA+	4.6	0.0	0.3	0.0	33.4

The percentage and the standard error of all the experiments were used for the graph illustrated in the chapter III (figure 3.9).

Appendix III

Data from Chapter IV

A III Data for the repair experiments

A III.1-1 NER efficiency at high resolution at *URA3* gene for the NTS

The table below represent the repair efficiency at the specific CPD points for the NTS in the NRE and RE strains.

Exp 1	RE					NRE				
CPDs	Repair time (hours)					Repair time (hours)				
Position	0	1	2	3	4	0	1	2	3	4
Top band	1394203.9	1251552.7	1362670.6	1484348.6	1135776.3	1958276.6	1679756.3	1944286.6	2193285.4	1812283.8
244	41143.2	35692.1	40688.3	42488.1	34550.1	35386.0	26849.4	39489.1	29468.2	17027.4
257	98820.9	89147.1	104295.0	108868.3	84820.4	97602.5	62129.7	98718.7	69562.5	33334.3
292	46238.1	41725.9	54493.3	52866.4	42796.5	43203.0	30762.1	49173.5	45260.1	21781.0
302	2668.8	2017.2	2268.3	1831.8	1199.4	2573.1	2049.5	2057.0	2343.0	1683.8
313	14125.3	11111.8	12974.5	9433.8	8400.8	16909.0	11701.3	16571.5	12365.4	7583.5
326	70461.5	61326.6	76971.0	77977.9	61641.8	65216.4	46757.0	68640.2	70629.7	40862.4
363	43658.5	38757.6	49979.8	45291.0	34271.7	45452.1	28808.4	44781.5	32109.5	14309.2
388	10507.8	11324.3	13095.9	13669.5	11151.7	9813.7	7215.3	9674.4	8006.4	3873.7
399	4300.8	4909.3	6003.8	6572.9	5431.1	2946.6	2024.7	3912.0	2226.0	1783.1
407	4234.8	3320.5	4056.4	3758.7	2964.2	3943.7	3092.8	3006.2	2261.9	1980.3
440	14051.8	13841.6	16864.0	16050.5	12838.9	13488.6	9370.3	14019.5	10664.6	6684.2
460	9535.1	7731.4	8579.1	9875.1	7831.8	9533.3	7672.0	12762.7	12350.8	6473.5
480	28427.0	24304.7	29395.5	29491.3	23067.5	31805.4	21612.0	34752.0	32543.6	18082.2
503	9232.0	6290.1	8225.5	8447.8	6749.6	8985.5	7396.6	11875.0	11774.0	7240.4
521	7927.3	4537.2	6043.5	5830.2	4389.9	7026.4	3914.1	7807.8	7208.7	5321.7
540	29770.7	28987.1	34246.5	36056.2	28130.7	46820.2	30576.4	50054.8	38554.8	20683.4
560	6597.3	6594.0	9149.2	6594.1	6904.7	9252.3	6063.0	9405.0	7065.4	4118.3
594	22805.7	20607.4	26180.6	24447.4	18200.1	17858.6	12655.9	18950.6	18432.9	9189.5
600	13116.0	12323.1	14744.7	13809.4	10285.8	10323.2	6770.8	11675.2	9134.3	4243.3
604	10034.9	7932.9	9109.8	8496.5	6329.8	16992.8	11278.0	13273.3	10497.1	4656.3
608	4081.6	2934.2	3965.8	3436.5	3157.0	2692.3	1890.1	2402.8	2099.4	1163.2
616	7807.7	6434.6	8582.7	8191.9	7703.1	10279.2	6084.9	7888.0	5223.0	2428.5
627	34267.2	28264.8	38058.2	35179.8	29575.6	35883.6	22984.1	29083.9	20881.0	9413.3
654	7970.0	4210.5	5901.5	6728.1	5462.6	7944.6	6076.3	5782.8	4967.3	3265.3
661	14623.4	12641.3	16429.6	20650.2	15611.6	8976.6	5493.5	7603.6	9374.9	6078.7
722	32525.2	25989.7	31567.8	29774.8	23245.7	36849.5	30857.0	37546.9	28269.1	15547.5
Sum	1983136.4	1764509.9	1994540.8	2110166.8	1668207.2	2589432.7	2117452.4	2592459.3	2728424.7	2089650.3
ratio	0.9	0.8	0.9	1.0	0.7	0.9	0.8	1.0	1.0	0.8

The data was adjusted and illustrated in the table below.

Exp 1	RE					NRE				
CPDs	Repair time (hours)					Repair time (hours)				
Position	0	1	2	3	4	0	1	2	3	4
244	43610.4	42549.7	42836.3	42488.1	44493.9	37285.5	34596.5	41560.2	29468.2	22232.4
257	104746.9	106274.8	109801.0	108868.3	109232.4	102841.5	80056.6	103896.2	69562.5	43524.1
292	49010.9	49742.7	57370.2	52866.4	55113.7	45522.0	39638.2	51752.5	45260.1	28439.1
302	2828.9	2404.7	2388.0	1831.8	1544.6	2711.2	2640.9	2164.9	2343.0	2198.5
313	14972.4	13246.7	13659.5	9433.8	10818.6	17816.7	15077.6	17440.6	12365.4	9901.6
326	74686.8	73109.3	81034.5	77977.9	79382.8	68717.0	60248.3	72240.1	70629.7	53353.4
363	46276.6	46204.1	52618.3	45291.0	44135.4	47891.8	37120.8	47130.1	32109.5	18683.2
388	11138.0	13500.0	13787.2	13669.5	14361.3	10340.4	9297.2	10181.8	8006.4	5057.8
399	4558.7	5852.6	6320.8	6572.9	6994.3	3104.8	2608.9	4117.2	2226.0	2328.2
407	4488.8	3958.5	4270.6	3758.7	3817.3	4155.3	3985.2	3163.8	2261.9	2585.7
440	14894.4	16501.0	17754.3	16050.5	16534.0	14212.6	12074.0	14754.8	10664.6	8727.4
460	10106.9	9216.9	9032.0	9875.1	10085.8	10045.0	9885.7	13432.1	12350.8	8452.4
480	30131.6	28974.3	30947.3	29491.3	29706.5	33512.6	27848.0	36574.6	32543.6	23609.7
503	9785.6	7498.6	8659.7	8447.8	8692.2	9467.8	9530.9	12497.8	11774.0	9453.7
521	8402.7	5408.9	6362.5	5830.2	5653.4	7403.5	5043.4	8217.3	7208.7	6948.4
540	31555.9	34556.4	36054.5	36056.2	36226.9	49333.4	39398.9	52680.0	38554.8	27006.0
560	6992.9	7860.9	9632.2	6594.1	8891.9	9748.9	7812.4	9898.2	7065.4	5377.2
594	24173.2	24566.7	27562.7	24447.4	23438.2	18817.2	16307.7	19944.5	18432.9	11998.6
600	13902.5	14690.8	15523.2	13809.4	13246.1	10877.3	8724.5	12287.6	9134.3	5540.4
604	10636.7	9457.0	9590.7	8496.5	8151.6	17905.0	14532.2	13969.4	10497.1	6079.7
608	4326.4	3497.9	4175.1	3436.5	4065.6	2836.8	2435.5	2528.8	2099.4	1518.7
616	8275.9	7670.9	9035.8	8191.9	9920.1	10831.0	7840.7	8301.6	5223.0	3170.8
627	36322.1	33695.3	40067.3	35179.8	38087.7	37809.8	29616.0	30609.2	20881.0	12290.8
654	8448.0	5019.5	6213.0	6728.1	7034.8	8371.0	7829.5	6086.0	4967.3	4263.5
661	15500.3	15070.1	17296.9	20650.2	20104.7	9458.4	7078.6	8002.4	9374.9	7936.9
722	34475.6	30983.1	33234.4	29774.8	29936.0	38827.4	39760.5	39516.1	28269.1	20300.1

The remaining signal was calculated taking as 100 % of signal the 0 repair hour sample. The T_{50}% is the time required to repair 50 % of the lesion. The data is presented in the table below (%).

Exp 1	RE						NRE					
CPDs	Repair time (hours)					T50%	Repair time (hours)					T50%
Position	0	1	2	3	4		0	1	2	3	4	
244	100.0	97.6	98.2	97.4	100.0	10.0	100.0	92.8	111.5	79.0	59.6	4.2
257	100.0	101.5	100.8	103.9	104.3	10.0	100.0	77.8	101.0	67.6	42.3	3.8
292	100.0	101.5	100.1	100.9	112.5	10.0	100.0	87.1	103.7	99.4	62.5	4.5
302	100.0	85.0	84.4	64.8	54.6	4.3	100.0	97.4	79.8	86.4	81.1	10.0
313	100.0	88.5	91.2	63.0	72.3	10.0	100.0	84.6	97.9	69.4	55.6	4.1
326	100.0	97.9	108.5	104.4	106.3	10.0	100.0	87.7	105.1	102.8	77.6	5.5
363	100.0	99.8	103.7	97.9	95.4	10.0	100.0	77.5	98.4	67.0	39.0	3.7
388	100.0	101.2	103.8	102.7	128.9	10.0	100.0	89.9	98.5	77.4	48.9	4.0
399	100.0	108.4	108.7	104.2	103.4	10.0	100.0	84.0	102.6	71.7	75.0	4.7
407	100.0	88.2	95.1	83.7	85.0	10.0	100.0	95.9	76.1	54.4	62.2	10.0
440	100.0	110.8	109.2	107.8	111.0	10.0	100.0	85.0	103.8	75.0	61.4	4.5
460	100.0	91.2	89.4	97.7	99.8	10.0	100.0	98.4	103.7	103.0	84.1	10.0
480	100.0	96.2	102.7	97.9	98.6	10.0	100.0	83.1	109.1	97.1	70.5	5.0
503	100.0	76.6	88.5	86.3	88.8	10.0	100.0	100.7	102.0	124.4	99.9	10.0
521	100.0	64.4	75.7	69.4	67.3	10.0	100.0	68.1	101.0	97.4	93.9	10.0
540	100.0	109.5	114.3	114.3	114.8	10.0	100.0	79.9	106.8	78.2	54.7	4.2
560	100.0	112.4	107.7	94.3	107.2	10.0	100.0	80.1	101.5	72.5	55.2	5.2
594	100.0	101.6	104.0	101.1	97.0	10.0	100.0	86.7	106.0	98.0	63.8	4.7
600	100.0	105.7	101.7	99.3	95.3	10.0	100.0	80.2	103.0	84.0	50.9	4.1
604	100.0	88.9	90.2	79.9	76.6	10.0	100.0	81.2	78.0	58.6	34.0	3.4
608	100.0	80.9	96.5	79.4	94.0	10.0	100.0	85.9	89.1	74.0	53.5	4.2
616	100.0	92.7	109.2	99.0	119.9	10.0	100.0	72.4	76.6	48.2	29.3	3.0
627	100.0	92.8	110.3	96.9	104.9	10.0	100.0	78.3	81.0	55.2	32.5	3.3
654	100.0	59.4	73.5	79.6	83.3	10.0	100.0	93.5	72.7	59.3	50.9	4.0
661	100.0	97.2	111.6	103.2	129.7	10.0	100.0	74.8	84.6	99.1	83.9	10.0
722	100.0	89.9	96.4	86.4	86.8	10.0	100.0	102.4	101.8	72.8	52.3	4.0

AIII.1-2 NER efficiency at high resolution at *URA3* gene for the NTS

The table below represent the repair efficiency at the specific CPD points for the NTS in the NRE and RE strains.

Exp 2	RE					NRE				
CPDs	Repair time (hours)					Repair time (hours)				
Position	0	1	2	3	4	0	1	2	3	4
Top band	1205870.6	1473842.8	1472358.2	1602443.4	1572793.5	1639180.6	2083085.5	1763930.4	1601172.8	1646173.5
244	38846.0	36666.4	55115.5	62280.0	55685.8	33992.7	87382.5	28253.3	16466.3	14684.8
257	84950.1	80037.1	111109.8	135929.6	120028.0	104640.9	217048.5	68795.3	34618.4	30842.2
292	42971.1	38358.5	59839.8	61682.7	54993.2	48440.8	105943.1	41353.7	24421.1	24361.9
302	2343.3	2123.6	3267.1	2981.9	2422.8	3736.1	5246.4	2639.4	1544.8	2643.6
313	11462.5	10814.8	15162.4	15090.3	13467.3	15342.0	28472.2	12691.1	5638.4	3796.6
326	64482.2	63588.7	90902.2	100545.5	90458.3	71375.6	148512.0	70050.6	43467.4	37142.1
363	45763.8	40851.4	57157.2	60714.4	48304.7	47143.6	97650.4	30951.4	13984.0	10953.5
388	10898.7	7964.9	16549.2	14735.2	11645.0	11164.1	27495.0	7441.6	3562.1	5378.8
399	5246.9	3696.5	7494.0	8680.5	6277.1	2775.0	9546.8	1974.2	826.6	238.5
407	3859.9	3438.8	4961.0	5057.9	3429.7	5142.1	8972.1	2446.9	1272.7	1116.5
440	15144.9	13642.5	21299.6	22749.9	18775.4	15097.0	33892.2	9940.0	4662.5	3296.8
460	7950.8	12016.5	11667.8	11453.7	11316.8	14714.5	20318.2	9980.9	6044.7	3825.0
480	26229.4	29941.9	37006.1	39903.8	34231.3	35627.1	63880.3	28205.0	16826.8	17265.3
503	7982.6	7269.7	11103.4	10972.9	9367.9	10472.8	18110.5	9662.6	6064.6	5530.8
521	5332.9	4900.1	6587.9	6393.7	6226.1	7634.5	11889.5	7303.7	4907.0	6638.1
540	27254.2	34225.3	39038.2	44987.1	42259.6	50827.1	67910.5	35372.3	20100.5	19122.4
560	7203.6	7641.0	8965.2	9636.8	9492.4	11511.0	17672.7	8088.0	4599.9	2879.5
594	24455.5	16270.7	29595.9	35749.6	33945.5	23597.3	53565.3	18965.3	10454.0	8837.5
600	15063.9	13348.7	18355.8	18046.9	20536.3	8871.2	19503.1	6585.2	3346.4	2303.4
604	11797.9	13867.0	13619.4	13990.9	12104.3	19885.0	17422.9	11685.2	5597.8	4029.8
608	4838.6	2046.8	5401.3	5193.0	5709.9	3339.6	5609.1	1578.2	824.6	639.6
616	7236.3	3928.9	9910.9	9679.5	8784.6	6773.2	16504.5	5381.4	1069.7	1454.7
627	28891.2	22578.0	41500.7	44417.9	41258.9	38378.4	73380.4	19937.3	6628.5	6563.7
654	6798.2	6526.8	9706.1	10143.1	8370.2	10924.2	14380.3	5027.7	3262.9	1098.9
661	8302.3	7172.4	11064.2	15981.9	14424.7	6181.9	16167.9	3205.9	1565.1	995.7
722	29070.4	23686.6	38328.7	38429.4	32106.1	45097.8	53101.2	24108.2	9778.1	13008.9
Sum	1792017.9	2010880.3	2259209.0	2455474.6	2331556.5	2322437.3	3410884.0	2259444.6	1867352.7	1895453.5
ratio	0.7	0.8	0.9	1.0	0.9	1.0	1.5	1.0	0.8	0.8

The data was adjusted and presented in the next table.

Exp 2	RE					NRE				
CPDs	Repair time (hours)					Repair time (hours)				
Position	0	1	2	3	4	0	1	2	3	4
244	53228.0	44773.1	59903.6	62280.0	58645.4	33992.7	59497.9	29041.0	20479.3	17992.8
257	116401.1	97732.8	120762.3	135929.6	126407.3	104640.9	147786.2	70713.3	43055.2	37789.9
292	58880.2	46839.4	65038.3	61682.7	57916.0	48440.8	72135.6	42506.6	30372.6	29849.9
302	3210.8	2593.2	3551.0	2981.9	2551.6	3736.1	3572.2	2712.9	1921.3	3239.1
313	15706.2	13205.9	16479.6	15090.3	14183.1	15342.0	19386.5	13044.9	7012.5	4651.9
326	88355.4	77647.8	98799.2	100545.5	95266.0	71375.6	101120.4	72003.6	54060.6	45509.0
363	62706.9	49883.4	62122.7	60714.4	50872.0	47143.6	66489.2	31814.4	17392.0	13421.0
388	14933.7	9725.9	17986.9	14735.2	12263.9	11164.1	18721.1	7649.0	4430.2	6590.5
399	7189.5	4513.8	8145.1	8680.5	6610.7	2775.0	6500.4	2029.2	1028.0	292.3
407	5289.0	4199.1	5392.0	5057.9	3612.0	5142.1	6109.0	2515.1	1582.9	1368.0
440	20752.0	16658.8	23150.0	22749.9	19773.3	15097.0	23076.9	10217.1	5798.8	4039.4
460	10894.4	14673.3	12681.4	11453.7	11918.2	14714.5	13834.4	10259.1	7517.8	4686.6
480	35940.2	36561.9	40221.0	39903.8	36050.7	35627.1	43495.5	28991.3	20927.5	21154.6
503	10938.0	8876.9	12068.0	10972.9	9865.8	10472.8	12331.3	9932.0	7542.6	6776.7
521	7307.3	5983.5	7160.3	6393.7	6557.0	7634.5	8095.4	7507.3	6102.9	8133.4
540	37344.5	41792.4	42429.6	44987.1	44505.6	50827.1	46239.6	36358.5	24999.1	23430.0
560	9870.6	9330.4	9744.1	9636.8	9996.9	11511.0	12033.2	8313.5	5720.9	3528.2
594	33509.6	19868.0	32167.0	35749.6	35749.7	23597.3	36472.1	19494.1	13001.7	10828.3
600	20641.0	16300.1	19950.5	18046.9	21627.7	8871.2	13279.4	6768.8	4161.9	2822.3
604	16165.8	16932.9	14802.6	13990.9	12747.7	19885.0	11863.1	12011.0	6962.0	4937.5
608	6630.0	2499.3	5870.6	5193.0	6013.4	3339.6	3819.2	1622.2	1025.5	783.7
616	9915.4	4797.6	10771.9	9679.5	9251.5	6773.2	11237.7	5531.4	1330.3	1782.4
627	39587.6	27569.9	45106.0	44417.9	43451.7	38378.4	49964.0	20493.1	8243.9	8042.2
654	9315.2	7969.9	10549.3	10143.1	8815.0	10924.2	9791.4	5167.9	4058.1	1346.5
661	11376.1	8758.2	12025.4	15981.9	15191.3	6181.9	11008.6	3295.2	1946.6	1220.0
722	39833.1	28923.6	41658.4	38429.4	33812.5	45097.8	36156.1	24780.3	12161.1	15939.4

The remaining signal was calculated taking as 100 % of signal the 0 repair hour sample. The T_{50}% is the time required to repair 50 % of the lesion. The data is presented in the table below (%).

Exp 2	RE						NRE					
CPDs	Repair time (hours)					T50%	Repair time (hours)					T50%
Position	0	1	2	3	4		0	1	2	3	4	
244	100.0	84.1	112.5	107.0	110.2	10.0	100.0	105.0	85.4	60.2	52.9	4.0
257	100.0	84.0	103.7	106.8	108.6	10.0	100.0	101.2	67.6	41.1	36.1	2.8
292	100.0	79.6	110.5	104.8	98.4	10.0	100.0	108.9	87.7	62.7	61.6	4.7
302	100.0	80.8	110.6	92.9	79.5	10.0	100.0	95.6	72.6	51.4	86.7	3.0
313	100.0	84.1	104.9	96.1	90.3	10.0	100.0	106.4	85.0	45.7	30.3	2.3
326	100.0	87.9	111.8	113.8	107.8	10.0	100.0	101.7	100.9	75.7	63.8	4.4
363	100.0	79.6	99.1	96.8	81.1	10.0	100.0	101.0	67.5	36.9	28.5	2.7
388	100.0	65.1	100.4	98.7	82.1	10.0	100.0	107.7	68.5	39.7	59.0	2.5
399	100.0	62.8	113.3	120.7	91.9	10.0	100.0	100.2	73.1	37.0	10.5	2.7
407	100.0	79.4	101.9	95.6	68.3	5.2	100.0	100.8	48.9	30.8	26.6	1.9
440	100.0	80.3	111.6	109.6	95.3	10.0	100.0	100.9	67.7	38.4	26.8	2.7
460	100.0	134.7	116.4	105.1	109.4	10.0	100.0	94.0	69.7	51.1	31.9	3.1
480	100.0	101.7	101.9	111.0	100.3	10.0	100.0	100.1	81.4	58.7	59.4	5.8
503	100.0	81.2	110.3	100.3	90.2	10.0	100.0	100.7	94.8	72.0	64.7	4.6
521	100.0	81.9	98.0	87.5	89.7	10.0	100.0	106.0	98.3	79.9	106.5	10.0
540	100.0	111.9	113.6	110.5	109.2	10.0	100.0	91.0	71.5	49.2	46.1	3.0
560	100.0	94.5	98.7	97.6	101.3	10.0	100.0	104.5	72.2	49.7	30.7	2.9
594	100.0	59.3	96.0	106.7	106.7	10.0	100.0	100.6	82.6	55.1	45.9	3.7
600	100.0	79.0	96.7	87.4	104.8	10.0	100.0	100.7	76.3	46.9	31.8	3.0
604	100.0	104.7	91.6	86.5	78.9	6.5	100.0	59.7	60.4	35.0	24.8	2.4
608	100.0	37.7	88.5	78.3	90.7	10.0	100.0	114.4	48.6	30.7	23.5	1.9
616	100.0	48.4	108.6	97.6	93.3	10.0	100.0	105.9	81.7	19.6	26.3	2.7
627	100.0	69.6	113.9	112.2	109.8	10.0	100.0	103.2	53.4	21.5	21.0	2.1
654	100.0	85.6	113.2	108.9	94.6	10.0	100.0	89.6	47.3	37.1	12.3	2.0
661	100.0	77.0	105.7	100.5	103.5	10.0	100.0	108.1	53.3	31.5	19.7	2.1
722	100.0	72.6	104.6	96.5	84.9	10.0	100.0	80.2	54.9	27.0	35.3	2.0

AIII.1-3 NER efficiency at high resolution at *URA3* gene for the NTS

The table below represent the repair efficiency at the specific CPD points for the NTS at the NRE and RE strains.

Exp 3	RE					NRE				
CPDs	Repair time (hours)					Repair time (hours)				
Position	0	1	2	3	4	0	1	2	3	4
Top band	1182692.2	1228784.8	1338145.5	1571877.9	1404117.8	1037831.7	1073665.9	1264345.1	1311940.6	1173248.2
244	27931.1	28737.3	24902.3	26968.1	19845.0	17199.2	14050.3	12481.0	8879.1	5457.6
257	62232.6	59268.3	49609.4	40010.0	48905.4	47035.7	33208.1	38587.1	24908.8	12399.0
292	30560.0	30848.7	25954.8	23478.7	20110.3	21078.5	19462.6	20762.1	14979.3	10737.3
302	1709.9	1408.2	1034.9	1216.9	874.7	1080.4	905.3	954.5	907.9	1189.7
313	7998.5	7750.4	5592.2	5478.7	4344.8	6624.0	5771.7	5018.5	4279.2	3210.9
326	46887.1	48907.1	44383.6	44825.5	37740.7	31733.5	34231.9	39054.9	28324.4	20417.3
363	36235.0	35043.9	30385.7	29025.1	24810.9	22746.7	19410.0	18600.1	12224.4	8380.8
388	8478.8	9440.4	8420.1	8310.6	5796.5	2800.6	3377.6	3222.7	1926.0	2053.5
399	5941.6	3093.7	4338.2	5426.0	5720.1	1614.3	1997.6	1748.1	1118.7	1586.1
407	4507.8	5952.7	5757.0	4662.4	5359.9	3699.3	1541.8	4691.0	11676.4	32099.5
440	20418.1	19353.9	19078.3	18989.4	16871.5	8138.0	6618.8	8309.8	5206.7	8151.6
460	3935.4	5263.0	4826.1	5824.0	3897.0	4795.2	5914.8	6669.8	5639.9	4003.9
480	16977.0	18622.1	14699.0	15741.0	13947.3	14353.6	15114.5	14629.6	9498.0	6567.3
503	15487.7	16615.4	19111.3	26649.5	16395.2	20891.2	1927.9	11878.9	15813.4	19413.7
521	17736.2	15670.7	17876.6	27056.3	16855.8	22789.6	3978.7	13128.9	15085.4	19675.0
540	31626.4	28627.1	26613.6	32145.6	26915.7	35391.1	22927.0	25460.6	20974.1	18786.6
560	4443.8	4209.4	3175.6	3202.0	2221.8	4141.2	4817.5	4146.8	2831.2	2372.6
594	17196.4	14011.4	10970.8	13319.0	8062.1	1346.6	155.5	309.8	1096.0	3630.8
600	9742.1	8748.7	6028.6	6421.4	4711.8	11130.6	10282.1	11107.2	7707.0	6062.2
604	9565.9	7632.9	5043.6	5596.7	4182.9	7126.6	7038.6	7055.6	4615.8	3474.3
608	3499.0	3933.0	2115.7	1950.7	1365.0	10148.4	7631.5	7362.2	7162.4	4098.9
616	5584.1	3438.3	2666.8	3489.0	3601.2	2777.7	2432.8	3026.6	1348.0	614.3
627	22259.5	21826.7	17890.7	20123.6	17747.4	16048.8	12148.8	11648.5	7247.4	6513.5
654	3994.4	3541.0	3882.1	6235.4	4344.6	3516.0	782.0	1435.6	2183.4	3442.9
661	27569.0	24567.5	16306.0	31676.8	25180.1	33335.4	4576.1	8624.4	16088.1	21666.2
722	59608.4	54462.4	43988.5	62196.1	54596.4	42567.3	10615.3	19055.7	28224.4	43764.4
Sum	1711985.6	1732216.9	1771944.7	2056954.2	1809165.5	1449353.0	1342719.1	1576924.8	1583220.1	1452022.1
ratio	0.8	0.8	0.9	1.0	0.9	0.9	0.8	1.0	1.0	0.9

The data was adjusted and illustrated in the table below.

Exp 3	RE					NRE				
CPDs	Repair time (hours)					Repair time (hours)				
Position	0	1	2	3	4	0	1	2	3	4
244	33559.3	34124.6	28907.7	26968.1	22563.0	18787.8	16566.9	12530.9	8879.1	5950.7
257	74772.7	70379.3	57588.8	40010.0	55603.6	51380.1	39156.2	38741.2	24908.8	13519.3
292	36717.9	36631.9	30129.5	23478.7	22864.7	23025.4	22948.7	20845.0	14979.3	11707.5
302	2054.5	1672.2	1201.3	1216.9	994.5	1180.2	1067.5	958.3	907.9	1297.2
313	9610.2	9203.3	6491.7	5478.7	4939.9	7235.8	6805.5	5038.6	4279.2	3501.0
326	56335.0	58075.7	51522.5	44825.5	42909.8	34664.5	40363.3	39210.8	28324.4	22262.1
363	43536.4	41613.5	35273.1	29025.1	28209.1	24847.7	22886.6	18674.4	12224.4	9138.0
388	10187.2	11210.2	9774.4	8310.6	6590.4	3059.3	3982.6	3235.5	1926.0	2239.0
399	7138.8	3673.7	5036.0	5426.0	6503.5	1763.5	2355.4	1755.1	1118.7	1729.4
407	5416.2	7068.7	6683.0	4662.4	6094.0	4041.0	1818.0	4709.8	11676.4	34999.9
440	24532.4	22982.2	22147.0	18989.4	19182.3	8889.6	7804.4	8342.9	5206.7	8888.2
460	4728.4	6249.7	5602.4	5824.0	4430.8	5238.1	6974.2	6696.4	5639.9	4365.7
480	20397.9	22113.1	17063.3	15741.0	15857.5	15679.3	17821.7	14688.0	9498.0	7160.6
503	18608.6	19730.2	22185.3	26649.5	18640.7	22820.8	2273.2	11926.3	15813.4	21167.9
521	21310.0	18608.5	20751.9	27056.3	19164.5	24894.6	4691.4	13181.3	15085.4	21452.8
540	37999.2	33993.8	30894.3	32145.6	30602.2	38660.0	27033.5	25562.3	20974.1	20484.1
560	5339.3	4998.6	3686.4	3202.0	2526.1	4523.7	5680.4	4163.4	2831.2	2587.0
594	20661.5	16638.1	12735.4	13319.0	9166.3	1470.9	183.3	311.1	1096.0	3958.9
600	11705.2	10388.8	6998.2	6421.4	5357.2	12158.6	12123.8	11151.6	7707.0	6609.9
604	11493.4	9063.9	5854.9	5596.7	4755.8	7784.9	8299.4	7083.7	4615.8	3788.3
608	4204.0	4670.3	2456.0	1950.7	1552.0	11085.7	8998.4	7391.6	7162.4	4469.2
616	6709.3	4082.9	3095.7	3489.0	4094.5	3034.2	2868.5	3038.7	1348.0	669.8
627	26744.8	25918.5	20768.3	20123.6	20178.1	17531.1	14324.9	11695.0	7247.4	7102.1
654	4799.2	4204.8	4506.6	6235.4	4939.6	3840.7	922.1	1441.4	2183.4	3754.0
661	33124.2	29173.1	18928.8	31676.8	28628.8	36414.4	5395.7	8658.9	16088.1	23623.8
722	71619.6	64672.4	51063.9	62196.1	62074.1	46498.9	12516.6	19131.7	28224.4	47718.8

The remaining signal was calculated taking as 100 % of signal the 0 repair hour sample. The T_{50}% is the time required to repair 50 % of the lesion. The data is presented in the table below (%).

Exp 3	RE						NRE					
CPDs	Repair time (hours)					T50%	Repair time (hours)					T50%
Position	0	1	2	3	4		0	1	2	3	4	
244	100.0	101.7	86.1	80.4	67.2	5.4	100.0	88.2	66.7	47.3	31.7	3.0
257	100.0	94.1	77.0	53.5	74.4	3.0	100.0	76.2	75.4	48.5	26.3	2.9
292	100.0	99.8	82.1	63.9	62.3	5.5	100.0	99.7	90.5	65.1	50.8	4.0
302	100.0	81.4	58.5	59.2	48.4	3.9	100.0	90.4	81.2	76.9	109.9	5.3
313	100.0	95.8	67.6	57.0	51.4	4.2	100.0	94.1	69.6	59.1	48.4	3.2
326	100.0	103.1	91.5	79.6	76.2	10.0	100.0	116.4	113.1	81.7	64.2	5.3
363	100.0	95.6	81.0	66.7	64.8	10.0	100.0	92.1	75.2	49.2	36.8	3.0
388	100.0	110.0	95.9	81.6	64.7	4.6	100.0	100.2	105.8	63.0	73.2	10.0
399	100.0	51.5	70.5	76.0	91.1	10.0	100.0	103.6	99.5	63.4	98.1	10.0
407	100.0	100.5	123.4	86.1	112.5	10.0	100.0	45.0	106.5	108.9	106.1	10.0
440	100.0	93.7	90.3	77.4	78.2	10.0	100.0	87.8	93.9	58.6	100.0	10.0
460	100.0	132.2	118.5	123.2	93.7	10.0	100.0	103.1	107.8	107.7	83.3	10.0
480	100.0	108.4	83.7	77.2	77.7	10.0	100.0	113.7	93.7	60.6	45.7	3.2
503	100.0	106.0	109.2	103.2	100.2	10.0	100.0	100.0	92.8	69.3	52.3	4.3
521	100.0	87.3	97.4	107.0	89.9	10.0	100.0	108.8	86.2	60.6	52.9	4.2
540	100.0	89.5	81.3	84.6	80.5	10.0	100.0	29.9	26.1	24.3	23.0	0.5
560	100.0	93.6	69.0	60.0	47.3	3.8	100.0	105.6	92.0	62.6	57.2	4.1
594	100.0	80.5	61.6	64.5	44.4	3.7	100.0	109.1	74.5	21.1	12.5	2.8
600	100.0	88.8	59.8	54.9	45.8	3.2	100.0	99.7	91.7	63.4	54.4	4.5
604	100.0	78.9	50.9	48.7	41.4	2.3	100.0	106.6	91.0	59.3	48.7	3.2
608	100.0	111.1	58.4	46.4	36.9	2.7	100.0	81.2	66.7	64.6	40.3	3.8
616	100.0	60.9	46.1	52.0	61.0	2.0	100.0	94.5	100.1	44.4	22.1	2.7
627	100.0	96.9	77.7	75.2	75.4	10.0	100.0	81.7	66.7	41.3	40.5	2.2
654	100.0	87.6	93.9	129.9	102.9	10.0	100.0	97.7	56.8	37.5	24.0	2.3
661	100.0	88.1	57.1	95.6	86.4	10.0	100.0	14.8	23.8	44.2	64.9	0.5
722	100.0	90.3	71.3	86.8	86.7	10.0	100.0	26.9	41.1	60.7	102.6	0.5

A III.1-4 NER efficiency at high resolution at *URA3* gene for the NTS

The table below represent the repair efficiency at the specific CPD points for the NTS at the NRE and RE strains.

Exp 4	RE					NRE				
CPDs	Repair time (hours)					Repair time (hours)				
Position	0	1	2	3	4	0	1	2	3	4
Top band	469964.6	711529.7	752569.3	952474.4	709734.0	391694.9	507832.5	398948.5	674007.9	740834.4
244	6578.5	10020.5	9659.6	7868.9	12416.3	4958.5	5185.3	2506.4	1896.2	1962.1
257	14017.2	21527.8	18385.5	19428.4	10810.2	10437.4	11454.4	5011.4	4966.3	2854.2
292	6379.9	9758.3	8304.0	9155.8	4605.0	3810.0	6022.4	3303.4	4351.7	2660.9
302	323.3	352.3	328.8	457.3	121.6	330.6	403.6	112.5	121.8	167.4
313	1440.3	2608.3	2111.6	2105.6	1322.9	1023.0	1531.9	722.4	737.1	625.5
326	8595.9	13805.6	12577.7	15853.8	9248.2	6335.5	8318.5	5546.9	6146.6	4543.9
363	5298.7	8524.9	7810.7	8143.9	4767.2	4353.0	5292.1	2585.6	2154.5	1563.8
388	1404.2	2007.4	2011.3	2246.4	1660.1	776.9	1271.0	314.5	443.8	431.8
399	974.0	1841.0	1375.0	1429.5	815.6	565.9	1160.6	487.5	298.6	381.6
407	685.2	1098.4	674.8	557.2	210.6	379.8	753.2	229.3	218.6	827.3
440	2208.9	3268.9	2624.8	2278.1	986.8	1569.1	2645.8	701.5	538.8	593.2
460	1242.4	1943.0	1936.2	2239.6	1235.8	1465.3	1719.9	824.5	1123.7	883.0
480	3947.8	5885.2	4811.5	5295.3	3241.6	3394.9	4903.6	2312.6	2873.1	2153.4
503	397.6	742.2	937.5	1314.8	723.2	965.3	1258.4	601.9	757.7	803.8
521	1147.2	1653.2	1674.0	1715.4	1126.0	398.6	277.8	491.0	1217.6	664.5
540	6365.8	9208.0	8511.9	7747.6	4640.4	984.4	884.7	681.6	1064.1	610.4
560	779.9	1186.1	1051.7	1357.7	872.2	868.4	1204.2	518.9	531.3	508.6
594	2595.8	3373.5	2872.5	4057.1	1915.1	1460.0	2137.3	926.7	755.4	889.3
600	1103.3	2202.5	1818.5	2064.6	1282.3	959.8	1551.8	517.8	507.9	363.1
604	1122.5	2240.4	2310.4	2317.1	1230.3	1370.0	1604.2	663.5	638.5	399.1
608	832.1	1484.9	1248.8	1392.3	416.6	166.0	259.0	113.1	78.3	96.2
616	163.6	362.1	385.3	655.3	369.3	362.5	441.9	194.0	137.6	110.5
627	2614.7	4108.4	4098.9	5448.2	2080.4	2154.7	2591.7	1010.9	595.4	584.6
654	1214.8	2512.4	1829.6	2043.3	1105.6	1019.7	783.4	757.6	968.9	401.8
661	5699.7	7579.9	9155.1	7052.0	4897.5	1060.0	1158.8	586.8	441.6	462.3
722	3575.9	4527.6	3614.2	4217.5	2473.8	9213.2	8852.6	4078.1	6973.4	6313.8
Sum	555559.7	844717.7	870481.4	1078520.4	788664.1	455339.0	585914.1	437515.9	716328.7	775680.2
ratio	0.6	1.0	1.0	1.2	0.9	0.6	0.8	0.6	1.0	1.1

The data was adjusted and illustrated in the table below.

Exp 4	RE					NRE				
CPDs	Repair time (hours)					Repair time (hours)				
Position	0	1	2	3	4	0	1	2	3	4
244	10307.6	10326.1	9659.6	6351.0	13704.4	7800.6	6339.5	4103.6	1896.2	1812.0
257	21962.9	22184.4	18385.5	15680.8	11931.7	16419.8	14004.0	8205.0	4966.3	2635.9
292	9996.3	10055.9	8304.0	7389.7	5082.7	5993.8	7362.9	5408.6	4351.7	2457.3
302	506.6	363.1	328.8	369.1	134.3	520.1	493.4	184.1	121.8	154.6
313	2256.8	2687.9	2111.6	1699.4	1460.1	1609.4	1872.8	1182.7	737.1	577.6
326	13468.5	14226.7	12577.7	12795.7	10207.7	9966.9	10170.1	9081.7	6146.6	4196.2
363	8302.2	8784.9	7810.7	6573.0	5261.8	6848.0	6470.1	4233.3	2154.5	1444.2
388	2200.2	2068.6	2011.3	1813.0	1832.3	1222.3	1553.9	515.0	443.8	398.8
399	1526.1	1897.1	1375.0	1153.7	900.3	890.3	1419.0	798.1	298.6	352.4
407	1073.6	1131.9	674.8	449.7	232.5	597.5	920.9	375.4	218.6	764.0
440	3461.0	3368.7	2624.8	1838.7	1089.1	2468.5	3234.7	1148.5	538.8	547.8
460	1946.6	2002.3	1936.2	1807.6	1364.0	2305.2	2102.7	1349.9	1123.7	815.5
480	6185.6	6064.7	4811.5	4273.8	3577.9	5340.7	5995.0	3786.3	2873.1	1988.6
503	622.9	764.8	937.5	1061.2	798.3	1518.5	1538.4	985.4	757.7	742.3
521	1797.5	1703.6	1674.0	1384.5	1242.9	627.1	339.7	804.0	1217.6	613.7
540	9974.4	9488.8	8511.9	6253.1	5121.8	1548.6	1081.7	1115.9	1064.1	563.7
560	1222.1	1222.2	1051.7	1095.8	962.7	1366.2	1472.3	849.6	531.3	469.7
594	4067.2	3476.4	2872.5	3274.5	2113.8	2296.8	2613.0	1517.3	755.4	821.3
600	1728.7	2269.7	1818.5	1666.3	1415.3	1509.9	1897.2	847.8	507.9	335.3
604	1758.8	2308.7	2310.4	1870.2	1358.0	2155.2	1961.3	1086.4	638.5	368.5
608	1303.9	1530.2	1248.8	1123.7	459.8	261.2	316.7	185.2	78.3	88.8
616	256.3	373.1	385.3	528.9	407.6	570.3	540.3	317.6	137.6	102.0
627	4096.9	4233.7	4098.9	4397.3	2296.2	3389.7	3168.6	1655.1	595.4	539.9
654	1903.4	2589.1	1829.6	1649.1	1220.3	1604.2	957.8	1240.4	968.9	371.0
661	8930.6	7811.1	9155.1	5691.8	5405.6	1667.6	1416.7	960.7	441.6	427.0
722	5602.9	4665.7	3614.2	3404.0	2730.5	14494.0	10823.1	6676.9	6973.4	5830.7

The remaining signal was calculated taking as 100 % of signal the 0 repair hour sample. The T_{50}% is the time required to repair 50 % of the lesion. The data is presented in the table below (%).

Exp 4	RE						NRE					
CPDs Position	Repair time (hours)					T50%	Repair time (hours)					T50%
	0	1	2	3	4		0	1	2	3	4	
244	100.0	101.0	93.7	123.2	133.0	10.0	100.0	81.3	52.6	24.3	23.2	2.1
257	100.0	100.6	83.7	71.4	54.3	4.1	100.0	85.3	50.0	30.2	16.1	2.3
292	100.0	100.6	83.1	73.9	50.8	4.0	100.0	122.8	90.2	72.6	41.0	3.8
302	100.0	71.7	64.9	72.9	26.5	3.5	100.0	94.9	35.4	23.4	29.7	1.8
313	100.0	119.1	93.6	75.3	64.7	4.6	100.0	116.4	73.5	45.8	35.9	2.9
326	100.0	105.6	93.4	95.0	75.8	5.7	100.0	102.0	91.1	61.7	42.1	3.4
363	100.0	105.8	94.1	79.2	63.4	4.6	100.0	94.5	61.8	31.5	21.1	2.5
388	100.0	94.0	91.4	82.4	83.3	10.0	100.0	127.1	42.1	36.3	32.6	1.9
399	100.0	124.3	90.1	75.6	59.0	4.4	100.0	109.4	89.6	33.5	39.6	2.75
407	100.0	105.4	62.9	41.9	21.7	2.9	100.0	104.1	62.8	36.6	107.9	2.6
440	100.0	97.3	75.8	53.1	31.5	3.3	100.0	101.0	46.5	21.8	22.2	1.9
460	100.0	102.9	99.5	92.9	70.1	4.9	100.0	91.2	58.6	48.7	35.4	2.8
480	100.0	98.0	77.8	69.1	57.8	4.5	100.0	112.3	70.9	53.8	37.2	3.1
503	100.0	102.8	105.5	107.4	128.1	10.0	100.0	101.3	64.9	49.9	48.9	3.0
521	100.0	94.8	93.1	77.0	69.1	5.2	100.0	54.2	128.2	104.2	97.9	10.0
540	100.0	95.1	85.3	62.7	51.3	4.1	100.0	69.8	72.1	68.7	36.4	3.6
560	100.0	100.0	86.1	89.7	78.8	10.0	100.0	107.8	62.2	38.9	34.4	2.65
594	100.0	85.5	70.6	80.5	52.0	4.3	100.0	113.8	66.1	32.9	35.8	2.6
600	100.0	131.3	105.2	96.4	81.9	10.0	100.0	125.6	56.1	33.6	22.2	2.5
604	100.0	131.3	131.4	106.3	77.2	10.0	100.0	91.0	50.4	29.6	17.1	2.3
608	100.0	117.4	95.8	86.2	35.3	3.8	100.0	121.2	70.9	30.0	34.0	2.6
616	100.0	105.5	100.3	106.3	109.0	10.0	100.0	94.7	55.7	24.1	17.9	2.35
627	100.0	103.3	100.0	107.3	56.0	4.2	100.0	93.5	48.8	17.6	15.9	2.2
654	100.0	106.0	96.1	86.6	64.1	10.0	100.0	59.7	77.3	60.4	23.1	3.2
661	100.0	87.5	102.5	63.7	60.5	6.1	100.0	85.0	57.6	26.5	25.6	2.3
722	100.0	83.3	64.5	60.8	48.7	3.7	100.0	74.7	46.1	48.1	40.2	1.9

AIII.2-1 NER efficiency at high resolution at *URA3* gene for the TS

The table below represent the repair efficiency at the specific CPD points for the TS at the NRE and RE strains.

Exp 1	RE					NRE				
CPDs	Repair time (hours)					Repair time (hours)				
Position	0	1	2	3	4	0	1	2	3	4
Top band	444159.8	506112.2	461191.1	511010.1	370202.2	452906.2	633401.8	617061.9	716990.0	737363.6
596	18990.2	20793.2	17292.1	16490.5	13259.3	18990.2	20793.2	17292.1	16490.5	13259.3
544	19252.8	23236.0	20396.1	18611.0	14860.8	19252.8	23236.0	20396.1	18611.0	14860.8
531	8816.1	10051.4	8062.3	7145.2	5679.6	8816.1	10051.4	8062.3	7145.2	5679.6
561	8738.8	9722.5	8824.7	9342.5	7382.5	8738.8	9722.5	8824.7	9342.5	7382.5
506	8588.6	9918.1	7562.1	6534.3	5864.7	8588.6	9918.1	7562.1	6534.3	5864.7
499	7291.7	8813.6	7035.8	5579.3	4322.4	7291.7	8813.6	7035.8	5579.3	4322.4
491	9971.0	12176.7	10454.6	9189.2	7005.7	9971.0	12176.7	10454.6	9189.2	7005.7
485	5282.0	5728.4	5204.6	4656.2	3957.0	5282.0	5728.4	5204.6	4656.2	3957.0
478	4097.6	4412.5	3574.5	3659.3	2451.9	4097.6	4412.5	3574.5	3659.3	2451.9
467	14871.2	18945.8	16353.3	13532.2	9984.3	14871.2	18945.8	16353.3	13532.2	9984.3
451	15183.2	18655.6	15703.1	14780.5	8428.0	15183.2	18655.6	15703.1	14780.5	8428.0
434	6452.0	8210.8	6947.7	5838.0	4335.7	6452.0	8210.8	6947.7	5838.0	4335.7
367	7238.8	8969.1	7700.5	7689.6	3961.5	7238.8	8969.1	7700.5	7689.6	3961.5
335	6806.5	6104.9	5323.2	5541.6	4458.4	6806.5	6104.9	5323.2	5541.6	4458.4
331	3961.5	4354.4	3582.9	4033.3	2373.5	3961.5	4354.4	3582.9	4033.3	2373.5
322	358.9	354.0	331.2	511.4	273.6	358.9	354.0	331.2	511.4	273.6
305	9058.1	10391.7	8655.6	8255.2	5668.2	9058.1	10391.7	8655.6	8255.2	5668.2
293	2065.8	1859.9	1419.6	1450.1	896.9	2065.8	1859.9	1419.6	1450.1	896.9
269	32548.2	37681.5	31260.1	30824.1	24861.7	32548.2	37681.5	31260.1	30824.1	24861.7
Sum	1983136.4	1764509.9	1994540.8	2110166.8	1668207.2	677710.0	775820.2	684186.1	725799.7	531168.7
ratio	0.9	0.8	0.9	1.0	0.8	0.9	1.0	0.9	0.9	0.7

The data was adjusted and illustrated in the table below.

Exp 1	RE					NRE				
CPDs	Repair time (hours)					Repair time (hours)				
Position	0	1	2	3	4	0	1	2	3	4
596	21739.3	20793.2	19608.0	17627.0	19366.4	30659.7	26170.7	17754.3	18216.1	19020.0
544	22040.0	23236.0	23127.8	19893.6	21705.6	24154.9	20029.7	12248.3	6688.3	5599.9
531	10092.4	10051.4	9142.1	7637.6	8295.6	10137.3	7244.0	3986.5	2203.9	1672.5
561	10003.8	9722.5	10006.6	9986.3	10782.8	9673.9	9191.3	6444.0	3907.7	2805.8
506	9832.0	9918.1	8574.9	6984.6	8566.0	8946.2	7953.6	5121.6	2901.0	2206.9
499	8347.3	8813.6	7978.1	5963.8	6313.3	7175.1	7365.1	5705.6	3528.7	2368.7
491	11414.4	12176.7	11854.8	9822.5	10232.5	10851.2	10535.1	9601.3	6187.2	5148.5
485	6046.7	5728.4	5901.7	4977.1	5779.6	6422.5	6106.1	5200.5	3123.2	2706.8
478	4690.8	4412.5	4053.2	3911.5	3581.2	4905.1	3884.3	2501.9	1887.0	1509.8
467	17024.0	18945.8	18543.5	14464.8	14583.0	17627.7	16481.9	12194.7	6968.0	5454.8
451	17381.2	18655.6	17806.2	15799.1	12309.9	14540.7	12925.5	8427.6	5692.7	3907.0
434	7386.0	8210.8	7878.2	6240.3	6332.6	6011.4	6130.9	3673.9	2344.2	1692.0
367	8286.7	8969.1	8731.9	8219.5	5786.1	5507.8	5579.5	5169.6	2953.9	1131.1
335	7791.9	6104.9	6036.1	5923.5	6512.0	10800.6	6394.1	5280.7	5360.9	4527.1
331	4535.0	4354.4	4062.8	4311.3	3466.7	6577.3	5206.5	4519.0	3213.2	2557.1
322	410.8	354.0	375.6	546.6	399.7	706.8	264.5	247.2	106.7	139.5
305	10369.4	10391.7	9814.9	8824.2	8278.9	9556.0	10312.2	8571.1	6680.9	5901.1
293	2364.9	1859.9	1609.7	1550.0	1310.0	2081.2	2203.8	1493.8	712.5	723.9
269	37260.1	37681.5	35446.9	32948.4	36312.8	25959.2	20849.6	15118.7	12927.0	10514.6

The remaining signal was calculated taking as 100 % of signal the 0 repair hour sample. The T_{50}% is the time required to repair 50 % of the lesion. The data is presented in the table below (%).

Exp 1	RE						NRE					
CPDs	Repair time (hours)					T50%	Repair time (hours)					T50%
Position	0	1	2	3	4		0	1	2	3	4	
596	100.0	95.6	90.2	81.1	89.1	10.0	100.0	85.4	57.9	59.4	62.0	2.0
544	100.0	105.4	104.9	90.3	98.5	10.0	100.0	82.9	50.7	27.7	23.2	2.1
531	100.0	99.6	90.6	75.7	82.2	10.0	100.0	71.5	39.3	21.7	16.5	1.6
561	100.0	97.2	100.0	99.8	107.8	10.0	100.0	95.0	66.6	40.4	29.0	2.9
506	100.0	100.9	87.2	71.0	87.1	10.0	100.0	88.9	57.2	32.4	24.7	2.4
499	100.0	105.6	95.6	71.4	75.6	5.8	100.0	102.6	79.5	49.2	33.0	3.3
491	100.0	106.7	103.9	86.1	89.6	10.0	100.0	97.1	88.5	57.0	47.4	3.8
485	100.0	94.7	97.6	82.3	95.6	10.0	100.0	95.1	81.0	48.6	42.1	2.9
478	100.0	94.1	86.4	83.4	76.3	10.0	100.0	79.2	51.0	38.5	30.8	2.1
467	100.0	111.3	108.9	85.0	85.7	10.0	100.0	93.5	69.2	39.5	30.9	2.9
451	100.0	107.3	102.4	90.9	70.8	4.9	100.0	88.9	58.0	39.2	26.9	2.6
434	100.0	111.2	106.7	84.5	85.7	10.0	100.0	102.0	61.1	39.0	28.1	2.8
367	100.0	108.2	105.4	99.2	69.8	10.0	100.0	101.3	93.9	53.6	20.5	3.3
335	100.0	78.3	77.5	76.0	83.6	10.0	100.0	59.2	48.9	49.6	41.9	1.9
331	100.0	96.0	89.6	95.1	76.4	10.0	100.0	79.2	68.7	48.9	38.9	3.0
322	100.0	86.2	91.4	133.1	97.3	10.0	100.0	37.4	35.0	15.1	19.7	0.5
305	100.0	100.2	94.7	85.1	79.8	10.0	100.0	107.9	89.7	69.9	61.8	4.5
293	100.0	78.6	68.1	65.5	55.4	10.0	100.0	105.9	71.8	34.2	34.8	2.2
269	100.0	101.1	95.1	88.4	97.5	10.0	100.0	80.3	58.2	49.8	40.5	3.0

AIII.2-2 NER efficiency at high resolution at *URA3* gene for the TS

The table below represent the repair efficiency at the specific CPD points for the TS at the NRE and RE strains.

Exp 2	RE					NRE				
CPDs	Repair time (hours)					Repair time (hours)				
Position	0	1	2	3	4	0	1	2	3	4
Top band	802335.7	803099.1	822715.6	890498.0	648278.6	484903.1	365737.7	637702.0	570431.3	539947.5
596	32297.5	27460.5	28897.7	19087.8	11319.8	24429.2	16304.9	34474.4	24072.7	20587.8
544	32042.7	24184.8	23515.1	13553.7	4504.3	24679.4	18132.6	37658.2	34025.9	27294.4
531	14884.3	10947.5	9262.8	4789.5	1987.9	11089.9	8711.4	15962.0	13194.2	10222.6
561	13312.0	12213.4	12332.7	8603.2	3860.3	9529.9	7995.1	15170.1	14710.0	12157.9
506	11676.6	9447.0	8890.3	5519.3	1858.5	9795.5	7206.9	14630.1	13265.1	10389.1
499	10989.9	11121.9	10145.5	6631.5	3468.9	8993.8	6235.1	13088.6	10895.0	9996.1
491	15854.7	15681.9	14098.1	10759.9	5890.4	12722.5	9179.7	17710.9	16144.1	14205.3
485	10043.6	9368.3	8379.9	5709.0	3009.3	7343.1	5478.8	10427.3	9740.0	7988.1
478	6893.5	4814.9	4914.9	2943.8	2018.6	4887.6	3161.6	5938.5	4443.6	3748.8
467	25465.6	21437.0	21565.5	13651.9	6585.2	18773.4	12474.5	25899.4	20956.8	16256.1
451	21579.2	19477.6	15481.3	9413.8	4131.2	17366.8	12930.3	23759.1	21597.9	17996.0
434	9324.8	8855.4	7043.9	4479.0	2261.7	9269.4	6764.6	14777.9	11541.8	11087.6
367	6674.9	5921.2	5717.3	3457.5	2362.2	7058.5	5305.3	9085.1	7853.7	7220.1
335	5682.4	5061.4	5386.9	3895.7	3777.1	2902.7	2694.2	4508.7	3667.0	3611.4
331	6105.5	8321.8	5893.7	4822.0	4210.7	4513.8	2863.5	6264.2	4964.0	4898.9
322	1042.6	799.4	525.3	508.4	412.0	1186.2	661.2	1133.4	221.9	358.9
305	13645.2	14243.9	9132.1	9092.9	3959.9	8671.9	6794.2	9613.9	8402.2	7306.5
293	3709.6	4502.7	3610.2	3508.8	2917.2	3168.4	2724.1	3900.0	3755.2	3643.9
269	57224.3	63762.4	66175.7	46591.4	35787.4	61088.8	67990.1	63524.5	48469.7	39182.8
Sum	1166147.7	1131619.3	1133072.9	1093832.2	766220.1	776840.6	601859.5	1030165.8	888658.4	810416.1
ratio	1.0	1.0	1.0	0.9	0.7	0.8	0.6	1.0	0.9	0.8

The data was adjusted and illustrated in the table below.

Exp 2	RE					NRE				
CPDs	Repair time (hours)					Repair time (hours)				
Position	0	1	2	3	4	0	1	2	3	4
596	32395.4	27908.0	34474.4	27906.0	26170.3	32297.5	28298.4	29741.3	20349.7	17228.2
544	32727.3	31036.4	37658.2	39444.1	34695.5	32042.7	24922.7	24201.5	14449.8	6855.3
531	14706.2	14910.8	15962.0	15295.2	12994.5	14884.3	11281.5	9533.2	5106.2	3025.5
561	12637.6	13684.8	15170.1	17052.4	15454.5	13312.0	12586.1	12692.7	9172.0	5875.2
506	12989.8	12335.7	14630.1	15377.4	13206.1	11676.6	9735.2	9149.8	5884.2	2828.5
499	11926.6	10672.2	13088.6	12629.9	12706.7	10989.9	11461.2	10441.6	7070.0	5279.5
491	16871.3	15712.4	17710.9	18714.8	18057.2	15854.7	16160.4	14509.6	11471.3	8964.9
485	9737.7	9377.6	10427.3	11291.0	10154.1	10043.6	9654.1	8624.5	6086.4	4580.0
478	6481.4	5411.5	5938.5	5151.2	4765.3	6893.5	4961.8	5058.4	3138.5	3072.2
467	24895.4	21351.8	25899.4	24293.9	20664.0	25465.6	22091.1	22195.0	14554.5	10022.4
451	23030.1	22132.1	23759.1	25037.1	22875.7	21579.2	20071.9	15933.2	10036.2	6287.5
434	12292.1	11578.5	14777.9	13379.7	14094.1	9324.8	9125.6	7249.5	4775.1	3442.2
367	9360.3	9080.8	9085.1	9104.3	9177.9	6674.9	6101.9	5884.2	3686.1	3595.2
335	3849.3	4611.5	4508.7	4250.9	4590.7	5682.4	5215.8	5544.2	4153.3	5748.6
331	5985.8	4901.3	6264.2	5754.4	6227.3	6105.5	8575.7	6065.8	5140.8	6408.5
322	1573.0	1131.7	1133.4	257.2	456.2	1042.6	823.8	540.6	542.0	627.1
305	11499.8	11629.2	9613.9	9740.1	9287.7	13645.2	14678.6	9398.6	9694.1	6026.8
293	4201.6	4662.7	3900.0	4353.2	4632.0	3709.6	4640.1	3715.6	3740.8	4439.8
269	81009.6	116374.5	63524.5	56187.9	49807.5	57224.3	65707.9	68107.4	49671.7	54466.6

The remaining signal was calculated taking as 100 % of signal the 0 repair hour sample. The T_{50}% is the time required to repair 50 % of the lesion. The data is presented in the table below (%).

Exp 2	RE						NRE					
CPDs	Repair time (hours)					T50%	Repair time (hours)					T50%
Position	0	1	2	3	4		0	1	2	3	4	
596	100.0	87.6	92.1	63.0	53.3	4.3	100.0	85.4	57.9	59.4	62.0	3.6
544	100.0	77.8	75.5	45.1	21.4	2.9	100.0	82.9	50.7	27.7	23.2	2.1
531	100.0	75.8	64.0	34.3	20.3	2.4	100.0	71.5	39.3	21.7	16.5	1.7
561	100.0	94.5	95.3	68.9	44.1	4.7	100.0	95.0	66.6	40.4	29.0	2.6
506	100.0	83.4	78.4	50.4	24.2	3.0	100.0	88.9	57.2	32.4	24.7	2.2
499	100.0	104.3	95.0	64.3	48.0	3.9	100.0	102.6	79.5	49.2	33.0	3.0
491	100.0	101.9	91.5	72.4	56.5	4.3	100.0	97.1	88.5	57.0	47.4	3.8
485	100.0	96.1	85.9	60.6	45.6	3.8	100.0	95.1	81.0	48.6	42.1	2.9
478	100.0	72.0	73.4	45.5	44.6	2.8	100.0	79.2	51.0	38.5	30.8	2.1
467	100.0	86.7	87.2	57.2	39.4	3.3	100.0	93.5	69.2	39.5	30.9	2.6
451	100.0	93.0	73.8	46.5	29.1	2.9	100.0	88.9	58.0	39.2	26.9	2.4
434	100.0	97.9	77.7	51.2	36.9	3.0	100.0	102.0	61.1	39.0	28.1	2.4
367	100.0	91.4	88.2	55.2	53.9	4.5	100.0	101.3	93.9	53.6	20.5	3.2
335	100.0	91.8	97.6	73.1	101.2	10.0	100.0	59.2	48.9	49.6	41.9	1.9
331	100.0	140.5	99.3	84.2	105.0	10.0	100.0	79.2	68.7	48.9	38.9	2.9
322	100.0	79.0	51.9	52.0	60.1	2.3	100.0	37.4	35.0	15.1	19.7	0.8
305	100.0	107.6	68.9	71.0	44.2	3.8	100.0	107.9	89.7	69.9	61.8	5.0
293	100.0	125.1	100.2	100.8	119.7	10.0	100.0	105.9	71.8	34.2	34.8	2.5
269	100.0	114.8	119.0	86.8	95.2	10.0	100.0	80.3	58.2	49.8	40.5	3.0

AIII.2-3 NER efficiency at high resolution at *URA3* gene for the TS

The table below represent the repair efficiency at the specific CPD points for the TS at the NRE and RE strains.

Exp 3	RE					NRE				
CPDs	Repair time (hours)					Repair time (hours)				
Position	0	1	2	3	4	0	1	2	3	4
Top band	476121.5	384794.7	324379.1	377834.0	143586.6	770833.1	585392.2	781504.8	377351.0	935088.6
596	20489.1	15529.8	14614.0	14363.5	5725.2	27383.1	14077.8	15578.7	4748.3	9861.3
544	17056.8	15806.7	16004.8	17528.5	6220.0	32512.1	20431.7	20286.4	4083.3	4808.4
531	9063.6	7748.0	7982.0	6993.9	2715.2	14505.6	7531.4	7490.8	1538.7	1856.1
561	8473.1	10645.4	9184.9	10343.6	5640.9	16350.3	6980.6	11748.3	2542.2	5158.0
506	8688.4	11377.9	8456.0	8398.3	3235.3	14073.1	8033.6	8987.1	1471.9	4246.3
499	8562.4	8919.2	8965.8	9597.0	2973.6	15121.9	9685.4	12751.6	2643.0	5987.3
491	13386.2	12638.3	11321.5	11930.6	3373.0	20645.5	12915.4	16120.5	4142.3	9582.9
485	8865.1	5989.8	5644.7	5972.7	3097.4	10859.9	5601.2	6633.9	1946.2	3791.8
478	5138.0	3018.6	2081.8	1918.1	1122.5	4759.2	2803.6	3438.3	941.4	1360.5
467	18125.2	14991.3	15517.0	14826.3	4453.5	25736.8	16708.3	20455.5	3865.7	10554.3
451	17315.3	13833.9	15872.7	14819.2	4994.8	22693.2	10052.9	16478.7	2808.0	6280.7
434	9050.2	7481.5	7904.8	6599.1	4230.4	11866.4	5674.1	8930.7	1728.9	4424.6
367	3624.4	3137.2	3272.0	3969.2	3625.1	8567.5	4880.3	5899.1	1876.7	3324.1
335	8077.3	6125.9	5747.0	5509.8	3096.1	14435.9	11894.1	21000.7	4443.7	7561.3
331	7720.2	5789.4	6820.8	5262.5	2258.6	13777.9	8275.6	11660.6	1540.5	6038.9
322	3132.9	1775.3	2824.9	2406.0	1624.0	4507.8	2398.7	2872.3	647.5	943.8
305	6003.8	4333.4	4345.1	3891.1	1676.8	6308.9	3063.4	6515.0	347.6	1435.5
293	3419.7	3625.3	3452.3	2907.3	1607.0	4101.1	3411.0	6350.1	2118.6	3133.7
269	56528.3	47260.7	43778.4	37053.1	24442.7	56933.3	39495.9	57964.4	24148.6	31063.6
Sum	751761.1	616828.6	552626.9	597811.1	240450.9	1180710.9	820175.0	1083688.6	458092.9	1080762.4
ratio	1.0	0.8	0.7	0.8	0.3	1.0	0.7	0.9	0.4	0.9

The data was adjusted and the illustrated in the table below.

Exp 3	RE					NRE				
CPDs	Repair time (hours)					Repair time (hours)				
Position	0	1	2	3	4	0	1	2	3	4
596	20489.1	18926.9	19880.1	18062.4	17899.6	27383.1	20266.1	16973.5	12238.5	10773.2
544	17056.8	19264.4	21771.9	22042.5	19446.6	32512.1	29413.1	22102.6	10524.4	5253.0
531	9063.6	9442.9	10858.3	8795.0	8488.8	14505.6	10842.1	8161.4	3966.0	2027.8
561	8473.1	12974.1	12494.6	13007.4	17636.1	16350.3	10049.2	12800.1	6552.5	5635.0
506	8688.4	13866.9	11503.0	10561.0	10115.0	14073.1	11565.0	9791.7	3793.8	4639.0
499	8562.4	10870.2	12196.6	12068.4	9296.8	15121.9	13942.9	13893.3	6812.1	6541.1
491	13386.2	15403.0	15401.2	15003.0	10545.6	20645.5	18592.8	17563.8	10676.7	10469.1
485	8865.1	7300.0	7678.7	7510.8	9684.0	10859.9	8063.4	7227.8	5016.2	4142.5
478	5138.0	3679.0	2831.9	2412.1	3509.3	4759.2	4036.1	3746.1	2426.3	1486.3
467	18125.2	18270.7	21108.5	18644.4	13923.7	25736.8	24053.0	22286.9	9963.7	11530.3
451	17315.3	16860.0	21592.3	18635.5	15616.2	22693.2	14472.0	17954.0	7237.5	6861.5
434	9050.2	9118.1	10753.2	8298.6	13226.1	11866.4	8168.3	9730.3	4456.2	4833.8
367	3624.4	3823.4	4451.0	4991.3	11333.7	8567.5	7025.6	6427.2	4837.2	3631.5
335	8077.3	7465.9	7817.9	6928.8	9679.8	14435.9	17122.6	22880.9	11453.4	8260.6
331	7720.2	7055.8	9278.5	6617.7	7061.4	13777.9	11913.5	12704.6	3970.5	6597.3
322	3132.9	2163.7	3842.8	3025.6	5077.4	4507.8	3453.1	3129.5	1668.9	1031.1
305	6003.8	5281.3	5910.8	4893.1	5242.4	6308.9	4410.1	7098.3	895.8	1568.2
293	3419.7	4418.3	4696.3	3656.0	5024.3	4101.1	4910.4	6918.6	5460.7	3423.5
269	56528.3	57599.1	59553.5	46595.1	76419.2	56933.3	56857.7	63153.9	62241.8	33936.3

The remaining signal was calculated taking as 100 % of signal the 0 repair hour sample. The T_{50}% is the time required to repair 50 % of the lesion. The data is presented in the table below (%).

Exp 3	RE						NRE					
CPDs	Repair time (hours)					T50%	Repair time (hours)					T50%
Position	0	1	2	3	4		0	1	2	3	4	
596	100.0	92.4	97.0	88.2	87.4	10.0	100.0	74.0	62.0	44.7	39.3	2.6
544	100.0	112.9	127.6	129.2	114.0	10.0	100.0	90.5	68.0	32.4	16.2	2.6
531	100.0	104.2	119.8	97.0	93.7	10.0	100.0	74.7	56.3	27.3	14.0	2.2
561	100.0	103.1	107.5	103.5	108.1	10.0	100.0	61.5	78.3	40.1	34.5	2.7
506	100.0	109.6	102.4	101.6	116.4	10.0	100.0	82.2	69.6	27.0	33.0	2.4
499	100.0	127.0	142.4	140.9	108.6	10.0	100.0	92.2	91.9	45.0	43.3	2.9
491	100.0	115.1	115.1	112.1	78.8	5.9	100.0	90.1	85.1	51.7	50.7	4.0
485	100.0	82.3	86.6	84.7	109.2	10.0	100.0	74.2	66.6	46.2	38.1	2.7
478	100.0	71.6	55.1	46.9	68.3	2.4	100.0	84.8	78.7	51.0	31.2	3.1
467	100.0	100.8	116.5	102.9	76.8	6.0	100.0	93.5	86.6	38.7	44.8	2.7
451	100.0	97.4	124.7	107.6	90.2	5.7	100.0	63.8	79.1	31.9	30.2	2.6
434	100.0	100.8	118.8	91.7	146.1	10.0	100.0	68.8	82.0	37.6	40.7	2.7
367	100.0	105.5	122.8	137.7	112.7	10.0	100.0	82.0	75.0	56.5	42.4	3.4
335	100.0	92.4	96.8	85.8	119.8	10.0	100.0	118.6	158.5	79.3	57.2	4.2
331	100.0	91.4	120.2	85.7	91.5	10.0	100.0	86.5	92.2	28.8	47.9	2.6
322	100.0	69.1	122.7	96.6	162.1	10.0	100.0	76.6	69.4	37.0	22.9	2.6
305	100.0	88.0	98.5	81.5	87.3	10.0	100.0	69.9	112.5	14.2	24.9	2.6
293	100.0	129.2	137.3	106.9	106.9	10.0	100.0	119.7	168.7	133.2	83.5	10.0
269	100.0	101.9	105.4	82.4	135.2	10.0	100.0	99.9	110.9	109.3	59.6	4.2

AIII.3-1 NER efficiency at high resolution at *URA3* gene for the TS

The table below represent the repair efficiency at the specific CPD points for the TS at the NRE*sir2Δ* and RE*sir2Δ* strains.

Exp 1	RE*sir2Δ*					NRE*sir2Δ*				
CPDs	**Repair time (hours)**					**Repair time (hours)**				
Position	**0**	**1**	**2**	**3**	**4**	**0**	**1**	**2**	**3**	**4**
Top band	2027106.4	2494535.3	2440160.0	2574888.0	1902392.2	3117769.6	3352185.3	3521046.2	3334730.5	3112306.8
596	950922.3	1008696.0	795921.9	556735.3	167323.7	81216.4	119403.8	77336.8	66366.8	60805.6
544	199892.8	101675.8	49402.5	43637.6	12082.6	83977.3	108634.5	49740.9	20620.6	20610.7
531	183095.5	91675.4	42193.5	46685.2	6757.1	49393.3	51741.7	29024.7	12468.7	10799.7
561	73824.0	36036.1	19365.9	19415.5	4611.4	30242.6	51634.0	38096.7	7892.3	2750.1
506	67515.4	32053.2	14782.5	11581.1	1567.6	32055.6	38891.5	15026.8	8194.0	7080.7
499	65435.5	28640.2	13260.2	13028.3	2042.6	23757.4	38848.5	24120.2	14373.6	13573.5
491	62553.3	38887.2	18357.3	17126.1	4774.9	34625.5	58939.2	46389.8	7499.7	3670.7
485	95328.6	59798.1	29275.6	19399.7	3246.7	27113.6	46287.4	29841.0	16913.1	11786.8
478	55287.9	26949.4	16369.7	15599.1	3329.8	12572.7	19697.0	13669.3	8116.2	8559.9
467	29309.9	17551.4	11102.4	13805.6	1922.3	47341.3	84598.7	74405.3	28846.4	20039.2
451	108169.2	70227.0	39886.5	43514.5	5458.9	55515.3	87577.2	51576.3	15662.0	10436.1
434	115934.8	53686.5	24816.8	27151.8	4216.1	28446.6	39907.1	17579.8	10159.0	3104.0
367	46758.4	30199.5	19822.7	14664.2	1931.1	16377.6	21632.9	17484.9	5918.2	2919.7
335	11481.5	6193.2	4924.2	6724.6	980.6	7783.8	17021.6	31753.8	17210.4	6572.3
331	5931.0	2983.3	1980.2	4955.3	819.1	12114.9	24937.6	30697.0	3799.2	1794.7
322	29156.8	12842.4	6368.3	7130.9	756.1	1250.7	2821.4	4065.1	2614.9	930.1
305	9695.9	4885.4	4784.3	9676.6	1142.0	15324.3	31333.2	39979.6	6968.2	2390.6
293	14434.9	11509.9	9882.8	19856.6	2701.9	22901.2	41776.9	51558.3	20851.3	11485.3
269	41176.6	24950.1	13520.6	19771.2	2477.1	31149.6	53119.0	91187.4	53912.3	45705.4
Sum	4193010.7	4153975.4	3576178.2	3485347.1	2130533.8	4314115.8	4925645.0	4885345.6	4107744.9	3757756.0
ratio	1.0	1.0	0.9	0.8	0.5	0.9	1.0	1.0	0.8	0.8

The data was adjusted and illustrated in the table below.

Exp 1	RE*sir2Δ*					NRE*sir2Δ*				
CPDs	Repair time (hours)					Repair time (hours)				
Position	0	1	2	3	4	0	1	2	3	4
596	950922.3	1018174.8	933205.5	669774.7	329302.5	92728.9	119403.8	77974.7	79581.2	79703.6
544	199892.8	102631.3	57923.6	52497.8	23779.3	95881.1	108634.5	50151.2	24726.4	27016.3
531	183095.5	92536.9	49471.2	56164.1	13298.3	56394.8	51741.7	29264.2	14951.3	14156.2
561	73824.0	36374.7	22706.2	23357.6	9075.4	34529.5	51634.0	38411.0	9463.7	3604.9
506	67515.4	32354.4	17332.2	13932.5	3085.1	36599.5	38891.5	15150.8	9825.5	9281.4
499	65435.5	28909.3	15547.4	15673.5	4020.0	27125.1	38848.5	24319.1	17235.6	17792.1
491	62553.3	39252.7	21523.6	20603.3	9397.3	39533.7	58939.2	46772.5	8993.0	4811.5
485	95328.6	60360.0	34325.2	23338.6	6389.8	30957.0	46287.4	30087.2	20280.7	15450.1
478	55287.9	27202.7	19193.3	18766.3	6553.2	14354.9	19697.0	13782.0	9732.2	11220.3
467	29309.9	17716.3	13017.4	16608.6	3783.2	54052.0	84598.7	75019.1	34590.1	26267.3
451	108169.2	70887.0	46766.3	52349.7	10743.4	63384.6	87577.2	52001.8	18780.5	13679.5
434	115934.8	54191.0	29097.3	32664.7	8297.6	32479.0	39907.1	17724.8	12181.8	4068.7
367	46758.4	30483.3	23241.8	17641.7	3800.4	18699.2	21632.9	17629.1	7096.5	3827.1
335	11481.5	6251.4	5773.6	8090.0	1929.8	8887.1	17021.6	32015.7	20637.1	8614.9
331	5931.0	3011.3	2321.8	5961.4	1612.0	13832.2	24937.6	30950.2	4555.7	2352.5
322	29156.8	12963.1	7466.8	8578.8	1488.0	1427.9	2821.4	4098.6	3135.5	1219.2
305	9695.9	4931.3	5609.5	11641.3	2247.6	17496.5	31333.2	40309.4	8355.6	3133.6
293	14434.9	11618.0	11587.4	23888.2	5317.5	26147.5	41776.9	51983.6	25003.0	15054.9
269	41176.6	25184.6	15852.7	23785.6	4875.0	35565.1	53119.0	91939.6	64646.8	59910.4

The remaining signal was calculated taking as 100 % of signal the 0 repair hour sample. The T_{50}% is the time required to repair 50 % of the lesion. The data is presented in the table below (%).

Exp 1	RES*ir2Δ*						NRES*ir2Δ*					
CPDs	**Repair time (hours)**					**T50%**	**Repair time (hours)**					**T50%**
Position	**0**	**1**	**2**	**3**	**4**		**0**	**1**	**2**	**3**	**4**	
596	100.0	107.1	98.1	70.4	34.6	3.6	100.0	128.8	84.1	85.8	86.0	10.0
544	100.0	51.3	29.0	26.3	11.9	1.0	100.0	113.3	52.3	25.8	28.2	2.1
531	100.0	50.5	27.0	30.7	7.3	1.0	100.0	91.7	51.9	26.5	25.1	2.1
561	100.0	49.3	30.8	31.6	12.3	1.0	100.0	149.5	111.2	27.4	10.4	2.6
506	100.0	47.9	25.7	20.6	4.6	0.9	100.0	106.3	41.4	26.8	25.4	1.8
499	100.0	44.2	23.8	24.0	6.1	0.9	100.0	143.2	89.7	63.5	65.6	4.8
491	100.0	62.8	34.4	32.9	15.0	1.4	100.0	149.1	118.3	22.7	12.2	2.6
485	100.0	63.3	36.0	24.5	6.7	1.4	100.0	149.5	97.2	65.5	49.9	4.0
478	100.0	49.2	34.7	33.9	11.9	1.0	100.0	137.2	96.0	67.8	78.2	10.0
467	100.0	60.4	44.4	56.7	12.9	1.4	100.0	156.5	138.8	64.0	48.6	4.0
451	100.0	65.5	43.2	48.4	9.9	1.6	100.0	138.2	82.0	29.6	21.6	2.6
434	100.0	46.7	25.1	28.2	7.2	0.9	100.0	122.9	54.6	37.5	12.5	2.2
367	100.0	65.2	49.7	37.7	8.1	2.0	100.0	115.7	94.3	38.0	20.5	2.7
335	100.0	54.4	50.3	70.5	16.8	2.0	100.0	191.5	106.2	103.2	96.9	10.0
331	100.0	50.8	39.1	100.5	27.2	1.0	100.0	108.3	103.8	32.9	17.0	2.7
322	100.0	44.5	25.6	29.4	5.1	0.9	100.0	107.6	107.0	109.6	85.4	10.0
305	100.0	50.9	57.9	120.1	23.2	1.0	100.0	109.1	100.4	47.8	17.9	2.9
293	100.0	80.5	80.3	100.5	36.8	3.8	100.0	159.8	198.8	95.6	57.6	4.4
269	100.0	61.2	38.5	57.8	11.8	1.4	100.0	149.4	108.5	101.8	108.5	10.0

AIII.3-2 NER efficiency at high resolution at *URA3* gene for the TS

The table below represent the repair efficiency at the specific CPD points for the TS at the NRE*sir2Δ* and RE*sir2Δ* strains.

Exp 2	RE*sir2Δ*					NRE*sir2Δ*				
CPDs	**Repair time (hours)**					**Repair time (hours)**				
Position	**0**	**1**	**2**	**3**	**4**	**0**	**1**	**2**	**3**	**4**
Top band	4514801.7	4615176.4	4429386.5	5110168.4	4951650.6	5402293.7	5367882.6	5164580.4	5339430.9	5223766.9
596	347439.6	208622.2	116519.1	85900.5	60394.7	142200.8	208372.3	72036.5	57387.1	47919.8
544	672445.4	346747.7	198062.3	130428.9	102673.3	361156.6	401038.2	146682.8	81458.6	58163.3
531	168351.2	83556.8	50198.8	33224.6	31460.0	137727.1	128355.4	37699.0	17964.8	10830.5
561	219744.1	96691.3	64048.8	41840.7	31586.3	118827.7	163176.2	90824.1	53192.0	31131.4
506	187951.8	86875.8	44087.7	32843.1	30077.4	113377.3	119480.8	51286.2	30971.5	13622.6
499	201588.1	110129.1	61869.0	37300.4	31776.4	101690.6	147441.1	83372.5	56671.4	50399.3
491	296934.9	178704.1	108103.1	64618.2	50925.3	147808.0	205013.5	129148.0	87355.6	45485.7
485	168826.2	76329.4	46416.1	31251.1	23346.1	95141.1	130723.6	64679.6	39779.7	25016.7
478	95216.8	47952.7	35977.4	23738.0	21715.0	49008.2	63195.5	34365.6	16786.0	17199.3
467	432944.9	231396.8	151540.1	105542.6	86047.1	229883.4	321578.2	183202.8	110166.1	61891.5
451	476741.1	202645.8	131376.0	90104.5	72448.2	268311.5	341450.8	159295.7	90588.7	53456.0
434	177050.8	91001.6	58746.2	42808.0	33253.1	108588.6	125612.0	57414.8	33095.5	22668.9
367	129658.4	61059.1	31962.0	21834.5	17952.4	111194.1	105002.6	45299.3	26268.6	16702.6
335	46216.2	20488.9	10686.9	10595.9	8530.1	23638.7	28887.5	16144.9	7977.7	6259.2
331	33127.9	22947.0	13687.2	12235.3	11419.7	27453.5	40880.9	34502.5	22919.1	61021.2
322	166163.1	96491.2	63177.5	42257.8	32254.9	95788.1	85870.1	60473.8	39024.3	132922.9
305	244133.9	145830.2	94069.8	48423.5	40066.1	175648.3	258936.4	150482.5	106159.6	72494.9
293	97209.8	71443.9	47439.4	44446.8	31759.4	60015.2	81963.7	52154.1	38330.5	34248.2
269	499898.5	306331.8	237924.5	194241.6	187113.9	297523.6	366833.3	230140.0	187677.8	211957.2
Sum	9176444.6	7100421.8	5995278.3	6203804.4	5856449.9	8067276.1	8691694.7	6863785.0	6443205.6	6197158.0
ratio	1.0	0.8	0.7	0.7	0.6	0.9	1.0	0.8	0.7	0.7

The data was adjusted and illustrated in the next table.

Exp 2	RE*sir2Δ*					NRE*sir2Δ*				
CPDs	**Repair time (hours)**					**Repair time (hours)**				
Position	**0**	**1**	**2**	**3**	**4**	**0**	**1**	**2**	**3**	**4**
596	347439.6	269619.3	178345.5	127061.0	94632.2	153207.4	208372.3	91220.7	77413.6	67208.9
544	672445.4	448129.9	303156.6	192925.7	160878.3	389110.6	401038.2	185746.3	109885.2	81575.7
531	168351.2	107987.1	76834.9	49144.7	49294.6	148387.3	128355.4	47738.7	24233.9	15190.1
561	219744.1	124961.9	98033.8	61889.3	49492.5	128025.1	163176.2	115011.6	71754.5	43662.7
506	187951.8	112276.5	67481.1	48580.3	47128.1	122152.9	119480.8	64944.4	41779.6	19106.1
499	201588.1	142328.7	94697.4	55173.5	49790.2	109561.6	147441.1	105575.7	76448.0	70686.5
491	296934.9	230953.7	165463.8	95580.9	79794.6	159248.6	205013.5	163541.6	117840.2	63795.0
485	168826.2	98646.6	71045.0	46225.4	36580.9	102505.2	130723.6	81904.5	53661.6	35086.6
478	95216.8	61973.1	55067.4	35112.3	34025.1	52801.5	63195.5	43517.6	22643.8	24122.6
467	432944.9	299052.7	231949.1	156114.8	134826.8	247676.7	321578.2	231991.9	148610.8	86804.6
451	476741.1	261895.4	201085.7	133279.4	113518.8	289079.2	341450.8	201718.0	122201.5	74973.6
434	177050.8	117608.7	89917.7	63320.1	52104.2	116993.5	125612.0	72705.1	44644.9	31793.8
367	129658.4	78911.5	48921.5	32296.7	28129.5	119800.6	105002.6	57363.1	35435.5	23425.8
335	46216.2	26479.4	16357.5	15673.0	13365.7	25468.4	28887.5	20444.4	10761.7	8778.7
331	33127.9	29656.2	20949.9	18098.1	17893.4	29578.4	40880.9	43690.9	30917.2	85584.0
322	166163.1	124703.4	96700.2	62506.3	50540.0	103202.3	85870.1	76578.8	52642.6	186428.3
305	244133.9	188468.0	143984.4	71626.4	62779.4	189243.7	258936.4	190557.8	143206.2	101676.2
293	97209.8	92332.7	72611.3	65744.1	49763.7	64660.5	81963.7	66043.3	51706.7	48034.1
269	499898.5	395897.2	364170.0	287315.1	293188.0	320552.4	366833.3	291429.1	253171.9	297276.1

The remaining signal was calculated taking as 100 % of signal the 0 repair hour sample. The T_{50}% is the time required to repair 50 % of the lesion. The data is presented in the table below (%).

Exp 2	RES*ir2Δ*						NRES*ir2Δ*					
CPDs	Repair time (hours)					T50%	Repair time (hours)					T50%
Position	0	1	2	3	4		0	1	2	3	4	
596	100.0	77.6	51.3	36.6	27.2	2.0	100.0	136.0	59.5	50.5	43.9	3.0
544	100.0	66.6	87.3	28.7	23.9	2.8	100.0	103.1	47.7	28.2	21.0	1.8
531	100.0	64.1	22.1	29.2	29.3	1.7	100.0	86.5	32.2	16.3	10.2	1.6
561	100.0	56.9	28.2	28.2	22.5	1.4	100.0	127.5	89.8	56.0	34.1	3.2
506	100.0	59.7	19.4	25.8	25.1	1.3	100.0	97.8	53.2	34.2	15.6	2.2
499	100.0	70.6	27.3	27.4	24.7	1.9	100.0	134.6	96.4	69.8	64.5	4.6
491	100.0	77.8	47.6	32.2	26.9	2.0	100.0	128.7	102.7	74.0	40.1	3.7
485	100.0	58.4	20.4	27.4	21.7	1.4	100.0	127.5	79.9	52.4	34.2	3.1
478	100.0	65.1	15.8	36.9	35.7	1.2	100.0	119.7	82.4	42.9	45.7	2.5
467	100.0	69.1	66.8	36.1	31.1	2.2	100.0	129.8	93.7	60.0	35.0	3.4
451	100.0	54.9	57.9	28.0	23.8	2.2	100.0	118.1	69.8	42.3	25.9	2.7
434	100.0	66.4	25.9	35.8	29.4	1.4	100.0	107.4	62.1	38.2	27.2	2.5
367	100.0	60.9	14.1	24.9	21.7	1.4	100.0	87.6	47.9	29.6	19.6	1.9
335	100.0	57.3	4.7	33.9	28.9	1.2	100.0	113.4	80.3	42.3	34.5	2.8
331	100.0	89.5	6.0	54.6	54.0	1.5	100.0	108.2	107.7	104.5	109.3	10.0
322	100.0	75.0	27.8	37.6	30.4	1.4	100.0	83.2	74.2	51.0	180.6	3.0
305	100.0	77.2	41.4	29.3	25.7	1.3	100.0	136.8	100.7	75.7	53.7	4.1
293	100.0	95.0	20.9	67.6	51.2	1.5	100.0	106.8	102.1	80.0	74.3	10.0
269	100.0	79.2	104.8	57.5	58.6	4.5	100.0	114.4	90.9	79.0	92.7	10.0

A III.4-1 NER efficiency at high resolution at *URA3* gene for the NTS

The table below represent the repair efficiency at the specific CPD points for the NTS at the NRE*sir2Δ* and RE*sir2Δ* strains.

Exp 1	RE*sir2Δ*				NRE*sir2Δ*				
CPDs	**Repair time (hours)**				**Repair time (hours)**				
Position	**0**	**1**	**2**	**3**	**0**	**1**	**2**	**3**	**4**
Top band	2575721.9	2530840.3	2855642.1	2785117.6	2501726.0	2400901.1	2312925.0	2463705.5	2896314.6
244	60478.4	43616.3	26039.4	15648.5	49274.1	41349.2	28176.9	19512.3	16992.1
257	137260.3	112031.2	73191.9	54870.7	146810.9	102332.3	58784.7	40532.4	37312.4
292	68464.5	65647.8	46075.5	31456.9	49270.5	44961.2	29355.2	28935.6	28751.3
302	2534.5	1848.1	1336.7	573.6	3324.1	2396.5	1059.5	833.0	883.0
313	20931.8	15780.3	5506.3	3487.8	27107.0	16391.1	5668.6	5452.3	5514.0
326	78913.8	90174.2	59663.8	41652.3	100755.6	85848.3	51205.3	56473.1	52638.9
363	57180.1	46394.6	23199.0	12921.7	51258.2	59396.9	28074.9	19316.7	18865.0
388	7772.8	8932.3	5174.8	3540.3	5134.1	9213.0	3774.8	3615.8	3295.8
399	10829.4	10321.4	5816.4	4657.0	2416.5	6250.3	2898.8	2593.3	3068.2
407	7854.9	4900.8	2284.8	1336.9	11221.4	5418.9	2232.8	1700.4	1501.3
440	28599.0	24684.5	15011.3	10155.1	16037.1	20105.1	10570.5	6803.8	7444.9
460	10624.5	19521.1	5783.2	6024.6	15794.8	12920.6	6379.0	6294.7	7598.2
480	56331.4	57835.5	30885.0	22171.9	50646.7	45762.0	31115.2	24347.3	26920.8
503	13601.4	11758.8	6288.1	3959.8	17049.5	10718.8	6097.2	7458.7	7238.1
521	11974.6	9199.6	4387.4	2014.8	17571.6	11191.8	7613.2	5573.5	7087.6
540	71340.9	60482.8	26040.9	13605.9	78406.6	73173.9	47351.3	34835.4	27507.9
560	11463.7	8832.7	3732.3	2697.1	17167.0	15820.8	7622.5	5686.4	5622.9
594	31867.8	30559.7	13291.8	9530.2	30740.1	31718.0	20363.0	15097.3	13398.9
600	20845.0	14650.2	5137.7	2326.7	13427.7	22686.3	11696.0	8310.0	6228.6
604	18767.0	10692.1	3061.9	1948.2	36640.9	26414.9	12254.2	8975.6	6305.6
608	3677.7	3376.3	2364.2	756.2	5532.3	4762.9	4970.0	4421.8	4134.3
616	17669.9	15137.3	4596.4	3026.9	9571.6	6788.4	2538.5	1523.0	1186.0
627	49924.1	39772.3	15978.7	9167.2	56565.8	35612.1	19395.1	12310.7	10823.2
654	14682.9	9118.4	6647.3	4993.3	14471.9	9688.7	4525.8	3664.1	3078.6
661	15167.8	16100.2	12083.7	9352.6	10240.1	11420.4	8310.2	4148.2	4915.7
722	66749.8	65698.0	44385.5	29024.2	59825.6	35872.4	21815.1	14866.2	14451.7
Sum	3471229.9	3327906.7	3303605.8	3086017.9	3397987.8	3149116.1	2746773.1	2806987.1	3219079.6
ratio	1.0	1.0	1.0	0.9	1.0	0.9	0.8	0.8	0.9

The data was adjusted and illustrated in the table below.

Exp 1	RE*sir2Δ*				NRE*sir2Δ*				
CPDs	Repair time (hours)				Repair time (hours)				
Position	0	1	2	3	0	1	2	3	4
244	60478.4	45494.7	27360.6	17601.8	49274.1	44617.0	34857.2	23620.6	17936.5
257	137260.3	116856.1	76905.6	61720.0	146810.9	110419.6	72721.6	49066.4	39386.1
292	68464.5	68475.1	48413.4	35383.5	49270.5	48514.4	36314.8	35027.9	30349.2
302	2534.5	1927.7	1404.5	645.2	3324.1	2585.9	1310.7	1008.3	932.1
313	20931.8	16459.9	5785.7	3923.1	27107.0	17686.5	7012.6	6600.2	5820.5
326	78913.8	94057.7	62691.1	46851.5	100755.6	92632.8	63345.2	68363.4	55564.4
363	57180.1	48392.7	24376.1	14534.6	51258.2	64091.0	34731.0	23383.7	19913.4
388	7772.8	9317.0	5437.4	3982.2	5134.1	9941.1	4669.7	4377.1	3479.0
399	10829.4	10765.9	6111.5	5238.3	2416.5	6744.3	3586.0	3139.4	3238.7
407	7854.9	5111.8	2400.7	1503.7	11221.4	5847.2	2762.1	2058.4	1584.7
440	28599.0	25747.6	15773.0	11422.7	16037.1	21693.9	13076.6	8236.3	7858.7
460	10624.5	20361.8	6076.6	6776.6	15794.8	13941.7	7891.4	7620.1	8020.5
480	56331.4	60326.3	32452.1	24939.5	50646.7	49378.5	38492.1	29473.5	28417.0
503	13601.4	12265.2	6607.2	4454.0	17049.5	11565.9	7542.7	9029.0	7640.3
521	11974.6	9595.8	4610.0	2266.3	17571.6	12076.3	9418.2	6747.0	7481.5
540	71340.9	63087.6	27362.2	15304.3	78406.6	78956.8	58577.5	42169.9	29036.7
560	11463.7	9213.1	3921.7	3033.7	17167.0	17071.1	9429.7	6883.6	5935.4
594	31867.8	31875.8	13966.2	10719.8	30740.1	34224.6	25190.7	18275.9	14143.6
600	20845.0	15281.1	5398.3	2617.1	13427.7	24479.1	14468.9	10059.6	6574.7
604	18767.0	11152.5	3217.3	2191.4	36640.9	28502.5	15159.5	10865.3	6656.0
608	3677.7	3521.7	2484.2	850.6	5532.3	5139.3	6148.3	5352.8	4364.0
616	17669.9	15789.2	4829.6	3404.8	9571.6	7324.9	3140.3	1843.6	1252.0
627	49924.1	41485.1	16789.4	10311.5	56565.8	38426.5	23993.4	14902.7	11424.7
654	14682.9	9511.1	6984.5	5616.6	14471.9	10454.4	5598.8	4435.6	3249.7
661	15167.8	16793.5	12696.8	10520.1	10240.1	12323.0	10280.4	5021.6	5188.9
722	66749.8	68527.5	46637.6	32647.2	59825.6	38707.4	26987.1	17996.2	15254.9

The remaining signal was calculated taking as 100 % of signal the 0 repair hour sample. The T_{50}% is the time required to repair 50 % of the lesion. The data is presented in the table below (%).

Exp 1	RE*sir2Δ*					NRE*sir2Δ*					
CPDs	**Repair time (hours)**				**T50%**	**Repair time (hours)**					**T50%**
Position	**0**	**1**	**2**	**3**		**0**	**1**	**2**	**3**	**4**	
244	100.0	75.2	45.2	29.1	1.8	100.0	90.5	70.7	47.9	36.4	2.9
257	100.0	85.1	56.0	45.0	2.4	100.0	75.2	49.5	33.4	26.8	2.0
292	100.0	100.0	70.7	51.7	3.0	100.0	98.5	73.7	71.1	61.6	5.0
302	100.0	76.1	55.4	25.5	2.2	100.0	77.8	39.4	30.3	28.0	1.7
313	100.0	78.6	27.6	18.7	1.5	100.0	65.2	25.9	24.3	21.5	1.4
326	100.0	119.2	79.4	59.4	3.2	100.0	91.9	62.9	67.9	55.1	4.2
363	100.0	84.6	42.6	25.4	1.8	100.0	125.0	67.8	45.6	38.8	2.7
388	100.0	119.9	70.0	51.2	3.2	100.0	100.0	91.0	85.3	67.8	5.0
399	100.0	99.4	56.4	48.4	2.5	100.0	179.1	148.4	129.9	134.0	10.0
407	100.0	65.1	30.6	19.1	1.4	100.0	52.1	24.6	18.3	14.1	1.0
440	100.0	90.0	55.2	39.9	2.2	100.0	135.3	81.5	51.4	49.0	3.2
460	100.0	101.6	57.2	63.8	4.1	100.0	88.3	50.0	48.2	50.8	2.0
480	100.0	107.1	57.6	44.3	2.4	100.0	97.5	76.0	58.2	56.1	4.0
503	100.0	90.2	48.6	32.7	2.0	100.0	67.8	44.2	53.0	44.8	1.6
521	100.0	80.1	38.5	18.9	1.7	100.0	68.7	53.6	38.4	42.6	2.2
540	100.0	88.4	38.4	21.5	1.8	100.0	100.7	74.7	53.8	37.0	3.2
560	100.0	80.4	34.2	26.5	1.6	100.0	99.4	54.9	40.1	34.6	2.2
594	100.0	100.0	43.8	33.6	1.9	100.0	111.3	81.9	59.5	46.0	3.7
600	100.0	73.3	25.9	12.6	1.5	100.0	182.3	107.8	74.9	49.0	4.0
604	100.0	59.4	17.1	11.7	1.2	100.0	77.8	41.4	29.7	18.2	1.7
608	100.0	95.8	67.5	23.1	2.4	100.0	92.9	111.1	96.8	78.9	10.0
616	100.0	89.4	27.3	19.3	1.6	100.0	76.5	32.8	19.3	13.1	1.6
627	100.0	83.1	33.6	20.7	1.7	100.0	67.9	42.4	26.3	20.2	1.7
654	100.0	64.8	47.6	38.3	1.8	100.0	72.2	38.7	30.6	22.5	1.6
661	100.0	110.7	83.7	69.4	3.8	100.0	120.3	100.4	49.0	50.7	3.0
722	100.0	102.7	69.9	48.9	2.9	100.0	64.7	45.1	30.1	25.5	1.7

A III.4-2 NER efficiency at high resolution at *URA3* gene for the NTS

The table below represent the repair efficiency at the specific CPD points for the NTS at the NRE*sir2Δ* and RE*sir2Δ* strains.

Exp 2	RE*sir2Δ*					NRE*sir2Δ*				
CPDs	Repair time (hours)					Repair time (hours)				
Position	0	1	2	3	4	0	1	2	3	4
Top band	3692569.5	2260410.8	3956975.3	5023657.3	3086801.8	2974950.1	4064532.2	3699521.9	3763294.3	3581282.0
244	61770.7	123179.8	82904.0	44064.7	22259.1	86309.8	168155.8	30528.9	53064.3	87430.0
257	188322.8	335076.9	278704.8	208988.4	106691.3	309757.9	495124.7	84289.0	133234.8	64227.9
292	64336.9	134814.7	116323.7	81426.1	40706.1	94007.0	175392.7	38568.8	80322.6	48328.8
302	1871.7	1694.1	1056.1	1002.3	2239.4	4847.7	8335.1	683.1	5917.8	19539.4
313	16848.7	26840.9	11732.7	5706.1	5749.2	37716.2	71598.2	3465.7	7549.1	4202.1
326	128571.1	238992.0	190149.6	131602.9	59188.5	211062.5	381728.8	72511.9	172806.3	89227.5
363	85105.5	134088.8	76751.8	47572.3	22110.5	117825.9	213337.7	19987.8	43223.0	19726.6
388	17682.4	47364.0	19978.5	16125.9	8812.2	20948.1	27315.5	1324.6	6439.5	5570.0
399	12134.7	27809.1	17272.3	10173.1	3004.4	2946.5	9255.5	1989.8	5437.3	7205.5
407	10355.7	11619.5	7630.4	4456.9	955.0	14994.1	36114.0	2110.4	3413.7	1480.6
440	29599.5	54140.2	44771.0	28331.2	10647.2	29881.6	77621.4	8456.5	12788.8	5515.6
460	6365.2	22940.4	17772.1	12658.7	5208.2	24821.8	37396.7	6659.9	14178.2	16728.6
480	53762.5	109625.0	87715.8	62670.7	31018.1	94795.3	195733.6	43552.2	85155.0	50438.8
503	9943.7	28570.0	18963.5	8712.8	2991.0	28873.7	48490.4	9317.6	18234.9	17756.6
521	16320.0	20473.5	13906.2	12110.4	9051.5	38483.1	93978.0	12920.5	28112.2	18050.0
540	63856.2	131160.2	79741.4	56008.7	26328.7	125002.1	264739.6	36781.7	62233.5	36858.3
560	4184.4	18778.3	9550.6	3653.3	563.1	21296.9	49890.5	4426.4	6686.2	4546.2
594	22405.6	51796.2	36569.0	23126.3	8593.3	47668.0	94221.3	14438.1	32385.2	19225.0
600	17885.1	35558.5	17116.1	12127.2	4305.3	22735.0	48007.1	8569.5	14507.5	6585.4
604	13470.6	20459.5	11955.3	6952.8	3020.4	48781.6	76583.5	10053.2	19511.9	10085.3
608	3981.1	7987.4	6080.8	4563.1	2123.9	8505.0	15056.5	2582.9	5328.6	3855.1
616	10721.4	23831.8	13937.3	8323.5	3405.4	19513.4	30526.9	2384.6	4938.2	4449.9
627	34451.4	83824.7	52204.2	29448.3	10899.0	99975.8	154910.5	17840.6	29806.4	16807.3
654	7844.2	23942.7	17832.0	10026.5	4036.0	18997.0	23370.1	6007.9	11166.6	18966.7
661	12262.7	39576.5	40127.2	29764.5	13290.9	80453.8	130536.0	62138.6	104998.9	83630.4
722	24684.4	109259.9	112933.0	72933.9	28884.5	86230.5	135449.1	16826.0	38197.7	24455.0
Sum	4611307.6	4123815.4	5340654.7	5956188.0	3522884.0	4671380.3	7127401.4	4217937.9	4762932.4	4266174.7
ratio	0.8	0.7	0.9	1.0	0.6	1.0	1.5	0.9	1.0	0.9

The data was adjusted and illustrated in the table below.

Exp 2	RE*sir2Δ*					NRE*sir2Δ*				
CPDs	**Repair time (hours)**					**Repair time (hours)**				
Position	**0**	**1**	**2**	**3**	**4**	**0**	**1**	**2**	**3**	**4**
244	79786.0	177913.4	92459.1	44064.7	37633.7	88001.4	112371.2	34473.5	53064.3	97610.5
257	243246.8	483964.7	310826.7	208988.4	180384.4	315828.7	330870.3	95179.8	133234.8	71706.6
292	83100.6	194718.2	129730.5	81426.1	68822.3	95849.4	117207.3	43552.2	80322.6	53956.2
302	2417.6	2446.8	1177.8	1002.3	3786.1	4942.7	5570.0	771.4	5917.8	21814.6
313	21762.6	38767.4	13085.0	5706.1	9720.2	38455.4	47845.9	3913.5	7549.1	4691.3
326	166068.6	345185.5	212065.2	131602.9	100070.8	215199.0	255092.7	81881.1	172806.3	99617.2
363	109926.4	193669.6	85597.8	47572.3	37382.5	120135.1	142564.3	22570.4	43223.0	22023.5
388	22839.5	68409.7	22281.1	16125.9	14898.9	21358.6	18253.8	1495.8	6439.5	6218.6
399	15673.7	40165.8	19263.0	10173.1	5079.5	3004.3	6185.1	2246.9	5437.3	8044.6
407	13376.0	16782.6	8509.8	4456.9	1614.6	15288.0	24133.4	2383.1	3413.7	1653.0
440	38232.2	78196.8	49931.0	28331.2	18001.4	30467.3	51871.0	9549.1	12788.8	6157.9
460	8221.6	33133.6	19820.4	12658.7	8805.7	25308.3	24990.6	7520.5	14178.2	18676.5
480	69442.2	158335.6	97825.4	62670.7	52442.7	96653.1	130800.3	49179.6	85155.0	56311.9
503	12843.8	41264.8	21149.1	8712.8	5056.9	29439.6	32404.0	10521.5	18234.9	19824.2
521	21079.7	29570.7	15509.0	12110.4	15303.5	39237.3	62801.4	14590.0	28112.2	20151.7
540	82479.7	189439.8	88932.0	56008.7	44514.2	127451.9	176914.0	41534.2	62233.5	41150.1
560	5404.7	27122.2	10651.3	3653.3	952.0	21714.3	33339.6	4998.3	6686.2	5075.6
594	28940.1	74811.3	40783.8	23126.3	14528.8	48602.2	62964.0	16303.6	32385.2	21463.6
600	23101.2	51358.5	19088.8	12127.2	7279.0	23180.6	32081.0	9676.8	14507.5	7352.2
604	17399.3	29550.5	13333.1	6952.8	5106.7	49737.7	51177.4	11352.1	19511.9	11259.7
608	5142.2	11536.6	6781.6	4563.1	3591.0	8671.7	10061.6	2916.6	5328.6	4304.0
616	13848.3	34421.2	15543.6	8323.5	5757.6	19895.8	20399.8	2692.7	4938.2	4968.0
627	44499.0	121071.3	58220.9	29448.3	18427.1	101935.2	103519.9	20145.8	29806.4	18764.4
654	10132.0	34581.4	19887.2	10026.5	6823.7	19369.3	15617.3	6784.1	11166.6	21175.2
661	15839.1	57161.9	44752.0	29764.5	22471.1	82030.5	87231.5	70167.4	104998.9	93368.4
722	31883.6	157808.4	125949.0	72933.9	48835.5	87920.5	90514.7	19000.1	38197.7	27302.6

The remaining signal was calculated taking as 100 % of signal the 0 repair hour sample. The T_{50}% is the time required to repair 50 % of the lesion. The data is presented in the table below (%).

Exp 2	RE*sir2Δ*						NRE*sir2Δ*					
CPDs	**Repair time (hours)**					**T50%**	**Repair time (hours)**					**T50%**
Position	**0**	**1**	**2**	**3**	**4**		**0**	**1**	**2**	**3**	**4**	
244	100.0	103.0	105.9	55.2	47.2	3.5	100.0	127.7	39.2	60.3	110.9	1.5
257	100.0	100.0	107.8	85.9	74.2	10.0	100.0	104.8	30.1	42.2	22.7	1.3
292	100.0	104.3	106.1	98.0	82.8	10.0	100.0	122.3	45.4	83.8	56.3	1.7
302	100.0	101.2	48.7	41.5	156.6	2.0	100.0	112.7	15.6	119.7	441.3	1.3
313	100.0	108.1	60.1	26.2	44.7	2.2	100.0	124.4	10.2	19.6	12.2	1.1
326	100.0	100.9	127.7	79.2	60.3	10.0	100.0	118.5	38.0	80.3	46.3	1.4
363	100.0	106.2	77.9	43.3	34.0	2.8	100.0	118.7	18.8	36.0	18.3	1.1
388	100.0	100.5	97.6	70.6	65.2	4.4	100.0	85.5	7.0	30.1	29.1	1.2
399	100.0	106.3	122.9	64.9	32.4	3.3	100.0	105.9	74.8	101.0	100.8	10.0
407	100.0	125.5	63.6	33.3	12.1	2.4	100.0	157.9	15.6	22.3	10.8	1.1
440	100.0	104.5	130.6	74.1	47.1	3.9	100.0	100.3	31.3	42.0	20.2	1.4
460	100.0	100.0	100.0	100.0	107.1	10.0	100.0	98.7	29.7	56.0	73.8	1.3
480	100.0	100.0	100.9	90.2	75.5	10.0	100.0	135.3	50.9	88.1	58.3	2.0
503	100.0	100.3	100.7	67.8	39.4	3.6	100.0	110.1	35.7	61.9	67.3	1.4
521	100.0	140.3	73.6	57.5	72.6	3.3	100.0	160.1	37.2	71.6	51.4	1.4
540	100.0	109.7	107.8	67.9	54.0	6.0	100.0	138.8	32.6	48.8	32.3	1.4
560	100.0	101.8	107.1	67.6	17.6	3.1	100.0	153.5	23.0	30.8	23.4	1.2
594	100.0	158.5	140.9	79.9	50.2	4.1	100.0	129.5	33.5	66.6	44.2	1.4
600	100.0	122.3	82.6	52.5	31.5	3.1	100.0	138.4	41.7	62.6	31.7	1.6
604	100.0	169.8	76.6	40.0	29.3	2.7	100.0	102.9	22.8	39.2	22.6	1.2
608	100.0	104.3	101.9	88.7	69.8	10.0	100.0	116.0	33.6	61.4	49.6	1.4
616	100.0	148.6	112.2	60.1	41.6	3.8	100.0	102.5	13.5	24.8	25.0	1.1
627	100.0	102.1	100.8	66.2	41.4	3.4	100.0	101.6	19.8	29.2	18.4	1.2
654	100.0	101.3	106.3	99.0	67.3	10.0	100.0	80.6	35.0	57.7	109.3	1.4
661	100.0	100.9	102.5	107.9	141.9	10.0	100.0	106.3	85.5	128.0	113.8	10.0
722	100.0	105.0	100.0	100.0	100.0	10.0	100.0	103.0	21.6	43.4	31.1	1.2

A III.4-3 NER efficiency at high resolution at *URA3* gene for the NTS

The table below represent the repair efficiency at the specific CPD points for the NTS at the NRE*sir2Δ* and RE*sir2Δ* strains.

Exp 3	RE*sir2Δ*					NRE*sir2Δ*				
CPDs	Repair time (hours)					Repair time (hours)				
Position	0	1	2	3	4	0	1	2	3	4
Top band	917724.5	952378.8	961931.3	934051.6	903051.4	1363223.4	1455363.7	1410266.4	1374671.5	1373085.8
244	46569.1	39031.1	28599.1	11472.7	12815.0	24354.2	36440.2	17547.4	7734.1	6979.5
257	104150.7	108757.5	96037.2	49381.1	53714.2	72370.0	92058.0	48638.0	22173.6	21527.1
292	40722.1	46422.4	39470.6	19703.7	23598.0	29098.2	45748.8	28331.3	16741.2	18145.4
302	1480.7	1827.3	1131.2	565.1	581.6	1681.0	1468.1	575.7	669.5	2610.4
313	11614.4	10293.3	5436.1	2298.9	3062.8	28673.1	44609.6	27176.5	16310.9	18479.6
326	60202.4	57586.7	47697.7	20340.5	24595.6	56778.8	80399.7	54015.7	33178.9	30216.1
363	45043.7	36361.6	22042.3	7099.4	10092.1	31423.0	46735.6	20355.0	10160.3	6731.2
388	13468.3	10914.8	6103.4	1868.7	3433.0	3545.3	5784.6	2611.8	2086.0	2296.6
399	7728.6	7297.1	4897.1	2316.3	2843.5	1260.4	4074.6	2642.8	1284.4	1912.6
407	3047.2	2235.8	1749.0	647.1	800.0	4210.4	4097.8	1583.1	431.5	1272.5
440	16253.5	15242.4	12975.4	5176.3	7356.1	8334.3	13288.5	7343.5	1837.3	1981.7
460	8107.3	6853.0	7143.4	4871.6	4720.8	7813.3	9157.8	5326.7	3163.7	5811.7
480	31769.6	30805.3	25520.9	10603.6	12903.5	20696.6	31207.2	18569.8	10956.5	9818.9
503	8915.8	8571.6	6061.7	2503.5	3248.8	6516.9	7913.2	4266.2	1928.1	2720.8
521	5515.9	5064.4	3042.1	1399.8	2649.5	5550.5	6638.0	3351.3	1709.2	2024.3
540	34183.9	30081.9	18417.4	7523.9	9582.9	25280.3	38195.6	19322.2	8177.1	7982.6
560	5864.5	6974.2	3413.6	1009.9	2349.7	5134.8	7179.6	6245.0	1747.9	1577.2
594	18152.8	17540.2	10912.3	3840.9	4690.0	13970.0	20983.3	13506.8	6575.1	5099.5
600	13848.6	9121.0	3977.8	1531.2	2466.4	5524.8	10919.8	7120.0	2575.1	1418.6
604	10868.0	6484.9	3018.0	707.1	1963.7	13957.0	17281.4	8212.9	3566.7	2237.9
608	2905.9	2518.6	1490.5	412.1	1283.4	2124.1	3543.8	1896.5	863.4	1298.4
616	8751.2	7508.9	5412.9	1862.6	2444.7	5160.1	5531.3	2506.6	1098.9	1612.3
627	27040.1	21944.9	14939.6	4962.7	6765.4	25026.5	24996.8	10786.7	4568.1	4547.6
654	11448.8	13485.6	6863.2	7635.7	11142.3	26644.2	17011.3	5453.5	16978.6	21404.5
661	11219.0	12872.9	9319.5	5144.3	6555.2	7000.2	5652.9	1500.7	6205.0	6346.3
722	30287.3	30062.1	26488.9	7934.0	14698.5	19344.1	19932.2	9304.3	5384.5	4030.1
Sum	1635952.4	1607694.3	1477681.4	1185140.3	1203366.0	1895747.9	2167405.6	1787535.3	1595150.4	1594013.1
ratio	1.0	1.0	0.9	0.7	0.7	0.9	1.0	0.8	0.7	0.7

The data was adjusted and illustrated in the table below.

Exp 3	RE*sir2Δ*					NRE*sir2Δ*				
CPDs	**Repair time (hours)**					**Repair time (hours)**				
Position	**0**	**1**	**2**	**3**	**4**	**0**	**1**	**2**	**3**	**4**
244	46569.1	39717.1	31662.2	15836.8	17421.7	27844.1	36440.2	21276.4	10508.7	9490.1
257	104150.7	110669.2	106323.5	68165.0	73023.4	82740.6	92058.0	58974.0	30128.3	29270.7
292	40722.1	47238.3	43698.2	27198.7	32081.1	33267.9	45748.8	34352.0	22747.1	24672.6
302	1480.7	1859.4	1252.3	780.0	790.6	1921.9	1468.1	698.1	909.7	3549.4
313	11614.4	10474.2	6018.3	3173.3	4163.8	32781.9	44609.6	32951.7	22162.4	25127.1
326	60202.4	58598.9	52806.5	28077.7	33437.3	64915.1	80399.7	65494.7	45081.7	41085.4
363	45043.7	37000.7	24403.2	9799.9	13720.0	35925.9	46735.6	24680.7	13805.2	9152.5
388	13468.3	11106.6	6757.2	2579.6	4667.1	4053.3	5784.6	3166.9	2834.3	3122.7
399	7728.6	7425.4	5421.6	3197.4	3865.7	1441.0	4074.6	3204.4	1745.1	2600.6
407	3047.2	2275.1	1936.3	893.2	1087.6	4813.8	4097.8	1919.5	586.3	1730.3
440	16253.5	15510.3	14365.2	7145.3	10000.5	9528.6	13288.5	8904.1	2496.5	2694.5
460	8107.3	6973.5	7908.5	6724.7	6417.9	8933.0	9157.8	6458.7	4298.7	7902.3
480	31769.6	31346.8	28254.4	14637.1	17542.0	23662.4	31207.2	22516.1	14887.1	13350.9
503	8915.8	8722.2	6711.0	3455.8	4416.7	7450.8	7913.2	5172.9	2619.8	3699.5
521	5515.9	5153.4	3368.0	1932.2	3601.9	6345.9	6638.0	4063.5	2322.3	2752.5
540	34183.9	30610.6	20390.1	10385.9	13027.7	28902.9	38195.6	23428.4	11110.6	10854.1
560	5864.5	7096.8	3779.3	1394.1	3194.3	5870.6	7179.6	7572.1	2374.9	2144.5
594	18152.8	17848.6	12081.0	5301.9	6376.0	15971.9	20983.3	16377.2	8933.9	6933.9
600	13848.6	9281.3	4403.9	2113.7	3353.0	6316.5	10919.8	8633.0	3498.9	1928.8
604	10868.0	6598.9	3341.2	976.1	2669.6	15957.0	17281.4	9958.2	4846.2	3042.9
608	2905.9	2562.9	1650.2	568.8	1744.7	2428.5	3543.8	2299.6	1173.2	1765.5
616	8751.2	7640.8	5992.7	2571.1	3323.6	5899.5	5531.3	3039.3	1493.2	2192.3
627	27040.1	22330.6	16539.8	6850.5	9197.4	28612.8	24996.8	13079.0	6206.9	6183.4
654	11448.8	13722.6	7598.2	10540.2	15147.7	30462.3	17011.3	6612.5	23069.6	29104.1
661	11219.0	13099.1	10317.7	7101.1	8911.7	8003.3	5652.9	1819.6	8431.1	8629.2
722	30287.3	30590.5	29326.0	10951.9	19982.3	22116.0	19932.2	11281.6	7316.1	5479.8

The remaining signal was calculated taking as 100 % of signal the 0 repair hour sample. The T_{50}% is the time required to repair 50 % of the lesion. The data is presented in the table below (%).

Exp 3	RE*sir2Δ*						NRE*sir2Δ*					
CPDs	**Repair time (hours)**					**T50%**	**Repair time (hours)**					**T50%**
Position	**0**	**1**	**2**	**3**	**4**		**0**	**1**	**2**	**3**	**4**	
244	100.0	85.3	68.0	34.0	37.4	2.5	100.0	130.9	76.4	37.7	34.1	2.6
257	100.0	106.3	102.1	65.4	70.1	4.8	100.0	111.3	71.3	36.4	35.4	2.6
292	100.0	116.0	107.3	66.8	78.8	6.0	100.0	137.5	103.3	68.4	74.2	5.2
302	100.0	125.6	84.6	52.7	53.4	3.0	100.0	76.4	36.3	47.3	184.7	1.6
313	100.0	90.2	51.8	27.3	35.9	2.0	100.0	136.1	100.5	67.6	76.6	5.6
326	100.0	97.3	87.7	46.6	55.5	2.9	100.0	123.9	100.9	69.4	63.3	4.4
363	100.0	82.1	54.2	21.8	30.5	2.1	100.0	130.1	68.7	38.4	25.5	2.6
388	100.0	82.5	50.2	19.2	34.7	2.0	100.0	142.7	78.1	69.9	77.0	10.0
399	100.0	96.1	70.1	41.4	50.0	2.6	100.0	102.8	100.0	100.0	100.0	10.0
407	100.0	74.7	63.5	29.3	35.7	2.4	100.0	85.1	39.9	12.2	35.9	1.8
440	100.0	95.4	88.4	44.0	61.5	2.8	100.0	139.5	93.4	26.2	28.3	2.6
460	100.0	86.0	97.5	82.9	79.2	10.0	100.0	102.5	72.3	48.1	88.5	2.7
480	100.0	98.7	88.9	46.1	55.2	2.9	100.0	131.9	95.2	62.9	56.4	4.1
503	100.0	97.8	75.3	38.8	49.5	2.6	100.0	106.2	69.4	35.2	49.7	2.5
521	100.0	93.4	61.1	35.0	65.3	2.3	100.0	104.6	64.0	36.6	43.4	2.4
540	100.0	89.5	59.6	30.4	38.1	2.3	100.0	132.2	81.1	38.4	37.6	2.7
560	100.0	121.0	64.4	23.8	54.5	2.3	100.0	122.3	129.0	40.5	36.5	2.8
594	100.0	98.3	66.6	29.2	35.1	2.4	100.0	131.4	102.5	55.9	43.4	3.3
600	100.0	67.0	31.8	15.3	24.2	1.5	100.0	102.9	136.7	55.4	30.5	3.2
604	100.0	60.7	30.7	9.0	24.6	1.3	100.0	108.3	62.4	30.4	19.1	2.3
608	100.0	88.2	56.8	19.6	60.0	2.2	100.0	145.9	94.7	48.3	72.7	2.9
616	100.0	87.3	68.5	29.4	38.0	2.4	100.0	93.8	51.5	25.3	37.2	2.0
627	100.0	82.6	61.2	25.3	34.0	2.3	100.0	87.4	45.7	21.7	21.6	1.9
654	100.0	119.9	66.4	92.1	132.3	10.0	100.0	55.8	21.7	75.7	95.5	1.1
661	100.0	116.8	92.0	63.3	79.4	10.0	100.0	70.6	22.7	105.3	107.8	1.4
722	100.0	101.0	96.8	36.2	66.0	2.7	100.0	90.1	51.0	33.1	24.8	2.0

A III.4-4 NER efficiency at high resolution at *URA3* gene for the NTS

The table below represent the repair efficiency at the specific CPD points for the NTS at the NRE*sir2Δ* and RE*sir2Δ* strains.

Exp 4	RE*sir2Δ*					NRE*sir2Δ*				
CPDs	**Repair time (hours)**					**Repair time (hours)**				
Position	**0**	**1**	**2**	**3**	**4**	**0**	**1**	**2**	**3**	**4**
Top band	2807599.0	2842366.2	3055074.8	3172540.0	3033466.5	2174268.5	2422070.5	2605494.7	2511200.5	2114603.0
244	58336.0	44266.6	23730.1	15737.7	6594.2	24322.8	33886.4	14093.2	11287.2	8293.3
257	111592.5	121967.6	70810.0	56835.0	30110.4	130843.4	135024.4	51339.2	28592.7	18422.3
292	52313.1	51035.8	39085.0	24808.2	19363.0	54210.8	70357.4	36231.7	37726.4	24015.5
302	1625.6	1535.0	950.5	793.2	160.4	12713.8	14657.6	8430.6	26609.2	24920.0
313	20880.9	10261.0	4727.8	3957.5	6622.0	22044.0	21040.2	12976.0	21971.7	22204.2
326	83890.5	69008.5	50067.9	31491.6	18459.9	91323.7	113711.3	75522.4	50397.2	25512.9
363	44279.0	30586.7	15547.8	10499.4	7864.5	40109.8	41336.4	16344.1	4879.0	2640.0
388	5315.9	3569.4	2838.6	3702.1	1988.6	11006.5	5449.8	3295.8	5702.9	2976.2
399	5478.4	11406.1	7415.4	6448.6	5089.6	6689.2	10030.6	4588.8	9481.6	5362.2
407	6903.7	6644.5	449.2	830.9	382.0	11167.6	7506.7	1883.8	1347.1	492.7
440	11779.7	14081.3	9588.2	4819.0	3872.2	7182.8	9073.5	4796.2	3041.6	2716.6
460	12211.1	10276.2	9083.1	5355.1	4272.9	14360.7	13943.6	6336.8	8940.5	5879.2
480	54394.5	47965.5	34629.1	19022.7	17978.3	38827.2	53617.2	34918.5	21892.0	13501.8
503	15572.1	12121.1	7844.9	7268.9	3554.6	10113.2	12079.7	5565.4	3469.3	1592.1
521	12291.3	7606.4	3706.2	4421.3	4462.0	14588.6	12522.8	8406.5	14196.1	14016.1
540	62651.1	50334.3	28555.3	17715.6	14509.5	74850.4	83353.0	34360.1	31296.3	17098.8
560	8832.1	7358.5	3761.6	2667.2	1217.0	10985.6	13547.8	6466.1	2348.1	2858.2
594	32170.6	32883.6	17619.6	13094.5	7040.2	22408.4	31122.0	20514.9	13795.9	8389.8
600	13000.0	10638.0	4808.7	2166.8	1675.7	7811.3	10589.3	5396.5	1228.2	911.7
604	22538.5	11689.1	3407.6	1630.0	1560.3	31813.6	25284.2	10151.9	3920.6	1362.5
608	4870.8	3571.7	2631.6	1029.5	854.3	5161.3	4199.2	3248.9	2239.6	2228.4
616	17370.6	10824.8	5384.2	3303.7	1000.9	7571.3	4773.1	2722.8	452.7	129.3
627	57933.8	35309.4	16623.2	9359.1	5876.0	58085.6	41489.1	15713.2	6674.6	2342.2
654	15422.0	12974.8	6798.6	6498.7	6116.8	33705.8	16592.5	6737.0	11884.7	8799.8
661	10821.9	21583.3	18806.1	13777.2	12807.8	9509.2	11428.6	8014.2	7195.9	4273.8
722	96424.9	82067.1	61002.8	34137.9	24636.2	48591.5	33841.1	12257.8	9491.6	4559.3
Sum	3646499.5	3563932.7	3504947.9	3473911.4	3241535.8	2974266.6	3252527.7	3015807.2	2851263.3	2340101.6
ratio	1.0	1.0	1.0	1.0	0.9	0.9	1.0	0.9	0.9	0.7

The data was adjusted and illustrated in the table below.

Exp 4	RE*sir2Δ*					NRE*sir2Δ*				
CPDs	Repair time (hours)					Repair time (hours)				
Position	0	1	2	3	4	0	1	2	3	4
244	58336.0	45292.2	24688.5	16519.6	7418.1	26598.3	33886.4	15199.4	12875.7	11526.9
257	111592.5	124793.3	73669.8	59658.6	33872.1	143084.7	135024.4	55369.0	32616.6	25605.3
292	52313.1	52218.1	40663.4	26040.7	21782.0	59282.5	70357.4	39075.6	43035.8	33379.3
302	1625.6	1570.5	988.9	832.6	180.4	13903.2	14657.6	9092.3	30354.0	34636.5
313	20880.9	10498.7	4918.7	4154.1	7449.3	24106.4	21040.2	13994.5	25063.8	30861.8
326	83890.5	70607.3	52090.0	33056.2	20766.1	99867.6	113711.3	81450.4	57489.7	35460.6
363	44279.0	31295.3	16175.7	11021.1	8847.1	43862.4	41336.4	17627.0	5565.6	3669.3
388	5315.9	3652.1	2953.3	3886.0	2237.1	12036.2	5449.8	3554.5	6505.5	4136.6
399	5478.4	11670.4	7714.9	6769.0	5725.5	7315.0	10030.6	4949.0	10816.0	7453.0
407	6903.7	6798.5	467.3	872.2	429.8	12212.4	7506.7	2031.7	1536.7	684.8
440	11779.7	14407.6	9975.4	5058.4	4355.9	7854.8	9073.5	5172.6	3469.6	3775.8
460	12211.1	10514.2	9449.9	5621.2	4806.7	15704.2	13943.6	6834.2	10198.7	8171.5
480	54394.5	49076.8	36027.7	19967.8	20224.4	42459.7	53617.2	37659.4	24972.9	18766.2
503	15572.1	12401.9	8161.7	7630.0	3998.6	11059.4	12079.7	6002.3	3957.5	2212.8
521	12291.3	7782.6	3855.8	4641.0	5019.4	15953.4	12522.8	9066.3	16194.0	19481.1
540	62651.1	51500.4	29708.6	18595.7	16322.1	81853.1	83353.0	37057.1	35700.7	23765.8
560	8832.1	7529.0	3913.5	2799.7	1369.0	12013.4	13547.8	6973.6	2678.5	3972.6
594	32170.6	33645.4	18331.2	13745.0	7919.7	24504.9	31122.0	22125.2	15737.4	11661.1
600	13000.0	10884.5	5002.9	2274.4	1885.0	8542.1	10589.3	5820.1	1401.0	1267.2
604	22538.5	11959.9	3545.3	1711.0	1755.3	34790.0	25284.2	10948.8	4472.4	1893.8
608	4870.8	3654.4	2737.9	1080.7	961.0	5644.2	4199.2	3503.9	2554.8	3097.3
616	17370.6	11075.6	5601.7	3467.9	1125.9	8279.6	4773.1	2936.5	516.4	179.7
627	57933.8	36127.5	17294.6	9824.1	6610.1	63519.9	41489.1	16946.6	7613.9	3255.4
654	15422.0	13275.4	7073.2	6821.5	6880.9	36859.1	16592.5	7265.9	13557.3	12230.9
661	10821.9	22083.3	19565.6	14461.7	14407.9	10398.8	11428.6	8643.3	8208.6	5940.1
722	96424.9	83968.4	63466.5	35833.9	27714.0	53137.5	33841.1	13220.0	10827.4	6337.1

The remaining signal was calculated taking as 100 % of signal the 0 repair hour sample. The T_{50}% is the time required to repair 50 % of the lesion. The data is presented in the table below (%).

Exp 4	RES*ir2Δ*						NRES*ir2Δ*					
CPDs	Repair time (hours)					T50%	Repair time (hours)					T50%
Position	0	1	2	3	4		0	1	2	3	4	
244	100.0	77.6	42.3	28.3	12.7	1.8	100.0	127.4	57.1	48.4	43.3	2.5
257	100.0	111.8	66.0	53.5	30.4	3.2	100.0	94.4	38.7	22.8	17.9	1.8
292	100.0	99.8	77.7	49.8	41.6	3.0	100.0	118.7	65.9	72.6	56.3	4.5
302	100.0	96.6	60.8	51.2	11.1	3.0	100.0	105.4	65.4	118.3	149.1	10.0
313	100.0	50.3	23.6	19.9	35.7	1.0	100.0	87.3	58.1	104.0	128.0	2.5
326	100.0	84.2	62.1	39.4	24.8	2.5	100.0	113.9	81.6	57.6	35.5	3.3
363	100.0	70.7	36.5	24.9	20.0	1.6	100.0	94.2	40.2	12.7	8.4	1.8
388	100.0	68.7	55.6	73.1	42.1	3.8	100.0	45.3	29.5	54.0	34.4	0.9
399	100.0	113.0	140.8	123.6	104.5	10.0	100.0	137.1	67.7	107.9	101.9	10.0
407	100.0	98.5	6.8	12.6	6.2	1.5	100.0	61.5	16.6	12.6	5.6	1.3
440	100.0	122.3	84.7	42.9	37.0	2.8	100.0	115.5	65.9	44.2	48.1	2.6
460	100.0	86.1	77.4	46.0	39.4	2.8	100.0	88.8	43.5	64.9	52.0	1.8
480	100.0	90.2	66.2	36.7	37.2	2.5	100.0	126.3	88.7	58.8	44.2	3.5
503	100.0	79.6	52.4	49.0	25.7	2.2	100.0	109.2	54.3	35.8	20.0	2.2
521	100.0	63.3	31.4	37.8	40.8	1.4	100.0	78.5	56.8	101.5	122.1	2.5
540	100.0	82.2	47.4	29.7	26.1	1.9	100.0	101.8	45.3	43.6	29.0	1.8
560	100.0	85.2	44.3	31.7	15.5	1.8	100.0	112.8	58.0	22.3	33.1	2.2
594	100.0	104.6	57.0	42.7	24.6	2.3	100.0	127.0	90.3	64.2	47.6	3.8
600	100.0	83.7	38.5	17.5	14.5	1.7	100.0	124.0	68.1	16.4	14.8	2.4
604	100.0	53.1	15.7	7.6	7.8	1.1	100.0	72.7	31.5	12.9	5.4	1.5
608	100.0	75.0	56.2	22.2	19.7	2.2	100.0	74.4	62.1	45.3	54.9	2.6
616	100.0	63.8	32.2	20.0	6.5	1.4	100.0	57.6	35.5	6.2	2.2	1.3
627	100.0	62.4	29.9	17.0	11.4	1.4	100.0	65.3	26.7	12.0	5.1	1.4
654	100.0	86.1	45.9	44.2	44.6	1.9	100.0	45.0	19.7	36.8	33.2	0.9
661	100.0	104.1	100.8	103.6	133.1	10.0	100.0	109.9	83.1	78.9	57.1	5.0
722	100.0	87.1	65.8	37.2	28.7	2.5	100.0	63.7	24.9	20.4	11.9	1.3

Appendix IV

Data from Chapter VI

AIV.1-1 Histone H4K16 acetylation levels at the 540 fragment in the *URA3* coding region for the NRE and NRE*sir2Δ* strains

The table below represent the % IP/input before (U) and after the UV exposure (30, 60 mins) for each independent experiment in the *URA3* coding region for the NRE and NRE*sir2Δ* strains.

samples	Exp1	Exp2	Exp3
	%IP/input	% IP/input	%IP/input
NRE/U	0.48916754	0.733898	0.076183
NRE/30	0.78729399	0.429999	0.075955
NRE/60	0.85031826	1.412909	0.051438
NRE*sir2Δ*/U	0.4473313	0.414967	0.155998
NRE*sir2Δ*/30	0.78714376	0.462891	0.116686
NRE*sir2Δ*/60	0.74286132	1.989736	0.126045

AIV.1-2 The ratio, average and standard error

The ratio was calculated considering as 1 the % IP/input obtained at NRE/U sample, so all the values could be compared with the NRE/U sample. The averages and the standard errors were also calculated.

samples	ratio	ratio	ratio	average	St. error
NRE/U	1	1	1	1	0
NRE/30	1.609457	0.585911	0.997008	1.064125	0.297372
NRE/60	1.738297	1.925211	0.675181	1.446229	0.389282
NRE*sir2Δ* /U	0.914475	0.565429	2.047657	1.175854	0.447396
NRE*sir2Δ*/30	1.60915	0.630729	1.531647	1.257175	0.314021
NRE*sir2Δ*/60	1.518623	2.711187	1.654496	1.961436	0.376922

AIV.1-3 Summary of the results

The table below summarized the data used to plot the graph (figure 6.3, B) at chapter VI.

samples	average	St. error
NRE/U	1	0
NRE/30	1.064125	0.297372
NRE/60	1.446229	0.389282
NRE*sir2Δ*/U	1.175854	0.447396
NR*sir2Δ*/30	1.257175	0.314021
NRE*sir2Δ*/60	1.961436	0.376922

AIV.2-1 Histone H4K16 acetylation levels at the 222 fragment in the *URA3* coding region for the NRE and the NRE*sir2Δ* strains

The table below represent the % IP/input before (U) and after the UV exposure (30, 60 mins) for each independent experiment in the *URA3* coding region for the NRE and NRE*sir2Δ* strains.

Samples	Exp1	Exp2	Exp3
	%IP/input	%IP/input	%IP/input
NRE/U	0.040618	0.228559	0.214514
NRE/30'	0.036245	0.300626	0.167126
NRE/60'	0.121613	0.376111	1.092574
NRE*sir2Δ*/U	0.029814	0.188196	0.337241
NRE*sir2Δ*/30'	0.093684	0.419503	0.220874
NRE*sir2Δ*/60'	0.12768	0.371033	0.954698

AIV.2-2 The ratio, average and standard error

The ratio was calculated considering as 1 the % IP/input obtained at the NRE/U sample, so all the values could be compared with the NRE/U sample. The averages and the standard errors were also calculated.

Samples	ratio	ratio	ratio	average	St. error
NRE/U	1	1	1	1	0
NRE/30'	0.892334	1.31531344	0.779091	0.99558	0.163175
NRE/60'	2.994059	1.645574371	5.093261	3.244298	1.003095
NRE*sir2Δ*/U	0.734	0.823401955	1.572117	1.043173	0.265728
NRE*sir2Δ*/30'	2.306449	1.835427264	1.029648	1.723842	0.372779
NRE*sir2Δ*/60'	3.143418	1.623360359	4.450523	3.072434	0.816903

AIV.2-3 Summary of the results

The table below summarized the data used to plot the graph (figure 6.3, A) at chapter VI.

Samples	average	St. error
NRE/U	1	0
NRE/30'	0.99558	0.163175
NRE/60'	3.244298	1.003095
NRE*sir2Δ*/U	1.043173	0.265728
NRE*sir2Δ*/30'	1.723842	0.372779
NRE*sir2Δ*/60'	3.072434	0.816903

AIV.3-1 Histone H4K16 acetylation levels at the 222 fragment in the RE and RE*sir2Δ* strains

The table below represent the % IP/input before (U) and after the UV exposure (30, 60 mins) for each independent experiment in the *URA3* coding region for the RE and RE*sir2Δ* strains.

Samples	Exp1	Exp2	Exp3
	% IP/input	% IP/input	% IP/input
RE	0.037705	0.625085	2.874351
RE/30'	0.044068	0.135482	1.690622
RE/60'	0.017299	0.068901	3.820301
RE*sir2Δ*/U	0.112434	0.998444	3.520819
RE*sir2Δ*/30	0.07272	0.787705	9.527634
RE*sir2Δ*/60	0.161283	9.888026	39.17646

AIV.3-2 The ratio, average and standard error

The ratio was calculated considering as 1 the % IP/input obtained at RE/U sample, so all the values from the rest of samples could be compared with the RE/U sample. The averages and the standard errors were also calculated.

Samples	ratio	ratio	ratio	average	St. error
RE	1	1	1	1	0
RE/30'	1.168764	0.216741	0.588175	0.657894	0.277027
RE/60'	0.458783	0.110227	1.329101	0.632704	0.362445
RE*sir2Δ*/U	2.981917	1.597293	1.224909	1.934706	0.534526
RE*sir2Δ*/30	1.92866	1.260155	3.314708	2.167841	0.605035
RE*sir2Δ*/60	4.277477	15.81868	13.62967	11.24194	3.539105

AIV.3-3 Summary of the results

The table below summarized the data used to plot the graph (figure 6.3, C) at chapter VI.

Samples	average	St. error
RE	1	0
RE/30'	0.657894	0.277027
RE/60'	0.632704	0.362445
RE*sir2Δ*/U	1.934706	0.534526
RE*sir2Δ*/30	2.167841	0.605035
RE*sir2Δ*/60	11.24194	3.539105

AIV.4-1 Histone H4K16 acetylation levels at the 540 fragment in the *URA3* coding region for the RE and the RE*sir2Δ* strains

The table below represent the % IP/input before (U) and after the UV exposure (30, 60 mins) for each independent experiment in the *URA3* coding region for the RE and RE*sir2Δ* strains.

samples	Exp1	Exp2	Exp3
	%IP/input	%IP/input	%IP/input
RE/U	0.318319	0.144873	6.806998
RE/30'	0.268757	0.105458	0.575942
RE/60'	0.147058	0.225506	0.581568
RE*sir2Δ*//U	0.28507	0.142445	0.661527
RE*sir2Δ*//30'	0.272882	0.34069	2.548198
RE*sir2Δ*//60'	13.53714	3.076403	5.668798

AIV.4-2 The ratio, average and standard error

The ratio was calculated considering as 1 the % IP/input obtained at RE/U sample, so all the values could be compared with the RE/U sample. The averages and the standard errors were also calculated.

samples	ratio	ratio	ratio	average	St. error
RE/U	1	1	1	1	0
RE/30'	0.8443	0.727935	0.08461	0.55228178	0.236236
RE/60'	0.461982	1.55658	0.08544	0.701332907	0.441223
RE*sir2Δ*/U	0.895548	0.983239	0.09718	0.658656908	0.281876
RE*sir2Δ*/30'	0.85726	2.351649	0.37435	1.194419543	0.595171
RE*sir2Δ*/60'	42.52696	21.23522	0.83279	21.5316552	12.03698

AIV.4-3 Summary of the results

The table below summarized the data used to plot the graph (figure 6.3, D) at chapter VI

samples	average	St. error
RE/U	1	0
RE/30'	0.55228178	0.236236
RE/60'	0.701332907	0.441223
RE*sir2Δ*/U	0.658656908	0.281876
RE*sir2Δ*/30'	1.194419543	0.595171
RE*sir2Δ*/60'	21.5316552	12.03698

AIV.5-1 Histone H3K (9, 14) acetylation levels at the 540 fragment in the *URA3* coding region for the RE and the RE*sir2Δ* strains

The table below represent the % IP/input before (U) and after the UV exposure (30, 60 mins) for each independent experiment in the *URA3* coding region for the RE and RE*sir2Δ* strains.

samples	Exp1	Exp2	Exp3
	%IP/input	%IP/input	%IP/input
RE/U	4.26492287	4.53482	2.92099699
RE/30'	1.82839933	6.448002	0.44830836
RE/60'	0.61065673	2.354346	0.3982511
RE*sir2Δ*/U	4.12378805	14.61661	2.84217309
RE*sir2Δ*/30'	3.49645246	9.0598	1.50085152
RE*sir2Δ*/60'	35.4463807	60.29981	22.7656844

AIV.5-2 The ratio, average and standard error

The ratio was calculated considering as 1 the % IP/input obtained at RE/U sample, so all the values from the rest of samples could be compared with the RE/U sample. The averages and the standard errors were also calculated.

Samples	ratio	ratio	ratio	average	St. error
RE/U	1	1	1	1	0
RE/30'	0.42870631	1.421887	0.15347786	0.6680237	0.385214264
RE/60'	0.14318119	0.519171	0.13634081	0.2662309	0.126485338
RE*sir2Δ*/U	0.966908	3.223194	0.97301473	1.721039	0.751079728
RE*sir2Δ*/30'	0.81981611	1.99783	0.51381481	1.110487	0.452379779
RE*sir2Δ*/60'	8.31114227	13.29707	7.79380618	9.8006719	1.754564928

AIV.5-3 Summary of the results

The table below summarized the data used to plot the graph (figure 6.4, B) at chapter VI.

Samples	average	St. error
RE/U	1	0
RE/30'	0.6680237	0.385214264
RE/60'	0.2662309	0.126485338
RE*sir2Δ*/U	1.721039	0.751079728
RE*sir2Δ*/30'	1.110487	0.452379779
RE*sir2Δ*/60'	9.8006719	1.754564928

AIV.6-1 Histone H3K (9, 14) acetylation levels at the 222 fragment in the *URA3* coding region for the RE and the RE*sir2Δ* strains

The table below represent the % IP/input before (U) and after the UV exposure (30, 60 mins) for each independent experiment in the *URA3* coding region for the RE and RE*sir2Δ* strains.

samples	Exp1	Exp2	Exp3
	%IP/input	%IP/input	%IP/input
RE/U	5.084514	3.87326	2.967820704
RE/30'	17.335775	1.835121	0.597588198
RE/60'	1.2206204	0.538402	0.494276763
RE*sir2Δ*/U	13.733972	7.802302	4.240825879
RE*sir2Δ*/30'	3.2998583	4.016002	1.958442819
RE*sir2Δ*/60'	45.417892	5.197365	29.59001546

AIV.6-2 The ratio, average and standard error

The ratio was calculated taking as 1 the % IP/input obtained at RE/U sample, so all the values from the rest of samples could be compared with the RE/U sample. The averages and the standard errors were also calculated.

Samples	ratio	ratio	ratio	average	St. error
RE/U	1	1	1	1	0
RE/30'	3.4095245	0.201356	0.473792404	1.361557613	0.79551
RE/60'	0.2400663	0.166545	0.139004972	0.181872209	0.023365
RE*sir2Δ*/U	2.7011377	1.428936	2.014401884	2.048158536	0.284773
RE*sir2Δ*/30'	0.6490017	0.659893	1.036853279	0.781915852	0.098767
RE*sir2Δ*/60'	8.9325926	9.970284	1.341858115	6.748244922	2.106702

AIV.6-3 Summary of the results

The table below summarized the data used to plot the graph (figure 6.4, A) at chapter VI.

Samples	average	St. error
RE/U	1	0
RE/30'	1.361557613	0.79551
RE/60'	0.181872209	0.023365
RE*sir2Δ*/U	2.048158536	0.284773
RE*sir2Δ*/30'	0.781915852	0.098767
RE*ssir2Δ*/60'	6.748244922	2.106702